NUMERICAL APPROXIMATION OF FLUID-STRUCTURE INTERACTION PROBLEMS WITH APPLICATION TO HAEMODYNAMICS

THÈSE N° 2458 (2001)

PRÉSENTÉE AU DÉPARTEMENT DE MATHÉMATIQUES

ÉCOLE POLYTECHNIQUE FÉDÉRALE DE LAUSANNE

POUR L'OBTENTION DU GRADE DE DOCTEUR ÈS SCIENCES

PAR

Fabio NOBILE

laurea in ingegneria elettronica, Politecnico di Milano, Italie
de nationalité italienne

acceptée sur proposition du jury:

Prof. A. Quarteroni, directeur de thèse
Prof. M. Grote, rapporteur
Prof. Y. Maday, rapporteur
Prof. J. Rappaz, rapporteur

Lausanne, EPFL
2001

Abstract

The purpose of this thesis is the numerical approximation of the fluid-structure interaction problem appearing when an incompressible fluid flows in a compliant vessel. This is indeed the typical situation arising in the hemodynamics of large arteries. The vessel wall dynamics is described by means of a thin elastic membrane model while the fluid motion by the Navier-Stokes equations for incompressible Newtonian fluids.

We account for quite large deformations of the structure, which induce a non negligible movement of the fluid domain. The fluid equations are described resorting to an *Arbitrary Lagrangian Eulerian* (ALE) formulation.

The first part of this work deals with the analysis of the ALE technique in the context of a finite element approximation. Stability and convergence properties of a few finite element ALE schemes, and their relation with the so called *Geometric Conservation Laws* (GCL) are investigated on a linear advection diffusion equation. The obtained results are then generalised to the incompressible Navier-Stokes equations in a moving domain. Moreover we show how inexact factorisation schemes can be extended straightforwardly to the ALE framework.

In the second part of this thesis we focus on the fluid-structure problem. We consider a finite element approximation in space, which allows for possible non-conformities between fluid and structure discretisation. Moreover, we propose three fully implicit time-advancing schemes and we analyse their stability properties. In particular we prove an unconditional stability result for two of them, while for the third one, which employs an explicit structure solver, we show that the stability condition is not more restrictive than the one associated to the structure discretisation. Finally, we present several numerical results on a simplified 2D geometry. In particular we are able to simulate the propagation inside the vessel of a pressure pulse imposed at the inflow section.

One of the peculiar features of the coupled problem at hand is, indeed, the appearance of pressure and flow rate waves inside the vessel. This fact introduces the further difficulty of devising suitable boundary conditions which allow to "absorb" the outgoing waves. To this aim, we couple the 3D fluid-structure model with a reduced mono-dimensional model which acts as an "absorbing" device for the waves exiting the computational domain. Numerical results showing the effectiveness of this technique are presented as well.

Version abrégée

Cette thèse concerne l'approximation numérique des problèmes d'intéraction fluide-structure qui apparaissent dans l'étude de l'écoulement d'un fluide incompressible à l'intérieur d'un vaisseau déformable. Cela est, en effet, la situation type en hemodynamique, c'est-à-dire dans l'étude de l'écoulement sanguin dans les grandes artères. Le mouvement de la paroi du vaisseau est décrit à l'aide d'un modèle élastique membranaire; quant à l'écoulement fluide, il est décrit par les équations de Navier-Stokes pour un fluide newtonien incompressible. On considère le cas où les déformations de la structure peuvent être assez grandes et induisent un mouvement non négligeable du domaine fluide. Le problème fluide est alors décrit en utilisant une formulation ALE.

La première partie de ce travail porte sur l'analyse de la technique ALE dans le contexte d'une approximation par éléments finis. On étudie, sur une équation de diffusion et transport linéaire, les propriétés de stabilité et de convergence de plusieurs schémas ALE éléments finis, ainsi que leur relation avec les lois de conservation géométrique (GCL). Les résultats obtenus sont ensuite généralisés aux équations de Navier-Stokes incompressibles dans un domaine mobile. De plus, on montre comment des schémas de factorisation inexacte pour la résolution des équations du fluide peuvent être étendus dans le cas d'une formulation ALE.

Dans la deuxième partie de la thèse, on se concentre sur le problème fluide-structure. On considère une approximation en espace par éléments finis qui permet des non-conformités entre les discrétisations fluide et structure. Ensuite, on propose trois schémas en temps complètement implicites et on analyse leurs propriétés de stabilité. En particulier, pour deux d'entre eux, on démontre un résultat de stabilité inconditionnelle; pour le troisième, qui utilise un solveur explicite structure, on démontre que la condition de stabilité n'est pas plus restrictive que celle qui est associée à la discrétisation de la structure. Enfin, on présente plusieurs résultats numériques sur une géométrie simplifiée bi-dimensionnelle. En particulier, on est capable de simuler la propagation, à l'intérieur du domaine, d'une impulsion de pression imposée sur la section d'entrée.

Un des aspects caractéristiques du problème couplé est, en effet, la formation des ondes de pression et de débit à l'intérieur du vaisseau. Cela introduit des difficultés supplémentaires pour établir des conditions au bord permettant d'absorber les ondes sortantes. Cette difficulté est surmontée par le couplage du modèle fluide-structure 3D avec un modèle réduit, mono-dimensionnel, qui agit comme un "dispositif absorbant" pour les ondes sortantes du domaine de calcul. Enfin, on présente des résultats numériques qui montrent l'éfficacité de cette technique.

Acknowledgements

I would like to thank, firstly, Prof. Quarteroni, who has introduced me to the world of Finite Elements and Computational Fluid Dynamics and has given me the opportunity to work on a very interesting subject. He has devoted me a lot of time to guide me in my research and has continuously stimulated me to investigate further aspects of the problem. This has given me the possibility to learn really a lot of things during my PhD. I am particularly grateful to him for the confidence he has always had in me and for the enthusiasm in scientific research he could transmit to me.

I am very grateful also to Dr. Luca Formaggia who has always been present and ready to give me suggestions and indications on mathematical topics and to help me in overcoming the numerous difficulties encountered. I thank him also for his priceless help with software problems.

I would like to thank, moreover, Dr. Alessandro Veneziani, with whom I started collaborating on this fascinating subject four years ago, Dr. Jean-Frederic Gerbeau with whom I worked during the first year of my PhD and who enlightened me on the more theoretical aspects of PDEs and Dr. Céline Grandmont for the fruitful discussions on the theoretical aspects of fluid-structure interaction problems.

I also thank Prof. Jacques Rappaz, Prof. Yvon Maday and Prof. Marcus Grote who accepted to be members of the jury and read carefully the manuscript, giving me precious suggestions, as well as Prof. Robert Dalang who presided the jury.

Thanks, finally, to my colleagues in the group of Prof. Quarteroni, and the other people of the Department of Mathematics at the EPFL with whom I shared many experiences during these three years, as well as my parents who have always encouraged me.

I acknowledge the Fonds National Suisse that has supported this work.

Contents

Introduction

Fluid structure interaction problems appear in many different applications of physics and engineering. We may cite, for instance, aeroelasticity problems or fluttering of wings and structures, wind induced oscillations of bridges, gas explosions in pipelines or buildings, hydraulic shock absorbers, vibrations or water hammer effects in pipe network and, of course, the application we are interested in, that is blood flow in large arteries. These are only a few examples drawn from a wide range of applications.

In all the aforementioned situations, fluid and structure dynamics influence each other. Indeed, the structure deforms under the action of the fluid stresses and, conversely, the fluid follows the structure displacement; that means not only that the fluid velocity equals that of the structure at the interface, but that the region itself in which the fluid is confined changes as a consequence of the structure motion.

Typically, structure dynamics (displacement, strains and stresses) is described in a Lagrangian frame of reference, i.e. with respect to a fixed configuration Ω_0^S. On the other hand, the fluid equations are tackled in an Eulerian framework, which allows us to describe the fluid quantities at each time t and at each point x of the physical domain Ω^F that is considered in the application.

In those cases where the structure deformation is very small, the fluid domain Ω^F may be thought of as fixed and the presence of the structure accounted for by suitable boundary conditions (called *transpiration* conditions). Standard formulations and numerical approximation schemes may thus be adopted for both the fluid and the structure. This approach is widely used for instance in the study of wing fluttering or more generally structure vibrations induced by a fluid flow.

In the case where the structure displacement induces non negligible deformations of the fluid domain, as for instance in hemodynamics where, during a cardiac beat, the diameter of an artery may undergo a variation of about 10%, we are faced with the problem of solving fluid equations on a moving domain. The first part of this work deals precisely with this aspect.

Different techniques have been proposed in the literature to numerically approximate equations on moving domains. We mention, among others, the Arbitrary Lagrangian Eulerian (ALE) formulation, proposed at the beginning of the eighties (see e.g. [20, 48]); the space time approach, see e.g. [88, 89, 59] and [61] for an application to fluid structure problems; the fictitious domain method ([37, 38]); the level set method ([12]); and finally the immersed boundary method proposed by C. Peskin [69, 68] and applied successfully since the seventies, to the simulation of heart contractions. Among these techniques, very likely the most popular is the ALE formulation. It is based on the introduction of an appropriate (arbitrary) mapping

$\mathcal{A}_t$ from a reference fixed configuration Ω_0^F to the current moving domain $\Omega^F(t)$:

$$\mathcal{A}_t : \Omega_0^F \to \Omega^F(t), \qquad \mathbf{x}(\mathbf{Y},t) = \mathcal{A}_t(\mathbf{Y}), \ \forall \mathbf{Y} \in \Omega_0^F.$$

We will refer to $\mathbf{Y}$ as the *ALE coordinate* and $\mathbf{x}$ as the *Eulerian coordinate*. A triangulation $\mathcal{T}_{h,t}$ of the physical domain $\Omega^F(t)$ can be easily obtained as the image through the mapping $\mathcal{A}_t$ of a triangulation $\mathcal{T}_{h,0}$ on Ω_0^F, provided $\mathcal{A}_t$ is invertible and sufficiently regular.

In this way, we will obtain a mesh $\mathcal{T}_{h,t}$ that naturally follows the boundary movement. In order to effectively apply the ALE technique, one has then to rewrite the equations in a moving frame of reference: the space derivative terms are left expressed as a function of the Eulerian coordinate $\mathbf{x}$, since their expression is much simpler; on the contrary, the time derivatives will be computed along a constant $\mathbf{Y}$ line. Introducing the notion of *domain velocity* $\mathbf{w} = \frac{\partial \mathcal{A}_t}{\partial t}$ (also frequently called *mesh velocity* since it represents in fact the velocity of each mesh node in the physical space), a generic conservation law of the following type

$$\frac{\partial u}{\partial t} + \nabla_{\mathbf{x}} \cdot \mathbf{F}(u) = f, \tag{0.0.1}$$

defined on a moving domain $\Omega^F(t)$, can be written in ALE form as

$$\left.\frac{\partial u}{\partial t}\right|_{\mathbf{Y}} - \mathbf{w} \cdot \nabla_{\mathbf{x}} u + \nabla_{\mathbf{x}} \cdot \mathbf{F}(u) = f, \qquad \text{in } \Omega^F(t), \tag{0.0.2}$$

thanks to relation

$$\left.\frac{\partial u}{\partial t}\right|_{\mathbf{Y}} = \left.\frac{\partial u}{\partial t}\right|_{\mathbf{x}} + \mathbf{w} \cdot \nabla_{\mathbf{x}} u.$$

Formulation (0.0.2) is not the only possible one in the ALE context. Another frequently used formulation, equivalent to (0.0.2), which has the advantage of maintaining the conservation properties of equation (0.0.1), reads

$$\left.\frac{\partial (J_{\mathcal{A}_t} u)}{\partial t}\right|_{\mathbf{Y}} + J_{\mathcal{A}_t} \nabla_{\mathbf{x}} \cdot (\mathbf{F} - \mathbf{w}u) = J_{\mathcal{A}_t} f, \tag{0.0.3}$$

where $J_{\mathcal{A}_t}$ is the jacobian of the ALE transformation $\mathcal{A}_t$. Its derivation will be presented in Chapter 1. We will refer to formulation (0.0.2) as the *non-conservative* form and to (0.0.3) as the *conservative* one.

In spite of the popularity that ALE formulations have gained in the last years, a rigorous mathematical analysis of both conservative and non-conservative forms as well as a thorough investigation of the properties of the numerical approximations deriving from them is still missing. The present work is a contribution to the study of ALE numerical schemes based on finite element approximations.

Another relevant aspect in the investigation of ALE schemes concerns the so-called *Geometric Conservation Laws* (GCL). The ALE formulation has been used extensively for fluid structure interaction problems particularly for compressible fluid dynamics and aero–elasticity, using mainly finite difference and finite volume schemes. In some of those works numerical instabilities and oscillations were noted. The main cause has been related to a misrepresentation of the convective fluxes due to an inaccurate calculation of geometrical quantities such as surface normals and volumes of the control cells used in finite-volume

computations. When dealing with a moving domain it is possible to write the differential equations governing the "evolution" of such geometrical quantities during the domain movement. A failure of the numerical scheme in correctly representing such an evolution may cause a loss of the conservation properties, which may lead to instabilities. Ways to overcome the problem have been devised for finite volume schemes and they result in an appropriate evaluation of the geometric quantities to be used in the time advancing scheme. This led to the development of the GCL. Unfortunately, no clear-cut analysis is so far available and the real significance of those conditions in terms of scheme stability and accuracy properties has not yet been established. In [56], M. Lesoinne and C. Farhat have analysed a spatial finite volume ALE formulation and have related the GCL to a minimal condition on the precision of the quadrature formula used to compute time-integrals. Notably, the minimal degree of exactness must depend on the number of space dimensions. In the same work, a preliminary analysis on the form of the GCL conditions for finite element schemes is given. In a later work [44], H. Guillard and C. Farhat have proved that the GCL are sufficient to guarantee that particular finite volume schemes remain at least first order accurate in time, independently of the law according to which the domain moves.

Nevertheless, a thorough analysis of the implication and possible limits of the ALE formulation in the context of finite element methods is still missing.

In part I of this thesis we will focus on some aspects of the ALE formulation. We begin by investigating the smoothness conditions on the ALE mapping required to obtain a proper discretisation. We carry out a comparison between conservative and non-conservative formulation, reinterpret the GCL in a finite element context and analyse stability and accuracy properties of a few time marching schemes. The major part of this investigation will be made on a linear scalar advection diffusion equation.

We then discuss time discretisation. We may ask the following general question: given a time marching scheme which features some stability and accuracy properties when applied to a differential equation defined on a fixed domain, does it preserve the same properties when applied to the same equation defined on a moving domain and written in ALE from? And, furthermore, what role do the GCL play in this regard?

We will show that for an Implicit Euler scheme applied to the conservative formulation (0.0.3), GCL are sufficient conditions to recover an unconditional stability result.

This result is not as general as we would have hoped; indeed, we will see that other time discretisation schemes (first or second order accurate), which are unconditionally stable when applied to a differential equation on a fixed domain, do not preserve the same stability properties when written in ALE form.

On the contrary, our conclusion is that the accuracy of time discretisation schemes does not degrade when solving problems on moving domains in ALE form; we prove this theoretically for one scheme and numerically for others. In this regard, GCL seem not to play any relevant role in the accuracy of the numerical schemes.

Part of our work on the ALE formulation, notably the derivation of the conservative and non-conservative ALE formulation and their corresponding finite element approximation, and the stability result for the Implicit Euler scheme, has already been published in a work coauthored with L. Formaggia, entitled *A stability analysis for the Arbitrary Lagrangian Eulerian formulation with finite elements* [30].

In Chapter 3, much of the work done in Chapters 1 and 2 on a linear advection diffusion equation will be generalised to the incompressible Navier-Stokes equations. In particular, we will discuss the finite element approximation of the fluid equations in the ALE framework and

we will extend to this situation the unconditional stability result obtained for the Implicit Euler scheme, satisfying the GCL, that was introduced in Chapter 1. We are interested in solving the Navier-Stokes equations with inexact factorisation schemes, which allow us to decouple the computation of the pressure from that of the velocity field; in particular we focus on the *Yosida* projection scheme proposed in [77]. We will describe how these techniques can be extended to the ALE framework and we will show their effectiveness on a numerical test case.

This analysis represents a necessary step toward the approximation of the fluid-structure interaction problem that we propose to investigate.

The second part of this thesis is dedicated to the study of the fluid-structure interaction problem arising in hemodynamic applications.

Cardiovascular diseases are one of the leading causes of death in Western countries. They are closely related to altered flow conditions such as separation and flow reversal zones or low and oscillatory shear stress zones. A detailed understanding of the local hemodynamic environment can have useful clinical applications, mainly in predicting of the consequences of a surgical intervention.

In large arteries, the mechanical interaction between blood and the arterial wall plays an important role in the control of blood flow in the overall circulatory system. Indeed, during the first part of the cardiac beat (*systolic* phase), the wall deformation accumulates part of the mechanical energy as elastic energy which will afterwards be returned back to the fluid in the second part (*diastolic* phase). This mechanism allows the propagation toward the peripheral vessels of pressure waves coming from the heart and guarantees an almost uniform flow rate at capillary level. Hence, fluid/structure interaction phenomena must be appropriately accounted for in the modelling of blood flow. In particular, the deformation of the geometry should be properly described since, as we have already mentioned, the radius of an artery may vary up to 10% between diastole and systole.

The mathematical modelling of this problem is a hard task because of the complexity of blood and arterial tissues and the lack of "in-vivo" measurements. Blood is a complex suspension, in an aqueous polymer solution called *plasma*, of different particles: *red cells*, *white cells* and *platelets*. Yet, in large arteries, these particles have dimensions much smaller than the diameter of the vessel and blood can be considered a homogeneous and incompressible fluid. Furthermore, it can be assumed to behave as a Newtonian fluid. This assumption is no longer true in small vessels or capillaries.

The modelling of arterial wall is even more difficult. Indeed, arteries are formed by three layers: an *intima*, a *media* and an *adventitia*, each of them being constituted by different materials with different mechanical features such as collagen fibers, elastin, smooth muscle and water. For an overview on the mathematical modelling of blood flow we refer to [79]. In the present work we will consider a very simple model both for blood and artery: for blood dynamics we adopt Navier-Stokes equations for incompressible Newtonian fluids, while the arterial wall will be described as a thin membrane in cylindrical configuration. Moreover, we will account only for radial displacements.

Figure 1 shows an idealised configuration of a segment of an artery. The boundary Γ_l^w represents the deformable arterial wall while the two sections $\mathcal{S}_1$ and $\mathcal{S}_2$ are "artificial" boundaries introduced only to bound the computational domain. In the geometry depicted in figure 1

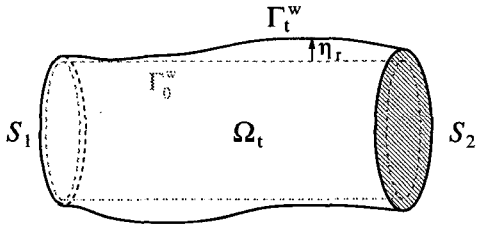

Figure 1: A sketch of a segment of an artery.

we will consider the coupled problem

$$\begin{cases} \rho\partial_t \mathbf{u} + \rho\mathbf{u}\cdot\boldsymbol{\nabla}\mathbf{u} - \operatorname{div}(2\mu\mathbf{D}(\mathbf{u}) - p\mathbf{I}) = 0 \\ \operatorname{div}\mathbf{u} = 0 \end{cases} \quad \text{in } \Omega_t, \tag{0.0.4}$$

$$\tilde{\rho}_w \frac{\partial^2\eta_r}{\partial t^2} - a\frac{\partial^2\eta_r}{\partial z^2} + b\eta_r - c\frac{\partial^3\eta_r}{\partial^2 z\partial t} = \Phi, \quad \text{on } \Gamma_0^w \tag{0.0.5}$$

$$\begin{cases} \mathbf{u} = \dot{\eta}\mathbf{e}_r \\ [(p - p_{ext})\mathbf{n} - 2\mu\mathbf{D}(\mathbf{u})\cdot\mathbf{n}]\cdot\mathbf{e}_r = \Phi \end{cases} \quad \text{on } \Gamma_t^w \tag{0.0.6}$$

where $\mathbf{u}$ is the fluid velocity, p the fluid pressure and η_r the wall displacement (in the radial direction) computed with respect to the reference cylindrical configuration Γ_0^w. We have denoted by $\mathbf{D}(\mathbf{u})$ the strain tensor $\mathbf{D}(\mathbf{u}) = (\boldsymbol{\nabla}\mathbf{u} + \boldsymbol{\nabla}^T\mathbf{u})/2$ and by $\mathbf{I}$ the identity tensor. The parameters appearing in (0.0.4) and (0.0.5) characterise the physical properties of blood and arterial tissue. Finally, equations (0.0.6) enforce the continuity of velocity and stresses at the fluid-structure interface and constitute the coupling conditions between fluid and structure equations. Here $\mathbf{n}$ is the normal outward unit vector to Γ_t^w and $\mathbf{e}_r$ the unit radial vector. This model will be addressed in Chapter 4. We will consider and analyse a global weak formulation for this coupled problem, which accounts at the same time for the fluid and the structure equations, and we will describe in detail a finite element approximation in the case of both a conforming and a non-conforming discretisation between fluid and structure.

About time discretisation, many strategies can be envisaged in order to effectively solve the coupled problem. See, for instance, [41] for an overview of possible coupling algorithms. The simplest strategies, known as *staggered* or *partitioned* procedures, are obtained by making the coupling explicit and allow to solve at each time step the fluid and the structure equations only once and independently. For instance, in our case, given an approximation η^n of the wall displacement at time t^n, we may solve the fluid equations with an imposed velocity, provided from the previous time step, at the fluid-structure interface (which means to use the first of the coupling conditions (0.0.6) as a Dirichlet boundary condition), thus obtaining a fluid velocity and pressure; then, we solve the structure equation with a forcing term Φ which depends on the newly computed values of $\mathbf{u}$ and p, and we obtain the wall displacement at the new time step t^{n+1}.

Unfortunately, we have experienced that staggered algorithms are unstable for the problem

at hand when the wall density is comparable with that of the fluid, which is indeed the case when the parameters of the model are chosen within a physiological range.

For this reason, in this work we will consider only implicit coupled algorithms. In particular, we will propose three algorithms; the first two use an implicit structure solver and will be proven to be unconditionally stable. The third one employs an explicit structure discretisation. We will obtain, in this case, a conditional stability result with a stability constant governed only by the structure discretisation (in other words, the proposed coupled algorithm does not engender a further condition on the time step).

The use of implicit coupled algorithms makes simulations much more costly. Indeed, at each time step we are faced with a non-linear system to solve. The strategy adopted in the present work to compute the solution of such a non-linear system consists of simply sub-iterating between fluid and structure until the coupling conditions (0.0.6) are satisfied within a fixed tolerance.

We will also present many numerical results on a simplified 2D geometry. In particular, we will simulate the propagation of a pressure pulse, imposed at the inflow section, inside the vessel. This simulation would represent the propagation, in a segment of straight artery, of a pressure wave coming from the heart and traveling towards the peripheral vessels.

Indeed, as already anticipated previously, a peculiar feature of this fluid-structure interaction problem is the appearance of traveling pressure waves along the vessel. Even if the flow is governed by parabolic equations such as the incompressible Navier-Stokes, the behaviour of the coupled fluid-structure system is in many respects more akin to that of a hyperbolic problem. As a consequence, an additional complexity arises in the treatment of the "inflow" and "outflow" boundaries (section $\mathcal{S}_1$ and $\mathcal{S}_2$, respectively), where one would like to have a correct representation of the traveling waves, without spurious reflections. In the case of compressible flows and more general hyperbolic equations, the problem of devising absorbing boundary conditions has been widely studied, see for instance [22, 35, 36]. However, in our case, where the propagation phenomena are due to the fluid-structure interaction and not to the fluid compressibility, little may be found in the literature.

In the present work, this issue is tackled by coupling the 3D fluid-structure problem with a reduced one-dimensional model, which acts as an "absorbing" device for the waves exiting the computational domain. This reduced model is obtained by integrating the fluid equations over each section normal to the axis of the vessel and describes the coupled system in terms of *transversally averaged* flow rate and pressure. Figure 2 illustrates this idea.

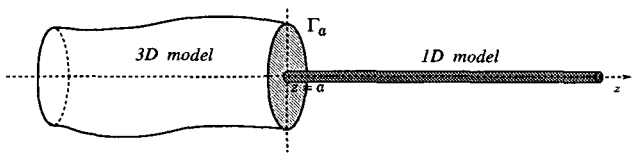

Figure 2: Coupling a 3D model with a 1D model

In Chapter 5 we will first present and analyse the 1D model. We will show that it is a hyperbolic system of equations with source term, hence well suited to describe propagative phenomena and we will derive an a priori energy inequality for the sub-critical case, which is the most relevant for our target application. The 1D model will be discretised with a finite

element Lax-Wendroff scheme.

We will next consider the coupling between the 3D fluid-structure model and the 1D reduced one. Referring to figure 2, suitable coupling conditions must be devised, at the interface Γ_a, in order to make the two models interact with one another. We will propose several Interaction Models and we will present numerical results for a few of them. The 1D model provides only averaged quantities at Γ_a, such as the averaged pressure or the mass flux. We are then faced with the problem of imposing averaged quantities as boundary conditions (called *defective*) to the fluid equations. This aspect is the subject of a paper coauthored with L. Formaggia, J.F. Gerbeau and A. Quarteroni, entitled *Numerical treatment of defective boundary conditions for the Navier-Stokes equations* [28]; the results obtained therein will be summarised in Section 5.2.2. Finally, numerical results are provided for a 2D/1D models coupling, showing the effectiveness of this technique in dramatically reducing spurious numerical reflections.

To our knowledge, this approach is completely new. It is the subject of two papers *On the Coupling of 3D and 1D Navier-Stokes equations for Flow Problems in Compliant Vessels* by L. Formaggia, J-F. Gerbeau, F. Nobile and A. Quarteroni [29] and *Multiscale Modelling of the Circulatory System: a Preliminary Analysis* by L. Formaggia, F. Nobile, A. Quarteroni and A. Veneziani [32].

Even though we are constantly inspired by the application to blood flow in arteries, many of the considerations in Chapters 4 and 5 can be applied to other situations as well; notably, whenever an incompressible fluid flows in a compliant vessel. An example is provided by the study of vibrations or water hammer effects in pipe network flows. This class of problems has been extensively investigated, see for instance the review article [90]. The methodology proposed in this work may be of interest in those situations as well. For this reason we have tried to give a presentation of the subject a little more general than the specific hemodynamic application.

This thesis is the synthesis of a three year work that has been partially carried out in collaboration with other people, as attested to by the coauthored papers cited in this Introduction. Yet, a considerable part of the present work, notably the results presented in Chapters 2, 3, 4 and some considerations on the equivalence between conservative and non-conservative ALE formulation presented in Chapter 1, are the fruit of an individual research and have not yet been published.

Part I

ALE approximation of differential problems in moving domains

Chapter 1

Parabolic equations in moving domains

Introduction

In this chapter we will describe in a rather abstract form the ALE approach for a generic conservation law of the following type

$$\frac{\partial U}{\partial t} + \nabla_{\mathbf{x}} \cdot \mathbf{F}(U) = f, \tag{1.0.1}$$

defined on a moving domain. We will derive the conservative and non-conservative formulations already presented in (0.0.2) and (0.0.3) and we will introduce their corresponding weak formulations. Moreover, we will investigate the smoothness condition that the ALE mapping should satisfy if we wish to maintain a H^1 spatial regularity which is the one enjoyed by piecewise continuous finite element spaces. The aim is to find a condition compatible with an approximation of the ALE mapping by means of finite elements base functions, which will be indeed addressed later on in the chapter.

In a second part of the chapter, we will consider a linear transport-diffusion model problem. Some considerations on the existence of weak solutions and the equivalence between the different formulations are made in section 1.6.2. Sections 1.7, 1.8 and 1.9 deal with the finite element space discretisation of the model problem and the Implicit Euler time discretisation both for the conservative and the non-conservative formulation; a stability analysis is carried out in the two cases. In this framework, we will introduce the Geometric Conservation Laws (GCL) which have been originally designed for finite-volume schemes as a sort of "patch test" to which the discrete scheme should obey. We will recognize their formulations in a finite element scheme and we will assess their relevance for obtaining a stability result independent of the domain movement law for the Implicit Euler discretisation of the conservative weak-ALE formulation.

The contents of this chapter, with the exception of subsection 1.6.2, have been already published in the paper by L. Formaggia and F. Nobile *A stability analysis for the Arbitrary Lagrangian Eulerian formulation with finite elements* [30].

1.1 The Arbitrary Lagrangian Eulerian (ALE) formulation

The Arbitrary Lagrangian Eulerian frame of reference, that we adopt when the computational domain changes, may be defined in a way similar to the Lagrangian frame that is widely used in continuum mechanics. Let $\mathcal{A}_t$ be a family of mappings, which at each $t \in (t_0, T)$ associate a point $\mathbf{Y}$ of a *reference configuration* Ω_0 (the domain configuration at time $t = t_0$) to a point $\mathbf{x}$ on the current domain configuration Ω_t :

$$\mathcal{A}_t : \Omega_0 \subset \mathbb{R}^d \to \Omega_t \subset \mathbb{R}^d, \qquad \mathbf{x}(\mathbf{Y}, t) = \mathcal{A}_t(\mathbf{Y}).$$

We assume $\mathcal{A}_t$ to be an homeomorphism, that is $\mathcal{A}_t \in C^0(\overline{\Omega_0})$ is invertible with continuous inverse $\mathcal{A}_t^{-1} \in C^0(\overline{\Omega_t})$. Furthermore, we assume that the application

$$t \to \mathbf{x}(\mathbf{Y}, t), \quad \mathbf{Y} \in \Omega_0$$

is differentiable almost everywhere in $[t_0, T]$. In the following, we will denote by I the interval $[t_0, T]$.
We name $\mathbf{Y} \in \Omega_0$ the *ALE coordinate* while $\mathbf{x} = \mathbf{x}(\mathbf{Y}, t)$ will be indicated as the spatial (or Eulerian) coordinate.
In the following we will often have the necessity of switching between the different frame of reference. For the sake of notation, we will use the shorthand notation $\Omega_t \times I$ to indicate the set

$$\{(\mathbf{x}, t) | \quad \mathbf{x} \in \Omega_t, t \in I\}.$$

Let $f : \Omega_t \times I \to \mathbb{R}$ be a function defined on the Eulerian frame and $\hat{f} := f \circ \mathcal{A}_t$ the corresponding function on the ALE frame, defined as

$$\hat{f} : \Omega_0 \times I \to \mathbb{R}, \quad \hat{f}(\mathbf{Y}, t) = f(\mathcal{A}_t(\mathbf{Y}), t).$$

The symbol $\left.\frac{\partial f}{\partial t}\right|_{\mathbf{Y}}$ will indicate the time derivative on the ALE frame, written in the spatial coordinate. It is defined as

$$\left.\frac{\partial f}{\partial t}\right|_{\mathbf{Y}} : \Omega_t \times I \to \mathbb{R}, \qquad \left.\frac{\partial f}{\partial t}\right|_{\mathbf{Y}} (\mathbf{x}, t) = \frac{\partial \hat{f}}{\partial t}(\mathbf{Y}, t), \quad \mathbf{Y} = \mathcal{A}_t^{-1}(\mathbf{x}) \tag{1.1.1}$$

For analogy, we will indicate by $\left.\frac{\partial f}{\partial t}\right|_{\mathbf{x}}$ the partial time derivative in the spatial frame.
We then define the *domain velocity* $\mathbf{w}$ as

$$\mathbf{w}(\mathbf{x}, t) = \left.\frac{\partial \mathbf{x}}{\partial t}\right|_{\mathbf{Y}} \tag{1.1.2}$$

1.1.1 Derivation of ALE formulation for first order time dependent problems in conservative form

Let us consider the time dependent problem

$$\text{find} \quad u : \Omega_t \times I \to \mathbb{R}, \qquad \text{such that} \quad \left.\frac{\partial u}{\partial t}\right|_{\mathbf{x}} + \mathcal{L}(u) = 0, \tag{1.1.3}$$

with appropriate initial and boundary conditions.
Here, $\mathcal{L}$ indicates a differential operator (linear or non linear) in the space variable $\mathbf{x}$. In order to find the equivalent equation for $u \circ \mathcal{A}_t$, a standard application of the chain rule to the time derivative gives

$$\left.\frac{\partial u}{\partial t}\right|_{\mathbf{Y}} = \left.\frac{\partial u}{\partial t}\right|_{\mathbf{x}} + \left.\frac{\partial \mathbf{x}}{\partial t}\right|_{\mathbf{Y}} \cdot \nabla_{\mathbf{x}} u = \left.\frac{\partial u}{\partial t}\right|_{\mathbf{x}} + \mathbf{w} \cdot \nabla_{\mathbf{x}} u. \tag{1.1.4}$$

The symbol $\nabla_{\mathbf{x}}$ is here used to indicate the gradient with respect to the $\mathbf{x}$ variable, while $\nabla_{\mathbf{Y}}$ will be used when the gradient is taken with respect to the reference domain. Thus

$$\left.\frac{\partial u}{\partial t}\right|_{\mathbf{Y}} + \mathcal{L}(u) - \mathbf{w} \cdot \nabla_{\mathbf{x}} u = 0 \tag{1.1.5}$$

is the ALE counterpart of (1.1.3). The main difference with the original formulation is the appearance of a convective-type term due to the domain movement.
Often, PDE's governing continuum mechanics problems are written in conservative form, which reflects the fact that they express indeed conservation properties. Since the context in which the ALE technique is used is normally that of conservation laws, in the following we will always refer to equation written in conservative form. Nevertheless, large part of the results illustrated in this work may be readily extended to the more general case. The conservation equation for a quantity u is written as

$$\left.\frac{\partial u}{\partial t}\right|_{\mathbf{x}} + \nabla_{\mathbf{x}} \cdot \mathbf{F} = f \tag{1.1.6}$$

where $\mathbf{F}$ indicates the flux vector which is generally a function of u and of its first and second space derivatives, while f is a possible *source term*. The application of relation (1.1.4) gives

$$\left.\frac{\partial u}{\partial t}\right|_{\mathbf{Y}} + \nabla_{\mathbf{x}} \cdot (\mathbf{F}) - \mathbf{w} \cdot \nabla_{\mathbf{x}} u = f. \tag{1.1.7}$$

Expression (1.1.7) represents one of the possible forms in which a conservation law may be cast in the ALE frame. Another possible ALE formulation may be directly derived from the integral formulation of the conservation equation. We indicate the Jacobian matrix of the ALE mapping as

$$\mathbf{J}_{\mathcal{A}_t} = \frac{\partial \mathbf{x}}{\partial \mathbf{Y}},$$

and its determinant,

$$J_{\mathcal{A}_t} = \det(\mathbf{J}_{\mathcal{A}_t}).$$

We now make use in the following derivation of the *Euler expansion formula*[2], which relates the time evolution of $J_{\mathcal{A}_t}$ to the divergence of the domain velocity field, according to the following differential equation

$$\left.\frac{\partial J_{\mathcal{A}_t}}{\partial t}\right|_{\mathbf{Y}} = J_{\mathcal{A}_t} \nabla_{\mathbf{x}} \cdot \mathbf{w}, \tag{1.1.8}$$

which is valid for $\mathbf{Y} \in \Omega_0$, $\mathbf{x} = \mathcal{A}_t(\mathbf{Y})$ and $t \in I$. Supplemented by the initial condition $J_{\mathcal{A}_t} = 1$ for $t = t_0$, expression (1.1.8) may be also interpreted as an evolution law for the Jacobian determinant, once the domain velocity field is known. This interpretation is not the usual one, since expression (1.1.8) is normally regarded as an identity satisfied at each time during the domain evolution process. Yet, considering (1.1.8) as an evolution law may shed some light on a possible interpretation of the Geometric Conservation Laws, as it will be discussed later on. The derivation of expression (1.1.8), yet relative to a full Lagrangian frame, may be found in[2]. It may be readily extended to the ALE frame.
We wish now to find an expression for a term in the form

$$\frac{d}{dt}\int_{V_t} u d\Omega, \tag{1.1.9}$$

where V_t is an arbitrary sub-domain $V_t \subset \Omega_t$. We will indicate with V_0 the subset of Ω_0 such that $V_t = \mathcal{A}_t(V_0)$. We have

$$\frac{d}{dt}\int_{V_t} u d\Omega = \frac{d}{dt}\int_{V_0} u J_{\mathcal{A}_t}\, d\Omega = \int_{V_0} \left.\frac{\partial (u J_{\mathcal{A}_t})}{\partial t}\right|_{\mathbf{Y}} d\Omega, \tag{1.1.10}$$

then, using expression (1.1.8), we finally obtain that

$$\frac{d}{dt}\int_{V_t} u d\Omega = \int_{V_t} \left[\left.\frac{\partial u}{\partial t}\right|_{\mathbf{Y}} + u \nabla_{\mathbf{x}} \cdot \mathbf{w}\right] d\Omega, \tag{1.1.11}$$

which is a generalisation of the well known *Reynolds transport formula*[2].
Consequently, the conservation equation (1.1.6) in integral form and ALE frame is

$$\frac{d}{dt}\int_{V_t} u d\Omega + \int_{V_t} \nabla_{\mathbf{x}} \cdot (\mathbf{F} - \mathbf{w}u)\, d\Omega = \int_{V_t} f\, d\Omega. \tag{1.1.12}$$

In the previous relation all integrals have been expressed in the current frame of reference. However, one may choose to write the equation with respect to the reference domain. This would lead to the following expression

$$\int_{V_0} \left\{ \left.\frac{\partial (J_{\mathcal{A}_t} u)}{\partial t}\right|_{\mathbf{Y}} + J_{\mathcal{A}_t} \left[\nabla_{\mathbf{x}} \cdot (\mathbf{F} - \mathbf{w}u) - f\right] \right\} d\Omega = 0, \tag{1.1.13}$$

and, due to the arbitrariness of V_0, we may write the following differential equation,

$$\left.\frac{\partial (J_{\mathcal{A}_t} u)}{\partial t}\right|_{\mathbf{Y}} + J_{\mathcal{A}_t} \nabla_{\mathbf{x}} \cdot (\mathbf{F} - \mathbf{w}u) = J_{\mathcal{A}_t} f, \tag{1.1.14}$$

which is another admissible form of the ALE equations (see, for instance,[54]).[1]. Relation (1.1.14) could have been derived directly from (1.1.7) by employing the Euler expansion formula (1.1.8).
The previous presentation had the objective of deriving some common forms in which the ALE equations are presented in the literature. Another approach may be followed by using a variational formulation as a starting point, which is the basis for the derivation of ALE finite elements.

[1]Relation (1.1.14) may be written completely on the reference domain by transforming the divergence term by exploiting the Piola-Kirchoff theorem[14]. We omit the derivation here; it may be found in [54].

1.2 Weak formulation in the ALE frame

The flux $\mathbf{F} = \mathbf{F}(u)$ in (1.1.6) may be often decomposed into two parts

$$\mathbf{F}(u) = \mathbf{F}_e(u) + \mathbf{F}_v(u) \tag{1.2.1}$$

where $\mathbf{F}_e$ does not contain any derivative of u, while $\mathbf{F}_v(u)$ contains first order spatial derivatives of the unknown. A typical case is the Navier-Stokes equations which govern fluid dynamics, where $\mathbf{F}_e$ contains the convective terms, while $\mathbf{F}_v$ represents the viscous fluxes.
A weak formulation of (1.1.6) may be formally obtained as

$$\int_{\Omega_t} \psi \left(\left.\frac{\partial u}{\partial t}\right|_{\mathbf{x}} + \nabla_{\mathbf{x}} \cdot \mathbf{F}_e(u) \right) d\Omega - \int_{\Omega_t} \mathbf{F}_v(u) \cdot \nabla_{\mathbf{x}} \psi \, d\Omega = \int_{\Omega_t} \psi f d\Omega, \quad \forall \psi \in \mathcal{W}(\Omega_t). \tag{1.2.2}$$

where $\mathcal{W}(\Omega_t)$ is the space of test functions defined in Ω_t, with the required regularity at each time t. For all t, u is sought in a suitable functional space, which essentially coincides with $\mathcal{W}(\Omega_t)$ up to the boundary behaviour. Relation (1.2.2) is formally the weak formulation of (1.1.5). Yet, in that form is impractical, since it contains a time derivative in the Eulerian frame, while it will be natural to work with variables that follow the domain evolution. Moreover, the test functions cannot be taken constant with time since they should vanish on the part of the moving boundary where essential boundary conditions are applied. It is then natural to recast them in the moving frame of reference as well.
To that purpose, we consider a space of admissible test functions $\mathcal{Y}(\Omega_0)$, defined on the *reference* domain, and made of functions $\hat{\psi} : \Omega_0 \to \mathbb{R}$ that are smooth enough. The ALE mapping then identifies a corresponding set $\mathcal{X}(\Omega_t)$ of weighting functions on the "current configuration", defined as follows,

$$\mathcal{X}(\Omega_t) = \{\psi : \Omega_t \times I \to \mathbb{R}, \quad \psi = \hat{\psi} \circ \mathcal{A}_t^{-1}, \ \hat{\psi} \in \mathcal{Y}(\Omega_0)\}. \tag{1.2.3}$$

At each time t, we must have $\mathcal{X}(\Omega_t) \subset \mathcal{W}(\Omega_t)$ in order for the function space to be admissible. This condition will impose constraints on the regularity of the mapping, as it will be analysed in a later section for the particular case in which $\mathcal{W}(\Omega_t) \equiv H^1(\Omega_t)$.

In the following of this section we will illustrate two possible ways of building a weak formulation in the ALE frame.

1.2.1 A non-conservative formulation

If we transform the Eulerian time derivative of relation (1.2.2) into its ALE counterpart the following weak formulation may be written

$$\int_{\Omega_t} \psi \left.\frac{\partial u}{\partial t}\right|_{\mathbf{Y}} d\Omega + \int_{\Omega_t} \psi \left(\nabla_{\mathbf{x}} \cdot \mathbf{F}_e(u) - \mathbf{w} \nabla_{\mathbf{x}} u\right) d\Omega - \int_{\Omega_t} \mathbf{F}_v(u) \cdot \nabla_{\mathbf{x}} \psi \, d\Omega = \int_{\Omega_t} \psi f d\Omega$$
$$\forall \psi \in \mathcal{X}(\Omega_t), \tag{1.2.4}$$

1.2.2 A conservative ALE formulation.

Another ALE variational formulation may be obtained bearing in mind that functions in $\mathcal{Y}(\Omega_0)$ do not depend on time. An immediate consequence is that:

$$0 = \left.\frac{\partial \psi}{\partial t}\right|_{\mathbf{Y}} = \left.\frac{\partial \psi}{\partial t}\right|_{\mathbf{x}} + \mathbf{w} \cdot \nabla_{\mathbf{x}} \psi, \qquad \forall \psi \in \mathcal{X}(\Omega_t), \tag{1.2.5}$$

and then, for any time-differentiable function $g = g(\mathbf{x}, t)$, we have that

$$\left.\frac{\partial(\psi g)}{\partial t}\right|_{\mathbf{Y}} = \psi \left.\frac{\partial g}{\partial t}\right|_{\mathbf{Y}}, \qquad \forall \psi \in \mathcal{X}(\Omega_t). \tag{1.2.6}$$

By recalling expression (1.1.11), one may then write the following useful formulae, valid for any $\psi, \chi \in \mathcal{X}(\Omega_t)$.

$$\frac{d}{dt}\int_{\Omega_t} \psi d\Omega = \int_{\Omega_t} \psi \nabla_{\mathbf{x}} \cdot \mathbf{w} d\Omega, \tag{1.2.7}$$

$$\frac{d}{dt}\int_{\Omega_t} \psi u d\Omega = \int_{\Omega_t} \psi \left(\left.\frac{\partial u}{\partial t}\right|_{\mathbf{Y}} + u \nabla_{\mathbf{x}} \cdot \mathbf{w}\right) d\Omega \tag{1.2.8}$$

$$\frac{d}{dt}\int_{\Omega_t} \psi \chi d\Omega = \int_{\Omega_t} \psi \chi \nabla_{\mathbf{x}} \cdot \mathbf{w} d\Omega. \tag{1.2.9}$$

The alternative ALE weak formulation may then be obtained following two routes. The first moves from (1.2.2), taking $\psi \in \mathcal{X}(\Omega_t)$, expanding the time derivative using (1.1.4) and finally exploiting relation (1.2.8). The result is the following expression

$$\frac{d}{dt}\int_{\Omega_t} \psi u \, d\Omega + \int_{\Omega_t} \psi(\nabla_{\mathbf{x}} \cdot (\mathbf{F}_e(u) - \mathbf{w}u)) \, d\Omega - \int_{\Omega_t} \mathbf{F}_v(u) \cdot \nabla_{\mathbf{x}} \psi \, d\Omega = \int_{\Omega_t} \psi f d\Omega, \qquad \forall \psi \in \mathcal{X}(\Omega_t). \tag{1.2.10}$$

The second formulation is obtained from the differential expression (1.1.14) which in weak form reads

$$\int_{\Omega_0} \hat{\psi} \left(\left.\frac{\partial(J_{\mathcal{A}_t} u)}{\partial t}\right|_{\mathbf{Y}} \right) d\Omega + \int_{\Omega_0} \hat{\psi} J_{\mathcal{A}_t} (\nabla_{\mathbf{x}} \cdot (\mathbf{F}_e(u) - \mathbf{w}u)) \, d\Omega - \int_{\Omega_0} J_{\mathcal{A}_t} \mathbf{F}_v(u) \cdot \nabla_{\mathbf{x}} \hat{\psi} \, d\Omega = \int_{\Omega_0} J_{\mathcal{A}_t} \hat{\psi} f d\Omega \qquad \forall \hat{\psi} \in \mathcal{Y}(\Omega_0). \tag{1.2.11}$$

By exploiting the fact that $\left.\frac{\partial \psi}{\partial t}\right|_{\mathbf{Y}} = 0$ (see (1.2.5)) the time derivative may be moved out of the integral sign and the integrals may be transformed on the current domain configuration, leading again to (1.2.10). In this formulation the transient term is expressed as a total time derivative while the ALE convection term appears in the form of the divergence of the product of the domain velocity field $\mathbf{w}$ and the solution u. The time derivative term accounts for both effects due to the variation of the solution u and the domain movement. For conservation equations, it has the advantage that the ALE term is itself in "conservation form", therefore the modification of an existing "fixed-grid" code is (at least apparently) straightforward, as it is just required to change the definition of the fluxes. In addition, the formulation is "conservative", in the sense that, taking any $V \subset \Omega_t$ with Lipschitz continuous boundary, should $\psi|_V = const$ be an admissible test function[2], we derive from (1.2.10), taking $f = 0$, that

$$\frac{d}{dt}\int_V u \, d\Omega + \int_{\partial V} \mathbf{F} \cdot \mathbf{n} d\Gamma - \int_{\partial V} u\mathbf{w} \cdot \mathbf{n} d\Gamma = 0, \tag{1.2.12}$$

[2]This is always the case if $\overline{V} \subset \Omega_t$

i.e. in absence of source terms, the variation of u over V is due only to boundary terms. It can be noted that also the contribution of the ALE term to the conservation reduces to a boundary term, which is indeed related to the additional "flux" of u through the boundary as a consequence of its movement[3].
Formulations (1.2.4) and (1.2.10) are equivalent at the continuous level, however they lead to different discrete problems. In particular, the conservation property just mentioned, may not be satisfied by the finite dimensional problem associated to (1.2.4).

1.3 On the regularity of the ALE mapping

We may note that the fulfillment of the appropriate regularity condition for the functions in $\mathcal{X}(\Omega_t)$ may impose a certain level of regularity to the ALE mapping. Since we are mainly interested in fluid flow and elastic structures, we would like to deal with functions $u(\mathbf{x}, t)$ that satisfy

$$u(\cdot, t) : I \to V(\Omega_t) \subset H^1(\Omega_t).$$

Therefore, we will investigate the regularity required on the mapping in order that if $\mathcal{Y}(\Omega_0) \subset H^1(\Omega_0)$ then, at each time t during the domain motion the 'transformed function space' $\mathcal{X}(\Omega_t)$ remains a subspace of $H^1(\Omega_t)$.

1.3.1 Some additional notation

In the following we will make use of standard function spaces. We will indicate by $L^p(\Omega)$, with $1 \leq p \leq \infty$, the set of measurable functions v defined on $\Omega \subset \mathbb{R}^d$ and such that

$$\int_\Omega |v(\mathbf{x})|^p d\Omega < \infty, \qquad 1 \leq p < \infty \tag{1.3.1}$$

or, when $p = \infty$

$$\exists C \text{ s.t. } |v(\mathbf{x})| \leq C \quad \text{a.e. in } \Omega \tag{1.3.2}$$

The set $L^p(\Omega)$ forms a Banach space when equipped with the norm

$$\|v\|_{L^p(\Omega)} = \left(\int_\Omega |v(\mathbf{x})|^p d\Omega \right)^{\frac{1}{p}}, \qquad 1 \leq p < \infty \tag{1.3.3}$$

$$\|v\|_{L^\infty(\Omega)} = \inf\{M | \quad |v(\mathbf{x})| < M \quad \text{a.e. in } \Omega\}, \qquad p = \infty \tag{1.3.4}$$

With the Sobolev space $W^{k,p}(\Omega)$, with $k > 0$ integer and $1 \leq p \leq \infty$, we indicate the class of functions

$$W^{k,p}(\Omega) = \{v \in L^p(\Omega) | \quad D^\alpha v \in L^p(\Omega), \quad |\alpha| \leq k\}, \tag{1.3.5}$$

[3] We may anticipate that for the Navier-Stokes equation the "ALE" fluxes will exactly balance the convective fluxes on the part of the boundary which moves at the same velocity as the fluid, reflecting the fact that there is no mass exchange through that portion of boundary.

being $\alpha = (\alpha_1, \cdots, \alpha_d)$, with $\alpha_i > 0$ integer, and $|\alpha| = \alpha_1 + \cdots + \alpha_d$. D^α indicates the distributional partial derivative

$$D^{\boldsymbol{\alpha}} v = \frac{\partial^{|\boldsymbol{\alpha}|} v}{\partial^{\alpha_1} x_1 \cdots \partial^{\alpha_d} x_d}. \tag{1.3.6}$$

With $H^p(\Omega)$ it is indicated the Hilbert space $W^{p,2}(\Omega)$. Finally, $H_0^1(\Omega)$ indicates the subspace of $H^1(\Omega)$ of functions with zero trace on $\partial\Omega$. We remind the Poincaré inequality

$$\int_\Omega v^2 \, d\Omega \leq C_\Omega \int_\Omega |\nabla v|^2 \, d\Omega, \qquad \forall v \in H_0^1(\Omega). \tag{1.3.7}$$

For vector functions, we will use the bold symbols. Hence $\mathbf{L}^p(\Omega)$ indicates the space of vector functions $\mathbf{v}$ such that each component v_i satisfies $v_i \in L^p(\Omega)$ (similar notations for $\mathbf{H}^k(\Omega)$). The associated norm is then defined by

$$\|\mathbf{v}\|^2_{\mathbf{L}^p(\Omega)} = \sum \|v_i\|^2_{L^p(\Omega)}. \tag{1.3.8}$$

When dealing with space-time functions

$$v(t, \mathbf{x}), \quad \text{with} \quad (t, \mathbf{x}) \in I \times \Omega,$$

we will make use of the spaces

$$L^2(I; H^p(\Omega)) = \{v : I \to H^p(\Omega) | \quad v \, measurable, \int_I \|v(t)\|^2_{H^p(\Omega)} dt < \infty\}, \tag{1.3.9}$$

equipped with the norm

$$\|v\|_{L^2(I;H^p(\Omega))} = \left(\int_I \|v(t)\|^2_{H^p(\Omega)} dt \right)^{\frac{1}{2}} \tag{1.3.10}$$

and

$$H^1(I; H^p(\Omega)) = \left\{ v \in L^2(I; H^p(\Omega)) | \quad \frac{\partial v}{\partial t} \in L^2(I; H^p(\Omega)) \right\}. \tag{1.3.11}$$

The dual space $H^{-1}(\Omega)$ of $H_0^1(\Omega)$, is formed by all continuous linear operators on functions belonging to $H_0^1(\Omega)$. We will indicate the duality paring between $H^{-1}(\Omega)$ and $H_0^1(\Omega)$ by

$$< f, v >, \qquad f \in H^{-1}(\Omega), \quad v \in H_0^1(\Omega). \tag{1.3.12}$$

The space $H^{-1}(\Omega)$ is equipped with the norm

$$\|f\|_{H^{-1}(\Omega)} = \sup_{\substack{v \in H_0^1(\Omega) \\ \|v\|_{H^1(\Omega)} \neq 0}} \frac{< f, v >}{\|v\|_{H^1(\Omega)}} \tag{1.3.13}$$

In the presence of a moving domain Ω_t, we extend the definition (1.3.9) as follows:

$$L^2(I; H^p(\Omega_t)) = \{v : \Omega_t \times I \to \mathbb{R}| \quad \int_I \|v(t)\|^2_{H^p(\Omega_t)} dt < \infty\},$$

equipped with the norm as in (1.3.10). Finally, we indicate with $L^2(I; H_0^1(\Omega_t))$ the closure of $\mathcal{D}(\Omega_t \times I)$ with respect to the norm $\| \cdot \|_{L^2(I;H^1(\Omega_t))}$, $\mathcal{D}(\Omega_t \times I)$ being the space of infinitely differentiable functions whose support is a compact subset of $\Omega_t \times I$.

1.3.2 Mapping regularity condition

The following problem will be addressed

Problem 1.3.1 *Find sufficient conditions for the ALE mapping $\mathcal{A}_t$ so that if $\hat{v} \in H^1(\Omega_0)$ then $v = \hat{v} \circ \mathcal{A}_t^{-1} \in H^1(\Omega_t)$, and vice-versa.*

Classical results [7] indicate that a sufficient condition is that $\mathcal{A}_t$ be a C^1-diffeomorphism, which implies that $\forall t \in I$

$$\mathcal{A}_t \in \mathbf{C}^1(\overline{\Omega_0}) \qquad \mathcal{A}_t^{-1} \in \mathbf{C}^1(\overline{\Omega_t}), \tag{1.3.14}$$

and, moreover,

$$\mathbf{J}_{\mathcal{A}_t} \in \mathbf{L}^\infty(\Omega_0) \qquad \mathbf{J}_{\mathcal{A}_t^{-1}} \in \mathbf{L}^\infty(\Omega_t). \tag{1.3.15}$$

Unfortunately, this requirement is too restrictive for our purposes. In fact, we would like to express the ALE mapping by means of finite element shape functions, which are required to be in $H^1(\Omega)$, but not necessarily in $C^1(\overline{\Omega})$. The reason is that in practical applications, we will reconstruct the ALE mapping from the boundary movement and, as we shall see later on, we will use for this purpose a finite element space discretisation. We need therefore to relax the above requirements. This is possible by imposing some mild constraints on Ω_t.
We can then state the following

Proposition 1.3.1 *Let Ω_0 be a bounded domain with Lipschitz continuous boundary and let $\mathcal{A}_t$ be invertible in $\overline{\Omega_0}$ and satisfy the following conditions: for each $t \in I$*

- *$\Omega_t = \mathcal{A}_t(\Omega_0)$ is bounded and $\partial\Omega_t$ is Lipschitz continuous*[4],
-

$$\mathcal{A}_t \in \mathbf{W}^{1,\infty}(\Omega_0), \qquad \mathcal{A}_t^{-1} \in \mathbf{W}^{1,\infty}(\Omega_t). \tag{1.3.16}$$

Then, $v \in H^1(\Omega_t)$ if and only if $\hat{v} = v \circ \mathcal{A}_t \in H^1(\Omega_0)$. Moreover, $\|v\|_{H^1(\Omega_t)}$ is equivalent to $\|\hat{v}\|_{H^1(\Omega_0)}$, $\forall v \in H^1(\Omega_0)$.

Proof. Under the assumption (1.3.16), Sobolev embedding theorem assures that

$$\mathcal{A}_t \in \mathbf{C}^0(\overline{\Omega_0}), \qquad \mathcal{A}_t^{-1} \in \mathbf{C}^0(\overline{\Omega_t}) \tag{1.3.17}$$

and, as consequence of the hypotheses, the Jacobian

$$\mathbf{J}_{\mathcal{A}_t} : \Omega_0 \to \mathbb{R}^{d\times d},$$

and

$$\mathbf{J}_{\mathcal{A}_t^{-1}} : \Omega_t \to \mathbb{R}^{d\times d}$$

belong to $\mathbf{L}^\infty(\Omega_0)$ and $\mathbf{L}^\infty(\Omega_t)$, respectively, and their determinants, $J_{\mathcal{A}_t}$ and $J_{\mathcal{A}_t^{-1}}$, being made of products of L^∞ functions defined on a bounded domain, are themselves in $L^\infty(\Omega_0)$ and $L^\infty(\Omega_t)$, respectively. Moreover, we have

$$\|\mathbf{J}_{\mathcal{A}_t} \circ \mathcal{A}_t^{-1}\|_{\mathbf{L}^\infty(\Omega_t)} = \|\mathbf{J}_{\mathcal{A}_t}\|_{\mathbf{L}^\infty(\Omega_0)}, \tag{1.3.18}$$

[4] if $\mathcal{A}_t$ were a C^1-diffeomorphism this requirement would be automatically satisfied, see, for example, [14]

$$\|\mathbf{J}_{\mathcal{A}_t^{-1}} \circ \mathcal{A}_t\|_{\mathbf{L}^\infty(\Omega_0)} = \|\mathbf{J}_{\mathcal{A}_t^{-1}}\|_{\mathbf{L}^\infty(\Omega_t)}. \tag{1.3.19}$$

Finally, because of the invertibility of $\mathcal{A}_t$, there is no loss of generality in assuming that there are two positive constants c_1, c_2 such that

$$J_{\mathcal{A}_t}(\mathbf{Y}) \geq c_1 \qquad \forall \mathbf{Y} \in \Omega_0, \forall t \in I,$$

and

$$J_{\mathcal{A}_t^{-1}}(\mathbf{x}) \geq c_2 \qquad \forall \mathbf{x} \in \Omega_t, \forall t \in I.$$

We then have

$$\|\hat{v}\|^2_{L_2(\Omega_0)} = \int_{\Omega_0} \hat{v}^2 d\Omega = \int_{\Omega_t} J_{\mathcal{A}_t^{-1}} v^2 d\Omega \leq \|J_{\mathcal{A}_t^{-1}}\|_{L_\infty(\Omega_t)} \|v\|^2_{L_2(\Omega_t)}, \tag{1.3.20}$$

$$\|v\|^2_{L_2(\Omega_t)} = \int_{\Omega_t} v^2 d\Omega = \int_{\Omega_0} J_{\mathcal{A}_t} \hat{v}^2 d\Omega \leq \|J_{\mathcal{A}_t}\|_{L_\infty(\Omega_0)} \|\hat{v}\|^2_{L_2(\Omega_0)}. \tag{1.3.21}$$

In addition,

$$|\hat{v}|^2_{H^1(\Omega_0)} = \int_{\Omega_0} \sum_{k=1}^d \left(\frac{\partial \hat{v}}{\partial Y_k}\right)^2 d\Omega = \int_{\Omega_t} J_{\mathcal{A}_t^{-1}} \sum_{k=1}^d \left(\sum_{j=1}^d \frac{\partial v}{\partial x_j}\frac{\partial x_j}{\partial Y_k}\right)^2 d\Omega. \tag{1.3.22}$$

We have

$$\sum_{k=1}^d \left(\sum_{j=1}^d \frac{\partial v}{\partial x_j}\frac{\partial x_j}{\partial Y_k}\right)^2 \leq \sum_{k=1}^d \left[\sum_{j=1}^d \left(\frac{\partial v}{\partial x_j}\right)^2\right]\left[\sum_{j=1}^d \left(\frac{\partial x_j}{\partial Y_k}\right)^2\right] \leq$$
$$d\sum_{k=1}^d \max_j \left(\frac{\partial x_j}{\partial Y_k}\right)^2 \sum_{j=1}^d \left(\frac{\partial v}{\partial x_j}\right)^2 \leq d^2 \left(\max_{jk} \left|\frac{\partial x_j}{\partial Y_k}\right|\right)^2 \sum_{j=1}^d \left(\frac{\partial v}{\partial x_j}\right)^2. \tag{1.3.23}$$

Then from (1.3.22) we obtain

$$|\hat{v}|^2_{H^1(\Omega_0)} \leq d^2 \|J_{\mathcal{A}_t^{-1}}\|_{L_\infty(\Omega_t)} \|\mathbf{J}_{\mathcal{A}_t}\|^2_{\mathbf{L}_\infty(\Omega_0)} |v|^2_{H^1(\Omega_t)}. \tag{1.3.24}$$

Analogously, by exchanging the role of v and $\hat{v}$ we have

$$|v|^2_{H^1(\Omega_t)} \leq d^2 \|J_{\mathcal{A}_t}\|_{L_\infty(\Omega_0)} \|\mathbf{J}_{\mathcal{A}_t^{-1}}\|^2_{\mathbf{L}_\infty(\Omega_t)} |\hat{v}|^2_{H^1(\Omega_0)}, \tag{1.3.25}$$

by which the theorem is proved. ■

As for the time regularity of the mapping, we will assume that the function $\mathbf{x}(\mathbf{Y}, t)$ satisfies

$$\mathbf{x} \in H^1\left(I; \mathbf{W}^{1,\infty}(\Omega_0)\right). \tag{1.3.26}$$

Proposition 1.3.2 *Under the assumption (1.3.26), we have that if* $\hat{v} \in H^1(I, H^1(\Omega_0))$ *then,* $v = \hat{v} \circ \mathcal{A}_t^{-1} \in H^1(I, H^1(\Omega_t))$ *and*

$$\left.\frac{\partial v}{\partial t}\right|_{\mathbf{Y}} \in L^2(I, H^1(\Omega_t)). \tag{1.3.27}$$

Proof. Owing to proposition 1.3.1 we have established an isomorphism between $H^1(\Omega_0)$ and $H^1(\Omega_t)$. Being $H^1(\Omega_0)$ a separable Hilbert space, we may express any $\hat{v} \in H^1(I; H^1(\Omega_0))$ as

$$\hat{v}(\mathbf{Y}, t) = \sum_{i=1}^{\infty} \hat{v}_i(t)\Psi_i(\mathbf{Y}), \tag{1.3.28}$$

where $\{\Psi_i(\mathbf{Y})\}$ is an orthonormal basis of $H^1(\Omega_0)$ and $\hat{v}_i(t) = (\hat{v}, \Psi_i)_{H^1(\Omega_0)}$ is the corresponding Fourier coefficient. We have indicated by $(\cdot,\cdot)_{H^1(\Omega_0)}$ the scalar product in $H^1(\Omega_0)$. Clearly, $\hat{v}_i(t) \in H^1(I)$. Then, we have

$$\left.\frac{\partial v}{\partial t}\right|_{\mathbf{Y}} \circ \mathcal{A}_t = \frac{\partial \hat{v}}{\partial t} = \sum_{i=1}^{\infty} \frac{d\hat{v}_i}{dt}\Psi_i \tag{1.3.29}$$

Therefore,

$$\left.\frac{\partial v}{\partial t}\right|_{\mathbf{Y}} \circ \mathcal{A}_t \in L^2(I; H^1(\Omega_0)) \tag{1.3.30}$$

Finally, we note that the set $\{\Phi_i |\quad \Phi_i = \Psi_i \circ \mathcal{A}_t^{-1}\}$ forms a complete basis (not necessarily orthogonal) of $H^1(\Omega_t)$, thanks to the equivalence of norms in $H^1(\Omega_t)$ and $H^1(\Omega_0)$ proved in proposition 1.3.1. Then we have,

$$v = \hat{v} \circ \mathcal{A}_t^{-1} = \sum_{i=1}^{\infty} \hat{v}_i \Psi_i \circ \mathcal{A}_t^{-1} = \sum_{i=1}^{\infty} \hat{v}_i \Phi_i, \tag{1.3.31}$$

thus $v \in H^1(I, H^1(\Omega_t))$. Furthermore,

$$\left.\frac{\partial v}{\partial t}\right|_{\mathbf{Y}} = \frac{\partial \hat{v}}{\partial t} \circ \mathcal{A}_t^{-1} = \sum_{i=1}^{\infty} \frac{d\hat{v}_i}{dt}\Psi_i \circ \mathcal{A}_t^{-1} = \sum_{i=1}^{\infty} \frac{d\hat{v}_i}{dt}\Phi_i \tag{1.3.32}$$

Then, $\left.\frac{\partial v}{\partial t}\right|_{\mathbf{Y}} \in L^2(I; H^1(\Omega_t))$. ■

1.4 A practical construction of the ALE mapping $\mathcal{A}_t$

In practice we are normally faced with the problem:

Problem 1.4.1 *Given the time evolution of the domain boundary*

$$\mathbf{g}: \quad \partial\Omega_0 \times I \to \partial\Omega_t$$

find an ALE mapping $\mathcal{A}_t$ such that, at each time $t \in I$,

$$\mathcal{A}_t(\mathbf{Y}) = \mathbf{g}(\mathbf{Y}, t), \qquad \forall \mathbf{Y} \in \partial\Omega_0.$$

Several techniques have been proposed in the literature to solve this problem. For instance, one may construct the domain motion by considering the domain as an 'elastic' or viscoelastic solid and solve the stated problem by resorting to the equations of elastodynamics. This approach is used, for example, in[26]. Yet, one may look to simplified models. Here, we present two possibilities without the pretension of being exhaustive.

1.4.1 Solving a parabolic system

It consists in finding a solution to the following problem.

Problem 1.4.2 *Given the initial configuration Ω_0 and the law of evolution of the domain boundary* $\mathbf{g}$*, find*

$$\mathbf{x} : \Omega_0 \times I \to \Omega_t$$

such that

$$\begin{cases} \dfrac{\partial \mathbf{x}}{\partial t} - \boldsymbol{\nabla}_{\mathbf{Y}} \cdot (\kappa \boldsymbol{\nabla}_{\mathbf{Y}} \mathbf{x}) = 0 & \mathbf{Y} \in \Omega_0, t \in I, \\ \mathbf{x}(\mathbf{Y}, 0) = \mathbf{Y} & \mathbf{Y} \in \Omega_0, \\ \mathbf{x}(\mathbf{Y}, t) = \mathbf{g}(\mathbf{Y}, t) & \mathbf{Y} \in \partial\Omega_0, t \in I. \end{cases} \tag{1.4.1}$$

Here κ is a positive constant (which may be taken equal to 1).

Remark 1.4.1 *We may note that a more complex expression for κ, by letting it be a tensor function with coefficients depending on the numerical solution of the problem at hand, may allow to implement a mesh adaption scheme based on node movement, at very little computational price, since the domain movement has to be computed anyway.*

1.4.2 Harmonic extension

Very often we need to know the ALE mapping only at discrete time levels, where the approximate solution of the problem at hand is sought. The data of the problem are the reference (initial) configuration and the new position of the boundary, which could be described as a function $\mathbf{h} : \partial\Omega_0 \to \partial\Omega_T$, being Ω_T the configuration at the given time T. In this case a simple alternative to the previously described technique consists in making a harmonic extension of $\mathbf{h}$ onto the whole domain Ω_0. That is, one solves the following problem

Problem 1.4.3 *Given Ω_0 and* $\mathbf{h}$*, find* $\mathbf{x} : \Omega_0 \to \Omega_T$ *such that*

$$\begin{cases} \boldsymbol{\nabla}_{\mathbf{Y}} \cdot (\kappa \boldsymbol{\nabla}_{\mathbf{Y}} \mathbf{x}) = 0 & \mathbf{Y} \in \Omega_0 \\ \mathbf{x}(\mathbf{Y}) = \mathbf{h}(\mathbf{Y}) & \mathbf{Y} \in \partial\Omega_0 \end{cases} \tag{1.4.2}$$

Again, if κ is a function of the numerical solution it may be used to drive an adaption type procedure.

1.5 Finite element discretisation of the ALE mapping

Our final objective will be the numerical solution of problems (1.2.4) or (1.2.10) by a finite element method. The choice of finite element space for the main variable u will undoubtedly affect the type of discretisation to be used for the ALE mapping. In particular, the discrete ALE mapping should be such that the domain triangulation maintains during its movement its suitability with respect to the chosen finite element space. For instance, if we use linear finite elements we need to ensure that the images of the mesh during the domain movement maintain straight edges.
There are thus two inter-related issues which must be faced:

1. finding the appropriate discrete formulation for (1.2.4) and (1.2.10);
2. finding a suitable finite element discretisation, $\mathcal{A}_{h,t}$, for the ALE mapping or, equivalently, of problems (1.4.1) or (1.4.2).

We briefly recall some basic concepts of the finite element method which are necessary for our discussion. The domain Ω_0 is discretised by partitioning it into a finite number of (possibly curved) polyhedra called finite elements. The set of finite elements is called mesh and it is indicated by $\mathcal{T}_{h,0}$. The discretised domain $\Omega_{h,0}$, formed by the union of all mesh elements, may differ from Ω_0 because of the approximation of the boundary. Yet, since this fact is not particularly relevant for our discussion, in the following we will assume $\Omega_{h,0} = \Omega_0$. We consider Lagrangian finite elements and the general case of a finite element function space $\mathcal{F}_{n,k}$ of degree n and parametric mapping degree k, defined as follows.

$$\mathcal{F}_{n,k}(\mathcal{T}_{h,0}) = \left\{ \widehat{\psi}_h : \Omega_0 \to \mathbb{R} | \quad \widehat{\psi}_h \in C^0(\overline{\Omega_0}),\ \widehat{\psi}_h\Big|_{K_0} \circ \mathcal{M}_k^{K_0} \in P_n(K_R),\ \forall K_0 \in \mathcal{T}_{h,0} \right\}, \tag{1.5.1}$$

where, $\widehat{\psi}_h\Big|_{K_0}$ indicates the restriction of $\widehat{\psi}_h$ to the finite element K_0, $P_n(K_R)$ is the space of polynomials of degree n defined on the simplex K_R and $\mathcal{M}_k^{K_0} \in P_k(K_R)$ is a homeomorphic mapping from K_R to K_0. In general $k \leq n$ and in particular it is either equal to 1 (affine mapping) or n (isoparametric mapping). Since we wish to consider the general case, we will indicate with the term "vertices" the finite element nodes which are used for the parametric mapping. $\mathcal{M}_k^{K_0}$ is defined as follows,

$$\mathcal{M}_k^{K_0} : K_R \to K_0, \quad \mathbf{Y}(\boldsymbol{\eta}) = \mathcal{M}_k^{K_0}(\boldsymbol{\eta}) = \sum_{i \in \mathcal{N}^K} \mathbf{Y}_i \tilde{\phi}_i(\boldsymbol{\eta}), \quad \boldsymbol{\eta} \in K_R, \quad \tilde{\phi}_i \in P_k(K_R). \tag{1.5.2}$$

Here, $\tilde{\phi}_i$ is the basis function associated to i-th vertex of the reference element, while $\mathbf{Y}_i$ is the coordinate of the correspondent vertex in $\mathcal{T}_{h,0}$. The sum extends over all vertices of K_R, here indicated by $\mathcal{N}^K$. It can be shown that $\mathcal{F}_{n,k}(\mathcal{T}_{h,0}) \subset H^1(\Omega_0)$, and, in particular, $\mathcal{F}_{n,k}(\mathcal{T}_{h,0}) \subset W^{1,\infty}(\Omega_0)$. In case of an affine mapping the finite element space $\mathcal{F}_{n,1}$ reduces to the more familiar expression,

$$\mathcal{F}_{n,1}(\mathcal{T}_{h,0}) = \{ \widehat{\psi}_h : \Omega_0 \to \mathbb{R} | \quad \widehat{\psi}_h \in C^0(\overline{\Omega_0}), \quad \widehat{\psi}_h\Big|_{K_0} \in P_n(K_0),\ \forall K_0 \in \mathcal{T}_{h,0} \}. \tag{1.5.3}$$

Should we wish to utilise a finite element discretisation for our problem, the space of test functions $\mathcal{Y}(\Omega_0)$ will be approximated by $\mathcal{X}_h(\Omega_0) = \mathcal{F}_{n,k}(\mathcal{T}_{h,0})$; we remark that this implies, in particular, that $\forall K_0 \in \mathcal{T}_{h,0}$, $\mathcal{M}_k^{K_0} \in P_k(K_R)$. In section 1.2 we have advocated that the proper ALE extension of the discrete test function space to a moving domain would be

$$\mathcal{X}_h(\Omega_{h,t}) = \{ \psi_h :\ \Omega_{h,t} \times I \to \mathbb{R}, \quad \psi_h \circ \mathcal{A}_{h,t} = \widehat{\psi}_h,\ \widehat{\psi}_h \in \mathcal{X}_h(\Omega_0) \}, \tag{1.5.4}$$

where $\Omega_{h,t} = \mathcal{A}_{h,t}(\Omega_0)$ is an approximation of Ω_t and we use in (1.5.4) the discrete ALE mapping. Therefore, in order to be consistent with the chosen finite element discretisation, we should require that at any t $\mathcal{X}_h(\Omega_{h,t}) = \mathcal{F}_{n,k}(\mathcal{T}_{h,t})$ where $\mathcal{T}_{h,t}$ is the image under the ALE mapping of $\mathcal{T}_{h,0}$. If $\mathbf{x}_i(t)$ denotes the position of the i-th vertex at time t, we may formally define $\mathcal{M}_k^{K_t}$ on each element K_t of $\mathcal{T}_{h,t}$ as follows (see figure 1.1 for a graphic representation),

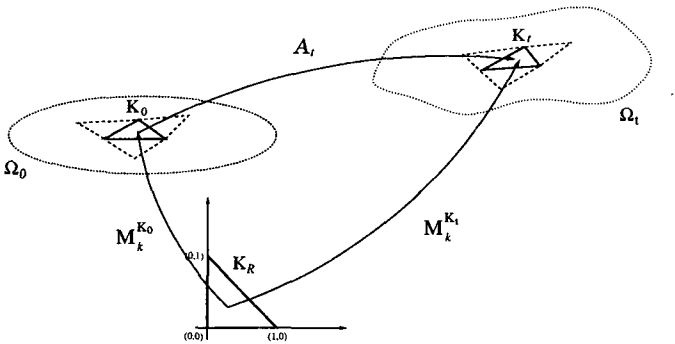

Figure 1.1: Finite element K_0 of $\mathcal{T}_{h,0}$ and K_t of $\mathcal{T}_{h,t}$ as images of the simplex K_R.

$$\mathcal{M}_k^{K_t} : K_R \to K_t, \quad \mathbf{x}(\boldsymbol{\eta}) = \mathcal{M}_k^{K_t}(\boldsymbol{\eta}) = \sum_{i \in \mathcal{N}^K} \mathbf{x}_i(t)\tilde{\phi}_i(\boldsymbol{\eta}), \quad \boldsymbol{\eta} \in K_R, \quad \tilde{\phi}_i \in P_k(K_R), \quad (1.5.5)$$

while $\mathcal{F}_{n,k}(\mathcal{T}_{h,t})$ is

$$\mathcal{F}_{n,k}(\mathcal{T}_{h,t}) = \left\{ \psi_h : \Omega_{h,t} \to \mathbb{R} \mid \quad \psi_h \in C^0(\Omega_{h,t}),\ \psi_h|_{K_t} \circ \mathcal{M}_k^{K_t} \in P_n(K_R),\ \forall K_t \in \mathcal{T}_{h,t} \right\}. \quad (1.5.6)$$

Proposition 1.5.1 *If, at any $t \in I$ the discrete ALE mapping satisfies*

$$\mathcal{A}_{h,t}|_{K_0} \circ \mathcal{M}_k^{K_0} = \mathcal{M}_k^{K_t}, \qquad \forall K_0 \in \mathcal{T}_{h,0}, \quad K_t = \mathcal{A}_t(K_0), \quad (1.5.7)$$

(equivalently $\mathcal{A}_{h,t}|_{K_0} = \mathcal{M}_k^{K_t} \circ (\mathcal{M}_k^{K_0})^{-1}$) and

$$\mathcal{X}_h(\Omega_0) = \mathcal{F}_{n,k}(\mathcal{T}_{h,0}), \qquad t = t_0, \quad (1.5.8)$$

then the space $\mathcal{X}_h(\Omega_{h,t})$, defined in (1.5.4) satisfies

$$\mathcal{X}_h(\Omega_{h,t}) = \mathcal{F}_{n,k}(\mathcal{T}_{h,t}), \qquad \forall t \in I. \quad (1.5.9)$$

Proof. We just note that the under the given hypothesis

$$\mathcal{X}_h(\Omega_0) = \left\{ \widehat{\psi}_h : \Omega_0 \to \mathbb{R} \mid \quad \widehat{\psi}_h \in C^0(\Omega_0),\ \widehat{\psi}_h\Big|_{K_0} \circ \mathcal{M}_k^{K_0} \in P_n(K_R),\ \forall K_0 \in \mathcal{T}_{h,0} \right\} \quad (1.5.10)$$

Then, from (1.5.4), we have that if $\psi_h \in \mathcal{X}_h(\Omega_{h,t})$ then

$$(\psi_h \circ \mathcal{A}_{h,t})|_{K_0} \circ \mathcal{M}_k^{K_0} \in P_n(K_R)$$

By recalling the definition of $\mathcal{F}_{n,k}(\mathcal{T}_{h,t})$, given in (1.5.6), and exploiting the continuity of the discrete ALE mapping, we finally obtain that $\psi_h \in \mathcal{F}_{n,k}(\mathcal{T}_{h,t})$. ■

As a consequence of condition (1.5.7) it is easily verified that the appropriate finite element function space for the discrete ALE mapping is the isoparametric space $\mathcal{F}_{k,k}(\mathcal{T}_{h,0})$, since, by

definition, if $\varphi \in \mathcal{F}_{k,k}(\mathcal{T}_{h,0})$ then $\varphi|_{K_0} \circ \mathcal{M}_k^{K_0} \in P_k(K_R)$, and condition (1.5.7) indeed implies that

$$\mathcal{A}_{h,t}|_{K_0} \circ \mathcal{M}_k^{K_0} \in P_k(K_R).$$

If we denote by

$$\{\psi_i, \quad i \in \mathcal{N}^{\mathcal{T}}\}$$

the set of nodal basis function of $\mathcal{F}_{k,k}$, the discrete ALE mapping would then provide the following discretisation for the function $\mathbf{x}$ in (1.4.1) or (1.4.2)

$$\mathbf{x}_h(\mathbf{Y},t) = \mathcal{A}_{h,t}(\mathbf{Y}) = \sum_{i \in \mathcal{N}^{\mathcal{T}}} \mathbf{x}_i(t)\psi_i(\mathbf{Y}) \tag{1.5.11}$$

We can then proceed to the solution of (1.4.1) or (1.4.2) by standard finite element procedures.

Remark 1.5.1 *We may note that the construction of the discrete ALE mapping depends on the degree k of the parametric mapping chosen for the finite element space where we wish to solve our problem, but not on the degree n of the finite element representation chosen for our principal unknown u_h. For instance, if we decide to use quadratic elements with an affine parametric mapping, the discrete ALE transformation should be built by using isoparametric linear elements.*

Remark 1.5.2 *By construction, the discrete ALE mapping satisfies the required regularity assumptions, and the mesh velocity field on Ω_0, can be expressed as*

$$\hat{\mathbf{w}}_h(\mathbf{Y},t) = \sum_{i \in \mathcal{N}^{\mathcal{T}}} \mathbf{w}_i(t)\psi_i(\mathbf{Y}), \qquad \text{in } \widehat{\Omega}_0 \times I. \tag{1.5.12}$$

Remark 1.5.3 *In practical applications, the ALE mapping will be computed only at some instants $t_i \in I$. A global mapping $\mathcal{A}_{h,t}$, defined for all $t \in I$, may then be obtained by interpolation in time of the transformations $\mathcal{A}_{h,t_i}$. We will always adopt this technique in the next sections when we will present the fully discrete schemes.*

A further discussion on the finite element spaces in the ALE frame will be carried out in Section 1.7, with respect to a specific model problem.

1.6 A linear advection diffusion problem

To analyse the properties of the discrete schemes resulting from the ALE formulation, we consider the following model problem

$$\begin{aligned} \frac{\partial u}{\partial t} + \nabla_{\mathbf{x}} \cdot (\boldsymbol{\beta} u) - \mu \Delta_{\mathbf{x}} u = f \quad & \text{for } \mathbf{x} \in \Omega_t, \ t \in I \\ u = u_0 \quad & \text{for } \mathbf{x} \in \Omega_0, \ t = t_0 \\ u = u_D \quad & \text{for } \mathbf{x} \in \partial\Omega_t, \ t \in I \end{aligned} \tag{1.6.1}$$

where $\boldsymbol{\beta}$ is a convection velocity, which is assumed to satisfy $\nabla_{\mathbf{x}} \cdot \boldsymbol{\beta} = 0$, μ a constant diffusivity, $\Delta_{\mathbf{x}}$ indicates the Laplacian operator and u_D is an assigned boundary condition

of Dirichlet type (in the case $\mu = 0$, the boundary condition should be applied only on the inflow part of the boundary). We may note that equation (1.6.1) is a special case of (1.1.6), with

$$\mathbf{F}_e(u) = \boldsymbol{\beta} u, \quad \mathbf{F}_v(u) = -\mu \nabla_{\mathbf{x}} u.$$

In this Section, we will investigate the stability of the continuous problem in ALE form and the existence of weak solutions of equation (1.6.1) rewritten either in conservative or non-conservative ALE form. We will consider only the case of homogeneous Dirichlet boundary conditions. An equivalence result stating that a weak solution of the ALE problem is also a weak solution of the model problem (1.6.1) will be given in Theorem 1.6.2.
In the next Sections, instead, we will consider the discrete scheme and derive some necessary conditions by which the numerical approximation satisfies the so called "Geometric Conservation Laws".

1.6.1 Stability analysis of the differential equation in ALE frame

We first verify that the differential equation written in the ALE frame maintains stability properties similar to those of an advection-diffusion problem on a fixed domain. Here we proceed formally by supposing the solution u be regular enough. A rigorous derivation of an a-priory estimate will be given in the next subsection. For the sake of completeness, we will consider a general convective field $\boldsymbol{\beta}$, satisfying $\|\nabla_{\mathbf{x}} \cdot \boldsymbol{\beta}\|_{L_\infty(\Omega_t \times I)} = \gamma < \infty$. We write the differential equation on the ALE frame in the form

$$\begin{aligned} \left.\frac{\partial u}{\partial t}\right|_{\mathbf{Y}} + \nabla_{\mathbf{x}} \cdot [(\boldsymbol{\beta} - \mathbf{w})u] - \mu \Delta_{\mathbf{x}} u + u \nabla_{\mathbf{x}} \cdot \mathbf{w} = f \quad & \text{for } \mathbf{x} \in \Omega_t, \ t \in I \\ u = u_0 \quad & \text{for } \mathbf{x} \in \Omega_0, \ t = t_0 \\ u = 0 \quad & \text{for } \mathbf{x} \in \partial\Omega_t, \ t \in I. \end{aligned} \tag{1.6.2}$$

We multiply the equation by u and integrate over Ω_t. Using the Reynolds transport formula, we have

$$\int_{\Omega_t} \left.\frac{\partial u^2}{\partial t}\right|_{\mathbf{Y}} d\Omega = \frac{d}{dt} \|u\|^2_{L_2(\Omega_t)} - \int_{\Omega_t} u^2 \nabla_{\mathbf{x}} \cdot \mathbf{w} d\Omega. \tag{1.6.3}$$

From (1.6.2) it may be derived that

$$\frac{1}{2}\frac{d}{dt} \|u\|^2_{L_2(\Omega_t)} + \mu \|\nabla_{\mathbf{x}} u\|^2_{L_2(\Omega_t)} + \int_{\Omega_t} \nabla_{\mathbf{x}} \cdot [(\boldsymbol{\beta} - \mathbf{w})u] u d\Omega + \frac{1}{2} \int_{\Omega_t} u^2 \nabla_{\mathbf{x}} \cdot \mathbf{w} d\Omega = \int_{\Omega_t} f u d\Omega. \tag{1.6.4}$$

Thanks to the homogeneous boundary conditions, we have

$$\int_{\Omega_t} \nabla_{\mathbf{x}} \cdot [(\boldsymbol{\beta} - \mathbf{w})u] u d\Omega = \frac{1}{2} \left[\int_{\Omega_t} u^2 \nabla_{\mathbf{x}} \cdot \boldsymbol{\beta} d\Omega - \int_{\Omega_t} u^2 \nabla_{\mathbf{x}} \cdot \mathbf{w} d\Omega \right] \tag{1.6.5}$$

and therefore relation (1.6.4) becomes:

$$\frac{1}{2}\frac{d}{dt} \|u\|^2_{L_2(\Omega_t)} + \mu \|\nabla_{\mathbf{x}} u\|^2_{L_2(\Omega_t)} = \int_{\Omega_t} f u d\Omega - \frac{1}{2} \int_{\Omega_t} u^2 \nabla_{\mathbf{x}} \cdot \boldsymbol{\beta} d\Omega. \tag{1.6.6}$$

We may observe that the terms depending on the domain velocity have been canceled out. Integrating in time between t_0 and t, we have:

$$\|u(t)\|^2_{L_2(\Omega_t)} + 2\mu \int_{t_0}^{t} \|\nabla_{\mathbf{x}} u\|^2_{L_2(\Omega_s)}\, ds = \|u(t_0)\|^2_{L_2(\Omega_{t_0})} + 2\int_{t_0}^{t} ds \int_{\Omega_s} f u d\Omega - \int_{t_0}^{t} ds \int_{\Omega_s} u^2 \nabla_{\mathbf{x}} \cdot \beta d\Omega. \quad (1.6.7)$$

Then, by using the definition of the H^{-1} norm and the Poincaré inequality (1.3.7), we deduce that

$$\|u(t)\|^2_{L_2(\Omega_t)} + \mu \int_{t_0}^{t} \|\nabla_{\mathbf{x}} u\|^2_{L_2(\Omega_s)}\, ds \leq \|u(t_0)\|^2_{L_2(\Omega_{t_0})} + \frac{(1+C_\Omega)}{\mu} \int_{t_0}^{t} \|f\|^2_{H^{-1}(\Omega_s)} + \gamma \int_{t_0}^{t} \|u\|^2_{L_2(\Omega_s)}\, ds. \quad (1.6.8)$$

Finally, by using the Gronwall lemma (see e.g. [80]), we obtain

$$\|u(t)\|^2_{L_2(\Omega_t)} + \mu \int_{t_0}^{t} \|\nabla_{\mathbf{x}} u\|^2_{L_2(\Omega_s)}\, ds \leq K\, e^{\gamma t} \quad (1.6.9)$$

where

$$K = \|u(t_0)\|^2_{L_2(\Omega_{t_0})} + \frac{(1+C_\Omega)}{\mu} \int_{t_0}^{t} \|f\|^2_{H^{-1}(\Omega_s)}\, ds. \quad (1.6.10)$$

If $\nabla_{\mathbf{x}} \cdot \beta = 0$ then the stability expression simplifies furtherly. At continuous level, then, the stability properties of the problem are not affected by the domain velocity field. Clearly, we may expect that this will not be true anymore for the discrete problem.

1.6.2 Existence and uniqueness results

Existence and uniqueness of a weak solution of problem (1.6.1) have been proven in different works. For instance, in [57] one can find a proof of existence and uniqueness of a solution $u \in L^2(I; H^1(\Omega_t))$, $\frac{\partial u}{\partial t} \in \left(L^2(I; H^1_0(\Omega_t))\right)'$[5] under the hypotheses that $f \in \left(L^2(I; H^1_0(\Omega_t))\right)'$, $\beta \in L^\infty(\Omega_t \times I)$ and the domain $\Omega_t \times I$ is sufficiently smooth; in particular Ω_0 and the lateral surface $\Sigma = \partial\Omega_t \times I$ are supposed to be infinitely differentiable surfaces of $\mathbb{R}^d$. Finally, the boundary and initial data are supposed to be traces of a function Φ belonging to the space $\mathcal{B}(\Omega_t \times I) \equiv \{v \in L^2(I; H^1(\Omega_t)),\ \frac{\partial v}{\partial t} \in \left(L^2(I; H^1_0(\Omega_t))\right)'\}$.
An alternative proof of existence of a weak solution in the same functional space mentioned before can be obtained through an elliptic regularization following the same guidelines as in [58, example 2.7, pages 343–345].
Other theoretical results of existence and uniqueness of the solution under weaker conditions on the domain regularity can be found in [10, 94], in [51] where a penalization method is used and in [11] where the problem is recast in an abstract semigroup setting.

We are going to provide a direct proof of existence of weak solutions of problem (1.6.2) rewritten in ALE formulation adopting a Faedo-Galerkin approach.

[5] With V' we indicated the dual of the functional space V.

Let Ω_0 be a bounded domain in $\mathbb{R}^d$ with a Lipschitz boundary. We consider an ALE mapping $\mathcal{A}_t \in \left[W^{1,\infty}(\Omega_0 \times I)\right]^d$ that satisfies the hypotheses of Proposition 1.3.1, an initial datum $u_0 \in L^2(\Omega_0)$ and a forcing term $f \in L^2(\Omega_t \times I)$[6]. Moreover, we take $\mathcal{Y}(\Omega_0) \equiv H_0^1(\Omega_0)$ and $\mathcal{X}(\Omega_t)$ defined as in (1.2.3). Then, the two weak formulations introduced in (1.2.4) and (1.2.10) read, respectively

Non-conservative formulation *find* $u : \Omega_t \times I \to \mathbb{R}$, $u = 0$ *on* $\partial\Omega_t$, *such that*

$$\int_{\Omega_t} \left.\frac{\partial u}{\partial t}\right|_{\mathbf{Y}} \psi \, d\Omega + \mu \int_{\Omega_t} \nabla_{\mathbf{x}} u \nabla_{\mathbf{x}} \psi \, d\Omega + \int_{\Omega_t} \psi \nabla_{\mathbf{x}} \cdot [(\boldsymbol{\beta} - \mathbf{w})u] \, d\Omega + \int_{\Omega_t} \psi u \nabla_{\mathbf{x}} \cdot \mathbf{w} \, d\Omega = \\ = \int_{\Omega_t} f\psi \, d\Omega \qquad \forall \psi \in \mathcal{X}(\Omega_t), \text{ a.e. in } I, \quad (1.6.11)$$

Conservative formulation *find* $u : \Omega_t \times I \to \mathbb{R}$, $u = 0$ *on* $\partial\Omega_t$, *such that*

$$\frac{d}{dt} \int_{\Omega_t} \psi u d\Omega + \mu \int_{\Omega_t} \nabla_{\mathbf{x}} \psi \nabla_{\mathbf{x}} u d\Omega + \int_{\Omega_t} \psi \nabla_{\mathbf{x}} \cdot [(\boldsymbol{\beta} - \mathbf{w})u] \, d\Omega = \\ = \int_{\Omega_t} f\psi \, d\Omega \qquad \forall \psi \in \mathcal{X}(\Omega_t), \text{ a.e. in } I, \quad (1.6.12)$$

and $u = u_0$ in Ω_0, at $t = t_0$ in both cases.
The time derivatives in the previous problems have to be intended in a way which will be clarified later on.
We first provide some useful properties of the functional spaces we will be using.

Lemma 1.6.1 *Under the aforementioned hypotheses on* Ω_0 *and* $\mathcal{A}_t$, *the application* $\hat{v} = v \circ \mathcal{A}_t$ *is an isomorphism from* $L^2(I; H^1(\Omega_t))$ *onto* $L^2(I; H^1(\Omega_0))$, *from* $L^\infty(I; L^2(\Omega_t))$ *onto* $L^\infty(I; L^2(\Omega_0))$ *as well as from* $H^1(\Omega_t \times I)$ *onto* $H^1(\Omega_0 \times I)$;

Proof. The first two properties derive directly from relations (1.3.20)-(1.3.21) and (1.3.24)-(1.3.25) observing that the quantities $\|J_{\mathcal{A}_t}\|_{L_\infty(\Omega_0)}$, $\|J_{\mathcal{A}_t^{-1}}\|_{L_\infty(\Omega_0)}$, $\|\mathbf{J}_{\mathcal{A}_t}\|^2_{\mathbf{L}_\infty(\Omega_t)}$ and $\|\mathbf{J}_{\mathcal{A}_t^{-1}}\|^2_{\mathbf{L}_\infty(\Omega_t)}$ belong all to $W^{1,\infty}(I)$. The third property can be proved in a similar way as in Proposition 1.3.1 accounting also for the time derivative. Indeed, we may introduce the space-time mapping $\tilde{\mathcal{A}} : \Omega_0 \times I \to \Omega_t \times I$,

$$(\mathbf{x}, t) = \tilde{\mathcal{A}}(\mathbf{Y}, \tau), \qquad \begin{cases} \mathbf{x} = \mathcal{A}_\tau(\mathbf{Y}), \\ t = \tau. \end{cases}$$

Clearly, $\tilde{\mathcal{A}} \subset \left[W^{1,\infty}(\Omega_0 \times I)\right]^{d+1}$ and the result is obtained by applying Proposition 1.3.1 on the mapping $\tilde{\mathcal{A}}$ and in the domain $\Omega_0 \times I$.
■
We start analyzing the conservative formulation (1.6.12). The first result we will prove is

[6]The derivation presented hereafter can be easily generalized to the case of a forcing term $f = \nabla_{\mathbf{x}} g$, $g \in L^2(\Omega_t \times I)$

Theorem 1.6.1 *Under the aforementioned hypotheses on Ω_0, $\mathcal{A}_t$, u_0 and f, problem (1.6.12) admits a unique solution $u \in L^2(I; H_0^1(\Omega_t)) \cap L^\infty(I; L^2(\Omega_t))$ such that*

$$\frac{d}{dt}\int_{\Omega_t} u\psi d\Omega \in L^2(I), \quad \forall \psi \in \mathcal{X}(\Omega_t).$$

Moreover, u satisfies the energy estimate (1.6.9).

Proof In order to study existence and uniqueness of the solution of problem (1.6.12) we rewrite (1.6.12) on the reference configuration Ω_0. To this aim we note in the following with $\hat{u}$ a function defined on Ω_t recast on Ω_0 : $\hat{u} = u \circ \mathcal{A}_t$. Then $\forall i = 1, \ldots, d$ we have

$$\frac{\partial u}{\partial x_i} = \sum_j \frac{\partial \hat{u}}{\partial Y_j}\frac{\partial Y_j}{\partial x_i}$$

$$\nabla_{\mathbf{x}} u \nabla_{\mathbf{x}} v = \sum_i \frac{\partial u}{\partial x_i}\frac{\partial v}{\partial x_i} = \sum_{jk}\left(\sum_i \frac{\partial Y_j}{\partial x_i}\frac{\partial Y_k}{\partial x_i}\right)\frac{\partial \hat{u}}{\partial Y_j}\frac{\partial \hat{v}}{\partial Y_k}$$

$$\nabla_{\mathbf{x}} \cdot \boldsymbol{\beta} = \sum_k \frac{\partial \beta_k}{\partial x_k} = \sum_j \left(\sum_k \frac{\partial Y_j}{\partial x_k}\frac{\partial \hat{\beta}_k}{\partial Y_j}\right).$$

The weak problem (1.6.12) written on the reference configuration reads then

$$\frac{d}{dt}\int_{\Omega_0} J_{\mathcal{A}_t}\hat{u}\hat{\psi}\, d\Omega + \sum_j \int_{\Omega_0} J_{\mathcal{A}_t}\hat{\psi}\sum_k \frac{\partial Y_j}{\partial x_k}\frac{\partial}{\partial Y_j}\left((\hat{\beta}_k - \hat{\mathbf{w}}_k)\hat{u}\right) d\Omega +$$
$$\sum_{jk}\mu\int_{\Omega_0} J_{\mathcal{A}_t}\left(\sum_i \frac{\partial Y_j}{\partial x_i}\frac{\partial Y_k}{\partial x_i}\right)\frac{\partial \hat{u}}{\partial Y_j}\frac{\partial \hat{\psi}}{\partial Y_k} d\Omega = \int_{\Omega_0} J_{\mathcal{A}_t}\hat{f}\hat{\psi}\, d\Omega \qquad \forall \hat{\psi} \in \mathcal{Y}(\Omega_0),\ t \in I, \tag{1.6.13}$$

Let us introduce the following notation : $\forall \hat{\phi}, \hat{\psi} \in \mathcal{Y}(\Omega_0)$

$$m(t; \hat{\phi}, \hat{\psi}) = \int_{\Omega_0} J_{\mathcal{A}_t}\hat{\phi}\hat{\psi}\, d\Omega$$

$$a(t; \hat{\phi}, \hat{\psi}) = \sum_j \int_{\Omega_0} J_{\mathcal{A}_t}\hat{\psi}\sum_k \frac{\partial Y_j}{\partial x_k}\frac{\partial}{\partial Y_j}\left((\hat{\beta}_k - \hat{\mathbf{w}}_k)\hat{\phi}\right) d\Omega +$$
$$+ \sum_{jk}\mu\int_{\Omega_0} J_{\mathcal{A}_t}\left(\sum_i \frac{\partial Y_j}{\partial x_i}\frac{\partial Y_k}{\partial x_i}\right)\frac{\partial \hat{\phi}}{\partial Y_j}\frac{\partial \hat{\psi}}{\partial Y_k} d\Omega$$

$$c(t; \hat{\phi}, \hat{\psi}) = \sum_j \int_{\Omega_0} J_{\mathcal{A}_t}\hat{\psi}\hat{\phi}\sum_k \frac{\partial Y_j}{\partial x_k}\frac{\partial \hat{\mathbf{w}}_k}{\partial Y_j} d\Omega$$

We analyse the conservative formulation (1.6.13) by adopting a Faedo-Galerkin method (see for instance [80, 87]). Let $\{\hat{\phi}_j\}_{j\geq 1}$ be a complete orthonormal basis of $H_0^1(\Omega_0)$, $V^N = span\{\hat{\phi}_1, \ldots, \hat{\phi}_N\}$, and consider the approximate problem :

find $\hat{u}^N(t) \in V^N$ *such that*

$$\begin{cases} \dfrac{d}{dt} m(t; \hat{u}^N(t), \hat{\phi}_j) + a(t; \hat{u}^N(t), \hat{\phi}_j) = \displaystyle\int_{\Omega_0} J_{\mathcal{A}_t} \hat{f} \hat{\phi}_j \, d\Omega \qquad \forall j = 1, \dots, N \\ \hat{u}^N(0) = u_0^N. \end{cases} \tag{1.6.14}$$

where u_0^N is the L^2 orthogonal projection of u_0 onto the space V^N.
We look for a solution of the form $\hat{u}^N(t) = \sum_{s=1}^N c_s(t)\hat{\phi}_s$ and we note $\mathbf{c}^N = [c_1(t), \dots, c_N(t)]^T$. Then, system (1.6.14) is equivalent to the system of ordinary differential equations

$$\begin{cases} \dfrac{d}{dt}\left(M(t)\mathbf{c}^N(t)\right) + A(t)\mathbf{c}^N(t) = \mathbf{F}(t), \qquad t \in I \\ \mathbf{c}^N(0) = \mathbf{c}_0 \end{cases} \tag{1.6.15}$$

where

$$M(t)_{ij} = m(t; \hat{\phi}_j, \hat{\phi}_i), \qquad A(t)_{ij} = a(t; \hat{\phi}_j, \hat{\phi}_i),$$
$$\mathbf{F}(t)_i = \int_{\Omega_0} J_{\mathcal{A}_t} \hat{f} \hat{\phi}_i \, d\Omega \qquad \text{and} \quad (\mathbf{c}_0)_i = \int_{\Omega_0} u_0 \hat{\phi}_i \, d\Omega.$$

We observe that

$$M(t) \in \left[W^{1,\infty}(I)\right]^{d^2}, \quad A(t) \in \left[L^\infty(I)\right]^{d^2}, \quad \mathbf{F}(t) \in \left[L^2(I)\right]^d, \tag{1.6.16}$$

and $M(t)$ is a symmetric and positive definite matrix for all $t \in I$ since, $\forall \mathbf{c}^N(t) \in \mathbb{R}^d$, $\mathbf{c}^N(t) \neq \mathbf{0}$,

$$\left(\mathbf{c}^N(t)\right)^T M(t)\mathbf{c}^N(t) = \int_{\Omega_0} J_{\mathcal{A}_t} |\hat{u}^N(t)|^2 \, d\Omega = \int_{\Omega_t} |u^N(t)|^2 = \left\|u^N(t)\right\|^2_{L_2(\Omega_t)} > 0$$

We introduce the vector $\mathbf{d}^N(t) = M(t)\mathbf{c}^N(t)$ which satisfies

$$\begin{cases} \dfrac{d}{dt}\mathbf{d}^N(t) + A(t)M^{-1}(t)\mathbf{d}^N(t) = \mathbf{F}(t), \qquad t \in I \\ \mathbf{d}^N(0) = M(t)\mathbf{c}_0. \end{cases}$$

This system admits a unique solution $\mathbf{d}^N(t) \in \left[H^1(I)\right]^N$ and consequently (1.6.15) admits a unique solution $\mathbf{c}^N(t) \in \left[H^1(I)\right]^N$ since $\mathbf{c}^N(t) = M^{-1}(t)\mathbf{d}^N(t)$ and $M^{-1}(t) \in \left[W^{1,\infty}(I)\right]^{d^2}$. As a consequence, $\hat{u}^N(t) \in H^1(I; H_0^1(\Omega_0))$.
We multiply now equation (1.6.15) by $\left(\mathbf{c}^N(t)\right)^T$ and we observe that for almost every $t \in I$

$$\frac{d}{dt}M(t)_{ij} = \frac{d}{dt}\int_{\Omega_0} J_{\mathcal{A}_t} \hat{\phi}_j \hat{\phi}_i \, d\Omega = \sum_l \int_{\Omega_0} J_{\mathcal{A}_t} \hat{\phi}_i \hat{\phi}_j \sum_k \frac{\partial Y_l}{\partial x_k} \frac{\partial \hat{\mathbf{w}}_k}{\partial Y_l} \, d\Omega = C(t)_{ij} \tag{1.6.17}$$

where we have exploited relation (1.1.8) and we have noted

$$C(t)_{ij} = c(t; \hat{\phi}_j, \hat{\phi}_i).$$

Hence

$$(\mathbf{c}^N)^T \frac{d}{dt}\left(M\mathbf{c}^N\right) = \frac{1}{2}(\mathbf{c}^N)^T \frac{d}{dt}\left(M\mathbf{c}^N\right) + \frac{1}{2}\frac{d}{dt}\left((\mathbf{c}^N)^T M\mathbf{c}^N\right) - \frac{1}{2}\frac{d}{dt}(\mathbf{c}^N)^T M\mathbf{c}^N =$$
$$\frac{1}{2}(\mathbf{c}^N)^T \frac{d}{dt}\left(M\mathbf{c}^N\right) + \frac{1}{2}\frac{d}{dt}\left((\mathbf{c}^N)^T M\mathbf{c}^N\right) - \frac{1}{2}(\mathbf{c}^N)^T M\frac{d}{dt}\mathbf{c}^N =$$
$$= \frac{1}{2}\frac{d}{dt}\left((\mathbf{c}^N)^T M\mathbf{c}^N\right) + \frac{1}{2}(\mathbf{c}^N)^T \frac{d}{dt}M(t)\mathbf{c}^N \quad (1.6.18)$$

We obtain then the equation

$$\frac{1}{2}\frac{d}{dt}\left(\mathbf{c}^N(t)^T M(t)\mathbf{c}^N(t)\right) + \mathbf{c}^N(t)^T A(t)\mathbf{c}^N(t) + \frac{1}{2}\mathbf{c}^N(t)^T C(t)\mathbf{c}^N(t) = \mathbf{c}^N(t)^T \mathbf{F}(t), \quad \forall t \in I \quad (1.6.19)$$

which is the algebraic counterpart of

$$\frac{1}{2}\frac{d}{dt}\int_{\Omega_t} |u^N(t)|^2 + \mu \int_{\Omega_t} |\boldsymbol{\nabla}_{\mathbf{x}} u^N(t)|^2 + \int_{\Omega_t} \boldsymbol{\nabla}_{\mathbf{x}} \cdot \left[(\boldsymbol{\beta} - \mathbf{w})u^N(t)\right] u^N(t) d\Omega +$$
$$+ \frac{1}{2}\int_{\Omega_t} |u^N(t)|^2 \boldsymbol{\nabla}_{\mathbf{x}} \cdot \mathbf{w} d\Omega = \int_{\Omega_t} f u^N(t) d\Omega.$$

We observe that, thanks to (1.6.16), the last three terms in (1.6.19) are measurable functions in time. Then, by integrating (1.6.19) between t_0 and τ, $\tau \in I$ and proceeding as in the previous section, we obtain the estimate :

$$\left\|u^N(\tau)\right\|^2_{L_2(\Omega_\tau)} + \mu \int_{t_0}^{\tau} \left\|\boldsymbol{\nabla}_{\mathbf{x}} u^N(s)\right\|^2_{L_2(\Omega_s)} ds \leq \left(\left\|u_0^N\right\|^2_{L_2(\Omega_0)} + \frac{(1+C_\Omega)}{\mu}\int_{t_0}^{\tau} \|f\|^2_{H^{-1}(\Omega_s)} ds\right) e^{\gamma\tau} \quad (1.6.20)$$

as in (1.6.9). According to Lemma 1.6.1, the norms $L^2(I; H_0^1(\Omega_t))$ and $L^\infty(I; L^2(\Omega_t))$ are equivalent to $L^2(I; H_0^1(\Omega_0))$ and $L^\infty(I; L^2(\Omega_0))$, respectively. The sequence $\{\hat{u}^N(t)\}$ is thus bounded in $L^\infty(I; L^2(\Omega_0)) \cap L^2(I; H^1(\Omega_0))$ and we can extract a subsequence $\{\hat{u}^{N,m}(t)\}$ converging to a limit function $\hat{u}(t)$ weakly in $L^2(I; H^1(\Omega_0))$ and weak* in $L^\infty(I; L^2(\Omega_0))$.

Passage to the limit

In order to pass to the limit in (1.6.14) we multiply each differential equation by $\theta(t) \in \mathcal{D}(I)$ and we integrate by parts the first term :

$$-\int_I \left(\int_{\Omega_0} J_{\mathcal{A}_t} \hat{u}^N(t)\hat{\phi}_j \, d\Omega\right) \frac{d}{dt}\theta(t)\, dt + \int_I a(t; \hat{u}^N(t), \hat{\phi}_j)\theta(t)\, dt = \int_I \int_{\Omega_0} J_{\mathcal{A}_t} \hat{f}\hat{\phi}_j \theta(t)\, d\Omega\, dt$$
$$\forall j = 1, \ldots, N, \quad \forall \theta(t) \in \mathcal{D}(I)$$

In all the terms we can pass to the limit for $N, m \to \infty$; moreover, since the linear combinations of $\hat{\phi}_j$ are dense in $H_0^1(\Omega_0)$ we obtain finally

$$-\int_I \left(\int_{\Omega_0} J_{\mathcal{A}_t} \hat{u}(t)\hat{\psi}\, d\Omega\right) \frac{d}{dt}\theta(t)\, dt + \int_I a(t; \hat{u}(t), \hat{\psi})\theta(t)\, dt = \int_I \int_{\Omega_0} J_{\mathcal{A}_t} \hat{f}\hat{\psi}\theta(t)\, d\Omega\, dt$$
$$\forall \hat{\psi} \in \mathcal{Y}(\Omega_0), \quad \forall \theta(t) \in \mathcal{D}(I) \quad (1.6.21)$$

which is nothing else then problem (1.6.13) where the time derivative has to be intended in a distributional sense. In a standard way it can be shown that also the initial condition is satisfied (see e.g. [80, Theorem 11.1.1, Chap 11]). We conclude that problem (1.6.13) admits a solution $\hat{u} \in L^\infty(I; L^2(\Omega_0)) \cap L^2(I; H_0^1(\Omega_0))$ and moreover from equation (1.6.13) we infer that

$$\frac{d}{dt}\int_{\Omega_0} J_{\mathcal{A}_t}\hat{u}\hat{\psi}\, d\Omega \in L^2(I) \;\; \forall \hat{\psi} \in \mathcal{Y}(\Omega_0) \qquad \text{i.e.} \qquad \frac{\partial(J_{\mathcal{A}_t}\hat{u})}{\partial t} \in L^2(I; H^{-1}(\Omega_0)). \tag{1.6.22}$$

Finally, equation (1.6.21), written on the domain Ω_t coincides with problem (1.6.12). Then, thanks to the isomorphism results of Lemma 1.6.1, the function $u = \hat{u} \circ \mathcal{A}_t^{-1}$ belongs to $L^2(I; H_0^1(\Omega_t)) \cap L^\infty(I; L^2(\Omega_t))$ and is a solution of (1.6.12); moreover, from (1.6.22)

$$\frac{d}{dt}\int_{\Omega_t} u\psi d\Omega \in L^2(I), \quad \forall \psi \in \mathcal{X}(\Omega_t).$$

In order to prove the a-priori estimate we need the following

Lemma 1.6.2 *Let E and F be two Banach spaces equipped with the norms $\|\cdot\|_E$ and $\|\cdot\|_F$. Let, moreover, $A : E \to F$ be an isomorphism between E and F. Then,*

a. There exists an isomorphism $B : E' \to F'$.

b. Given a sequence $\{\hat{\phi}^N\}$ such that $\{\hat{\phi}^N\} \to \hat{\phi}$ weakly in E, then $\{A\hat{\phi}^N\} \to A\hat{\phi}$ weakly in F.

Proof. We note in the following $\phi = A\hat{\phi}$. Since A is an isomorphism we have

$$\|A\|_{\mathcal{L}(E,F)} \le C_1, \quad \|A^{-1}\|_{\mathcal{L}(F,E)} \le C_2.$$

a. For every functional $\hat{f} \in E'$ we can define a functional $f \in F'$ such that

$$\forall \phi \in F, \qquad < f, \phi >=< \hat{f}, A^{-1}\phi >=< \hat{f}, \hat{\phi} >;$$

moreover

$$\|f\|_{F'} = \sup_{\substack{\phi \in F \\ \|\phi\|_F \neq 0}} \frac{< f, \phi >}{\|\phi\|_F} \le \sup_{\substack{\phi \in F \\ \|\phi\|_F \neq 0}} \frac{C_2 < \hat{f}, \hat{\phi} >}{\|\hat{\phi}\|_E} \le C_2 \|\hat{f}\|_{E'}$$

We set $f = B\hat{f}$; clearly $\|B\|_{\mathcal{L}(E',F')} \le C_2$ and with similar arguments it can be shown that $\|B^{-1}\|_{\mathcal{L}(F',E')} \le C_1$.

b. By the definition of weak convergence we have that

$$\forall \hat{f} \in E', \quad < \hat{f}, \hat{\phi}^N > \; \to \; < \hat{f}, \hat{\phi} > .$$

From item a. we know that $\forall f \in F'$ there exists $\hat{f} = B^{-1}f$. Then, we deduce immediately that

$$\forall f \in F', \quad < f, A\hat{\phi}^N >=< \hat{f}, \hat{\phi}^N > \; \to \; < \hat{f}, \hat{\phi} >=< f, A\hat{\phi} > .$$

and this concludes our proof.

■

Thanks to Lemma 1.6.2 and to the isomorphism between $L^2(I;H_0^1(\Omega_0))$ and $L^2(I;H_0^1(\Omega_t))$, proved in Lemma 1.6.1, we conclude that the sequence $\{u^{N,m}(t)\} = \{\hat{u}^{N,m}(t)\circ\mathcal{A}_t^{-1}\}$ converges weakly to $u(t) = \hat{u}(t)\circ\mathcal{A}_t^{-1}$ in $L^2(I;H_0^1(\Omega_t))$.
We prove now that the sequence $\{u^{N,m}(t)\} \to u(t)$ weakly* in $L^\infty(I;L^2(\Omega_t))$. Indeed, $\forall\phi \in L^1(I;L^2(\Omega_t))$ the function $\hat{\zeta} = J_{\mathcal{A}_t}\hat{\phi}$ belongs to $L^1(I;L^2(\Omega_0))$ and

$$\int_I\int_{\Omega_t} u^{N,m}(t)\phi\,d\Omega\,dt = \int_I\int_{\Omega_0} \hat{u}^{N,m}(t)\hat{\zeta}\,d\Omega\,dt \xrightarrow[N,m\to\infty]{} \int_I\int_{\Omega_0} \hat{u}(t)\hat{\zeta}\,d\Omega\,dt = \int_I\int_{\Omega_t} u(t)\phi\,d\Omega\,dt$$

We infer from (1.6.20) and the propertics of the weak convergence that the limit function $u(t)$ satisfies the estimate

$$\|u(\tau)\|^2_{L_2(\Omega_\tau)} + \mu\int_{t_0}^{\tau}\|\nabla_{\mathbf{x}}u(s)\|^2_{L_2(\Omega_s)}\,ds \le \left(\|u_0\|^2_{L_2(\Omega_0)} + \frac{(1+C_\Omega)}{\mu}\int_{t_0}^{\tau}\|f\|^2_{H^{-1}(\Omega_s)}\,ds\right)e^{\gamma\tau}. \tag{1.6.23}$$

Uniqueness of the solution is a direct consequence of (1.6.23) and the linearity of the problem.

■

The second result we will prove is the following

Theorem 1.6.2 *The solution u of (1.6.12) does not depend on the choice of the ALE mapping $\mathcal{A}_t$ and is the unique solution of problem (1.6.1) defined in the space $\left(L^2(I;H_0^1(\Omega_t))\right)'$.*

Proof. We remind that the solution $u = u(x,t)$ of (1.6.12) belongs to $L^2(I;H_0^1(\Omega_t)) \cap L^\infty(I;L^2(\Omega_t))$.

First step : we prove that $\frac{\partial u}{\partial t} \in H^{-1}(\Omega_t\times I)$.
Indeed, the distributional time derivative of u is defined as

$$< \frac{\partial u}{\partial t}, \phi >= -\int_I\int_{\Omega_t} u\frac{\partial\phi}{\partial t}\,d\Omega\,dt, \qquad \forall\phi\in\mathcal{D}(\Omega_t\times I).$$

Since $\mathcal{D}(\Omega_t\times I)$ is dense in $H_0^1(\Omega_t\times I)$ and $u\in L^2(\Omega_t\times I)$, the right hand side can be extended by continuity to all functions $\phi\in H_0^1(\Omega_t\times I)$ [7]. It follows immediately that $\frac{\partial u}{\partial t}\in \left(H_0^1(\Omega_t\times I)\right)' = H^{-1}(\Omega_t\times I)$.

Second step : We prove that $\frac{\partial u}{\partial t}\in\left(L^2(I;H_0^1(\Omega_t))\right)'$ and

$$< \frac{\partial u}{\partial t}, \phi > +\mu\int_I\int_{\Omega_t}\nabla_{\mathbf{x}}u\nabla_{\mathbf{x}}\phi\,d\Omega\,dt + \int_I\int_{\Omega_t}\nabla_{\mathbf{x}}\cdot(\boldsymbol{\beta}u)\phi\,d\Omega\,dt = \int_I\int_{\Omega_t} f\phi\,d\Omega\,dt, \tag{1.6.24}$$

for all $\phi\in L^2(I;H_0^1(\Omega_t))$.
Let $\{\hat{\psi}_i\}_{i\ge1}$ be a basis of $H_0^1(\Omega_0)$ and $\{\hat{\theta}_j\}_{j\ge1}$ be a basis of $H_0^1(I)$. We can write, as in (1.6.21), the equation

$$-\int_I\int_{\Omega_0} J_{\mathcal{A}_t}\hat{u}\hat{\psi}_i\frac{d}{dt}\hat{\theta}_j\,d\Omega\,dt + \int_I a(t;\hat{u},\hat{\psi}_i)\hat{\theta}_j\,dt = \int_I\int_{\Omega_0} J_{\mathcal{A}_t}\hat{f}\hat{\psi}_i\hat{\theta}_j\,d\Omega\,dt, \qquad \forall i,j\ge1 \tag{1.6.25}$$

[7] it can be extended to a larger class of test functions but this is enough for our purposes

where, as usual we have noted $\hat{u} = u \circ \mathcal{A}_t$. By setting $\hat{\zeta}_{ij}(\mathbf{Y}, t) = \hat{\psi}_i(\mathbf{Y})\hat{\theta}_j(t)$, equation (1.6.25) may be written equivalently

$$-\int_I \int_{\Omega_0} J_{\mathcal{A}_t} \hat{u} \frac{d\hat{\zeta}_{ij}}{dt}\, d\Omega\, dt + \int_I a(t; \hat{u}, \hat{\zeta}_{ij})\, dt = \int_I \int_{\Omega_0} J_{\mathcal{A}_t} \hat{f} \hat{\zeta}_{ij}\, d\Omega\, dt, \qquad \forall i, j \geq 1 \tag{1.6.26}$$

and since $\{\hat{\zeta}_{ij}\}_{i,j\geq 1}$ is a basis of $H_0^1(\Omega_0 \times I)$ relation (1.6.26) can be written for all test functions $\hat{\zeta} \in H_0^1(\Omega_0 \times I)$. Again from Lemma 1.6.1, the function $\zeta = \hat{\zeta} \circ \mathcal{A}_t^{-1}$ belongs to $H_0^1(\Omega_t \times I)$ and we can write all terms in (1.6.26) on the configuration Ω_t :

$$-\int_I \int_{\Omega_t} u \left.\frac{\partial \zeta}{\partial t}\right|_{\mathbf{Y}} d\Omega\, dt + \mu \int_I \int_{\Omega_t} \nabla_{\mathbf{x}} u \nabla_{\mathbf{x}} \zeta\, d\Omega\, dt + \int_I \int_{\Omega_t} \nabla_{\mathbf{x}} \cdot [(\beta - \mathbf{w})u] \zeta\, d\Omega\, dt =$$
$$= \int_I \int_{\Omega_t} f \zeta\, d\Omega\, dt, \qquad \forall \zeta \in H_0^1(\Omega_t \times I). \tag{1.6.27}$$

Exploiting relation (1.1.4) in the first term, we have

$$-\int_I \int_{\Omega_t} u \left.\frac{\partial \zeta}{\partial t}\right|_{\mathbf{Y}} d\Omega\, dt = -\int_I \int_{\Omega_t} u \left.\frac{\partial \zeta}{\partial t}\right|_{\mathbf{x}} d\Omega\, dt - \int_I \int_{\Omega_t} u\, \mathbf{w} \cdot \nabla_{\mathbf{x}} \zeta\, d\Omega\, dt =$$
$$= -\int_I \int_{\Omega_t} u \left.\frac{\partial \zeta}{\partial t}\right|_{\mathbf{x}} d\Omega\, dt + \int_I \int_{\Omega_t} \nabla_{\mathbf{x}} \cdot (\mathbf{w} u) \zeta\, d\Omega\, dt.$$

and (1.6.27) becomes

$$-\int_I \int_{\Omega_t} u \left.\frac{\partial \zeta}{\partial t}\right|_{\mathbf{x}} d\Omega\, dt + \mu \int_I \int_{\Omega_t} \nabla_{\mathbf{x}} u \nabla_{\mathbf{x}} \zeta\, d\Omega\, dt + \int_I \int_{\Omega_t} \nabla_{\mathbf{x}} \cdot (\beta u) \zeta\, d\Omega\, dt =$$
$$= \int_I \int_{\Omega_t} f \zeta\, d\Omega\, dt, \qquad \forall \zeta \in H_0^1(\Omega_t \times I). \tag{1.6.28}$$

or equivalently, $\forall \zeta \in H_0^1(\Omega_t \times I)$

$$< \frac{\partial u}{\partial t}, \zeta > = \int_I \int_{\Omega_t} f \zeta\, d\Omega\, dt - \mu \int_I \int_{\Omega_t} \nabla_{\mathbf{x}} u \nabla_{\mathbf{x}} \zeta\, d\Omega\, dt - \int_I \int_{\Omega_t} \nabla_{\mathbf{x}} \cdot (\beta u) \zeta\, d\Omega\, dt. \tag{1.6.29}$$

Since the right hand side in (1.6.29) is a linear continuous functional on $L^2(I; H_0^1(\Omega_t))$ and $H_0^1(\Omega_t \times I)$ is dense in $L^2(I; H_0^1(\Omega_t))$ we can extend (1.6.29) to all $\zeta \in L^2(I; H_0^1(\Omega_t))$. This implies that $\frac{\partial u}{\partial t} \in \left(L^2(I; H_0^1(\Omega_t))\right)'$ and u satisfies problem (1.6.1) in $\left(L^2(I; H_0^1(\Omega_t))\right)'$.

Third step : we prove now that the solution u of (1.6.12) does not depend on the ALE mapping $\mathcal{A}_t$.

Indeed, let us consider two possible different ALE mappings $\mathcal{A}_t^{(1)}$ and $\mathcal{A}_t^{(2)}$ (which describe, clearly, the evolution of the same domain Ω_t, $\forall t > 0$). Then, solving problem (1.6.12) with the two mappings, we obtain two solutions $u^{(1)}$ and $u^{(2)}$. Both solutions satisfy the same problem (1.6.1), thus the difference $v = u^{(1)} - u^{(2)}$ satisfies problem (1.6.1) with homogeneous data and, moreover, v satisfies the a-priori estimate (1.6.23). Then, necessarily, $v = 0$.
In other words, whatever ALE mapping we choose, the solution u on the actual configuration Ω_t is always the same.

■

About the non-conservative formulation (1.6.11), we would like to define the ALE derivative in a distributional sense by means of the Reynolds transport formula (1.1.11). To this aim, we observe that for a given function $v : \Omega_t \times I \to \mathbb{R}$, regular enough, we have, for all $\phi \in \mathcal{D}(\Omega_t \times I)$

$$\begin{aligned}\int_I \int_{\Omega_t} \left.\frac{\partial v}{\partial t}\right|_{\mathbf{Y}} \phi \, d\Omega dt &= -\int_I \int_{\Omega_t} v \left(\left.\frac{\partial \phi}{\partial t}\right|_{\mathbf{Y}} + \phi \nabla_{\mathbf{x}} \cdot \mathbf{w} \right) d\Omega dt \\ &= -\int_I \int_{\Omega_t} v \left(\frac{\partial \phi}{\partial t} + \nabla_{\mathbf{x}} \cdot (\phi \mathbf{w}) \right) d\Omega dt\end{aligned}$$

We may thus define the ALE derivative, in a distributional sense, of any function $v \in L^1(\Omega_t \times I)$ and ALE mapping $\mathcal{A}_t \in \left[W^{1,\infty}(\Omega_0 \times I)\right]^d$ as

$$< \left.\frac{\partial v}{\partial t}\right|_{\mathbf{Y}}, \phi > = - < v, \frac{\partial \phi}{\partial t} + \nabla_{\mathbf{x}} \cdot (\phi \mathbf{w}) >, \qquad \forall \phi \in \mathcal{D}(\Omega_t \times I). \tag{1.6.30}$$

If we consider, now, the weak-solution u of the conservative ALE formulation (1.6.12), which belongs in particular to $L^2(I; H_0^1(\Omega_t))$, we have

$$< \left.\frac{\partial u}{\partial t}\right|_{\mathbf{Y}}, \phi > = < \frac{\partial u}{\partial t}, \phi > + \int_I \int_{\Omega_t} \phi \mathbf{w} \cdot \nabla_{\mathbf{x}} u \, d\Omega dt, \qquad \forall \phi \in \mathcal{D}(\Omega_t \times I). \tag{1.6.31}$$

As we have shown in Theorem 1.6.2, u is also a solution of problem (1.6.1) in $\left(L^2(I; H_0^1(\Omega_t))\right)'$; thus, exploiting equation (1.6.29) in (1.6.31) we obtain

$$\begin{aligned}< \left.\frac{\partial u}{\partial t}\right|_{\mathbf{Y}}, \phi > = \int_I \int_{\Omega_t} f \phi \, d\Omega \, dt - \mu \int_I \int_{\Omega_t} \nabla_{\mathbf{x}} u \nabla_{\mathbf{x}} \phi \, d\Omega \, dt - \int_I \int_{\Omega_t} \nabla_{\mathbf{x}} \cdot (\beta - \mathbf{w}u) \phi \, d\Omega \, dt \\ - \int_I \int_{\Omega_t} \phi u \cdot \nabla_{\mathbf{x}} \cdot \mathbf{w} \, d\Omega dt, \qquad \forall \phi \in \mathcal{D}(\Omega_t \times I).\end{aligned} \tag{1.6.32}$$

The right hand side in (1.6.32) may be extended to all functions $\phi \in L^2(I; H_0^1(\Omega_t))$. Hence, the solution u of the ALE conservative formulation is also a solution of the non-conservative formulation

$$\left.\frac{\partial u}{\partial t}\right|_{\mathbf{Y}} + \nabla_{\mathbf{x}} \cdot [(\beta - \mathbf{w})u] - \mu \Delta_{\mathbf{x}} u + u \nabla_{\mathbf{x}} \cdot \mathbf{w} = f \qquad \text{in } \left(L^2(I; H_0^1(\Omega_t))\right)',$$

where the ALE derivative is defined in (1.6.30).
Observe that, in this way, we recover only a solution of the non-conservative equation in a weak formulation both in space and time. Yet, such a solution does not necessary satisfy equation (1.6.11) which, instead, should hold pointwise in time.

1.7 Finite element spaces in the ALE frame

We will use Lagrangian type finite elements and a discrete ALE mapping $\mathcal{A}_{h,t}$, as described in section 1.5, and a Galerkin formulation. Our discrete function space on Ω_0, $\mathcal{X}_h(\Omega_0)$, will then coincide with $\mathcal{F}_{n,k}(\mathcal{T}_{h,0})$, defined in (1.5.1). The corresponding finite element space on $\Omega_{h,t}$, $\mathcal{X}_h(\Omega_{h,t})$, will be formed by functions of $\mathcal{F}_{n,k}(\mathcal{T}_{h,t})$.

We will now indicate with $\mathcal{N}$ the set of nodes of the finite element mesh, and with $\mathcal{N}_{int} \subset \mathcal{N}$ the set of internal nodes. We also introduce the set of finite element nodal basis functions

$$\{\psi_i, \quad \psi_i \in \mathcal{X}_h(\Omega_{h,t}), \quad i \in \mathcal{N}\}$$

which forms a basis of $\mathcal{X}_h(\Omega_{h,t})$. Here, ψ_i is the finite element function associated with node i. With $\mathcal{X}_{0,h}(\Omega_{h,t})$ we indicate the discrete function space $\mathcal{X}_h(\Omega_{h,t}) \cap H_0^1(\Omega_{h,t})$. The set

$$\{\psi_i, \quad i \in \mathcal{N}_{int}\},$$

forms a basis of $\mathcal{X}_{0,h}(\Omega_{h,t})$.
The numerical solution u_h will then be sought in the space $\mathcal{X}_h(\Omega_{h,t})$. In particular, we have that u_h will be expressed as linear combination of nodal finite element basis functions,

$$u_h(\mathbf{x}, t) = \sum_{i \in \mathcal{N}} \psi_i(\mathbf{x}, t) u_i(t), \tag{1.7.1}$$

with time dependent coefficients $u_i(t)$. The set $\mathcal{X}_{0,h}(\Omega_{h,t})$ will be used as test function space. For the sake of simplicity, we will drop the subscript h when it is clear from the context that we are considering the discrete solution. This applies in particular to the computational domain which in the following will be indicated simply by Ω_t. We wish to remind that, because of the ALE mapping, functions in $\mathcal{X}_h(\Omega_{h,t})$ depend both on $\mathbf{x}$ and t, even if the functions in $\mathcal{X}_h(\Omega_0)$ do not depend on time. Thanks to relation (1.2.5) we may then write,

$$\left.\frac{\partial u_h}{\partial t}\right|_{\mathbf{Y}} (\mathbf{x}, t) = \sum_{i \in \mathcal{N}} \psi_i(\mathbf{x}, t) \frac{du_i}{dt}(t). \tag{1.7.2}$$

1.7.1 A remark on the significance of the Geometric Conservation Laws

Geometric Conservation Laws have been originally investigated in the context of finite difference and finite volume schemes for fluid dynamic problems. It stems from the basic idea that the solution should be minimally affected by the domain movement law. Indeed, at the continuous level, the ALE formulation is formally equivalent to the original problem; yet this is not generally true when the fully discrete system is considered. It has been proposed that some 'simple' solution of the differential problem should be also solutions of the discrete system. In particular, the attention has been concentrated on the capability of the discrete system of representing a constant solution, which is clearly a solution of the differential equation (in the absence of the source term and with the appropriate boundary and initial conditions). Following this approach we can state that *a numerical scheme satisfies the Geometric Conservation Laws if it is able to reproduce a constant solution.* It is therefore, similar to the "patch test" often used by finite element practitioners. As we will see, the GCL constraint involves only mesh geometrical quantities and the domain velocity field. The significance of this condition is still not completely clear. Recent results are available for special type of finite-volume schemes in [44] where the GCL have been linked to convergence properties of the proposed scheme.
In the following analysis, the GCL for a finite element scheme will be investigated in more detail and its relation with the stability properties of some time evolution schemes will be addressed.

1.8 Finite element approximation of the conservative formulation

The finite element semi-discrete approximation of (1.2.10) reads as follows,

$$\frac{d}{dt}\int_{\Omega_t}\psi_h u_h d\Omega + \mu\int_{\Omega_t}\nabla_{\mathbf{x}}\psi_h\nabla_{\mathbf{x}}u_h d\Omega + \int_{\Omega_t}\psi_h\nabla_{\mathbf{x}}\cdot[(\beta-\mathbf{w}_h)u_h]\,d\Omega = \\ = \int_{\Omega_t} f\psi_h\,d\Omega \qquad \forall\psi_h\in\mathcal{X}_{0,h}(\Omega_t), t\in I, \quad (1.8.1)$$

with

$$u_h = u_{Dh} \quad \text{for } \mathbf{x}\in\partial\Omega_t,\ t\in I$$
$$u_h = u_{0h} \quad \text{for } \mathbf{x}\in\Omega_0,\ t=t_0.$$

u_{Dh} and u_{0h} being suitable finite element approximations of u_D and u_0, respectively. Equation (1.8.1) may be equivalently written in algebraic form as follows

$$\frac{d}{dt}\left(\mathbf{M}(t)\,U\right) + \left(\mathbf{H}(t) - \mathbf{A}(t,\mathbf{w}_h)\right)U = \mathbf{F}, \\ u_i = u_D \qquad i\in\mathcal{N}\setminus\mathcal{N}_{int}, \quad (1.8.2)$$

where $U=\{u_i\}_{i\in\mathcal{N}}$ is the vector of the nodal values of the discrete solution,

$$\mathbf{M}(t) = \left\{\int_{\Omega_t}\psi_i\psi_j d\Omega\right\}_{i,j\in\mathcal{N}_{int}}$$

is the mass matrix, while $\mathbf{H}$ and $\mathbf{A}$ are defined as

$$\mathbf{H}(t) = \left\{\int_{\Omega_t}\psi_i\nabla_{\mathbf{x}}\cdot(\beta\psi_j)d\Omega + \mu\int_{\Omega_t}\nabla_{\mathbf{x}}\psi_i\cdot\nabla_{\mathbf{x}}\psi_j d\Omega\right\}_{i,j\in\mathcal{N}_{int}}$$

and

$$\mathbf{A}(t,\mathbf{w}_h) = \left\{\int_{\Omega_t}\psi_i\nabla_{\mathbf{x}}\cdot(\mathbf{w}_h\psi_j)d\Omega\right\}_{i,j\in\mathcal{N}_{int}}.$$

In this context the space integrals may be substituted by numerical quadrature. *In the following, we will always assume that the numerical quadrature rules employed are able to integrate exactly the terms involved.*

1.8.1 Stability analysis of the semi-discrete conservative scheme.

Unless for fixed domains, for the stability analysis of the semi-discrete scheme we cannot take $\psi_h = u_h$ since the two functions have, in general, a different time evolution. However, we can express the solution u_h as a linear combination of the test functions with time dependent coefficients, as indicated in (1.7.1). We then take $\psi_h = \psi_i$ and we multiply the equation for $u_i(t)$ obtaining:

$$u_i(t)\frac{d}{dt}\int_{\Omega_t}u_h\psi_i\,d\Omega + \int_{\Omega_t}\nabla_{\mathbf{x}}\cdot[(\beta-\mathbf{w}_h)u_h]\,u_i(t)\psi_i + \mu\int_{\Omega_t}\nabla_{\mathbf{x}}u_h\nabla_{\mathbf{x}}(u_i(t)\psi_i)\,d\Omega = \\ = \int_{\Omega_t} f u_i(t)\psi_i\,d\Omega \quad (1.8.3)$$

The first term can be rewritten as

$$\begin{aligned} u_i(t)\frac{d}{dt}\int_{\Omega_t} u_h\psi_i\,d\Omega &= \frac{d}{dt}\int_{\Omega_t} u_h u_i(t)\psi_i\,d\Omega - \int_{\Omega_t} u_h\psi_i\frac{du_i(t)}{dt}\,d\Omega \\ &= \frac{d}{dt}\int_{\Omega_t} u_h u_i(t)\psi_i\,d\Omega - \int_{\Omega_t} u_h\left.\frac{\partial\psi_i u_i(t)}{\partial t}\right|_{\mathbf{Y}}\,d\Omega. \end{aligned} \tag{1.8.4}$$

Summing over i all the equations, we obtain

$$\frac{d}{dt}\|u_h\|^2_{L_2(\Omega_t)} - \int_{\Omega_t} u_h\left.\frac{\partial u_h}{\partial t}\right|_{\mathbf{Y}}\,d\Omega + \int_{\Omega_t}\nabla_{\mathbf{x}}\cdot[(\beta-\mathbf{w}_h)u_h]\,u_h + \mu\,\|\nabla_{\mathbf{x}}u_h\|^2_{L_2(\Omega_t)} = \int_{\Omega_t} f u_h\,d\Omega. \tag{1.8.5}$$

The term

$$\int_{\Omega_t} u_h\left.\frac{\partial u_h}{\partial t}\right|_{\mathbf{Y}}\,d\Omega = \frac{1}{2}\int_{\Omega_t}\left.\frac{\partial(u_h^2)}{\partial t}\right|_{\mathbf{Y}}\,d\Omega$$

can be manipulated as in (1.6.3), leading to equation (1.6.4) written for the semi-discrete solution u_h of the problem. We can then proceed as in section 1.6.1, obtaining a stability inequality which is insensitive to the domain velocity field.

1.8.2 The discrete scheme

System (1.8.2) is a system of ODE's which needs to be integrated in time. With this aim, we will consider the following time integration schemes:

$$\mathbf{M}_{t_{n+1}}U_{n+1} - \mathbf{M}_{t_n}U_n + \mathcal{INT}_1{}_{t_n}^{t_{n+1}}[\mathbf{H}\,U] - \mathcal{INT}_2{}_{t_n}^{t_{n+1}}[\mathbf{A}\,U] = \mathbf{F}. \tag{1.8.6}$$

where $\mathcal{INT}_1$ and $\mathcal{INT}_2$ represent two quadrature formulae used to integrate numerically in time the terms $\mathbf{H}U$ and $\mathbf{A}\,U$:

$$\mathcal{INT}_1{}_{t_n}^{t_{n+1}}[\mathbf{H}\,U] \approx \int_{t_n}^{t_{n+1}} \mathbf{H}\,U dt$$

$$\mathcal{INT}_2{}_{t_n}^{t_{n+1}}[\mathbf{A}\,U] \approx \int_{t_n}^{t_{n+1}} \mathbf{A}\,U dt$$

In particular, the unknown U in the these two terms may be taken equal to U^{n+1} (implicit scheme) or U^n (explicit scheme).

1.8.3 The Geometric Conservation Laws

When $\mathbf{F} = 0$, sufficient conditions for a constant field to be a solution of the numerical scheme (1.8.6), for each time step interval $(t_n, t_{n+1}) \subset I$, are

$$\sum_{j\in\mathcal{N}}\int_{\Omega_t}\psi_i\nabla_{\mathbf{x}}\cdot(\beta\psi_j)d\Omega dt = 0, \quad \forall i \in \mathcal{N}_{int} \tag{1.8.7}$$

$$\sum_{j\in\mathcal{N}}\int_{\Omega_t}\nabla_{\mathbf{x}}\psi_i\cdot\nabla_{\mathbf{x}}\psi_j d\Omega dt = 0, \quad \forall i \in \mathcal{N}_{int} \tag{1.8.8}$$

and

$$\int_{\Omega_{t_{n+1}}} \psi_i(\mathbf{x}, t_{n+1}) d\Omega - \int_{\Omega_{t_n}} \psi_i(\mathbf{x}, t_n) d\Omega = \mathcal{INT}_{2_{t_n}}^{t_{n+1}} \left[\int_{\Omega_t} \psi_i \nabla_{\mathbf{x}} \cdot \mathbf{w}_h \, d\Omega \right] \quad \forall i \in \mathcal{N}_{int}. \tag{1.8.9}$$

Relation (1.8.7) and (1.8.8) are satisfied by the finite element shape functions. Indeed, they provide a partition of unity

$$\sum_{i \in \mathcal{N}} \psi_i(\mathbf{x}) = 1, \quad \forall \mathbf{x} \in \Omega_t. \tag{1.8.10}$$

Consequently, being $\nabla_{\mathbf{x}} \psi_i \in L^2(\Omega_t)$,

$$\sum_{i \in \mathcal{N}} \nabla_{\mathbf{x}} \psi_i = \mathbf{0} \quad \text{in } \Omega_t. \tag{1.8.11}$$

Remark 1.8.1 *In a finite volume context, a relation equivalent to (1.8.7) would furnish a condition for the computation of the normal unit vector to the surface of the moving control volumes. That condition is often called surface conservation law[92]. The reader may refer to[86] for a discussion about the relationship between Lagrangian finite element and finite volume schemes for conservation laws.*

Condition (1.8.9) expresses the *Geometric Conservation Laws* written for the FEM scheme which employs formulation (1.8.6). It states that the time integration scheme $\mathcal{INT}_2$ must be chosen in such a way that the identity

$$\int_{\Omega_{t_{n+1}}} \psi_h d\Omega - \int_{\Omega_{t_n}} \psi_h d\Omega = \mathcal{INT}_{2_{t_n}}^{t_{n+1}} \left[\int_{\Omega_t} \psi_h \nabla_{\mathbf{x}} \cdot \mathbf{w}_h \, d\Omega \right] \qquad \forall \psi_h \in \mathcal{X}_{0,h}(\Omega_t) \tag{1.8.12}$$

hold on each time-interval.

Remark 1.8.2 *Relation (1.8.12) may also be interpreted as the finite element discretisation of the weak form associated to relation (1.1.8). Indeed, we have already observed that relation (1.1.8) must be identically satisfied in order for the differential equation (1.1.14) (of which relation (1.2.10) is the weak form) to be equivalent to the original differential problem (1.1.7). The GCL enforce such condition at the discrete level.*

Remark 1.8.3 *In a finite element framework, it may be useful to consider another identity, namely relation (1.2.9). Requiring its fulfillment at discrete level would lead to*

$$\int_{\Omega_{t_{n+1}}} \psi_i \psi_j \, d\Omega - \int_{\Omega_{t_n}} \psi_i \psi_j \, d\Omega = \mathcal{INT}_{2_{t_n}}^{t_{n+1}} \left[\int_{\Omega_t} \psi_i \psi_j \nabla_{\mathbf{x}} \cdot \mathbf{w}_h \, d\Omega \right] \qquad \forall i, j \in \mathcal{N}_{int} \tag{1.8.13}$$

This relation may be considered as another form of the GCL for scheme (1.8.6), suited for a finite element approximation.

Proposition 1.8.1 *A sufficient condition for the fulfillment of (1.8.12) and (1.8.13) is to use a time integration scheme $\mathcal{INT}_2$ for the ALE term of degree $d \cdot s - 1$, where d is the space dimension and s is the degree of the polynomial used to represent the time evolution of the nodal displacement within each time step.*

Proof. In order to find out the degree of exactness of the time integration scheme necessary for the fulfillment of the GCL, we consider the time interval $[t_n, t_{n+1}]$ and we take Ω_{t_n} as the reference configuration. In the following, we indicate with $\mathcal{A}_{t_n,t_{n+1}}$ the ALE mapping between the two time levels, that is

$$\mathcal{A}_{t_n,t_{n+1}} = \mathcal{A}_{h,t_{n+1}} \circ \mathcal{A}_{h,t_n}^{-1}. \tag{1.8.14}$$

The following identity holds for all $\psi_h \in \mathcal{X}_{0,h}(\Omega_t)$.

$$\int_{\Omega_{t_{n+1}}} \psi_h \nabla_{\mathbf{x}} \cdot \mathbf{w}_h \, d\Omega = \int_{\Omega_{t_n}} \widehat{\psi}_h(\mathbf{Y})(\mathbf{J}_{cof} \nabla_{\mathbf{Y}}) \cdot \hat{\mathbf{w}}_h \, d\Omega, \tag{1.8.15}$$

where $\widehat{\psi}_h(\mathbf{Y}) = \psi_h \circ \mathcal{A}_{t_n,t_{n+1}}$ and $\hat{\mathbf{w}}_h = \mathbf{w}_h \circ \mathcal{A}_{t_n,t_{n+1}}$, while $\mathbf{J}_{cof}$ is the co-factor matrix of the ALE mapping Jacobian $\mathbf{J}_{\mathcal{A}_{t_n,t_{n+1}}}$. If the domain displacement law is taken to be a piecewise polynomial in time, then $\mathbf{J}_{cof}$ would be a polynomial in time in $[t_n, t_{n+1}]$, whose degree will depend also on the number of space dimensions. Expression (1.8.15) allows to determine the degree of the polynomial which has to be numerically integrated in time in the right hand side of relation (1.8.12). Assuming that the space integral is computed exactly, the satisfaction of the GCL conditions imposes some restrictions on the time integration rule employed for the ALE convection term.
Function $\hat{\psi}$ is constant in time. If the nodal displacement is represented on each time step by a polynomial in time of degree s then $\mathbf{w}_h$ is a polynomial of degree $s-1$, and $\mathbf{J}_{cof}$ of degree $(d-1)s$, being d the number of space dimensions. Consequently, a sufficient condition for the fulfillment of the GCL is obtained by employing a time advancing scheme of exactness (at least) $d \cdot s - 1$. Similar arguments apply for formulation (1.8.13).■

For instance, if we assume a linear time variation for $\mathbf{x}(\mathbf{Y}, t)$ on each time step ($s = 1$) the GCL are satisfied in $2D$ if we use the mid-point rule, which exactly integrates a linear function. These results are in agreement with what has been found by Leisoinne and Farhat in [56], in the context of finite volume formulation.

Remark 1.8.4 *It may be noted that the condition on the time advancing scheme just found for the fulfillment of the GCL involves only the numerical discretisation of the ALE convective term, without any direct involvement of u. Indeed, only terms related to the mesh movement are present. Consequently, as suggested in[56], we may in principle use a separate (possibly less accurate) time-integration rule for the other terms. For example, for a two dimensional problem and piecewise linear time evolution of mesh displacement, we may adopt an explicit treatment for the term* $\mathbf{H}U$*, using, for instance, a first-order forward Euler scheme, while adopting a mid-point rule just for the time integral of the ALE term.*

Remark 1.8.5 *Since there is no one-point integration scheme of exactness 2, in three dimensional problems the mesh quantities should be evaluated at (at least) two intermediate points. For example, we may use a 2 points Gauss quadrature formula for the ALE convective term.*

Remark 1.8.6 *For the case of linear finite elements, B. Nkonga and H. Guillard [62] have exploited the equivalence between Galerkin finite element discretisation and finite volumes on the dual grid in order to integrate exactly the ALE convection term, thus assuring the satisfaction of the GCL for their three dimensional numerical scheme.*

Remark 1.8.7 *The GCL formula for a finite volume scheme is readily inferred by noting that if we take $\psi = 1$ on a patch of elements $\Omega_i(t)$, expression (1.8.12) becomes*

$$\int_{\Omega_i(t_{n+1})} d\Omega - \int_{\Omega_i(t_n)} d\Omega = \mathcal{INT}_{2\,t_n}^{t_{n+1}} \left[\int_{\Omega_i(t)} \boldsymbol{\nabla}_{\mathbf{x}} \cdot \mathbf{w}_h \, d\Omega \right] = \mathcal{INT}_{2\,t_n}^{t_{n+1}} \left[\oint_{\partial\Omega_i(t)} \mathbf{w}_h \cdot \mathbf{n} \, d\Gamma \right], \tag{1.8.16}$$

which is the form which has been proposed in [97, 56].

1.8.4 A stability result for the implicit Euler method applied to the conservative scheme

Let us denote with u_h^n an approximation of $u_h(t^n)$. Clearly, u_h^n is defined on the domain Ω_{t^n}; yet it can be transported on any other configuration Ω_s, $s \neq t^n$, through the mapping $\mathcal{A}_{t^n,s} = \mathcal{A}_{h,s} \circ \mathcal{A}_{h,t^n}^{-1}$. To lighten the notation, whenever we need to integrate u_h^n on a domain Ω_s, $s \neq t^n$ we will write simpliy

$$\int_{\Omega_s} u_h^n \, d\Omega \qquad \text{instead of} \quad \int_{\Omega_s} u_h^n \circ \mathcal{A}_{t^n,s} \, d\Omega.$$

Let us consider, now, the following time discretisation of the semi-discrete problem (1.2.10) for a two dimensional problem. We assume a piecewise constant in time mesh velocity field and we adopt a mid-point time integration rule, thus satisfying the GCL. Yet, we will adopt an implicit Euler time discretisation for u_h. We obtain the following expression

$$\begin{aligned} &\int_{\Omega_{t^{n+1}}} u_h^{n+1} \psi_h \, d\Omega - \int_{\Omega_{t^n}} u_h^n \psi_h \, d\Omega + \Delta t \int_{\Omega_{t^{n+1/2}}} \mu \boldsymbol{\nabla}_{\mathbf{x}} u_h^{n+1} \boldsymbol{\nabla}_{\mathbf{x}} \psi_h \, d\Omega + \\ &\quad + \Delta t \int_{\Omega_{t^{n+1/2}}} \psi_h \boldsymbol{\nabla}_{\mathbf{x}} \cdot [(\boldsymbol{\beta} - \mathbf{w}_h) u_h^{n+1}] \, d\Omega = \Delta t \int_{\Omega_{t^{n+1/2}}} f^{n+1/2} \psi_h \, d\Omega \\ &\qquad\qquad \forall \psi_h \in \mathcal{X}_{0,h}(\Omega_t) \end{aligned} \tag{1.8.17}$$

with

$$\begin{aligned} u_h^i &= 0 \quad \text{on } \partial\Omega_t, \ i = 1, 2, \ldots \\ u_h^0 &= u_{0h} \quad \text{in } \Omega_0 \end{aligned}$$

Taking $\psi_h = u_h^{n+1}$ and integrating by parts the convective terms as in (1.6.5) we obtain

$$\begin{aligned} &\left\| u_h^{n+1} \right\|_{L_2(\Omega_{t^{n+1}})}^2 + \Delta t \mu \left\| \boldsymbol{\nabla}_{\mathbf{x}} u_h^{n+1} \right\|_{L_2(\Omega_{t^{n+1/2}})}^2 - \frac{1}{2} \Delta t \int_{\Omega_{t^{n+1/2}}} |u_h^{n+1}|^2 \boldsymbol{\nabla}_{\mathbf{x}} \cdot \mathbf{w}_h d\Omega \\ &\leq \int_{\Omega_{t^n}} u_h^n u_h^{n+1} \, d\Omega + \Delta t \int_{\Omega_{t^{n+1/2}}} f^{n+1/2} u_h^{n+1} \, d\Omega \ \leq \ \frac{1}{2} \left\| u_h^{n+1} \right\|_{L_2(\Omega_{t^n})}^2 + \frac{1}{2} \left\| u_h^n \right\|_{L_2(\Omega_{t^n})}^2 + \\ &\quad + \Delta t \frac{\mu}{2} \left\| \boldsymbol{\nabla}_{\mathbf{x}} u_h^{n+1} \right\|_{L_2(\Omega_{t^{n+1/2}})}^2 + \Delta t \frac{(1 + C_\Omega)}{2\mu} \left\| f^{n+1/2} \right\|_{H^{-1}(\Omega_{t^{n+1/2}})}^2. \end{aligned} \tag{1.8.18}$$

Since this scheme satisfies the GCL, the following equality holds (we exploit equation (1.8.13), where we set $\psi_i = \psi_j = u_h^{n+1}$):

$$\left\|u_h^{n+1}\right\|^2_{L_2(\Omega_{t^{n+1}})} - \left\|u_h^{n+1}\right\|^2_{L_2(\Omega_{t^n})} = \int_{t^n}^{t^{n+1}} \int_{\Omega_t} |u_h^{n+1}|^2 \nabla_{\mathbf{x}} \cdot \mathbf{w}_h d\Omega$$
$$= \Delta t \int_{\Omega_{t^{n+1/2}}} |u_h^{n+1}|^2 \nabla_{\mathbf{x}} \cdot \mathbf{w}_h d\Omega. \quad (1.8.19)$$

Substituting this equation in the previous inequality, we obtain the stability result:

$$\left\|u_h^{n+1}\right\|^2_{L_2(\Omega_{t^{n+1}})} + \Delta t\mu \left\|\nabla_{\mathbf{x}} u_h^{n+1}\right\|^2_{L_2(\Omega_{t^{n+1/2}})} \leq \left\|u_h^n\right\|^2_{L_2(\Omega_{t^n})} + \Delta t \frac{(1+C_\Omega)}{\mu} \left\|f^{n+1/2}\right\|^2_{H^{-1}(\Omega_{t^{n+1/2}})} \quad (1.8.20)$$

Finally, summing over all the time steps:

$$\left\|u_h^{n+1}\right\|^2_{L_2(\Omega_{t^{n+1}})} + \Delta t\mu \sum_{i=0}^{n} \left\|\nabla_{\mathbf{x}} u_h^{i+1}\right\|^2_{L_2(\Omega_{t^{i+1/2}})}$$
$$\leq \left\|u_h^0\right\|^2_{L_2(\Omega_{t^0})} + \Delta t \frac{(1+C_\Omega)}{\mu} \sum_{i=0}^{n} \left\|f^{i+1/2}\right\|^2_{H^{-1}(\Omega_{t^{i+1/2}})}. \quad (1.8.21)$$

In this case, one may observe that the stability result does not depend on the domain velocity field and that this property has been obtained thanks to the fulfillment of the GCL condition written in the form (1.8.13).

1.9 Finite element approximation of the non-conservative formulation

The semi-discrete counterpart of (1.2.4), based on the pure Galerkin finite element method, reads as follows:

$$\int_{\Omega_t} \left.\frac{\partial u_h}{\partial t}\right|_{\mathbf{Y}} \psi_h \, d\Omega + \int_{\Omega_t} \psi_h \, (\boldsymbol{\beta} - \mathbf{w}_h) \cdot \nabla_{\mathbf{x}} u_h \, d\Omega + \mu \int_{\Omega_t} \nabla_{\mathbf{x}} u_h \nabla_{\mathbf{x}} \psi_h \, d\Omega =$$
$$= \int_{\Omega_t} f \psi_h \, d\Omega \qquad \forall \psi_h \in \mathcal{X}_{0,h}(\Omega_t) \quad (1.9.1)$$

with

$$u_h = u_D \quad \text{for } \mathbf{x} \in \partial\Omega_t, \ t \in I;$$
$$u_h = u_{0h} \quad \text{for } \mathbf{x} \in \Omega_0, \ t = t_0$$

where we have written $\boldsymbol{\beta} \nabla_{\mathbf{x}} u_h$ instead of $\nabla_{\mathbf{x}} \cdot (\boldsymbol{\beta} u_h)$ thanks to the hypothesis of incompressibility of the convective field $\boldsymbol{\beta}$. System (1.9.1) may be equivalently written in algebraic form as we have done for the conservative scheme:

$$\mathbf{M}(t)\frac{dU}{dt} + \mathbf{H}(t)U - \mathbf{B}(t, \mathbf{w}_h)U = \mathbf{F}, \quad (1.9.2)$$

and

$$u_i(t_0) = u(\mathbf{x}_i(t_0), t_0) \qquad i \in \mathcal{N}, \tag{1.9.3}$$

$$u_i(t) = u_D(\mathbf{x}_i, t) \qquad i \in \mathcal{N} \setminus \mathcal{N}_{int}. \tag{1.9.4}$$

Here,

$$\mathbf{B}(t, \mathbf{w}_h) = \left\{ \int_{\Omega_t} \psi_i (\mathbf{w}_h \cdot \boldsymbol{\nabla}_{\mathbf{x}}) \psi_j \, d\Omega \right\}_{i,j \in \mathcal{N}_{\text{int}}}. \tag{1.9.5}$$

If the space integrals are computed exactly, it is immediately verified that a constant function will satisfy (1.9.2) (in the absence of forcing terms) independently of the numerical time integration formula adopted. Indeed,

$$\sum_{j \in \mathcal{N}} \int_{\Omega_t} \psi_i (\mathbf{w}_h \cdot \boldsymbol{\nabla}_{\mathbf{x}}) \psi_j \, d\Omega = 0 \qquad \forall i \in \mathcal{N}_{int}, \tag{1.9.6}$$

because of relation (1.8.11). Therefore, this scheme automatically satisfies the GCL since it is able to represent a constant solution. Unfortunately, while the discrete system (1.8.1), maintains the conservation property of the original problem this is not immediately true for relation (1.9.1).

1.9.1 Stability analysis of the semi-discrete scheme

As for the conservative scheme (1.8.1) analysed in the previous section, we cannot take $\psi_h = u_h$. Since each term in (1.9.1) is linear in ψ_h, if we take $\psi_h = \psi_i$, we multiply each term for $u_i(t)$ and sum over the index i, we get:

$$\int_{\Omega_t} \left. \frac{\partial u_h}{\partial t} \right|_{\mathbf{Y}} u_h \, d\Omega + \int_{\Omega_t} (\boldsymbol{\beta} - \mathbf{w}_h) \boldsymbol{\nabla}_{\mathbf{x}} u_h u_h \, d\Omega + \mu \int_{\Omega_t} |\boldsymbol{\nabla}_{\mathbf{x}} u_h|^2 \, d\Omega = \int_{\Omega_t} f u_h \, d\Omega, \tag{1.9.7}$$

The first term can be transformed exploiting (1.6.3) and obtaining:

$$\int_{\Omega_t} \left. \frac{\partial u_h}{\partial t} \right|_{\mathbf{Y}} u_h \, d\Omega = \frac{1}{2} \frac{d}{dt} \|u_h\|^2_{L_2(\Omega_t)} - \frac{1}{2} \int_{\Omega_t} u_h^2 \boldsymbol{\nabla}_{\mathbf{x}} \cdot \mathbf{w}_h d\Omega, \tag{1.9.8}$$

while the second one becomes:

$$\begin{aligned} \int_{\Omega_t} (\boldsymbol{\beta} - \mathbf{w}_h) \boldsymbol{\nabla}_{\mathbf{x}} u_h u_h \, d\Omega &= \frac{1}{2} \int_{\Omega_t} (\boldsymbol{\beta} - \mathbf{w}_h) \boldsymbol{\nabla}_{\mathbf{x}} |u_h|^2 \, d\Omega \\ &= -\frac{1}{2} \int_{\Omega_t} \boldsymbol{\nabla}_{\mathbf{x}} \cdot (\boldsymbol{\beta} - \mathbf{w}_h) |u_h|^2 \, d\Omega = \frac{1}{2} \int_{\Omega_t} \boldsymbol{\nabla}_{\mathbf{x}} \cdot \mathbf{w}_h |u_h|^2 \, d\Omega. \end{aligned} \tag{1.9.9}$$

Combining these two results into equation (1.9.7), we obtain exactly equation (1.6.6) written for the solution u_h of the semi-discrete problem at hand. Also in this case, we can proceed as in section 1.6.1, obtaining stability inequality without any intervention of the domain velocity field.

1.9.2 Stability result for the implicit Euler method

Let us consider the implicit Euler discretisation of problem (1.9.1),

$$\int_{\Omega_{t^{n+1}}} u_h^{n+1}\psi_h d\Omega - \int_{\Omega_{t^{n+1}}} u_h^n\psi_h d\Omega + \Delta t \int_{\Omega_{t^{n+1}}} \left[\psi_h(\boldsymbol{\beta}-\mathbf{w}_h)\boldsymbol{\nabla}_{\mathbf{x}}u_h^{n+1} + \mu\boldsymbol{\nabla}_{\mathbf{x}}u_h^{n+1}\boldsymbol{\nabla}_{\mathbf{x}}\psi_h\right] d\Omega$$
$$= \Delta t \int_{\Omega_{t^{n+1}}} f^{n+1}\psi_h d\Omega \qquad \forall \psi_h \in \mathcal{X}_{0,h}(\Omega_t) \quad (1.9.10)$$

with

$$u_h = 0 \quad \text{on } \partial\Omega_t, \ i = 1, 2, \ldots$$
$$u_h^0 = u_{0h} \quad \text{in } \Omega_0.$$

Again, we take $\psi_h = u_h^{n+1}$; by exploiting equation (1.9.9) for the treatment of the convective terms, we obtain

$$\left\|u_h^{n+1}\right\|^2_{L_2(\Omega_{t^{n+1}})} + \Delta t\mu \left\|\boldsymbol{\nabla}_{\mathbf{x}}u_h^{n+1}\right\|^2_{L_2(\Omega_{t^{n+1}})}$$
$$\leq -\frac{1}{2}\Delta t \int_{\Omega_{t^{n+1}}} \boldsymbol{\nabla}_{\mathbf{x}}\cdot\mathbf{w}_h|u_h^{n+1}|^2 d\Omega + \Delta t\int_{\Omega_{t^{n+1}}} f^{n+1}u_h^{n+1}\,d\Omega + \int_{\Omega_{t^{n+1}}} u_h^n u_h^{n+1}\,d\Omega$$
$$\leq -\frac{1}{2}\Delta t \int_{\Omega_{t^{n+1}}} \boldsymbol{\nabla}_{\mathbf{x}}\cdot\mathbf{w}_h|u_h^{n+1}|^2 d\Omega + \Delta t\frac{(1+C_\Omega)}{2\mu}\left\|f^{n+1}\right\|^2_{H^{-1}(\Omega_{t^{n+1}})}$$
$$+ \Delta t\frac{\mu}{2}\left\|\boldsymbol{\nabla}_{\mathbf{x}}u_h^{n+1}\right\|^2_{L_2(\Omega_{t^{n+1}})} + \frac{1}{2}\left\|u_h^{n+1}\right\|^2_{L_2(\Omega_{t^{n+1}})} + \frac{1}{2}\left\|u_h^n\right\|^2_{L_2(\Omega_{t^{n+1}})}, \quad (1.9.11)$$

where the last term is evaluated on the configuration at time t^{n+1}; such term can be modified as in (1.8.19):

$$\|u_h^n\|^2_{L_2(\Omega_{t^{n+1}})} = \|u_h^n\|^2_{L_2(\Omega_{t^n})} + \int_{t^n}^{t^{n+1}} \int_{\Omega_t} |u_h^n|^2 \boldsymbol{\nabla}_{\mathbf{x}}\cdot\mathbf{w}_h d\Omega dt. \quad (1.9.12)$$

Consequently we have

$$\left\|u_h^{n+1}\right\|^2_{L_2(\Omega_{t^{n+1}})} + \Delta t\mu \left\|\boldsymbol{\nabla}_{\mathbf{x}}u_h^{n+1}\right\|^2_{L_2(\Omega_{t^{n+1}})} \leq$$
$$\leq \left(\int_{t^n}^{t^{n+1}} \int_{\Omega_t} \boldsymbol{\nabla}_{\mathbf{x}}\cdot\mathbf{w}_h|u_h^n|^2 d\Omega dt - \Delta t\int_{\Omega_{t^{n+1}}} \boldsymbol{\nabla}_{\mathbf{x}}\cdot\mathbf{w}_h|u_h^{n+1}|^2 d\Omega\right)$$
$$+ \|u_h^n\|^2_{L_2(\Omega_{t^n})} + \Delta t\frac{(1+C_\Omega)}{\mu}\left\|f^{n+1}\right\|^2_{H^{-1}(\Omega_{t^{n+1}})} \quad (1.9.13)$$

In this case we cannot obtain a stability result independent on $\mathbf{w}_h$, because of the presence of the term

$$\left(\int_{t^n}^{t^{n+1}} \int_{\Omega_t} \boldsymbol{\nabla}_{\mathbf{x}}\cdot\mathbf{w}_h|u_h^n|^2 d\Omega dt - \Delta t\int_{\Omega_{t^{n+1}}} \boldsymbol{\nabla}_{\mathbf{x}}\cdot\mathbf{w}_h|u_h^{n+1}|^2 d\Omega\right). \quad (1.9.14)$$

Remark 1.9.1 *We may note that even if the scheme satisfies condition (1.8.13), i.e. in the 2D case we compute the second integral in the mid-configuration and consequently we can write:*

$$\Delta t \int_{\Omega_{t^{n+1/2}}} \nabla_{\mathbf{x}} \cdot \mathbf{w}_h |u_h^{n+1}|^2 d\Omega = \int_{t^n}^{t^{n+1}} \int_{\Omega_t} \nabla_{\mathbf{x}} \cdot \mathbf{w}_h |u_h^{n+1}|^2 d\Omega dt, \tag{1.9.15}$$

the term (1.9.14) is equal to

$$\int_{t^n}^{t^{n+1}} \int_{\Omega_t} \nabla_{\mathbf{x}} \cdot \mathbf{w}_h (|u_h^n|^2 - |u_h^{n+1}|^2) d\Omega dt \tag{1.9.16}$$

which is, in general, different than zero.

We can finally obtain a stability inequality, which depends on $\mathbf{w}_h$, from (1.9.13):

$$\begin{aligned} &\left\|u_h^{n+1}\right\|^2_{L_2(\Omega_{t^{n+1}})} + \Delta t\mu \left\|\nabla_{\mathbf{x}} u_h^{n+1}\right\|^2_{L_2(\Omega_{t^{n+1}})} \\ &\quad \leq \Delta t \left\|\nabla_{\mathbf{x}} \cdot \mathbf{w}_h(t^{n+1})\right\|_{L_\infty(\Omega_{t^{n+1}})} \left\|u_h^{n+1}\right\|^2_{L_2(\Omega_{t^{n+1}})} + \Delta t \frac{(1+C_\Omega)}{\mu} \left\|f^{n+1}\right\|^2_{H^{-1}(\Omega_{t^{n+1}})} \\ &\qquad + \left(1 + \Delta t \sup_{t\in(t^n,t^{n+1})} \left\|J_{\mathcal{A}_{t_n,t_{n+1}}} \nabla_{\mathbf{x}} \cdot \mathbf{w}_h\right\|_{L_\infty(\Omega_t)}\right) \left\|u_h^n\right\|^2_{L_2(\Omega_{t^n})}. \end{aligned} \tag{1.9.17}$$

Using the notations

$$\gamma_1^i = \left\|\nabla_{\mathbf{x}} \cdot \mathbf{w}_h(t^i)\right\|_{L_\infty(\Omega_{t^i})}$$

$$\gamma_2^i = \sup_{t\in(t^i,t^{i+1})} \left\|J_{\mathcal{A}_{t_i,t_{i+1}}} \nabla_{\mathbf{x}} \cdot \mathbf{w}_h\right\|_{L_\infty(\Omega_t)}$$

we can rewrite the previous inequality as

$$\begin{aligned} &\left\|u_h^{n+1}\right\|^2_{L_2(\Omega_{t^{n+1}})} + \Delta t\mu \left\|\nabla_{\mathbf{x}} u_h^{n+1}\right\|^2_{L_2(\Omega_{t^{n+1}})} \\ &\quad \leq \Delta t\gamma_1^{n+1} \left\|u_h^{n+1}\right\|^2_{L_2(\Omega_{t^{n+1}})} + (1+\Delta t\gamma_2^n) \left\|u_h^n\right\|^2_{L_2(\Omega_{t^n})} + \Delta t \frac{(1+C_\Omega)}{\mu} \left\|f^{n+1}\right\|^2_{H^{-1}(\Omega_{t^{n+1}})}. \end{aligned} \tag{1.9.18}$$

Summing over the index n we obtain:

$$\begin{aligned} &\left\|u_h^{n+1}\right\|^2_{L_2(\Omega_{t^{n+1}})} + \Delta t\mu \sum_{i=1}^{n+1} \left\|\nabla_{\mathbf{x}} u_h^i\right\|^2_{L_2(\Omega_{t^i})} \\ &\qquad \leq \Delta t\gamma_1^{n+1} \left\|u_h^{n+1}\right\|^2_{L_2(\Omega_{t^{n+1}})} + \Delta t \sum_{i=1}^{n} (\gamma_1^i + \gamma_2^i) \left\|u_h^i\right\|^2_{L_2(\Omega_{t^i})} \\ &\qquad + (1+\Delta t\gamma_2^0) \left\|u_h^0\right\|^2_{L_2(\Omega_{t^0})} + \Delta t \frac{(1+C_\Omega)}{\mu} \sum_{i=1}^{n+1} \left\|f^i\right\|^2_{H^{-1}(\Omega_{t^i})} \\ &\qquad\qquad \leq \Delta t \sum_{i=1}^{n+1} (\gamma_1^i + \gamma_2^i) \left\|u_h^i\right\|^2_{L_2(\Omega_{t^i})} + (1+\Delta t\gamma_2^0) \left\|u_h^0\right\|^2_{L_2(\Omega_{t^0})} \\ &\qquad\qquad\qquad + \Delta t \frac{(1+C_\Omega)}{\mu} \sum_{i=1}^{n+1} \left\|f^i\right\|^2_{H^{-1}(\Omega_{t^i})} \end{aligned} \tag{1.9.19}$$

Let us recall the following discrete Gronwall lemma (for the proof see for instance [80]).

Lemma 1.9.1 *Given $\delta, g_0, a_n, b_n, c_n, \gamma_n$ sequences of non negative numbers for $n \geq 0$, if the following inequality holds*

$$a_n + \delta \sum_{j=0}^{n} b_j \leq \delta \sum_{j=0}^{n} \gamma_j a_j + \delta \sum_{j=0}^{n} c_j + g_0$$

then, for all $n \geq 0$

$$a_n + \delta \sum_{j=0}^{n} b_j \leq exp\left(\delta \sum_{j=0}^{n} \sigma_j \gamma_j\right)\left[\delta \sum_{j=0}^{n} c_j + g_0\right]$$

where $\sigma_j = \frac{1}{1-\gamma_j \delta}$ and $\gamma_j \delta < 1$ for all j.

Then we conclude that

$$\begin{aligned} &\left\|u_h^{n+1}\right\|^2_{L_2(\Omega_{t^{n+1}})} + \Delta t \mu \sum_{i=1}^{n+1} \left\|\nabla_{\mathbf{x}} u_h^i\right\|^2_{L_2(\Omega_{t^i})} \\ &\leq \left((1 + \Delta t \gamma_2^0)\left\|u_h^0\right\|^2_{L_2(\Omega_{t^0})} + \Delta t \frac{(1 + C_\Omega)}{\mu} \sum_{i=1}^{n+1} \left\|f^i\right\|^2_{H^{-1}(\Omega_{t^i})}\right) \exp\left\{\Delta t \sum_{i=1}^{n+1} \frac{\gamma_1^i + \gamma_2^i}{1 - \Delta t(\gamma_1^i + \gamma_2^i)}\right\} \end{aligned} \tag{1.9.20}$$

provided that:

$$\Delta t < \frac{1}{\gamma_1^i + \gamma_2^i} = \left(\left\|\nabla_{\mathbf{x}} \cdot \mathbf{w}_h(t^i)\right\|_{L_\infty(\Omega_{t^i})} + \sup_{t \in (t^i, t^{i+1})} \left\|J_{\mathcal{A}_{t_i, t_{i+1}}} \nabla_{\mathbf{x}} \cdot \mathbf{w}_h\right\|_{L_\infty(\Omega_t)}\right)^{-1}$$

for all $i = 1, \cdots, n+1$. According to this stability analysis, we conclude that the scheme is only conditionally stable even if it is based on an implicit Euler method. Moreover, the maximum allowable time step will depend on the speed at which the domain is deforming.

Chapter 2

Convergence analysis and second order schemes

In the first part of this chapter we will carry out a convergence analysis for the discrete problems introduced in the Chapter 1.

A recent result of convergence for linear problems on moving two-dimensional domains has been obtained by L. Gastaldi in [34]. In that paper, the model problem (1.6.1) is addressed, and its discretisation in space with $\mathbb{P}_1$ finite elements and in time with the Implicit Euler scheme (1.8.17) that satisfies the GCL, are considered; moreover, the ALE mapping is constructed solving an elasticity problem. A linear convergence in both space and time is proved. What seems to emerge from this work is that GCL are important to recover the accuracy properties of the Implicit Euler discretisation.

Following the same approach as in [34], we will carry out a convergence analysis for a general discretisation in space with $\mathbb{P}_k$ isoparametric finite elements, under some regularity hypotheses on the discrete ALE mapping. In Subsection 2.1.1 we present some approximation error estimates for the finite element interpolation and projection operators in the ALE framework. In Subsection 2.1.2 the error on the semi-discrete problem is studied. We will prove a convergence rate of $O(h^k)$ provided the solution is regular enough and the mesh remains regular in time. The main result is contained in Proposition 2.1.1. In particular, we aim at highlighting how the constants appearing in the error estimate depend on the ALE mapping $\mathcal{A}_t$. In Subsection 2.1.4 we will consider a straightforward application of the Implicit Euler scheme to the semi-discrete problem in conservative form. This discretisation does not satisfy the GCL, in general. In Proposition 2.1.2 we will prove a linear convergence in time, under suitable hypotheses of regularity on the data of the differential problem and the discrete ALE mapping. This result shows that even though the GCL are not satisfied, the accuracy of the Implicit Euler scheme is not affected.

In the second part of this Chapter, we will introduce two second order temporal discretisation schemes, both for the conservative and non-conservative formulation, and we will derive the corresponding Geometric Conservation Laws. Both schemes are unconditionally stable when applied to a linear problem on a fixed domain; we will study their stability properties in the context of an ALE formulation. Unfortunately, we have been unable to generalise the unconditional stability result obtained for the Implicit Euler scheme, even when the GCL are satisfied. In all the cases, we could only prove a conditional stability where the maximum allowable time step depends on the rate of deformation of the domain. These results have

been confirmed numerically. Indeed, in Section 2.3 we will present many numerical tests showing how these schemes, when written in ALE form, do not preserve the same stability properties they feature on a fixed domain problem.
Always in Section 2.3 we will carry out a numerical convergence analysis of the time discretisation error.

2.1 Convergence and error analysis

Throughout this section we will adopt the following notations. We will indicate by $\mathcal{A}_{h,t}$ the discrete (finite element) ALE mapping constructed solving either problem (1.4.2) or more complex problems as suggested in [34]. We remind that $\mathcal{A}_{h,t}$ depends on the boundary displacement $g : \partial\Omega_0 \times I \to \mathbb{R}^{d-1}$ (or, more precisely, on its finite element interpolation g_h) and on the type of problem chosen to construct the mapping. We will note by $\Omega_{h,0}$ the finite element approximation of the reference domain Ω_0 and by $\Omega_{h,t} = \mathcal{A}_{h,t}(\Omega_{h,0})$ the computational domain at time t, which might differ from the exact domain Ω_t.
Moreover, as in Section 1.5, let $\mathcal{T}_{h,0}$ be a triangulation of $\Omega_{h,0}$, $\mathcal{T}_{h,t}$ the triangulation induced by the ALE mapping $\mathcal{A}_{h,t}$ on $\Omega_{h,t}$ and $\mathcal{X}_h^k(\Omega_{h,t}) = \mathcal{F}_{k,k}(\mathcal{T}_{h,t})$ the space of isoparametric finite elements of degree k. Finally, we set

$$\hat{h} = \max_{\hat{T}_j \in \mathcal{T}_{h,0}} \operatorname{diam}(\hat{T}_j) \qquad \text{and} \qquad h = \max_{T_j \in \mathcal{T}_{h,t}} \operatorname{diam}(T_j).$$

We will make the following hypotheses : the boundary displacement g and the discrete ALE mapping $\mathcal{A}_{h,t}$ are such that

$$\mathcal{T}_{h,t} \text{ remains a regular mesh } \forall t \in I, \tag{2.1.1}$$

$$\exists C_1, C_2 > 0 \text{ such that } C_1\hat{h} \le h \le C_2\hat{h}. \tag{2.1.2}$$

where the constants C_1 and C_2 might depend on g but not on $\hat{h}$ and t. Here we refer to the definition of regular isoparametric mesh given in [15, chap. 4, pag 241]

2.1.1 Finite element approximation errors in the ALE framework

We introduce the following finite element operators for every $k \ge 1$:

Interpolation operator

$$I_h^k : C^0(\bar{\Omega}_{h,t}) \to \mathcal{X}_h^k(\Omega_{h,t}), \qquad I_h^k u = \sum_{i \in \mathcal{N}^{\mathcal{T}}} u(x_i)\psi_i \tag{2.1.3}$$

where $\{\psi_i, \quad i \in \mathcal{N}^{\mathcal{T}}\}$ is the set of nodal basis functions of $\mathcal{F}_{k,k}(\mathcal{T}_{h,t})$.

Thanks to the hypothesis on the regularity of the mesh $\mathcal{T}_{h,t}$, standard finite element error estimates provide (see e.g. [15])

$$\left\| u - I_h^k u \right\|_{H^m(\Omega_{h,t})} \le C h^{l+1-m} \|u\|_{H^{l+1}(\Omega_{h,t})}, \qquad 1 \le l \le k, \quad m = 0, 1 \tag{2.1.4}$$

Thanks to hypothesis (2.1.2) these error estimates can be rewritten as functions of $\hat{h}$, which is indeed a parameter independent of time.

L^2 projection operator

$$\Pi_h^k:\ L^2(\Omega_{h,t}) \to \mathcal{X}_h^k(\Omega_{h,t}), \qquad \int_{\Omega_{h,t}} \Pi_h^k u\, \psi_h \, d\Omega = \int_{\Omega_{h,t}} u\, \psi_h \, d\Omega \quad \forall \psi_h \in \mathcal{X}_h^k(\Omega_{h,t}) \tag{2.1.5}$$

Again, thanks to the hypothesis on the regularity of the mesh $\mathcal{T}_{h,t}$, standard finite element error estimates provide (see e.g. [15] and [80])

$$\left\| u - \Pi_h^k u \right\|_{H^m(\Omega_{h,t})} \leq C h^{l+1-m} \|u\|_{H^{l+1}(\Omega_{h,t})}, \qquad 0 \leq l \leq k, \ \ m = 0, 1 \tag{2.1.6}$$

Also these error estimates can be rewritten as functions of $\hat{h}$.

Now, we consider a time dependent function $t \to u(t)$ which belongs to $H^{k+1}(\Omega_{h,t})$ for almost every $t \in I$ and with a time derivative $t \to \frac{\partial u}{\partial t}(t) \in H^k(\Omega_{h,t})$.
We are interested in estimating the approximation error on the time derivative $\frac{\partial u}{\partial t}$, both for the interpolation and the L^2 projection operators. We will prove the following two Lemmas :

Lemma 2.1.1 (Interpolation operator) *The following relations hold for all $k \geq 1$:*

$$a) \qquad \frac{\partial}{\partial t} I_h^k u \Big|_{\mathbf{Y}} = I_h^k \frac{\partial u}{\partial t}\Big|_{\mathbf{Y}} \tag{2.1.7}$$

$$b) \qquad \frac{\partial}{\partial t} I_h^k u = I_h^k \frac{\partial u}{\partial t} + \mathbf{w}_h \cdot \boldsymbol{\nabla}(u - I_h^k u) - \left(\mathbf{w}_h \cdot \boldsymbol{\nabla} u - I_h^k (\mathbf{w}_h \cdot \boldsymbol{\nabla} u) \right) \tag{2.1.8}$$

where $\mathbf{w}_h = \frac{\partial \mathcal{A}_{h,t}}{\partial t}$ is the grid velocity. Furthermore, under the assumption that there exists a constant γ, independent on h such that

$$\forall T_j \in \mathcal{T}_{h,t}, \quad \|\mathbf{w}_h\|_{W^{k,\infty}(T_j)} \leq \gamma \tag{2.1.9}$$

we have

$$\left\| \frac{\partial u}{\partial t} - \frac{\partial}{\partial t} I_h^k u \right\|_{L_2(\Omega_{h,t})} \leq C h^k \left(\left\| \frac{\partial u}{\partial t} \right\|_{H^k(\Omega_{h,t})} + \|\mathbf{w}_h\|_{L^\infty(\Omega_{h,t})}^{1/2} \|u\|_{H^{k+1}(\Omega_{h,t})} + \sqrt{\gamma}\, \|u\|_{H^{k+1}(\Omega_{h,t})} \right). \tag{2.1.10}$$

Proof. In the following, we will adopt the usual notation of $\hat{u}$ to indicate a function u defined on the actual domain $\Omega_{h,t}$ and recast to the reference domain $\Omega_{h,0}$ through the discrete ALE mapping $\mathcal{A}_{h,t}$.

a) We have

$$\begin{aligned} \frac{\partial}{\partial t} I_h^k u \Big|_{\mathbf{Y}} = \frac{\partial}{\partial t} \widehat{I_h^k u} \circ \mathcal{A}_{h,t}^{-1} &= \left(\frac{\partial}{\partial t} \sum_{i \in \mathcal{N}^{\mathcal{T}}} \hat{u}(\mathbf{Y}_i, t) \psi_i(\mathbf{Y}) \right) \circ \mathcal{A}_{h,t}^{-1} \\ &= \left(\sum_{i \in \mathcal{N}^{\mathcal{T}}} \frac{\partial}{\partial t} \hat{u}(\mathbf{Y}_i, t) \psi_i(\mathbf{Y}) \right) \circ \mathcal{A}_{h,t}^{-1} = I_h^k \frac{\partial u}{\partial t}\Big|_{\mathbf{Y}}. \end{aligned}$$

b)

$$\frac{\partial}{\partial t} I_h^k u = \frac{\partial}{\partial t} I_h^k u\Big|_{\mathbf{Y}} - \mathbf{w}_h \cdot \nabla I_h^k u = I_h^k \frac{\partial u}{\partial t}\Big|_{\mathbf{Y}} - \mathbf{w}_h \cdot \nabla I_h^k u = I_h^k \left(\frac{\partial u}{\partial t} + \mathbf{w}_h \cdot \nabla u\right) - \mathbf{w}_h \cdot \nabla I_h^k u$$
$$= I_h^k \frac{\partial u}{\partial t} + \mathbf{w}_h \cdot \nabla (u - I_h^k u) - \left(\mathbf{w}_h \cdot \nabla u - I_h^k (\mathbf{w}_h \cdot \nabla u)\right). \quad (2.1.11)$$

From b) we have immediately

$$\left\| \frac{\partial u}{\partial t} - \frac{\partial}{\partial t} I_h^k u \right\|_{L_2(\Omega_{h,t})} \leq \left\| \frac{\partial u}{\partial t} - I_h^k \frac{\partial u}{\partial t} \right\|_{L_2(\Omega_{h,t})} + \left\| \mathbf{w}_h \cdot \nabla (u - I_h^k u) \right\|_{L_2(\Omega_{h,t})}$$
$$+ \left\| \mathbf{w}_h \cdot \nabla u - I_h^k (\mathbf{w}_h \cdot \nabla u) \right\|_{L_2(\Omega_{h,t})}$$

The first two terms in the right hand side give directly the first two terms of the estimate (2.1.10). The third term is more troublesome since the function $\mathbf{w}_h \cdot \nabla u$ does not possess more regularity than $W^{1,\infty}$ on all the domain $\Omega_{h,t}$. Yet, if we consider this term evaluated elementwise, we have :

$$\left\| \mathbf{w}_h \cdot \nabla u - I_h^k (\mathbf{w}_h \cdot \nabla u) \right\|^2_{L_2(\Omega_{h,t})} = \sum_{T_j \in \mathcal{T}_{h,t}} \| \mathbf{w}_h \cdot \nabla u - I_h^k (\mathbf{w}_h \cdot \nabla u) \|^2_{L^2(T_j)}$$
$$\leq \sum_{T_j \in \mathcal{T}_{h,t}} C h^{2k} \| \mathbf{w}_h \cdot \nabla u \|^2_{H^k(T_j)} \leq C \gamma h^{2k} \| u \|^2_{H^{k+1}(\Omega_{h,t})} \quad (2.1.12)$$

and the thesis follows immediately. ■

Lemma 2.1.2 (Projection operator) *The following relations hold*

a) $$\frac{\partial}{\partial t} \Pi_h^k u\Big|_{\mathbf{Y}} = \Pi_h^k \left[\frac{\partial u}{\partial t}\Big|_{\mathbf{Y}} + \nabla_{\mathbf{x}} \cdot \mathbf{w}_h \left(u - \Pi_h^k u\right)\right] \quad (2.1.13)$$

b) $$\frac{\partial}{\partial t} \Pi_h^k u = \Pi_h^k \frac{\partial u}{\partial t} + \Pi_h^k \left[\nabla_{\mathbf{x}} \cdot \mathbf{w}_h \left(u - \Pi_h^k u\right)\right] + \Pi_h^k (\mathbf{w}_h \cdot \nabla u) - \mathbf{w}_h \cdot \nabla (\Pi_h^k u). \quad (2.1.14)$$

Moreover, under the same hypothesis (2.1.9) as in the previous Lemma, we have

$$\left\| \frac{\partial u}{\partial t} - \Pi_h^k \frac{\partial u}{\partial t} \right\|_{L_2(\Omega_{h,t})} \leq C h^k \left(\left\| \frac{\partial u}{\partial t} \right\|_{H^k(\Omega_{h,t})} + h \| \nabla_{\mathbf{x}} \cdot \mathbf{w}_h \|^{1/2}_{L^\infty(\Omega_{h,t})} \| u \|_{H^{k+1}(\Omega_{h,t})} \right.$$
$$\left. + \| \mathbf{w}_h \|^{1/2}_{L^\infty(\Omega_{h,t})} \| u \|_{H^{k+1}(\Omega_{h,t})} + \sqrt{\gamma} \| u \|_{H^{k+1}(\Omega_{h,t})} \right). \quad (2.1.15)$$

Proof

a) In order to characterize the ALE derivative of the L^2 projection of u, we derive in time relation (2.1.5)

$$\frac{d}{dt} \int_{\Omega_t} \Pi_h^k u(t) \psi_h \, d\Omega = \frac{d}{dt} \int_{\Omega_t} u(t) \psi_h \, d\Omega,$$

which is equivalent to

$$\int_{\Omega_{h,0}} J_{\mathcal{A}_{h,t}} \nabla_{\mathbf{x}} \cdot \mathbf{w}_h \widehat{\Pi_h^k u} \, \widehat{\psi}_h + \int_{\Omega_{h,0}} J_{\mathcal{A}_{h,t}} \frac{\partial}{\partial t} \widehat{\Pi_h^k u} \, \widehat{\psi}_h = \int_{\Omega_{h,0}} J_{\mathcal{A}_{h,t}} \nabla_{\mathbf{x}} \cdot \mathbf{w}_h \hat{u} \, \widehat{\psi}_h + \int_{\Omega_{h,0}} J_{\mathcal{A}_{h,t}} \frac{\partial \hat{u}}{\partial t} \, \widehat{\psi}_h.$$

i.e.

$$\int_{\Omega_{h,t}} \frac{\partial}{\partial t}\Pi_h^k u\Big|_{\mathbf{Y}} \psi_h = \int_{\Omega_{h,t}} \frac{\partial u}{\partial t}\Big|_{\mathbf{Y}} \psi_h + \int_{\Omega_{h,t}} \boldsymbol{\nabla}_{\mathbf{x}} \cdot \mathbf{w}_h u\, \psi_h - \int_{\Omega_{h,t}} \boldsymbol{\nabla}_{\mathbf{x}} \cdot \mathbf{w}_h \Pi_h^k u\, \psi_h. \quad (2.1.16)$$

For all $t \in I$, $\widehat{\Pi_h^k u(t)} \in \mathcal{X}_h^k(\Omega_{h,0})$, thus it can be expanded on the basis $\{\widehat{\psi}_i,\ i \in \mathcal{N}^{\mathcal{T}}\}$ of $\mathcal{X}_h^k(\Omega_{h,0})$:

$$\widehat{\Pi_h^k u}(\mathbf{Y},t) = \sum_{i\in\mathcal{N}^{\mathcal{T}}} \alpha_i(t)\widehat{\psi}_i(\mathbf{Y}).$$

Then,

$$\frac{\partial}{\partial t}\widehat{\Pi_h^k u} = \frac{\partial}{\partial t}\sum_{i\in\mathcal{N}^{\mathcal{T}}} \alpha_i(t)\widehat{\psi}_i(\mathbf{Y}) = \sum_{i\in\mathcal{N}^{\mathcal{T}}} \frac{d\alpha_i(t)}{dt}\widehat{\psi}_i(\mathbf{Y}) \in \mathcal{X}_h^k(\Omega_{h,0})$$

and

$$\frac{\partial}{\partial t}\Pi_h^k u\Big|_{\mathbf{Y}} = \sum_{i\in\mathcal{N}^{\mathcal{T}}} \frac{d\alpha_i(t)}{dt}\psi_i(\mathbf{x},t) \in \mathcal{X}_h^k(\Omega_{h,t}).$$

We deduce, from (2.1.16), that

$$\frac{\partial}{\partial t}\Pi_h^k u\Big|_{\mathbf{Y}} = \Pi_h^k\left[\frac{\partial u}{\partial t}\Big|_{\mathbf{Y}} + \boldsymbol{\nabla}_{\mathbf{x}} \cdot \mathbf{w}_h(u - \Pi_h^k u)\right].$$

b) By applying the definition of the distributional Eulerian derivative, we have $\forall \zeta \in \mathcal{D}(\Omega_{h,t}\times I)$

$$\begin{aligned} < \frac{\partial}{\partial t}\Pi_h^k u, \zeta > &= -\int_I\int_{\Omega_{h,t}} \Pi_h^k u \frac{\partial \zeta}{\partial t} = -\int_I\int_{\Omega_{h,t}} \Pi_h^k u\left(\frac{\partial \zeta}{\partial t}\Big|_{\mathbf{Y}} - \mathbf{w}_h \cdot \boldsymbol{\nabla}\zeta\right) \\ &= -\int_I\int_{\Omega_{h,t}} \Pi_h^k u \frac{\partial \zeta}{\partial t}\Big|_{\mathbf{Y}} - \int_I\int_{\Omega_{h,t}} \boldsymbol{\nabla}_{\mathbf{x}} \cdot \left(\mathbf{w}_h \Pi_h^k u\right)\zeta \quad (2.1.17) \end{aligned}$$

The first term on the right hand side can be developed as follows

$$\begin{aligned} -\int_I\int_{\Omega_{h,t}} \Pi_h^k u \frac{\partial \zeta}{\partial t}\Big|_{\mathbf{Y}} &= -\int_I\int_{\Omega_{h,0}} J_{\mathcal{A}_{h,t}} \widehat{\Pi_h^k u}\frac{\partial \hat{\zeta}}{\partial t} \\ &= \int_I\int_{\Omega_{h,0}} J_{\mathcal{A}_{h,t}} \boldsymbol{\nabla}_{\mathbf{x}} \cdot \mathbf{w}_h \widehat{\Pi_h^k u}\,\hat{\zeta} + \int_I\int_{\Omega_{h,0}} J_{\mathcal{A}_{h,t}} \frac{\partial}{\partial t}\widehat{\Pi_h^k u}\,\hat{\zeta} \\ &= \int_I\int_{\Omega_{h,t}} \boldsymbol{\nabla}_{\mathbf{x}} \cdot \mathbf{w}_h \Pi_h^k u\,\zeta + \int_I\int_{\Omega_{h,t}} \frac{\partial}{\partial t}\Pi_h^k u\Big|_{\mathbf{Y}}\zeta = \{\text{using (2.1.13)}\} \\ &= \int_I\int_{\Omega_{h,t}} \boldsymbol{\nabla}_{\mathbf{x}} \cdot \mathbf{w}_h \Pi_h^k u\,\zeta + \int_I\int_{\Omega_{h,t}} \Pi_h^k\left[\frac{\partial u}{\partial t}\Big|_{\mathbf{Y}} + \boldsymbol{\nabla}_{\mathbf{x}} \cdot \mathbf{w}_h(u - \Pi_h^k u)\right]\zeta \\ &= \int_I\int_{\Omega_{h,t}} \boldsymbol{\nabla}_{\mathbf{x}} \cdot \mathbf{w}_h \Pi_h^k u\,\zeta + \int_I\int_{\Omega_{h,t}} \Pi_h^k\left[\frac{\partial u}{\partial t} + \boldsymbol{\nabla}_{\mathbf{x}} \cdot (\mathbf{w}_h u) - \boldsymbol{\nabla}_{\mathbf{x}} \cdot \mathbf{w}_h \Pi_h^k u\right]\zeta \end{aligned}$$

Using this result in (2.1.17) we obtain (2.1.14) for almost every $(\mathbf{x},t) \in \Omega_{h,t} \times I$.

Equation (2.1.14) can be rewritten equivalently as

$$\frac{\partial}{\partial t}\Pi_h^k u = \Pi_h^k \frac{\partial u}{\partial t} + \Pi_h^k \left[\nabla_{\mathbf{x}} \cdot \mathbf{w}_h (u - \Pi_h^k u)\right] + \mathbf{w}_h \cdot \nabla (u - \Pi_h^k u) - \left[\mathbf{w}_h \cdot \nabla u - \Pi_h^k (\mathbf{w}_h \cdot \nabla u)\right] \tag{2.1.18}$$

Then we have directly

$$\begin{aligned}\left\| \frac{\partial u}{\partial t} - \frac{\partial}{\partial t}\Pi_h^k u \right\|_{L_2(\Omega_{h,t})} \leq & \left\| \frac{\partial u}{\partial t} - \Pi_h^k \frac{\partial u}{\partial t} \right\|_{L_2(\Omega_{h,t})} + \left\| \nabla_{\mathbf{x}} \cdot \mathbf{w}_h (u - \Pi_h^k u) \right\|_{L_2(\Omega_{h,t})} \\ & + \left\| \mathbf{w}_h \cdot \nabla (u - \Pi_h^k u) \right\|_{L_2(\Omega_{h,t})} + \left\| \mathbf{w}_h \cdot \nabla u - \Pi_h^k (\mathbf{w}_h \cdot \nabla u) \right\|_{L_2(\Omega_{h,t})}\end{aligned}$$

where we have exploited the fact that $\|\Pi_h^k\|_{\mathcal{L}(L^2(\Omega_{h,t}),L^2(\Omega_{h,t}))} = 1$. By proceeding as in the proof of Lemma 2.1.1 and evaluating the last term elementwise we obtain the desired result. ■

2.1.2 Error estimate for the semi-discrete problem

We aim at comparing the solution of the differential problem (1.6.1) with that of its semi-discrete counterpart (1.8.1). We remark that the error estimate we will obtain is valid also for problem (1.9.1) in non-conservative formulation. Indeed, the two formulations (1.8.1) and (1.9.1) are equivalent as far as no discretisation in time is carried out.

To begin with, in order to lighten the presentation, we will make first the hypothesis that the real domain Ω_t can be represented exactly by the discrete ALE mapping $\mathcal{A}_{h,t}$, i.e. $\Omega_{h,t} \equiv \Omega_t$, $\forall t \in I$. We will remove this hypothesis in Remark 2.1.1. Then, we can write problem (1.6.1) in weak-ALE form (1.6.12) adopting the discrete ALE mapping. Thus, we have to compare the differential problem : *find* $u(t) \in H_0^1(\Omega_{h,t})$, $u(t_0) = u_0$, *such that*

$$\begin{aligned}\frac{d}{dt}\int_{\Omega_{h,t}} \psi u d\Omega + \mu \int_{\Omega_{h,t}} \nabla_{\mathbf{x}}\psi \nabla_{\mathbf{x}} u d\Omega + \int_{\Omega_{h,t}} \psi \nabla_{\mathbf{x}} \cdot [(\boldsymbol{\beta} - \mathbf{w}_h)u]\, d\Omega = \\ = \int_{\Omega_{h,t}} f\psi\, d\Omega \qquad \forall \psi \in \mathcal{X}(\Omega_t), \text{ a.e. in } I,\end{aligned} \tag{2.1.19}$$

with the semi-discrete one : *find* $u_h(t) \in \mathcal{X}_{0,h}^k(\Omega_{h,t})$, $u_h(t_0) = u_{0h}$, *such that*

$$\begin{aligned}\frac{d}{dt}\int_{\Omega_{h,t}} \psi_h u_h d\Omega + \mu \int_{\Omega_{h,t}} \nabla_{\mathbf{x}}\psi_h \nabla_{\mathbf{x}} u_h d\Omega + \int_{\Omega_{h,t}} \psi_h \nabla_{\mathbf{x}} \cdot [(\boldsymbol{\beta} - \mathbf{w}_h)u_h]\, d\Omega = \\ = \int_{\Omega_{h,t}} f\psi_h\, d\Omega \qquad \forall \psi_h \in \mathcal{X}_{0,h}^k(\Omega_{h,t}), \text{ a.e. in } I,\end{aligned} \tag{2.1.20}$$

where we have noted $\mathcal{X}_{0,h}^k(\Omega_{h,t}) = \mathcal{X}_h^k(\Omega_{h,t}) \cap H_0^1(\Omega_{h,t})$. For the purpose of the convergence analysis, we define the space $V(I; \mathcal{X}_{0,h}^k)$ of functions $t \to v_h(t) \in \mathcal{X}_{0,h}^k(\Omega_{h,t})$ such that

$$v_h(t) = \sum_{i \in \mathcal{N}^{\mathcal{T}}} \alpha_i(t)\psi_i, \quad \alpha_i(t) \in H^1(I), \ \forall i \in \mathcal{N}^{\mathcal{T}} \tag{2.1.21}$$

Proposition 2.1.1 *The following estimate holds*

$$\frac{1}{2}\|(u(t)-u_h(t))\|^2_{L_2(\Omega_{h,t})}+\frac{\mu}{4}\int_{t_0}^{t}\|\nabla_{\mathbf{x}}(u(s)-u_h(s))\|^2_{L_2(\Omega_{h,s})}\,ds\leq$$

$$\|u_0-u_{0h}\|^2_{L_2(\Omega_{h,0})}+\inf_{v_h\in V(I;\mathcal{X}^k_{0,h})}\left\{\|u(t)-v_h(t)\|^2_{L_2(\Omega_{h,t})}\right.$$

$$+\|u_0-v_h(t_0)\|^2_{L_2(\Omega_{h,0})}+\int_{t_0}^{t}\left[\frac{2C_\Omega}{\mu}\left\|\frac{\partial}{\partial t}(u(s)-v_h(s))\right\|^2_{L_2(\Omega_{h,s})}\right.$$

$$\left.\left.+\left(\frac{5\mu}{2}+\frac{2C_\Omega\|\beta\|^2_{L_\infty(\Omega_{h,s})}}{\mu}\right)\|\nabla_{\mathbf{x}}(u(s)-v_h(s))\|^2_{L_2(\Omega_{h,s})}\right]ds\right\}. \quad (2.1.22)$$

Moreover, should the exact solution u belong to $L^2(I;H^{k+1}(\Omega_{h,t}))\cap L^\infty(I;H^k(\Omega_{h,t}))$, $k\geq 1$, with time derivative $\frac{\partial u}{\partial t}\in L^2(I;H^k(\Omega_{h,t}))$, then, under the hypotheses (2.1.1),(2.1.2) and (2.1.9) on the discrete ALE mapping and the condition $\|u_0-u_{0h}\|_{L_2(\Omega_{h,0})}\leq C\hat{h}^k\|u_0\|_{H^k(\Omega_{h,0})}$, we have the following error estimate

$$\frac{1}{2}\|(u(t)-u_h(t))\|^2_{L_2(\Omega_{h,t})}+\frac{\mu}{4}\int_{t_0}^{t}\|\nabla_{\mathbf{x}}(u(s)-u_h(s))\|^2_{L_2(\Omega_{h,t})}\,ds$$

$$\leq C\hat{h}^{2k}\left\{\|u(t)\|^2_{H^k(\Omega_{h,t})}+\|u_0\|^2_{H^k(\Omega_{h,0})}+\int_{t_0}^{t}\left(\frac{5\mu}{2}+\frac{2C_\Omega\|\beta\|^2_{L_\infty(\Omega_{h,s})}}{\mu}\right)\|u(s)\|^2_{H^{k+1}(\Omega_{h,s})}\,ds\right.$$

$$\left.+\int_{t_0}^{t}\frac{2C_\Omega}{\mu}\left(\left\|\frac{\partial u(s)}{\partial t}\right\|_{H^k(\Omega_{h,s})}+\left(\|\mathbf{w}_h\|^{1/2}_{L^\infty(\Omega_{h,s})}+\sqrt{\gamma}\right)\|u(s)\|_{H^{k+1}(\Omega_{h,s})}\right)^2 ds\right\}. \quad (2.1.23)$$

Proof. We take in (2.1.19) as test function a discrete function ψ_h and we subtract it to equation (2.1.20). We obtain, $\forall\psi_h\in\mathcal{X}^k_{0,h}(\Omega_{h,t})$

$$\frac{d}{dt}\int_{\Omega_{h,t}}\psi_h(u_h-u)d\Omega+\mu\int_{\Omega_{h,t}}\nabla_{\mathbf{x}}\psi_h\nabla_{\mathbf{x}}(u_h-u)d\Omega+\int_{\Omega_{h,t}}\psi_h\nabla_{\mathbf{x}}\cdot[(\boldsymbol{\beta}-\mathbf{w}_h)(u_h-u)]\,d\Omega=0. \quad (2.1.24)$$

Should we allow the test function ψ_h to be time dependent, i.e. $\psi_h(t)\in V(I;\mathcal{X}^k_{0,h})$, equation (2.1.24) should be rewritten in the form (see section 1.8.1 and in particular equation (1.8.5))

$$\frac{d}{dt}\int_{\Omega_{h,t}}\psi_h(u_h-u)d\Omega-\int_{\Omega_{h,t}}(u_h-u)\left.\frac{\partial\psi_h}{\partial t}\right|_{\mathbf{Y}}d\Omega+\mu\int_{\Omega_{h,t}}\nabla_{\mathbf{x}}\psi_h\nabla_{\mathbf{x}}(u_h-u)d\Omega$$

$$+\int_{\Omega_{h,t}}\psi_h\nabla_{\mathbf{x}}\cdot[(\boldsymbol{\beta}-\mathbf{w}_h)(u_h-u)]\,d\Omega=0. \quad (2.1.25)$$

We write, now, $\psi_h(t) = u_h(t) - v_h(t)$ and we elaborate (2.1.25) as follows

$$\frac{d}{dt}\|u_h - v_h\|^2_{L_2(\Omega_{h,t})} - \int_{\Omega_{h,t}} (u_h - v_h)\left.\frac{\partial(u_h - v_h)}{\partial t}\right|_{\mathbf{Y}} d\Omega + \mu\,\|\nabla_{\mathbf{x}}(u_h - v_h)\|^2_{L_2(\Omega_{h,t})}$$
$$+ \int_{\Omega_{h,t}} (u_h - v_h)\nabla_{\mathbf{x}} \cdot [(\boldsymbol{\beta} - \mathbf{w}_h)(u_h - v_h)]\, d\Omega = \frac{d}{dt}\int_{\Omega_{h,t}} (u_h - v_h)(u - v_h)d\Omega$$
$$- \int_{\Omega_{h,t}} (u - v_h)\left.\frac{\partial(u_h - v_h)}{\partial t}\right|_{\mathbf{Y}} d\Omega + \mu \int_{\Omega_{h,t}} \nabla_{\mathbf{x}}(u_h - v_h)\nabla_{\mathbf{x}}(u - v_h)d\Omega$$
$$+ \int_{\Omega_{h,t}} (u_h - v_h)\nabla_{\mathbf{x}} \cdot [(\boldsymbol{\beta} - \mathbf{w}_h)(u - v_h)]\, d\Omega \quad (2.1.26)$$

The left hand side can be manipulated as in section 1.8.1, leading to

$$\text{left hand side } = \frac{1}{2}\frac{d}{dt}\|u_h - v_h\|^2_{L_2(\Omega_{h,t})} + \mu\,\|\nabla_{\mathbf{x}}(u_h - v_h)\|^2_{L_2(\Omega_{h,t})}. \quad (2.1.27)$$

On the other hand, the first term on the right hand side gives

$$\frac{d}{dt}\int_{\Omega_{h,t}} (u_h - v_h)(u - v_h)d\Omega$$
$$= \int_{\Omega_{h,t}} \frac{\partial}{\partial t}\left[(u_h - v_h)(u - v_h)\right]\Big|_{\mathbf{Y}} d\Omega + \int_{\Omega_{h,t}} \nabla_{\mathbf{x}} \cdot \mathbf{w}_h\left[(u_h - v_h)(u - v_h)\right] d\Omega$$
$$= \int_{\Omega_{h,t}} (u - v_h)\left.\frac{\partial(u_h - v_h)}{\partial t}\right|_{\mathbf{Y}} d\Omega + \int_{\Omega_{h,t}} \frac{\partial(u - v_h)}{\partial t}(u_h - v_h)d\Omega$$
$$+ \int_{\Omega_{h,t}} \nabla_{\mathbf{x}} \cdot [\mathbf{w}_h(u - v_h)]\,(u_h - v_h)d\Omega. \quad (2.1.28)$$

Inserting (2.1.27) and (2.1.28) in (2.1.26) we obtain then

$$\frac{1}{2}\frac{d}{dt}\|u_h - v_h\|^2_{L_2(\Omega_{h,t})} + \mu\,\|\nabla_{\mathbf{x}}(u_h - v_h)\|^2_{L_2(\Omega_{h,t})} = \int_{\Omega_{h,t}} \frac{\partial(u - v_h)}{\partial t}(u_h - v_h)d\Omega$$
$$+ \mu \int_{\Omega_{h,t}} \nabla_{\mathbf{x}}(u_h - v_h)\nabla_{\mathbf{x}}(u - v_h)d\Omega + \int_{\Omega_{h,t}} (u_h - v_h)\boldsymbol{\beta} \cdot \nabla_{\mathbf{x}}(u - v_h)d\Omega \quad (2.1.29)$$

where, in the last term, we have exploited the fact that $\nabla_{\mathbf{x}} \cdot \boldsymbol{\beta} = 0$. The right hand side in

(2.1.29) can be bounded as follows

$$\begin{aligned}
&\int_{\Omega_{h,t}} \frac{\partial(u-v_h)}{\partial t}(u_h-v_h)d\Omega + \mu\int_{\Omega_{h,t}} \nabla_{\mathbf{x}}(u_h-v_h)\nabla_{\mathbf{x}}(u-v_h)d\Omega \\
&\qquad + \int_{\Omega_{h,t}} (u_h-v_h)\,\boldsymbol{\beta}\cdot\nabla_{\mathbf{x}}(u-v_h)d\Omega \\
&\leq \left\|\frac{\partial}{\partial t}(u-v_h)\right\|_{L_2(\Omega_{h,t})} \|(u_h-v_h)\|_{L_2(\Omega_{h,t})} \\
&\qquad + \mu\,\|\nabla_{\mathbf{x}}(u_h-v_h)\|_{L_2(\Omega_{h,t})}\,\|\nabla_{\mathbf{x}}(u-v_h)\|_{L_2(\Omega_{h,t})} \\
&\qquad + \|\boldsymbol{\beta}\|_{L_\infty(\Omega_{h,t})}\,\|(u_h-v_h)\|_{L_2(\Omega_{h,t})}\,\|\nabla_{\mathbf{x}}(u-v_h)\|_{L_2(\Omega_{h,t})} \\
&\leq \frac{C_\Omega}{\mu}\left\|\frac{\partial}{\partial t}(u-v_h)\right\|^2_{L_2(\Omega_{h,t})} + \frac{\mu}{4}\,\|\nabla_{\mathbf{x}}(u_h-v_h)\|^2_{L_2(\Omega_{h,t})} \\
&\qquad + \frac{\mu}{4}\,\|\nabla_{\mathbf{x}}(u_h-v_h)\|^2_{L_2(\Omega_{h,t})} + \mu\,\|\nabla_{\mathbf{x}}(u-v_h)\|^2_{L_2(\Omega_{h,t})} \\
&\qquad + \frac{\mu}{4}\,\|\nabla_{\mathbf{x}}(u_h-v_h)\|^2_{L_2(\Omega_{h,t})} + \frac{C_\Omega\,\|\boldsymbol{\beta}\|^2_{L_\infty(\Omega_{h,t})}}{\mu}\,\|\nabla_{\mathbf{x}}(u-v_h)\|^2_{L_2(\Omega_{h,t})}.
\end{aligned}$$

By putting this result in (2.1.29) and integrating in time between t_0 and t, $t\in I$, we have the following estimate for $\|u_h(t)-v_h(t)\|^2_{L_2(\Omega_{h,t})}$:

$$\begin{aligned}
&\|u_h(t)-v_h(t)\|^2_{L_2(\Omega_{h,t})} + \frac{\mu}{2}\int_{t_0}^{t}\|\nabla_{\mathbf{x}}(u_h(s)-v_h(s))\|^2_{L_2(\Omega_{h,t})}\,ds \\
&\qquad \leq \|u_h(t_0)-v_h(t_0)\|^2_{L_2(\Omega_{h,t})} + \int_{t_0}^{t}\left\{\frac{2C_\Omega}{\mu}\left\|\frac{\partial}{\partial t}(u(s)-v_h(s))\right\|^2_{L_2(\Omega_{h,t})}\right. \\
&\qquad\qquad \left. + \left(2\mu + \frac{2C_\Omega\,\|\boldsymbol{\beta}\|^2_{L_\infty(\Omega_{h,t})}}{\mu}\right)\|\nabla_{\mathbf{x}}(u(s)-v_h(s))\|^2_{L_2(\Omega_{h,t})}\right\}ds. \quad (2.1.30)
\end{aligned}$$

Finally, by observing that

$$\|u_h(t_0)-v_h(t_0)\|^2_{L_2(\Omega_{h,t})} \leq \|u_{0h}-u_0\|^2_{L_2(\Omega_{h,t})} + \|u_0-v_h(t_0)\|^2_{L_2(\Omega_{h,t})}$$

and that

$$\begin{aligned}
&\frac{1}{2}\,\|u(t)-u_h(t)\|^2_{L_2(\Omega_{h,t})} + \frac{\mu}{4}\int_{t_0}^{t}\|\nabla_{\mathbf{x}}(u(s)-u_h(s))\|^2_{L_2(\Omega_{h,t})}\,ds \\
&\qquad \leq \|u(t)-v_h(t)\|^2_{L_2(\Omega_{h,t})} + \frac{\mu}{2}\int_{t_0}^{t}\|\nabla_{\mathbf{x}}(u(s)-v_h(s))\|^2_{L_2(\Omega_{h,t})}\,ds \\
&+ \|u_h(t)-v_h(t)\|^2_{L_2(\Omega_{h,t})} + \frac{\mu}{2}\int_{t_0}^{t}\|\nabla_{\mathbf{x}}(u_h(s)-v_h(s))\|^2_{L_2(\Omega_{h,t})}\,ds, \qquad \forall v_h(t)\in V(I;\mathcal{X}^k_{0,h}),
\end{aligned}$$

inequality (2.1.22) follows immediately.

We can take, now, $v_h(t) = I^k_h u(t)$ (or, equivalently $v_h(t) = \Pi^k_h u(t)$ [1]) Observe that form (2.1.8) we deduce that $\frac{\partial}{\partial t} I^k_h u(t) \in L^2(I;\mathcal{X}^k_{0,h}(\Omega_{h,t}))$ and then $I^k_h u(t)\in V(I;\mathcal{X}^k_{0,h})$. Thus, the

[1] The operator Π^k_h should be defined in this case as the L^2 projection onto the subspace $\mathcal{X}^k_{0,h}(\Omega_{h,t})$, i.e. $\int_{\Omega_{h,t}} \Pi^k_h u\,\psi_h\,d\Omega = \int_{\Omega_{h,t}} u\,\psi_h\,d\Omega \quad \forall\psi_h\in\mathcal{X}^k_{0,h}(\Omega_{h,t})$. Inequalities (2.1.6) and (2.1.15) still hold $\forall u\in H^1_0(\Omega_{h,t})$.

choice $v_h(t) = I_h^k u(t)$ in (2.1.22) is admissible (analogous arguments hold for $v_h(t) = \Pi_h^k u(t)$). Hence, by exploiting in (2.1.22) inequalities (2.1.4) and (2.1.10), under the hypotheses (2.1.1), (2.1.2) and (2.1.9) on the discrete ALE mapping and the condition $\|u_{0h} - u_0\|_{L_2(\Omega_{h,0})} \leq C\hat{h}^k \|u_0\|_{H^k(\Omega_{h,0})}$, we easily obtain the error estimate (2.1.23).
■

Remark 2.1.1 *Should the computational domain $\Omega_{h,t}$ differs form the exact domain Ω_t (given that the boundary $\partial\Omega_{h,t}$ is the finite element interpolation of $\partial\Omega_t$) we could proceed as proposed in [34] (see also [15]). We consider a domain $\widetilde{\Omega_t}$ which contains both Ω_t and $\Omega_{h,t}$ for all $t \in I$. Should the solution $u(t)$ of (1.6.1) belong to $L^2(I; H^{k+1}(\Omega_t)) \cap L^\infty(I; H^k(\Omega_t))$, $k \geq 1$ with time derivative $\frac{\partial u}{\partial t} \in L^2(I; H^k(\Omega_t))$, we can always introduce an extension $\widetilde{u(t)}$ of $u(t)$ to $\widetilde{\Omega_t}$ such that*

$$\widetilde{u} \in L^2(I; H^{k+1}(\widetilde{\Omega_t})) \cap L^\infty(I; H^k(\widetilde{\Omega_t})), \quad \frac{\partial \widetilde{u}}{\partial t} \in L^2(I; H^k(\widetilde{\Omega_t}))$$

and

$$\begin{aligned}
&\|\widetilde{u}\|_{L^2(I;H^{k+1}(\widetilde{\Omega_t}))} \leq C\|u\|_{L^2(I;H^{k+1}(\Omega_t))} \\
&\|\widetilde{u}\|_{L^\infty(I;H^k(\widetilde{\Omega_t}))} \leq C\|u\|_{L^\infty(I;H^k(\Omega_t))} \\
&\left\|\frac{\partial \widetilde{u}}{\partial t}\right\|_{L^2(I;H^k(\widetilde{\Omega_t}))} \leq C \left\|\frac{\partial u}{\partial t}\right\|_{L^2(I;H^k(\Omega_t))}
\end{aligned}$$

Clearly, this extension should be an extension both in space and time to allow the time derivative to belong to $L^2(I; H^k(\widetilde{\Omega_t}))$. We can not just take an extension $\tilde{u} \in H^{k+1}(\widetilde{\Omega_t})$ at each give $t \in I$. If now $\beta \in \left[W^{1,\infty}(\Omega_t)\right]^d$, a.e. in I, we can introduce suitable extensions $\widetilde{f}$ and $\widetilde{\beta}$ of f and β on $\widetilde{\Omega_t}$ such that

$$\frac{\partial \widetilde{u}}{\partial t} - \mu\Delta\widetilde{u} + \boldsymbol{\nabla}_{\mathbf{x}} \cdot (\widetilde{\beta}\widetilde{u}) = \widetilde{f}, \quad \text{in } \widetilde{\Omega_t}. \tag{2.1.31}$$

By multiplying (2.1.31) by a discrete test function ψ_h (extended by zero outside $\Omega_{h,t}$) and integrating over $\Omega_{h,t}$, we can write (2.1.31) in the weak-ALE formulation, using the discrete ALE mapping $\mathcal{A}_{h,t}$:

$$\begin{aligned}
\frac{d}{dt}\int_{\Omega_{h,t}} \psi_h \widetilde{u} d\Omega + \mu \int_{\Omega_{h,t}} \boldsymbol{\nabla}_{\mathbf{x}}\psi_h \boldsymbol{\nabla}_{\mathbf{x}}\widetilde{u} d\Omega + \int_{\Omega_{h,t}} \psi_h \boldsymbol{\nabla}_{\mathbf{x}} \cdot \left[(\widetilde{\beta} - \mathbf{w}_h)\widetilde{u}\right] d\Omega = \\
= \int_{\Omega_{h,t}} \widetilde{f}\psi_h \, d\Omega \qquad \forall \psi_h \in \mathcal{X}_{0,h}^k(\Omega_{h,t}), \text{ a.e. in } I,
\end{aligned} \tag{2.1.32}$$

which has to be compared to the semi-discrete problem : find $u_h(t) \in \mathcal{X}_{0,h}^k(\Omega_{h,t})$, $u_h(t_0) = u_{0h}$, such that

$$\begin{aligned}
\frac{d}{dt}\int_{\Omega_{h,t}} \psi_h u_h d\Omega + \mu \int_{\Omega_{h,t}} \boldsymbol{\nabla}_{\mathbf{x}}\psi_h \boldsymbol{\nabla}_{\mathbf{x}} u_h d\Omega + \int_{\Omega_{h,t}} \psi_h \boldsymbol{\nabla}_{\mathbf{x}} \cdot \left[(\widetilde{\beta} - \mathbf{w}_h)u_h\right] d\Omega = \\
= \int_{\Omega_{h,t}} \widetilde{f}\psi_h \, d\Omega \qquad \forall \psi_h \in \mathcal{X}_{0,h}^k(\Omega_{h,t}), \text{ a.e. in } I.
\end{aligned} \tag{2.1.33}$$

For problems (2.1.32) and (2.1.33), exactly the same error estimate as in Proposition 2.1.1 hold, replacing u by $\widetilde{u}$
To avoid the practical construction of the extended data $\widetilde{f}$ and $\widetilde{\beta}$, we may adopt numerical integration schemes, which use only quadrature nodes internal to Ω_t to compute the integrals in (2.1.33) (so that the values of $\widetilde{f}$ and $\widetilde{\beta}$ coincide with those of f and β, respectively, provided that f and β are continuous functions). In such a case, in estimates (2.1.22) and (2.1.23) terms deriving from the numerical approximations of the integrals will appear as well. The rate of convergence will be in general preserved if k-th order quadrature rules are employed.

2.1.3 A priori estimates for the semi-discrete solution

In order to carry out an error analysis for the fully-discrete problem, which will be presented in the next section, we need firstly to derive some a-priori estimates for the solution of the semi-discrete problem (2.1.20). A first result has already been given in section 1.8.1, stating that

$$\|u_h(t)\|^2_{L_2(\Omega_{h,t})} + \mu \int_{t_0}^{t} \|\nabla_{\mathbf{x}} u_h(s)\|^2_{L_2(\Omega_{h,s})}\, ds \leq C_1 \tag{2.1.34}$$

where the constant C_1 depends on $\|u_{0h}\|^2_{L_2(\Omega_0)}$ and $\int_0^t \|f(s)\|^2_{H^{-1}(\Omega_s)}\, ds$ but is independent of h.
Let us now consider a discrete ALE mapping $\mathcal{A}_{h,t} \in \left[W^{1,\infty}(\Omega_0 \times I)\right]^d$ that satisfies the hypothesis of Proposition 1.3.1; we introduce the matrix

$$A : \Omega_0 \times I \to \mathbb{R}^{d^2}, \qquad A = J^{-1}_{\mathcal{A}_{h,t}} \frac{\partial}{\partial t} \left(Cof \mathbf{J}_{\mathcal{A}_{h,t}}\right) \mathbf{J}^T_{\mathcal{A}_{h,t}} \tag{2.1.35}$$

where $\mathbf{J}_{\mathcal{A}_{h,t}}$ is the Jacobian matrix of $\mathcal{A}_{h,t}$ and $Cof \mathbf{J}_{\mathcal{A}_{h,t}}$ is the co-factor matrix of $\mathbf{J}_{\mathcal{A}_{h,t}}$. Observe that, thanks to the hypotheses on $\mathcal{A}_{h,t}$, the quantity $\|A\|_{L^\infty(\Omega_0 \times I)}$ is bounded.
Further regularity results on the solution of the semi-discrete problem (2.1.20) can be found in the work by L. Gastaldi [34]. We may summarize them as follows

Lemma 2.1.3 *Given a forcing term $f \in L^2(\Omega_t \times I)$, the solution of the semi-discrete problem (2.1.20) satisfies*

$$\int_{t_0}^{t} \left\| \left. \frac{\partial u_h}{\partial t} \right|_{\mathbf{Y}} (s) \right\|^2_{L_2(\Omega_s)} ds + \frac{\mu}{2} \|\nabla_{\mathbf{x}} u_h(t)\|^2_{L_2(\Omega_t)} \leq C_2 \tag{2.1.36}$$

where C_2 depends on the constant C_1 introduced in (2.1.34), as well as on $\|A\|_{L^\infty(\Omega_0 \times I)}$, $\|\nabla_{\mathbf{x}} \cdot \mathbf{w}_h\|_{L^\infty(\Omega_t \times I)}$, $\|f\|_{L^2(\Omega_t \times I)}$ and $\|\nabla_{\mathbf{x}} u_{0h}\|^2_{L_2(\Omega_0)}$.
Moreover, assumed that there exist two positive constants γ_1 and γ_2 independent of h such that

$$\int_{t_0}^{t} \left(\left\| \nabla_{\mathbf{x}} \cdot \left(\left. \frac{\partial(\beta - \mathbf{w}_h)}{\partial t} \right|_{\mathbf{Y}} \right) \right\|^2_{L_\infty(\Omega_s)} + \left\| \left. \frac{\partial f}{\partial t} \right|_{\mathbf{Y}} \right\|^2_{L_2(\Omega_s)} \right) ds \leq \gamma_1 \tag{2.1.37}$$

$$\left\| \left. \frac{\partial(\beta - \mathbf{w}_h)}{\partial t} \right|_{\mathbf{Y}} \right\|_{L^\infty(\Omega_t \times I)} \leq \gamma_2 \tag{2.1.38}$$

and that $\left.\frac{\partial u_h}{\partial t}\right|_{\mathbf{Y}}(t_0) \in L^2(\Omega_0)$, *then the following a priori estimate holds true*

$$\left\| \left.\frac{\partial u_h}{\partial t}\right|_{\mathbf{Y}}(t) \right\|^2_{L_2(\Omega_t)} + \mu \int_{t_0}^{t} \left\| \nabla_{\mathbf{x}} \left.\frac{\partial u_h}{\partial t}\right|_{\mathbf{Y}}(s) \right\|^2_{L_2(\Omega_s)} ds \leq C_3, \tag{2.1.39}$$

where C_3 *depends on* C_1, C_2, γ_1, γ_2 *and* $\left\| \left.\frac{\partial u_h}{\partial t}\right|_{\mathbf{Y}}(t_0) \right\|_{L_2(\Omega_0)}$.

These results are not yet enough for the error estimates on the fully discrete problem that we will derive in next section. Let us then recall some useful relations that have been proven in [34] : *let* $\phi : \Omega_t \times I \to \mathbb{R}$ *be a differentiable function with respect to* t *and* $\mathbf{x}$ *and* $\mathbf{b}$ *a vector field such that* $\mathbf{b} \in \left[W^{1,\infty}(\Omega_t \times I)\right]^d$. *Then, for all* $v : \Omega_t \times I \to \mathbb{R}$ *such that* $v = \hat{v} \circ \mathcal{A}_{h,t}$, *with* $\hat{v} : \Omega_0 \to \mathbb{R}$ *differentiable, the following relations hold :*

- $$\frac{d}{dt}\int_{\Omega_t} \nabla_{\mathbf{x}}\phi \cdot \nabla_{\mathbf{x}} v \, d\Omega = \int_{\Omega_t} \nabla_{\mathbf{x}} \left(\left.\frac{\partial \phi}{\partial t}\right|_{\mathbf{Y}} \right) \cdot \nabla_{\mathbf{x}} v \, d\Omega + \int_{\Omega_t} (A \nabla_{\mathbf{x}} \phi) \cdot \nabla_{\mathbf{x}} v \, d\Omega$$
$$+ \int_{\Omega_t} \nabla_{\mathbf{x}} \phi \cdot (A \nabla_{\mathbf{x}} v) \, d\Omega - \int_{\Omega_t} \nabla_{\mathbf{x}} \cdot \mathbf{w}_h \nabla_{\mathbf{x}} \phi \cdot \nabla_{\mathbf{x}} v \, d\Omega \tag{2.1.40}$$
- $$\frac{d}{dt}\int_{\Omega_t} \phi \mathbf{b} \cdot \nabla_{\mathbf{x}} v \, d\Omega = \int_{\Omega_t} \left.\frac{\partial \phi}{\partial t}\right|_{\mathbf{Y}} \mathbf{b} \cdot \nabla_{\mathbf{x}} v \, d\Omega + \int_{\Omega_t} \phi \left.\frac{\partial \mathbf{b}}{\partial t}\right|_{\mathbf{Y}} \cdot \nabla_{\mathbf{x}} v \, d\Omega$$
$$+ \int_{\Omega_t} \phi \mathbf{b} \cdot (A \nabla_{\mathbf{x}} v) \, d\Omega \tag{2.1.41}$$

where the matrix A is given in (2.1.35). We are now in the position to prove the following

Lemma 2.1.4 *Under the same conditions (2.1.37) and (2.1.38) as in Lemma 2.1.3 the following estimate on the solution of the semi-discrete problem (2.1.20) holds for almost every* $t \in I$:

$$\left| \frac{d^2}{dt^2} \int_{\Omega_{h,t}} u_h(t) \psi_h \, d\Omega \right| \leq C_4(t) \left\| \nabla_{\mathbf{x}} \psi_h \right\|_{L_2(\Omega_t)} \tag{2.1.42}$$

where $C_4(t)$ *is a square integrable function on* I, *independent of* h *and the quantity*

$$\mathcal{Q} = \int_I (C_4(t))^2 \, dt \tag{2.1.43}$$

depends on the constants C_2, C_3, γ_1, γ_2 *introduced in Lemma 2.1.3, as well as on* $\|A\|_{L^\infty(\Omega_0 \times I)}$, $\|\nabla_{\mathbf{x}} \cdot \mathbf{w}_h\|_{L^\infty(\Omega_t \times I)}$.

Proof. Inequality (2.1.42) can be obtained by differentiating in time the semi-discrete problem. We have, $\forall \psi_h \in \mathcal{X}^k_{0,h}(\Omega_{h,t})$, and for almost every $t \in I$

$$\frac{d^2}{dt^2}\int_{\Omega_{h,t}} \psi_h u_h d\Omega = \frac{d}{dt}\int_{\Omega_{h,t}} f \psi_h \, d\Omega - \mu \frac{d}{dt}\int_{\Omega_{h,t}} \nabla_{\mathbf{x}} \psi_h \nabla_{\mathbf{x}} u_h d\Omega + \frac{d}{dt}\int_{\Omega_{h,t}} \nabla_{\mathbf{x}} \psi_h \cdot (\boldsymbol{\beta} - \mathbf{w}_h) u_h d\Omega. \tag{2.1.44}$$

where the last term has been integrated by parts. Observe that

$$\frac{d}{dt}\int_{\Omega_{h,t}} f \psi_h \, d\Omega = \int_{\Omega_{h,t}} \left.\frac{\partial f}{\partial t}\right|_{\mathbf{Y}} \psi_h \, d\Omega + \int_{\Omega_{h,t}} f \psi_h \nabla_{\mathbf{x}} \cdot \mathbf{w}_h \, d\Omega.$$

Then, by exploiting in (2.1.44) relations (2.1.40) and (2.1.41) we obtain

$$\left|\frac{d^2}{dt^2}\int_{\Omega_{h,t}} u_h(t)\psi_h\,d\Omega\right| \le \sqrt{C_\Omega}\left(\left\|\left.\frac{\partial f}{\partial t}\right|_{\mathbf{Y}}\right\|_{L_2(\Omega_t)} + \|\nabla_{\mathbf{x}}\cdot\mathbf{w}_h\|_{L_\infty(\Omega_t)}\,\|f\|_{L_2(\Omega_t)}\right)\|\nabla_{\mathbf{x}}\psi_h\|_{L_2(\Omega_t)}$$
$$+\mu\left\{\left\|\nabla_{\mathbf{x}}\left.\frac{\partial u_h}{\partial t}\right|_{\mathbf{Y}}\right\|_{L_2(\Omega_t)} + \left(2\,\|A\|_{L_\infty(\Omega_t)} + \|\nabla_{\mathbf{x}}\cdot\mathbf{w}_h\|_{L_\infty(\Omega_t)}\right)\|\nabla_{\mathbf{x}}u_h\|_{L_2(\Omega_t)}\right\}\|\nabla_{\mathbf{x}}\psi_h\|_{L_2(\Omega_t)}$$
$$+\left\{\left(\left\|\left.\frac{\partial(\boldsymbol{\beta}-\mathbf{w}_h)}{\partial t}\right|_{\mathbf{Y}}\right\|_{L_\infty(\Omega_t)} + \|A\|_{L_\infty(\Omega_t)}\,\|\boldsymbol{\beta}-\mathbf{w}_h\|_{L_\infty(\Omega_t)}\right)\|u_h\|_{L_2(\Omega_t)}\right.$$
$$\left.+\|\boldsymbol{\beta}-\mathbf{w}_h\|_{L_\infty(\Omega_t)}\left\|\left.\frac{\partial u_h}{\partial t}\right|_{\mathbf{Y}}\right\|_{L_2(\Omega_t)}\right\}\|\nabla_{\mathbf{x}}\psi_h\|_{L_2(\Omega_t)}$$

All the terms appearing in the previous inequality are square integrable functions thanks to hypotheses (2.1.37), (2.1.38) and the estimates provided in Lemma 2.1.3 and in (2.1.34). Thus, estimates (2.1.42) and (2.1.43) hold.

■

2.1.4 Error estimate for the fully-discrete problem

In this section we will analyse the discretisation error for a standard Implicit Euler scheme applied to the conservative formulation. We remind that this discretisation does not satisfy the GCL, in general. We would like to point out here that satisfying the GCL is not a necessary condition to preserve the accuracy of the Implicit Euler scheme.

In the fully-discrete problem, we will adopt a linear interpolation in time of the domain deformation. Thus, the discrete ALE mapping that we will employ, denoted by $\mathcal{A}_{h,\Delta t}$, is defined in each time slab $[t^n, t^{n+1}]$ as

$$\mathcal{A}_{h,\Delta t}(\mathbf{Y},t) = \frac{t-t^n}{\Delta t}\mathcal{A}_{h,t^n}(\mathbf{Y}) + \frac{t^{n+1}-t}{\Delta t}\mathcal{A}_{h,t^{n+1}}(\mathbf{Y})$$

where $\mathcal{A}_{h,t}$ is the time continuous ALE mapping adopted in the semi-discrete problem (2.1.20). The mesh velocity is thus constant on each time step and is given by

$$\hat{\mathbf{w}}^{n+1}_{h,\Delta t}(\mathbf{Y}) = \frac{\mathcal{A}_{h,t^{n+1}}(\mathbf{Y}) - \mathcal{A}_{h,t^n}(\mathbf{Y})}{\Delta t}$$

and $\mathbf{w}^{n+1}_{h,\Delta t}(\mathbf{x},t) = \hat{\mathbf{w}}^{n+1}_{h,\Delta t}(\mathbf{Y}) \circ \mathcal{A}^{-1}_{h,\Delta t}(\mathbf{x})$, $t \in (t^n, t^{n+1}]$.

We aim at comparing the semi-discrete problem (2.1.20), that we rewrite hereafter for convenience : *find* $u_h(t) \in \mathcal{X}^k_{0,h}(\Omega_{h,t})$, $u_h(t_0) = u_{0h}$, *such that*

$$\frac{d}{dt}\int_{\Omega_{h,t}}\psi_h u_h d\Omega + \mu\int_{\Omega_{h,t}}\nabla_{\mathbf{x}}\psi_h\nabla_{\mathbf{x}}u_h d\Omega + \int_{\Omega_{h,t}}\psi_h\nabla_{\mathbf{x}}\cdot[(\boldsymbol{\beta}(t)-\mathbf{w}_h(t))u_h]\,d\Omega =$$
$$= \int_{\Omega_{h,t}} f\psi_h\,d\Omega \qquad \forall\psi_h \in \mathcal{X}^k_{0,h}(\Omega_{h,t}),\ \text{a.e. in } I, \quad (2.1.45)$$

with the Implicit Euler discretisation : *find* $u_h^n \in \mathcal{X}_{0,h}^k(\Omega_{h,t^n})$, $n = 1, 2, \ldots$, $u_h^0 = u_{0h}$ *such that*

$$\frac{1}{\Delta t}\int_{\Omega_{h,t^{n+1}}} u_h^{n+1}\psi_h\, d\Omega - \frac{1}{\Delta t}\int_{\Omega_{h,t^n}} u_h^n\psi_h\, d\Omega + \int_{\Omega_{h,t^{n+1}}} \psi_h \nabla_{\mathbf{x}}\cdot[(\beta(t^{n+1}) - \mathbf{w}_{h,\Delta t}^{n+1})u_h^{n+1}]\, d\Omega$$
$$+ \int_{\Omega_{h,t^{n+1}}} \mu\nabla_{\mathbf{x}} u_h^{n+1}\nabla_{\mathbf{x}}\psi_h\, d\Omega = \int_{\Omega_{h,t^{n+1}}} f^{n+1}\psi_h\, d\Omega \qquad \forall\psi_h \in \mathcal{X}_{0,h}^k(\Omega_{h,t}),\ n \geq 0 \quad (2.1.46)$$

We will prove the following result

Proposition 2.1.2 *For a sufficiently small Δt the error estimate*

$$\left\|u_h^{n+1} - u_h(t^{n+1})\right\|^2_{L_2(\Omega_{h,t^{n+1}})} + \Delta t\mu\sum_{i=1}^{n+1}\left\|\nabla_{\mathbf{x}}\left(u_h^i - u_h(t^i)\right)\right\|^2_{L_2(\Omega_{h,t^i})}$$
$$\leq C\Delta t^2\left\{\max_{i=1,\ldots,n+1}\left(\sup_{s\in(t^{i-1},t^i)}\left\|J_{\mathcal{A}_{t^i,s}}\right\|_{L_\infty(\Omega_{t^i})}\right)\mathcal{Q}\right.$$
$$\left. + C_\Omega \sup_{s\in I}\left\|\left|\frac{\partial^2\mathcal{A}_{h,t}}{\partial t^2}(s)\right|^2\right\|_{L_\infty(\Omega_0)}\sum_{i=1}^{n+1}\Delta t\left\|\nabla_{\mathbf{x}}u_h^i\right\|^2_{L_2(\Omega_{t^i})}\right\} \quad (2.1.47)$$

holds, under the hypotheses of Lemma 2.1.3 and provided $\mathcal{A}_{h,t} \in \left[W^{1,\infty}(\Omega_0\times I)\right]^d \cap \left[W^{2,\infty}(I; L^\infty(\Omega_0))\right]^d$. *The constant $\mathcal{Q}$ is given in Lemma 2.1.4 while the constant C depends eventually on $\mathcal{A}_{h,t}$ but not on Δt. The quantity* $\sum_{i=1}^{n+1}\Delta t\left\|\nabla_{\mathbf{x}}u_h^i\right\|^2_{L_2(\Omega_{t^i})}$ *is bounded thanks to inequality (1.9.20).*

Proof We take the difference from equation (2.1.45) and (2.1.46) at the time level t^{n+1}. To lighten the notations, we drop out the subscript h to indicate the computational domain. Then, $\forall\psi_h \in \mathcal{X}_{0,h}^k(\Omega_{h,t})$, $n \geq 0$ we have

$$\frac{1}{\Delta t}\int_{\Omega_{t^{n+1}}} u_h^{n+1}\psi_h\, d\Omega - \frac{1}{\Delta t}\int_{\Omega_{t^n}} u_h^n\psi_h\, d\Omega - \frac{d}{dt}\int_{\Omega_t}\psi_h u_h(t)d\Omega\Big|_{t^{n+1}}$$
$$+ \int_{\Omega_{t^{n+1}}}\mu\nabla_{\mathbf{x}}(u_h^{n+1} - u_h(t^{n+1}))\nabla_{\mathbf{x}}\psi_h\, d\Omega + \int_{\Omega_{t^{n+1}}}\psi_h\nabla_{\mathbf{x}}\cdot\left[\beta(t^{n+1})(u_h^{n+1} - u_h(t^{n+1}))\right]\, d\Omega$$
$$- \int_{\Omega_{t^{n+1}}}\psi_h\nabla_{\mathbf{x}}\cdot\left[\mathbf{w}_{h,\Delta t}^{n+1}u_h^{n+1} - \mathbf{w}_h(t^{n+1})u_h(t^{n+1})\right]\, d\Omega = 0 \quad (2.1.48)$$

We set $e_h^{n+1} = u_h^{n+1} - u_h(t^{n+1})$; then, by taking in (2.1.48) $\psi_h = e_h^{n+1}$, integrating by parts the convective terms and exploiting the fact that $\nabla_{\mathbf{x}}\cdot\beta = 0$, we obtain

$$\frac{1}{\Delta t}\int_{\Omega_{t^{n+1}}} u_h^{n+1}\, e_h^{n+1}\, d\Omega - \frac{1}{\Delta t}\int_{\Omega_{t^n}} u_h^n\, e_h^{n+1}\, d\Omega - \frac{d}{dt}\int_{\Omega_t} u_h(t)\, e_h^{n+1}d\Omega\Big|_{t^{n+1}} + \mu\left\|\nabla_{\mathbf{x}}e_h^{n+1}\right\|^2_{L_2(\Omega_{t^{n+1}})}$$
$$+ \int_{\Omega_{t^{n+1}}}\nabla_{\mathbf{x}}e_h^{n+1}\cdot(\mathbf{w}_{h,\Delta t}^{n+1} - \mathbf{w}_h(t^{n+1}))\, u_h^{n+1}\, d\Omega + \int_{\Omega_{t^{n+1}}}\nabla_{\mathbf{x}}e_h^{n+1}\cdot\mathbf{w}_h(t^{n+1})\, e_h^{n+1}\, d\Omega = 0 \quad (2.1.49)$$

Observe that, in the second term of (2.1.49), the function e_h^{n+1} can be transported on Ω_{t^n} either through the mapping $\mathcal{A}_{h,t}$ or $\mathcal{A}_{h,\Delta t}$. In the sequel, we will adopt always the first possibility. We will use the following Taylor expansions around $t = t^{n+1}$:

$$\frac{d}{dt}\int_{\Omega_t} u_h(t)\psi_h d\Omega\Big|_{t^{n+1}} = \frac{1}{\Delta t}\int_{\Omega_{t^{n+1}}} u_h(t^{n+1})\,\psi_h\,d\Omega - \frac{1}{\Delta t}\int_{\Omega_{t^n}} u_h(t^n)\,\psi_h\,d\Omega + \frac{1}{\Delta t}\int_{t^n}^{t^{n+1}} (s-t^n)\frac{d^2}{ds^2}\left(\int_{\Omega_s} u_h(s)\psi_h d\Omega\right) ds, \quad (2.1.50)$$

which holds for all $\psi_h \in \mathcal{X}_{0,h}^k(\Omega_{h,t})$, and

$$\hat{\mathbf{w}}_h(\mathbf{Y}, t^{n+1}) = \frac{\partial \mathcal{A}_{h,t}}{\partial t}(\mathbf{Y}, t^{n+1}) = \frac{\mathcal{A}_{h,t^{n+1}}(\mathbf{Y}) - \mathcal{A}_{h,t^n}(\mathbf{Y})}{\Delta t} + \frac{1}{\Delta t}\int_{t^n}^{t^{n+1}} (s-t^n)\frac{\partial^2 \mathcal{A}_{h,s}}{\partial s^2}(\mathbf{Y}, s) ds \quad (2.1.51)$$

that, once written on the configuration $\Omega_{t^{n+1}}$ reads

$$\mathbf{w}_h(\mathbf{x}, t^{n+1}) = \mathbf{w}_{h,\Delta t}^{n+1}(\mathbf{x}) + \frac{1}{\Delta t}\left(\int_{t^n}^{t^{n+1}} (s-t^n)\frac{\partial^2 \mathcal{A}_{h,s}}{\partial s^2}(\mathbf{Y}, s)\, ds\right) \circ \mathcal{A}_{h,t^{n+1}}^{-1}(\mathbf{x}) \quad (2.1.52)$$

Exploiting (2.1.50) and (2.1.52) in (2.1.49), we obtain

$$\frac{1}{\Delta t}\left\|e_h^{n+1}\right\|^2_{L_2(\Omega_{t^{n+1}})} - \frac{1}{\Delta t}\int_{\Omega_{t^n}} e_h^n\, e_h^{n+1}\, d\Omega - \frac{1}{\Delta t}\int_{t^n}^{t^{n+1}} (s-t^n)\frac{d^2}{ds^2}\left(\int_{\Omega_s} u_h(s)\, e_h^{n+1} d\Omega\right) ds + \mu\left\|\nabla_{\mathbf{x}} e_h^{n+1}\right\|^2_{L_2(\Omega_{t^{n+1}})} - \frac{1}{2}\int_{\Omega_{t^{n+1}}} \nabla_{\mathbf{x}}\cdot \mathbf{w}_h(t^{n+1})\,(e_h^{n+1})^2\, d\Omega - \frac{1}{\Delta t}\int_{\Omega_{t^{n+1}}} \nabla_{\mathbf{x}} e_h^{n+1}\cdot\left(\int_{t^n}^{t^{n+1}} (s-t^n)\frac{\partial^2 \mathcal{A}_{h,s}}{\partial s^2}(\mathbf{Y}, s) ds\right) \circ \mathcal{A}_{h,t^{n+1}}^{-1}(\mathbf{x})\, u_h^{n+1} d\Omega = 0. \quad (2.1.53)$$

Then, by manipulating the term $\int_{\Omega_{t^n}} e_h^n\, e_h^{n+1}\, d\Omega$ (as done in section 1.8.4 or 1.9.2) as

$$\int_{\Omega_{t^n}} e_h^n\, e_h^{n+1}\, d\Omega \le \frac{1}{2}\left\|e_h^n\right\|^2_{L_2(\Omega_{t^n})} + \frac{1}{2}\left\|e_h^{n+1}\right\|^2_{L_2(\Omega_{t^n})} = \frac{1}{2}\left\|e_h^n\right\|^2_{L_2(\Omega_{t^n})} + \frac{1}{2}\left\|e_h^{n+1}\right\|^2_{L_2(\Omega_{t^{n+1}})} - \int_{t^n}^{t^{n+1}}\int_{\Omega_s} \nabla_{\mathbf{x}}\cdot \mathbf{w}_h(s)(e_h^{n+1})^2 d\Omega ds,$$

equation (2.1.53) can be elaborated as follows

$$\frac{1}{2\Delta t}\left\|e_h^{n+1}\right\|^2_{L_2(\Omega_{t^{n+1}})} + \mu\left\|\nabla_{\mathbf{x}} e_h^{n+1}\right\|^2_{L_2(\Omega_{t^{n+1}})} \le \frac{1}{2\Delta t}\left\|e_h^n\right\|^2_{L_2(\Omega_{t^n})}$$
$$+ \frac{1}{2}\left(\int_{\Omega_{t^{n+1}}} \nabla_{\mathbf{x}}\cdot \mathbf{w}_h(t^{n+1})(e_h^{n+1})^2 d\Omega - \frac{1}{\Delta t}\int_{t^n}^{t^{n+1}}\int_{\Omega_s} \nabla_{\mathbf{x}}\cdot \mathbf{w}_h(s)(e_h^{n+1})^2 d\Omega ds\right) \quad (T_2)$$
$$+ \frac{1}{\Delta t}\int_{t^n}^{t^{n+1}} (s-t^n)\frac{d^2}{ds^2}\left(\int_{\Omega_s} u_h(s)\, e_h^{n+1} d\Omega\right) ds \quad (T_3)$$
$$+ \frac{1}{\Delta t}\int_{\Omega_{t^{n+1}}} \nabla_{\mathbf{x}} e_h^{n+1}\cdot\left(\int_{t^n}^{t^{n+1}} (s-t^n)\frac{\partial^2 \mathcal{A}_{h,s}}{\partial s^2}(\mathbf{Y}, s) ds\right) \circ \mathcal{A}_{h,t^{n+1}}^{-1}(\mathbf{x})\, u_h^{n+1} d\Omega \quad (T_4)$$

We analyse separately the last three terms on the right hand side, noted T_2, T_3 and T_4 respectively. The term T_2 can be bound as

$$T_2 \leq \frac{1}{2}\gamma^{n+1}\left\|e_h^{n+1}\right\|^2_{L_2(\Omega_{t^{n+1}})}$$

where

$$\gamma^i = \left\|\nabla_{\mathbf{x}}\cdot\mathbf{w}_h(t^i)\right\|_{L_\infty(\Omega_{t^i})} + \sup_{s\in(t^{i-1},t^i)}\left\|J_{\mathcal{A}_{t_i,s}}\nabla_{\mathbf{x}}\cdot\mathbf{w}_h(s)\right\|_{L_\infty(\Omega_{t^i})},$$

and $\mathcal{A}_{t_i,s} = \mathcal{A}_{h,s}\circ\mathcal{A}_{h,t^i}$.

$$\begin{aligned}
T_3 &\leq \frac{1}{\Delta t}\int_{t^n}^{t^{n+1}}(s-t^n)C_4(s)\left\|\nabla_{\mathbf{x}}e_h^{n+1}\right\|_{L_2(\Omega_s)}ds\\
&\leq \frac{1}{\Delta t}\int_{t^n}^{t^{n+1}}\left\|J_{\mathcal{A}_{t^{n+1},s}}\right\|^{\frac{1}{2}}_{L_\infty(\Omega_{t^{n+1}})}(s-t^n)C_4(s)\left\|\nabla_{\mathbf{x}}e_h^{n+1}\right\|_{L_2(\Omega_{t^{n+1}})}ds\\
&\leq \frac{1}{\Delta t}\left(\int_{t^n}^{t^{n+1}}\left\|J_{\mathcal{A}_{t^{n+1},s}}\right\|_{L_\infty(\Omega_{t^{n+1}})}C_4^2(s)ds\right)^{\frac{1}{2}}\left(\int_{t^n}^{t^{n+1}}(s-t^n)^2\left\|\nabla_{\mathbf{x}}e_h^{n+1}\right\|^2_{L_2(\Omega_{t^{n+1}})}ds\right)^{\frac{1}{2}}\\
&\leq \sqrt{\frac{\Delta t}{3}}\sup_{s\in(t^n,t^{n+1})}\left\|J_{\mathcal{A}_{t^{n+1},s}}\right\|^{\frac{1}{2}}_{L_\infty(\Omega_{t^{n+1}})}\left(\int_{t^n}^{t^{n+1}}C_4^2(s)ds\right)^{\frac{1}{2}}\left\|\nabla_{\mathbf{x}}e_h^{n+1}\right\|_{L_2(\Omega_{t^{n+1}})}\\
&\leq \frac{\Delta t}{3\mu}\sup_{s\in(t^n,t^{n+1})}\left\|J_{\mathcal{A}_{t^{n+1},s}}\right\|_{L_\infty(\Omega_{t^{n+1}})}\int_{t^n}^{t^{n+1}}C_4^2(s)ds + \frac{\mu}{4}\left\|\nabla_{\mathbf{x}}e_h^{n+1}\right\|^2_{L_2(\Omega_{t^{n+1}})}.
\end{aligned}$$

Finally, for T_4 we have

$$\begin{aligned}
T_4 &= \frac{1}{\Delta t}\int_{t^n}^{t^{n+1}}\int_{\Omega_0}J_{\mathcal{A}_{h,t^{n+1}}}(s-t^n)\widehat{\nabla_{\mathbf{x}}e_h^{n+1}}\cdot\frac{\partial^2\mathcal{A}_{h,s}}{\partial s^2}\hat{u}_h^{n+1}d\Omega\,ds\\
&\leq \frac{1}{\Delta t}\left(\int_{t^n}^{t^{n+1}}(s-t^n)^2\left\|\nabla_{\mathbf{x}}e_h^{n+1}\right\|^2_{L_2(\Omega_{t^{n+1}})}\right)^{\frac{1}{2}}\left(\int_{t^n}^{t^{n+1}}\int_{\Omega_0}J_{\mathcal{A}_{h,t^{n+1}}}\left|\frac{\partial^2\mathcal{A}_{h,s}}{\partial s^2}\right|^2\left(\hat{u}_h^{n+1}\right)^2d\Omega\,ds\right)^{\frac{1}{2}}\\
&\leq \sqrt{\frac{\Delta t}{3}}\left\|\nabla_{\mathbf{x}}e_h^{n+1}\right\|_{L_2(\Omega_{t^{n+1}})}\left[\int_{t^n}^{t^{n+1}}\left\|\left|\frac{\partial^2\mathcal{A}_{h,s}}{\partial s^2}\right|^2\right\|_{L_\infty(\Omega_0)}\left\|u_h^{n+1}\right\|^2_{L_2(\Omega_{t^{n+1}})}ds\right]^{\frac{1}{2}}\\
&\leq \frac{\Delta t^2C_\Omega}{3\mu}\left\|\nabla_{\mathbf{x}}u_h^{n+1}\right\|^2_{L_2(\Omega_{t^{n+1}})}\sup_{s\in(t^n,t^{n+1})}\left\|\left|\frac{\partial^2\mathcal{A}_{h,s}}{\partial s^2}(s)\right|^2\right\|_{L_\infty(\Omega_0)} + \frac{\mu}{4}\left\|\nabla_{\mathbf{x}}e_h^{n+1}\right\|^2_{L_2(\Omega_{t^{n+1}})}.
\end{aligned}$$

Combining all these term we obtain finally

$$\begin{aligned}
\left\|e_h^{n+1}\right\|^2_{L_2(\Omega_{t^{n+1}})} + \Delta t\mu\left\|\nabla_{\mathbf{x}}e_h^{n+1}\right\|^2_{L_2(\Omega_{h,t^{n+1}})} &\leq \Delta t\gamma^{n+1}\left\|e_h^{n+1}\right\|^2_{L_2(\Omega_{t^{n+1}})}\\
&+ \left\|e_h^n\right\|^2_{L_2(\Omega_{t^n})} + \frac{2\Delta t^2}{3\mu}\sup_{s\in(t^n,t^{n+1})}\left\|J_{\mathcal{A}_{t^{n+1},s}}\right\|_{L_\infty(\Omega_{t^{n+1}})}\int_{t^n}^{t^{n+1}}C_4^2(s)ds\\
&+ \frac{2\Delta t^3C_\Omega}{3\mu}\left\|\nabla_{\mathbf{x}}u_h^{n+1}\right\|^2_{L_2(\Omega_{t^{n+1}})}\sup_{s\in(t^n,t^{n+1})}\left\|\left|\frac{\partial^2\mathcal{A}_{h,s}}{\partial s^2}(s)\right|^2\right\|_{L_\infty(\Omega_0)}
\end{aligned}$$

and, summing over n we have

$$\left\|e_h^{n+1}\right\|^2_{L_2(\Omega_{t^{n+1}})} + \Delta t\mu \sum_{i=1}^{n+1} \left\|\nabla_{\mathbf{x}} e_h^i\right\|^2_{L_2(\Omega_{h,t^i})} \leq \Delta t \sum_{i=1}^{n+1} \gamma^i \left\|e_h^i\right\|^2_{L_2(\Omega_{t^i})}$$
$$+ \frac{2\Delta t^2}{3\mu} \max_{i=1,\dots,n+1} \left(\sup_{s\in(t^{i-1},t^i)} \left\| J_{\mathcal{A}_{t^i,s}} \right\|_{L_\infty(\Omega_{t^i})} \right) \mathcal{Q}$$
$$+ \frac{2\Delta t^2 C_\Omega}{3\mu} \sup_{s\in I} \left\| \left| \frac{\partial^2 \mathcal{A}_{h,t}}{\partial t^2}(s) \right|^2 \right\|_{L_\infty(\Omega_0)} \sum_{i=1}^{n+1} \Delta t \left\|\nabla_{\mathbf{x}} u_h^i\right\|^2_{L_2(\Omega_{t^i})}$$

By applying the discrete Gronwall Lemma we obtain the desired inequality where the constant C is given by

$$C = \frac{2}{3\mu} \exp\left\{ t^{n+1} \frac{\gamma}{1-\Delta t\gamma} \right\}, \qquad \gamma = \max_{i=1,\dots,n+1} \gamma^i.$$

■

2.2 Second order time discretisation schemes

In sections 1.8 and 1.9 we have considered an Implicit Euler discretisation of model problem (1.6.1) applied to both the conservative and the non-conservative ALE formulation. In the first case, in particular, we have proposed a modified version of the scheme, which satisfies the GCL and we have shown that it is unconditionally stable. In this section, we would like to extend these considerations to higher order schemes. We will use the same notations as in Sections 1.8 and 1.9. In particular, we will drop the subscript h to indicate the computational domain. The finite element space will be indicated with $\mathcal{X}_h(\Omega_t)$ and may be taken as the finite element function space $\mathcal{F}_{n,k}(\mathcal{T}_{h,t})$ of degree n and parametric mapping degree k. Finially, the discrete ALE mapping adopted will be indicate always with $\mathcal{A}_{h,t}$ and will be supposed to be polynomial in time within each time step.

2.2.1 The Crank-Nicolson method

We will consider here a slight modification to the classical Crank-Nicolson method that, for a scalar ordinary differential equation

$$\dot{y}(t) = g(y(t), t), \quad t > 0, \quad \text{and} \quad y(0) = y_0 \tag{2.2.1}$$

reads

$$y^{n+1} - y^n = \Delta t g\left(\frac{y^{n+1} + y^n}{2}, t^{n+\frac{1}{2}} \right) \tag{2.2.2}$$

More precisely, it is a Gauss-Legendre implicit Runge-Kutta method of order 2. Nevertheless, for a linear advection diffusion equation on a fixed domain and with time-independent coefficients, this method coincides with the more classical Crank-Nicolson. With a little abuse on notations, we will refer to method (2.2.2) as a *Crank-Nicolson* method.

Discretisation of the conservative formulation

A straightforward application of scheme (2.2.2) to the conservative formulation (1.2.10) provides :

$$\int_{\Omega_{t^{n+1}}} u_h^{n+1}\psi_h\,d\Omega - \int_{\Omega_{t^n}} u_h^n\psi_h\,d\Omega + \Delta t\int_{\Omega_{t^{n+1/2}}} \mu\nabla_{\mathbf{x}}\frac{u_h^{n+1}+u_h^n}{2}\nabla_{\mathbf{x}}\psi_h\,d\Omega + \\ + \Delta t\int_{\Omega_{t^{n+1/2}}} \psi_h\nabla_{\mathbf{x}}\cdot\left[(\boldsymbol{\beta}-\mathbf{w}_h^{n+1/2})\frac{u_h^{n+1}+u_h^n}{2}\right]d\Omega = \Delta t\int_{\Omega_{t^{n+1/2}}} f^{n+1/2}\psi_h\,d\Omega \\ \forall\psi_h\in\mathcal{X}_{0,h}(\Omega_t),\quad n=0,1,\dots \qquad (2.2.3)$$

with

$$u_h^i = 0 \quad \text{on } \partial\Omega_t,\quad i=1,2,\dots$$
$$u_h^0 = u_{0h} \quad \text{in } \Omega_0$$

We remark that this formulation satisfies the GCL only for a 2D problem and a linear in time reconstruction of the geometry (i.e. a piecewise constant in time mesh velocity).
In order to satisfy the GCL in the more general case, we firstly observe that the right hand side of (2.2.2) can be seen as an approximation of

$$\Delta t g\left(\frac{y^{n+1}+y^n}{2}, t^{n+\frac{1}{2}}\right) \approx \int_{t^n}^{t^{n+1}} g(y(t),t)dt. \qquad (2.2.4)$$

We can adopt then a quadrature rule different to the midpoint one to integrate the right hand side in (2.2.4) while keeping $y(t)=\frac{y^{n+1}+y^n}{2}$, i.e.

$$y^{n+1}-y^n = \int_{t^n}^{t^{n+1}} g(y(t),t)dt \approx \mathcal{INT}_{t^n}^{t^{n+1}}\left[g\left(\frac{y^{n+1}+y^n}{2},t\right)\right].$$

We introduce, thus, a modified scheme

$$\int_{\Omega_{t^{n+1}}} u_h^{n+1}\psi_h\,d\Omega - \int_{\Omega_{t^n}} u_h^n\psi_h\,d\Omega \\ + \mathcal{INT}_{1\,t^n}^{t^{n+1}}\left[\int_{\Omega_t}\mu\nabla_{\mathbf{x}}\frac{u_h^{n+1}+u_h^n}{2}\nabla_{\mathbf{x}}\psi_h + \psi_h\nabla_{\mathbf{x}}\cdot\left(\boldsymbol{\beta}\frac{u_h^{n+1}+u_h^n}{2}\right)d\Omega\right] \\ - \mathcal{INT}_{2\,t^n}^{t^{n+1}}\left[\int_{\Omega_t}\psi_h\nabla_{\mathbf{x}}\cdot\left(\mathbf{w}_h(t)\frac{u_h^{n+1}+u_h^n}{2}\right)d\Omega\right] = \Delta t\int_{\Omega_{t^{n+1/2}}} f^{n+1/2}\psi_h\,d\Omega \\ \forall\psi_h\in\mathcal{X}_{0,h}(\Omega_t) \qquad (2.2.5)$$

where we take the liberty of using two different quadrature rules for the advection-diffusion terms and the term accounting for the domain deformation. In order to satisfy the GCL, the quadrature formula $\mathcal{INT}_{2\,t^n}^{t^{n+1}}$ must satisfy the requirements on the degree of exactness given in Proposition 1.8.1. We recall, in particular, that if we use a quadratic in time reconstruction of the ALE mapping for a 2D problem, we need for instance a 2 point Gaussian quadrature formula or the Simpson formula.

We are going now to study the stability of this scheme. We will present only the case of a two dimensional domain and a piecewise linear in time reconstruction of the geometry, which allows us to employ scheme (2.2.3). The results we will obtain can be easily extended to the more general scheme (2.2.5). We will first derive the following result :

Lemma 2.2.1 *The discrete solution u_h^n of scheme (2.2.3) satisfies the inequality*

$$\left\|u_h^{n+1}\right\|^2_{L_2(\Omega_{t^{n+1}})} + \frac{\Delta t}{4}\mu \left\|\nabla_{\mathbf{x}}(u_h^{n+1}+u_h^n)\right\|^2_{L_2(\Omega_{t^{n+1/2}})} - \frac{\Delta t}{4}\int_{\Omega_{t^{n+1/2}}} \nabla_{\mathbf{x}}\cdot\mathbf{w}_h|u_h^{n+1}-u_h^n|^2 d\Omega$$
$$\leq \|u_h^n\|^2_{L_2(\Omega_{t^n})} + \Delta t\frac{(1+C_\Omega)}{\mu}\left\|f^{n+1/2}\right\|^2_{H^{-1}(\Omega_{t^{n+1/2}})} \quad (2.2.6)$$

for all $n = 0, 1, \ldots$

Proof. We take in (2.2.3) $\psi_h = (u_h^{n+1} + u_h^n)$ and we use the identity

$$(a, a+b) = \frac{1}{2}\|a\| + \frac{1}{2}\|a+b\| - \frac{1}{2}\|b\|$$

to write the first two terms in (2.2.3) as

$$\int_{\Omega_{t^{n+1}}} u_h^{n+1}(u_h^{n+1}+u_h^n)\,d\Omega - \int_{\Omega_{t^n}} u_h^n(u_h^{n+1}+u_h^n)\,d\Omega$$
$$= \frac{1}{2}\left\|u_h^{n+1}\right\|^2_{L_2(\Omega_{t^{n+1}})} + \frac{1}{2}\left\|u_h^{n+1}+u_h^n\right\|^2_{L_2(\Omega_{t^{n+1}})} - \frac{1}{2}\|u_h^n\|^2_{L_2(\Omega_{t^{n+1}})}$$
$$- \frac{1}{2}\|u_h^n\|^2_{L_2(\Omega_{t^n})} - \frac{1}{2}\left\|u_h^{n+1}+u_h^n\right\|^2_{L_2(\Omega_{t^n})} + \frac{1}{2}\left\|u_h^{n+1}\right\|^2_{L_2(\Omega_{t^n})}$$
$$= \left\|u_h^{n+1}\right\|^2_{L_2(\Omega_{t^{n+1}})} - \|u_h^n\|^2_{L_2(\Omega_{t^n})} - \frac{1}{2}\Delta t\int_{\Omega_{t^{n+1/2}}} \nabla_{\mathbf{x}}\cdot\mathbf{w}_h|u_h^{n+1}|^2 d\Omega$$
$$- \frac{1}{2}\Delta t\int_{\Omega_{t^{n+1/2}}} \nabla_{\mathbf{x}}\cdot\mathbf{w}_h|u_h^n|^2 d\Omega + \frac{1}{2}\Delta t\int_{\Omega_{t^{n+1/2}}} \nabla_{\mathbf{x}}\cdot\mathbf{w}_h|u_h^{n+1}+u_h^n|^2 d\Omega$$
$$= \left\|u_h^{n+1}\right\|^2_{L_2(\Omega_{t^{n+1}})} - \|u_h^n\|^2_{L_2(\Omega_{t^n})} + \Delta t\int_{\Omega_{t^{n+1/2}}} \nabla_{\mathbf{x}}\cdot\mathbf{w}_h\, u_h^{n+1}u_h^n\,d\Omega, \quad (2.2.7)$$

where we have exploited relation (1.8.19). Then, equation (2.2.3) with $\psi_h = (u_h^{n+1} + u_h^n)$ becomes, after integration by parts of the convective term

$$\left\|u_h^{n+1}\right\|^2_{L_2(\Omega_{t^{n+1}})} - \|u_h^n\|^2_{L_2(\Omega_{t^n})} + \Delta t\int_{\Omega_{t^{n+1/2}}} \nabla_{\mathbf{x}}\cdot\mathbf{w}_h\, u_h^{n+1}u_h^n\,d\Omega$$
$$+ \frac{\Delta t}{2}\mu\left\|\nabla_{\mathbf{x}}(u_h^{n+1}+u_h^n)\right\|^2_{L_2(\Omega_{t^{n+1/2}})} - \frac{\Delta t}{4}\int_{\Omega_{t^{n+1/2}}} \nabla_{\mathbf{x}}\cdot\mathbf{w}_h|u_h^{n+1}+u_h^n|^2 d\Omega$$
$$\leq \Delta t\frac{(1+C_\Omega)}{\mu}\left\|f^{n+1/2}\right\|^2_{H^{-1}(\Omega_{t^{n+1/2}})} + \Delta t\frac{\mu}{4}\left\|\nabla_{\mathbf{x}}(u_h^{n+1}+u_h^n)\right\|^2_{L_2(\Omega_{t^{n+1/2}})} \quad (2.2.8)$$

and the thesis follows immediately.

■

We remark that, if $\nabla_{\mathbf{x}} \cdot \mathbf{w}_h < 0$, $\forall \mathbf{x} \in \Omega_{t^{n+1/2}}$ and $n = 0, 1, \dots$, (i.e. in the case of a uniform contraction of the domain), from (2.2.6) we could obtain a global stability independent on the mesh velocity as for the Implicit Euler scheme. In the more general case we can only obtain a conditioned stability where the maximum allowable time step will depend on the speed at which the domain is deforming. Indeed, we can write

$$\begin{aligned}
&\frac{\Delta t}{4} \int_{\Omega_{t^{n+1/2}}} \nabla_{\mathbf{x}} \cdot \mathbf{w}_h |u_h^{n+1} - u_h^n|^2 d\Omega \leq \frac{\Delta t}{2} \int_{\Omega_{t^{n+1/2}}} \nabla_{\mathbf{x}} \cdot \mathbf{w}_h \left(|u_h^{n+1}|^2 + |u_h^n|^2 \right) d\Omega \\
&\leq \frac{\Delta t}{2} \|\nabla_{\mathbf{x}} \cdot \mathbf{w}_h\|_{L_\infty(\Omega_{n+1/2})} \left\|u_h^{n+1}\right\|^2_{L_2(\Omega_{n+1/2})} + \frac{\Delta t}{2} \|\nabla_{\mathbf{x}} \cdot \mathbf{w}_h\|_{L_\infty(\Omega_{n+1/2})} \|u_h^n\|^2_{L_2(\Omega_{n+1/2})} \\
&\leq \Delta t \gamma_1^{n+1} \left\|u_h^{n+1}\right\|^2_{L_2(\Omega_{n+1})} + \Delta t \gamma_2^n \|u_h^n\|^2_{L_2(\Omega_n)}
\end{aligned}$$

where we have set

$$\begin{aligned}
\gamma_1^{n+1} &= \frac{1}{2} \|\nabla_{\mathbf{x}} \cdot \mathbf{w}_h\|_{L_\infty(\Omega_{n+1/2})} \left\| J_{\mathcal{A}_{t^{n+1}, t^{n+1/2}}} \right\|_{L_\infty(\Omega_{n+1})}, \\
\gamma_2^n &= \frac{1}{2} \|\nabla_{\mathbf{x}} \cdot \mathbf{w}_h\|_{L_\infty(\Omega_{n+1/2})} \left\| J_{\mathcal{A}_{t^n, t^{n+1/2}}} \right\|_{L_\infty(\Omega_n)}.
\end{aligned}$$

and inequality (2.2.6) becomes

$$\begin{aligned}
&\left\|u_h^{n+1}\right\|^2_{L_2(\Omega_{t^{n+1}})} + \frac{\Delta t}{4} \mu \left\|\nabla_{\mathbf{x}}(u_h^{n+1} + u_h^n)\right\|^2_{L_2(\Omega_{t^{n+1/2}})} \\
&\leq \Delta t \gamma_1^{n+1} \left\|u_h^{n+1}\right\|^2_{L_2(\Omega_{t^{n+1}})} + (1 + \Delta t \gamma_2^n) \|u_h^n\|^2_{L_2(\Omega_{t^n})} + \Delta t \frac{(1 + C_\Omega)}{\mu} \left\| f^{n+1/2} \right\|^2_{H^{-1}(\Omega_{t^{n+1/2}})}
\end{aligned} \tag{2.2.9}$$

which is very similar to (1.9.18). Then, applying the discrete Gronwall lemma we obtain a stability result similar to (1.9.20) under the condition

$$\Delta t \leq \frac{1}{\gamma_1^i + \gamma_2^i} = 2 \left(\|\nabla_{\mathbf{x}} \cdot \mathbf{w}_h\|_{L_\infty(\Omega_{i-1/2})} \left\| J_{\mathcal{A}_{t^i, t^{i-1/2}}} \right\|_{L_\infty(\Omega_i)} + \|\nabla_{\mathbf{x}} \cdot \mathbf{w}_h\|_{L_\infty(\Omega_{i+1/2})} \left\| J_{\mathcal{A}_{t^i, t^{i+1/2}}} \right\|_{L_\infty(\Omega_i)} \right)^{-1}$$

for all $i = 1, \dots, n$.

Discretisation of the non-conservative formulation

Scheme (2.2.2), applied to the non-conservative formulation (1.2.4), reads :

$$\begin{aligned}
&\int_{\Omega_{t^{n+1}}} u_h^{n+1} \psi_h \, d\Omega - \int_{\Omega_{t^{n+1}}} u_h^n \psi_h \, d\Omega + \Delta t \int_{\Omega_{t^{n+1/2}}} \mu \nabla_{\mathbf{x}} \frac{u_h^{n+1} + u_h^n}{2} \nabla_{\mathbf{x}} \psi_h \, d\Omega + \\
&+ \Delta t \int_{\Omega_{t^{n+1/2}}} \psi_h (\boldsymbol{\beta} - \mathbf{w}_h^{n+1/2}) \nabla_{\mathbf{x}} \cdot \left(\frac{u_h^{n+1} + u_h^n}{2} \right) d\Omega = \Delta t \int_{\Omega_{t^{n+1/2}}} f^{n+1/2} \psi_h \, d\Omega \\
&\qquad \forall \psi_h \in \mathcal{X}_{0,h}(\Omega_t)
\end{aligned} \tag{2.2.10}$$

As for the Implicit Euler scheme, this scheme always satisfies the GCL. A stability analysis can be carried out following the same guidelines as in the conservative case, by taking $\psi_h = u_h^{n+1} + u_h^n$ as a test function. As for the Implicit Euler method analyzed in section 1.9.2, it can be shown that this scheme is only conditionally stable and the stability condition depends on the mesh velocity. We omit the calculations for the sake of brevity.

2.2.2 The second order backward difference scheme BDF(2)

The second order backward difference scheme (in the following BDF(2)) applied to the scalar model equation (2.2.1) reads :

$$\frac{3}{2}y^{n+1} - 2y^n + \frac{1}{2}y^{n-1} = g\left(y^{n+1}, t^{n+1}\right), \qquad n \geq 1. \tag{2.2.11}$$

This scheme can be initialized by a one-step second order method such as, for instance, the Crank-Nicolson one presented in the previous section.

Discretisation of the conservative formulation

Scheme (2.2.11), applied to the conservative formulation (1.2.10) reads :

$$\begin{aligned}
&\frac{3}{2}\int_{\Omega_{t^{n+1}}} u_h^{n+1}\psi_h \, d\Omega - 2\int_{\Omega_{t^n}} u_h^n\psi_h \, d\Omega + \frac{1}{2}\int_{\Omega_{t^{n-1}}} u_h^{n-1}\psi_h \, d\Omega \\
&\quad + \Delta t \int_{\Omega_{t^{n+1}}} \mu \boldsymbol{\nabla}_{\mathbf{x}} u_h^{n+1} \boldsymbol{\nabla}_{\mathbf{x}}\psi_h \, d\Omega + \Delta t \int_{\Omega_{t^{n+1}}} \psi_h \boldsymbol{\nabla}_{\mathbf{x}} \cdot [(\boldsymbol{\beta} - \mathbf{w}_h^{n+1}) u_h^{n+1}] \, d\Omega \\
&\qquad = \Delta t \int_{\Omega_{t^{n+1}}} f^{n+1}\psi_h \, d\Omega \qquad \forall \psi_h \in \mathcal{X}_{0,h}(\Omega_t)
\end{aligned} \tag{2.2.12}$$

This scheme does not satisfy the GCL in general. However, we observe that

$$\frac{3}{2}y^{n+1} - 2y^n + \frac{1}{2}y^{n-1} = \frac{3}{2}\int_{t^n}^{t^{n+1}} g(y(t),t)dt - \frac{1}{2}\int_{t^{n-1}}^{t^n} g(y(t),t)dt. \tag{2.2.13}$$

Then, we can modify the scheme (2.2.11) in the following way

$$\frac{3}{2}y^{n+1} - 2y^n + \frac{1}{2}y^{n-1} = \frac{3}{2}\mathcal{INT}_{t^n}^{t^{n+1}}\left[g(y^{n+1},t)\right] - \frac{1}{2}\mathcal{INT}_{t^{n-1}}^{t^n}\left[g(y^{n+1},t)\right], \tag{2.2.14}$$

where, as usual, we use a quadrature formula to integrate the right hand side in (2.2.13) while keeping $y(t) = y^{n+1}$. The modified version of the BDF(2) scheme that satisfies the GCL reads then

$$\begin{aligned}
&\frac{3}{2}\int_{\Omega_{t^{n+1}}} u_h^{n+1}\psi_h \, d\Omega - 2\int_{\Omega_{t^n}} u_h^n\psi_h \, d\Omega + \frac{1}{2}\int_{\Omega_{t^{n-1}}} u_h^{n-1}\psi_h \, d\Omega \\
&+\frac{3}{2}\mathcal{INT}_{1\,t^n}^{t^{n+1}}\left[\int_{\Omega_t} \mu \boldsymbol{\nabla}_{\mathbf{x}} u_h^{n+1}\boldsymbol{\nabla}_{\mathbf{x}}\psi_h + \psi_h \boldsymbol{\nabla}_{\mathbf{x}} \cdot (\boldsymbol{\beta} u_h^{n+1}) \, d\Omega\right] - \frac{3}{2}\mathcal{INT}_{2\,t^n}^{t^{n+1}}\left[\int_{\Omega_t} \psi_h \boldsymbol{\nabla}_{\mathbf{x}} \cdot (\mathbf{w}_h(t) u_h^{n+1}) \, d\Omega\right] \\
&-\frac{1}{2}\mathcal{INT}_{1\,t^{n-1}}^{t^n}\left[\int_{\Omega_t} \mu \boldsymbol{\nabla}_{\mathbf{x}} u_h^{n+1}\boldsymbol{\nabla}_{\mathbf{x}}\psi_h + \psi_h \boldsymbol{\nabla}_{\mathbf{x}} \cdot (\boldsymbol{\beta} u_h^{n+1}) \, d\Omega\right] + \frac{1}{2}\mathcal{INT}_{2\,t^{n-1}}^{t^n}\left[\int_{\Omega_t} \psi_h \boldsymbol{\nabla}_{\mathbf{x}} \cdot (\mathbf{w}_h(t) u_h^{n+1}) \, d\Omega\right] \\
&\qquad = \Delta t \int_{\Omega_{t^{n+1}}} f^{n+1}\psi_h \, d\Omega \qquad \forall \psi_h \in \mathcal{X}_{0,h}(\Omega_t)
\end{aligned} \tag{2.2.15}$$

Again, we feel free to take to different quadrature formulae for the advection-diffusion terms and the term accounting for the domain deformation. It can be easily verified that this scheme satisfies the GCL provided the quadrature formula $\mathcal{INT}_2$ fulfills the requirement on the degree of exactness given in Proposition 1.8.1. In particular, for a 2D problem and a piecewise linear in time ALE mapping, at each time step we need to compute the matrix

associated to the term $\int_{\Omega_t} \psi_h \nabla_{\mathbf{x}} \cdot (\mathbf{w}_h u_h^{n+1})\, d\Omega$ on both configurations $\Omega_{t^{n+1/2}}$ and $\Omega_{t^{n-1/2}}$. For a 3D problem a 2 points Gaussian quadrature formula should be employed for $\mathcal{INT}_2$ thus implying four computations of the same matrix. This scheme has already been proposed by Farhat and Koobus in [52] in the context of a finite volume approximation.

In the remaining part of this section, we will derive a stability result for the BDF(2) scheme (2.2.15). We will limit ourselves to the case of a bidimensional domain and a piecewise linear in time ALE mapping. Furthermore, we will consider a standard BDF(2) approximation of the advection-diffusion terms, i.e. we set $\mathcal{INT}_{1\,t^{n-1}}^{\,t^n}[g(y(t),t)] = \mathcal{INT}_{1\,t^n}^{\,t^{n+1}}[g(y(t),t)] = \Delta t g(y^{n+1}, t^{n+1})$, while $\mathcal{INT}_2$ will be taken as the mid-point quadrature rule. The resulting scheme reads then

$$\begin{aligned}
&\frac{3}{2}\int_{\Omega_{t^{n+1}}} u_h^{n+1}\psi_h\, d\Omega - 2\int_{\Omega_{t^n}} u_h^n\psi_h\, d\Omega + \frac{1}{2}\int_{\Omega_{t^{n-1}}} u_h^{n-1}\psi_h\, d\Omega \\
&+ \Delta t\int_{\Omega_{t^{n+1}}} \left[\mu\nabla_{\mathbf{x}} u_h^{n+1}\nabla_{\mathbf{x}}\psi_h + \psi_h\nabla_{\mathbf{x}}\cdot(\boldsymbol{\beta} u_h^{n+1})\right] d\Omega - \frac{3}{2}\Delta t\int_{\Omega_{t^{n+1/2}}} \psi_h\nabla_{\mathbf{x}}\cdot(\mathbf{w}_h^{n+1/2}u_h^{n+1})\, d\Omega \\
&\quad + \frac{1}{2}\Delta t\int_{\Omega_{t^{n-1/2}}} \psi_h\nabla_{\mathbf{x}}\cdot(\mathbf{w}_h^{n-1/2}u_h^{n+1})\, d\Omega = \Delta t\int_{\Omega_{t^{n+1}}} f^{n+1}\psi_h\, d\Omega \qquad \forall\psi_h\in\mathcal{X}_{0,h}(\Omega_t)
\end{aligned} \tag{2.2.16}$$

We will first prove the following result :

Lemma 2.2.2 *The discrete solution u_h^n of scheme (2.2.16) satisfies the inequality*

$$\begin{aligned}
&\frac{1}{2}\left\|u_h^{n+1}\right\|^2_{L_2(\Omega_{t^{n+1}})} + \frac{1}{2}\left\|2u_h^{n+1} - u_h^n\right\|^2_{L_2(\Omega_{t^n})} + \frac{1}{2}\left\|u_h^{n+1} - 2u_h^n + u_h^{n-1}\right\|^2_{L_2(\Omega_{t^{n-1}})} \\
&\qquad + \Delta t\mu\left\|\nabla_{\mathbf{x}} u_h^{n+1}\right\|^2_{L_2(\Omega_{t^{n+1}})} + \Delta t\int_{\Omega_{t^{n+1/2}}} \nabla_{\mathbf{x}}\cdot\mathbf{w}_h^{n+1/2}|u_h^{n+1}|^2\, d\Omega \\
&\qquad + \Delta t\int_{\Omega_{t^{n-1/2}}} \nabla_{\mathbf{x}}\cdot\mathbf{w}_h^{n-1/2}\left(|u_h^{n+1}|^2 - 2u_h^{n+1}u_h^n\right) d\Omega \\
&\leq \frac{1}{2}\left\|u_h^n\right\|^2_{L_2(\Omega_{t^n})} + \frac{1}{2}\left\|2u_h^n - u_h^{n-1}\right\|^2_{L_2(\Omega_{t^{n-1}})} + \Delta t\frac{(1+C_\Omega)}{\mu}\left\|f^{n+1}\right\|^2_{H^{-1}(\Omega_{t^{n+1}})}
\end{aligned} \tag{2.2.17}$$

for all $n = 1, 2\ldots$

Proof. Let us take $\psi_h = u_h^{n+1}$ in (2.2.16). The first three terms can be developed in the following way

$$I = \frac{3}{2}\int_{\Omega_{t^{n+1}}} |u_h^{n+1}|^2\, d\Omega - 2\int_{\Omega_{t^n}} u_h^n u_h^{n+1}\, d\Omega + \frac{1}{2}\int_{\Omega_{t^{n-1}}} u_h^{n-1}u_h^{n+1}\, d\Omega \tag{2.2.18}$$

$$= \frac{3}{2}\int_{\Omega_{t^n}} |u_h^{n+1}|^2\, d\Omega - 2\int_{\Omega_{t^n}} u_h^n u_h^{n+1}\, d\Omega + \frac{1}{2}\int_{\Omega_{t^n}} u_h^{n-1}u_h^{n+1}\, d\Omega \tag{2.2.19}$$

$$+ \frac{3}{2}\Delta t\int_{\Omega_{t^{n+1/2}}} \nabla_{\mathbf{x}}\cdot\mathbf{w}_h^{n+1/2}|u_h^{n+1}|^2\, d\Omega - \frac{1}{2}\Delta t\int_{\Omega_{t^{n-1/2}}} \nabla_{\mathbf{x}}\cdot\mathbf{w}_h^{n-1/2}u_h^{n-1}u_h^{n+1}\, d\Omega \tag{2.2.20}$$

where we have employed relation (1.8.19). Let us observe, now, that

$$
\begin{aligned}
&\frac{3}{2}\int_{\Omega_{t^n}} |u_h^{n+1}|^2\,d\Omega - 2\int_{\Omega_{t^n}} u_h^n u_h^{n+1}\,d\Omega + \frac{1}{2}\int_{\Omega_{t^n}} u_h^{n-1}u_h^{n+1}\,d\Omega \\
&= \frac{1}{2}\int_{\Omega_{t^n}} \left(u_h^{n+1} - 2u_h^n + u_h^{n-1}\right) u_h^{n+1}\,d\Omega + \frac{1}{2}\int_{\Omega_{t^n}} \left(2u_h^{n+1} - u_h^n\right) 2u_h^{n+1}\,d\Omega - \int_{\Omega_{t^n}} |u_h^{n+1}|^2\,d\Omega \\
&= \frac{1}{4}\left\|u_h^{n+1}\right\|^2_{L_2(\Omega_{t^n})} + \frac{1}{4}\left\|u_h^{n+1} - 2u_h^n + u_h^{n-1}\right\|^2_{L_2(\Omega_{t^n})} - \frac{1}{4}\left\|2u_h^n - u_h^{n-1}\right\|^2_{L_2(\Omega_{t^n})} \\
&\quad + \frac{1}{4}\left\|2u_h^{n+1}\right\|^2_{L_2(\Omega_{t^n})} + \frac{1}{4}\left\|2u_h^{n+1} - u_h^n\right\|^2_{L_2(\Omega_{t^n})} - \frac{1}{4}\left\|u_h^n\right\|^2_{L_2(\Omega_{t^n})} - \left\|u_h^{n+1}\right\|^2_{L_2(\Omega_{t^n})} \\
&= \left(\frac{1}{4}\left\|u_h^{n+1}\right\|^2_{L_2(\Omega_{t^n})} + \frac{1}{4}\left\|2u_h^{n+1} - u_h^n\right\|^2_{L_2(\Omega_{t^n})}\right) + \frac{1}{4}\left\|u_h^{n+1} - 2u_h^n + u_h^{n-1}\right\|^2_{L_2(\Omega_{t^n})} \\
&\quad - \left(\frac{1}{4}\left\|u_h^n\right\|^2_{L_2(\Omega_{t^n})} + \frac{1}{4}\left\|2u_h^n - u_h^{n-1}\right\|^2_{L_2(\Omega_{t^n})}\right)
\end{aligned}
\tag{2.2.21}
$$

Then, applying (2.2.21) in (2.2.20) we obtain

$$
\begin{aligned}
I \;&= \frac{1}{4}\left\|u_h^{n+1}\right\|^2_{L_2(\Omega_{t^n})} + \frac{1}{4}\left\|2u_h^{n+1} - u_h^n\right\|^2_{L_2(\Omega_{t^n})} + \frac{1}{4}\left\|u_h^{n+1} - 2u_h^n + u_h^{n-1}\right\|^2_{L_2(\Omega_{t^n})} \\
&\quad - \frac{1}{4}\left\|u_h^n\right\|^2_{L_2(\Omega_{t^n})} - \frac{1}{4}\left\|2u_h^n - u_h^{n-1}\right\|^2_{L_2(\Omega_{t^n})} + \frac{3}{2}\Delta t\int_{\Omega_{t^{n+1/2}}} \boldsymbol{\nabla}_{\mathbf{x}}\cdot\mathbf{w}_h^{n+1/2}|u_h^{n+1}|^2\,d\Omega \\
&\quad - \frac{1}{2}\Delta t\int_{\Omega_{t^{n-1/2}}} \boldsymbol{\nabla}_{\mathbf{x}}\cdot\mathbf{w}_h^{n-1/2}u_h^{n-1}u_h^{n+1}\,d\Omega \\
&= \left(\frac{1}{4}\left\|u_h^{n+1}\right\|^2_{L_2(\Omega_{t^{n+1}})} + \frac{1}{4}\left\|2u_h^{n+1} - u_h^n\right\|^2_{L_2(\Omega_{t^n})}\right) + \frac{1}{4}\left\|u_h^{n+1} - 2u_h^n + u_h^{n-1}\right\|^2_{L_2(\Omega_{t^{n-1}})} \\
&\quad - \left(\frac{1}{4}\left\|u_h^n\right\|^2_{L_2(\Omega_{t^n})} + \frac{1}{4}\left\|2u_h^n - u_h^{n-1}\right\|^2_{L_2(\Omega_{t^{n-1}})}\right) + \frac{5}{4}\Delta t\int_{\Omega_{t^{n+1/2}}} \boldsymbol{\nabla}_{\mathbf{x}}\cdot\mathbf{w}_h^{n+1/2}|u_h^{n+1}|^2\,d\Omega \\
&\quad + \frac{1}{4}\Delta t\int_{\Omega_{t^{n-1/2}}} \boldsymbol{\nabla}_{\mathbf{x}}\cdot\mathbf{w}_h^{n-1/2}\left[\left(u_h^{n+1} - 2u_h^n + u_h^{n-1}\right)^2 - \left(2u_h^n - u_h^{n-1}\right)^2 - 2u_h^{n-1}u_h^{n+1}\right]\,d\Omega \\
&= \left(\frac{1}{4}\left\|u_h^{n+1}\right\|^2_{L_2(\Omega_{t^{n+1}})} + \frac{1}{4}\left\|2u_h^{n+1} - u_h^n\right\|^2_{L_2(\Omega_{t^n})}\right) + \frac{1}{4}\left\|u_h^{n+1} - 2u_h^n + u_h^{n-1}\right\|^2_{L_2(\Omega_{t^{n-1}})} \\
&\quad - \left(\frac{1}{4}\left\|u_h^n\right\|^2_{L_2(\Omega_{t^n})} + \frac{1}{4}\left\|2u_h^n - u_h^{n-1}\right\|^2_{L_2(\Omega_{t^{n-1}})}\right) + \frac{5}{4}\Delta t\int_{\Omega_{t^{n+1/2}}} \boldsymbol{\nabla}_{\mathbf{x}}\cdot\mathbf{w}_h^{n+1/2}|u_h^{n+1}|^2\,d\Omega \\
&\quad + \frac{1}{4}\Delta t\int_{\Omega_{t^{n-1/2}}} \boldsymbol{\nabla}_{\mathbf{x}}\cdot\mathbf{w}_h^{n-1/2}\left(|u_h^{n+1}|^2 - 4u_h^{n+1}u_h^n\right)\,d\Omega.
\end{aligned}
$$

Finally, by integrating by parts the convective terms in (2.2.16) and employing the previous

result we have

$$\left(\frac{1}{4}\left\|u_h^{n+1}\right\|^2_{L_2(\Omega_{t^{n+1}})}+\frac{1}{4}\left\|2u_h^{n+1}-u_h^n\right\|^2_{L_2(\Omega_{t^n})}\right)+\frac{1}{4}\left\|u_h^{n+1}-2u_h^n+u_h^{n-1}\right\|^2_{L_2(\Omega_{t^{n-1}})}$$
$$-\left(\frac{1}{4}\left\|u_h^{n}\right\|^2_{L_2(\Omega_{t^n})}+\frac{1}{4}\left\|2u_h^{n}-u_h^{n-1}\right\|^2_{L_2(\Omega_{t^{n-1}})}\right)+\frac{1}{2}\Delta t\int_{\Omega_{t^{n+1/2}}}\boldsymbol{\nabla}_{\mathbf{x}}\cdot\mathbf{w}_h^{n+1/2}|u_h^{n+1}|^2\,d\Omega$$
$$+\frac{1}{2}\Delta t\int_{\Omega_{t^{n-1/2}}}\boldsymbol{\nabla}_{\mathbf{x}}\cdot\mathbf{w}_h^{n-1/2}\left(|u_h^{n+1}|^2-2u_h^{n+1}u_h^n\right)\,d\Omega+\Delta t\mu\left\|\boldsymbol{\nabla}_{\mathbf{x}}u_h^{n+1}\right\|^2_{L_2(\Omega_{t^{n+1}})}$$
$$\leq\Delta t\frac{(1+C_\Omega)}{2\mu}\left\|f^{n+1}\right\|^2_{H^{-1}(\Omega_{t^{n+1}})}+\Delta t\frac{\mu}{2}\left\|\boldsymbol{\nabla}_{\mathbf{x}}u_h^{n+1}\right\|^2_{L_2(\Omega_{t^{n+1}})}\quad(2.2.22)$$

from which inequality (2.2.17) follows.

■

Should the domain be fixed, we would have the following global stability result

$$\frac{1}{2}\left\|u_h^{n+1}\right\|^2_{L_2(\Omega)}+\frac{1}{2}\left\|2u_h^{n+1}-u_h^n\right\|^2_{L_2(\Omega)}$$
$$+\frac{1}{2}\sum_{i=1}^{n}\left\|u_h^{i+1}-2u_h^i+u_h^{i-1}\right\|^2_{L_2(\Omega)}+\Delta t\mu\sum_{i=1}^{n}\left\|\boldsymbol{\nabla}_{\mathbf{x}}u_h^{i+1}\right\|^2_{L_2(\Omega)}$$
$$\leq\frac{1}{2}\left\|u_h^{1}\right\|^2_{L_2(\Omega)}+\frac{1}{2}\left\|2u_h^{1}-u_h^{0}\right\|^2_{L_2(\Omega)}+\Delta t\frac{(1+C_\Omega)}{\mu}\sum_{i=1}^{n}\left\|f^{i+1}\right\|^2_{H^{-1}(\Omega)}\quad(2.2.23)$$

without any condition on Δt.
In the case where the domain moves, we may use the bound

$$-\Delta t\int_{\Omega_{t^{n+1/2}}}\boldsymbol{\nabla}_{\mathbf{x}}\cdot\mathbf{w}_h^{n+1/2}|u_h^{n+1}|^2\,d\Omega-\Delta t\int_{\Omega_{t^{n-1/2}}}\boldsymbol{\nabla}_{\mathbf{x}}\cdot\mathbf{w}_h^{n-1/2}\left(|u_h^{n+1}|^2-2u_h^{n+1}u_h^n\right)\,d\Omega$$
$$\leq\Delta t\gamma_1^{n+1}\left\|u_h^{n+1}\right\|^2_{L_2(\Omega_{t^{n+1}})}+\Delta t\gamma_2^{n}\left\|u_h^{n}\right\|^2_{L_2(\Omega_{t^{n}})}.$$

Then, by applying the discrete Gronwall lemma, as in Section 1.9.2, we can recover a conditional stability. The limitation on the time step Δt is given by

$$\Delta t\leq\frac{1}{\gamma_1^i+\gamma_2^i},\qquad\forall i=2,3,\ldots$$

and depends on the mesh velocity.

Discretisation of the non-conservative formulation

The BDF(2) scheme applied to the non-conservative formulation (1.2.4) reads :

$$\int_{\Omega_{t^{n+1}}}\left(\frac{3}{2}u_h^{n+1}-2u_h^n+\frac{1}{2}u_h^{n-1}\right)\psi_h\,d\Omega+\Delta t\int_{\Omega_{t^{n+1}}}\mu\boldsymbol{\nabla}_{\mathbf{x}}u_h^{n+1}\boldsymbol{\nabla}_{\mathbf{x}}\psi_h\,d\Omega$$
$$+\Delta t\int_{\Omega_{t^{n+1}}}\psi_h(\boldsymbol{\beta}-\mathbf{w}_h^{n+1})\boldsymbol{\nabla}_{\mathbf{x}}\cdot u_h^{n+1}\,d\Omega=\Delta t\int_{\Omega_{t^{n+1}}}f^{n+1}\psi_h\,d\Omega$$
$$\forall\psi_h\in\mathcal{X}_{0,h}(\Omega_t)\quad(2.2.24)$$

As already pointed out for the other schemes previously proposed, this scheme always satisfies the GCL. A stability analysis can be carried out as in the previous section, by taking $\psi_h = u_h^{n+1}$. Again, it can be shown that this scheme is only conditionally stable as the Crank-Nicolson and the Implicit Euler ones. We omit the calculations for the sake of brevity.

2.3 Numerical assessment

We have considered the model advection-diffusion problem on a 2D domain. The ALE mapping has been constructed solving the Laplace problem (1.4.2) at each time step t^n. We have considered both a piecewise linear and piecewise quadratic in time interpolations; more precisely, we have considered the **linear interpolation** of the domain movement in $[t^n, t^{n+1}]$ given by

$$\mathbf{x}_h(Y,t) = \mathbf{x}_h^{n+1}(Y)\frac{(t-t^n)}{\Delta t} - \mathbf{x}_h^n(Y)\frac{(t-t^{n+1})}{\Delta t} \tag{2.3.1}$$

and consequently a constant in time mesh velocity

$$\mathbf{w}_h(Y,t) = \frac{\mathbf{x}_h^{n+1}(Y) - \mathbf{x}_h^n(Y)}{\Delta t}, \tag{2.3.2}$$

where we have noted $\mathbf{x}_h^n(Y) = \mathcal{A}_{h,t_n}(Y)$. As a **quadratic interpolation** of the domain movement in $[t^n, t^{n+1}]$ we have taken

$$\mathbf{x}_h(Y,t) = \mathbf{x}_h^{n+1}(Y)\frac{(t-t^n)(t-t^{n-1})}{2\Delta t^2} - \mathbf{x}_h^n(Y)\frac{(t-t^{n+1})(t-t^{n-1})}{\Delta t^2} + \mathbf{x}_h^{n-1}(Y)\frac{(t-t^{n+1})(t-t^n)}{2\Delta t^2} \tag{2.3.3}$$

and

$$\mathbf{w}_h(Y,t) = \mathbf{x}_h^{n+1}(Y)\frac{2t-t^n-t^{n-1}}{2\Delta t^2} - \mathbf{x}_h^n(Y)\frac{2t-t^{n+1}-t^{n-1}}{\Delta t^2} + \mathbf{x}_h^{n-1}(Y)\frac{2t-t^{n+1}-t^n}{2\Delta t^2}. \tag{2.3.4}$$

In this case, given $\mathbf{x}_h^0(Y)$ and the initial domain velocity $\mathbf{w}_h^0(Y)$, the domain deformation in the first time interval $[t^0, t^1]$ is given by

$$\mathbf{x}_h(Y,t) = \mathbf{x}_h^1(Y)\frac{(t-t^0)^2}{\Delta t^2} + \mathbf{x}_h^0(Y)\left[1 - \frac{(t-t^0)^2}{\Delta t^2}\right] - \mathbf{w}_h^0(Y)\frac{(t-t^0)(t-t^1)}{\Delta t}$$

and

$$\mathbf{w}_h(Y,t) = 2\left(\mathbf{x}_h^1(Y) - \mathbf{x}_h^0(Y)\right)\frac{(t-t^0)}{\Delta t^2} - \mathbf{w}_h^0(Y)\frac{(2t-t^1-t^0)}{\Delta t}$$

For both linear and quadratic interpolation, we have taken $\mathbf{w}_h(Y,t^n) = \lim_{t\to t^n_-} \mathbf{w}_h(Y,t)$ since $\mathbf{w}_h$ is discontinuous at the time instants t^n.

All the numerical schemes proposed in the previous sections, i.e. the Implicit Euler, the Crank-Nicolson and the BDF(2) schemes in both conservative and non-conservative formulation (in the following indicated by the suffixes *nc* and *c*, respectively) have been implemented. For the conservative formulation, we have considered the time discretisation which don't satisfy the GCL (in the following indicated with the suffix *noGCL*), the one which satisfies the GCL for a linear in time deformation of the domain (suffix *GCL1*) and the discretisation which satisfies the GCL for a quadratic in time domain deformation (suffix *GCL2*). The quadrature

formulae $\mathcal{INT}_1$ and $\mathcal{INT}_2$ have been taken as the mid-point rule for the schemes *GCL1* and as the two point Gaussian quadrature formula for the schemes *GCL2*. We remind that, for a 2D problem, the Crank-Nicolson scheme (2.2.3) always satisfies the GCL for a linear in time deformation of the domain. Then, in this case, the scheme GCL0 coincides with GCL1.
We will present hereafter two test cases. The first one aims at validating the stability results derived in the previous sections while the second one will focus on the time accuracy.

First test case - stability analysis

We have taken as reference domain Ω_0 the unit 2D square. The domain deformation is given by

$$\mathbf{x} = \mathcal{A}_t(\mathbf{Y}) : \quad \begin{cases} x_1 = Y_1[2 - \cos(20\pi t)] \\ x_2 = Y_2[2 - \cos(20\pi t)] \end{cases} \tag{2.3.5}$$

We observe that the deformed domain is still a square that expands and contracts periodically with a period $T = 1/10$. Moreover, since $\mathcal{A}_t(\mathbf{Y})$ is linear in $\mathbf{Y}$, by solving a Laplace problem at each time step t^n for the discrete ALE mapping, we recover the deformation given in (2.3.5) exactly. The mesh velocity on the domain Ω_t is given by

$$\mathbf{w} = \left[\frac{20\pi x_1 \sin(20\pi t)}{2 - \cos(20\pi t)}, \quad \frac{20\pi x_2 \sin(20\pi t)}{2 - \cos(20\pi t)}\right]^T$$

and its divergence is constant in whole the domain and is given by $\nabla_{\mathbf{x}} \cdot \mathbf{w} = \frac{40\pi \sin(20\pi t)}{2-\cos(20\pi t)}$.
We have considered the problem

$$\begin{cases} \dfrac{\partial u}{\partial t} - 0.01\Delta u = 0, & \text{in } \Omega_t \\ u = 0, & \text{on } \partial\Omega_t \\ u(0) = 1600 Y_1(1 - Y_1)Y_2(1 - Y_2), & \text{in } \Omega_0. \end{cases} \tag{2.3.6}$$

Observe that for such a problem $\|u(t)\|_{L_2(\Omega_t)}$ is a decreasing quantity (see inequality (1.6.8)). Problem (2.3.6) has been discretized in space with $\mathbb{P}_1$ finite elements. The monotonicity property of the L^2 norm of the solution is clearly valid for the semi-discrete problem as well. When problem (2.3.6) is defined on a fixed domain, the Implicit-Euler and the Crank-Nicolson schemes preserve that property, i.e. the computed solution u_h^n has a decreasing L^2 norm. On the other hand, when considering a moving domain, starting from our estimates, we should expect that only the Implicit Euler scheme applied to the conservative formulation and satisfying the GCL will preserve that property.
Figures 2.1 and 2.2 show, for the two schemes and the two cases of a linear and a quadratic interpolation of the domain deformation, the computed quantity $\|u_h^n\|^2_{L_2(\Omega_{t^n})}$ together with the "exact" norm $\|u_h(t)\|^2_{L_2(\Omega_t)}$ of the solution of the semi-discrete problem (computed on the same mesh but with a very small time step) during the time interval $[0, 0.4]$ (corresponding to 4 periods of oscillation of the domain). In all cases we have used a time step $\Delta t = 0.01$.
We can observe that, only the Implicit Euler discretisation which satisfies the GCL, applied to the conservative formulation, is strictly monotone, as it was predicted by our estimates. Furthermore, for the Crank-Nicolson scheme, the L^2 norm increases during the expansion of the domain and decreases during the contraction phase, coherently with estimate (2.2.6).

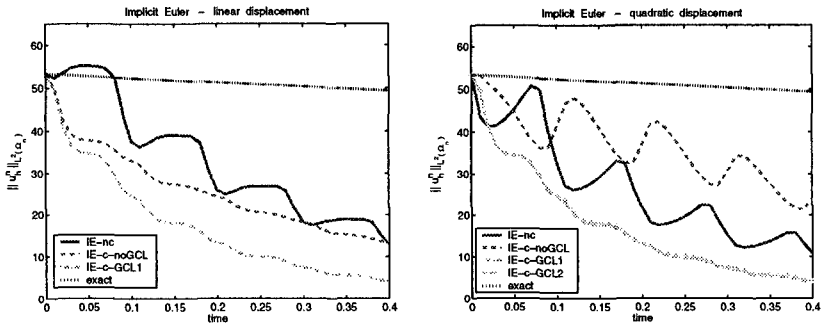

Figure 2.1: Test case 1 : L^2 norm of the computed and "exact" solution as a function of time for the Implicit Euler scheme. Interpolation in time of the domain deformation : linear on the left and quadratic on the right.

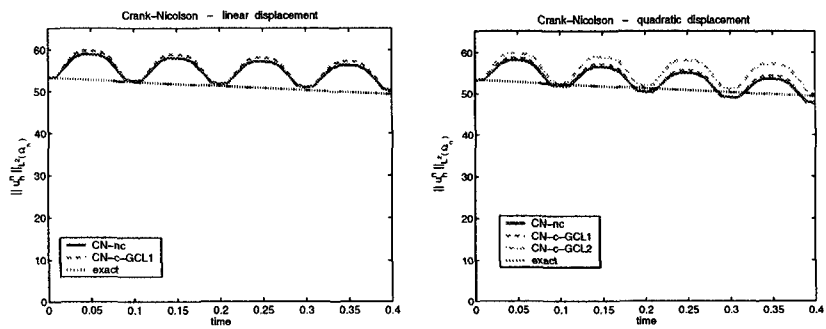

Figure 2.2: Test case 1 : L^2 norm of the computed and "exact" solution as a function of time for the Crank-Nicolson scheme. Interpolation in time of the domain deformation : linear on the left and quadratic on the right.

The BDF(2) scheme, even when applied to problem (2.3.6) on a fixed domain, does not feature the monotonicity property of the L^2 norm of the solution. On the other hand, as shown by estimate (2.2.17), the quantity which turns out to be decreasing, for a problem on a fixed domain, is $\varepsilon_h^n = \frac{1}{2}\|u_h^n\|^2_{L_2(\Omega_{t^n})} + \frac{1}{2}\|2u_h^n - u_h^{n-1}\|^2_{L_2(\Omega_{t^{n-1}})}$. Observe that $\varepsilon_h^n \to \|u_h(t^n)\|^2_{L_2(\Omega_t)}$ when $\Delta t \to 0$. Figure 2.3 shows the quantity ε_h^n for the different versions of the BDF(2) scheme and for the two cases of a linear and a quadratic in time interpolation of the domain deformation. On the same picture, we report also the norm $\|u_h(t)\|_{L_2(\Omega_t)}$ of the "exact" solution. It is evident that the quantity ε_h^n is not decreasing, coherently with estimate (2.2.17).

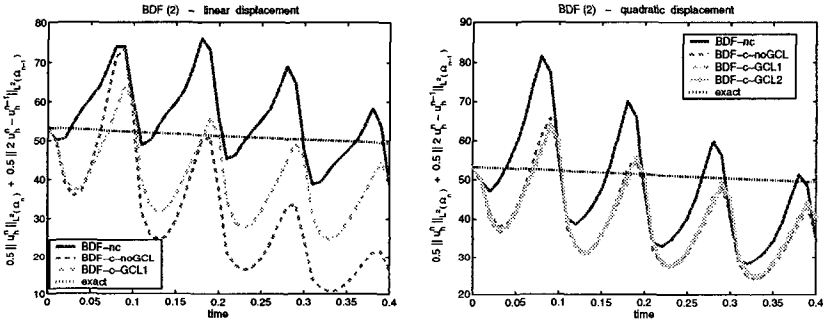

Figure 2.3: Test case 1 : quantity ε_h^n as a function of time computed by the BDF(2) scheme, compared to the "exact" value $\|u_h(t)\|_{L_2(\Omega_t)} = \lim_{\Delta t \to 0} \varepsilon_h^n$. Interpolation in time of the domain deformation : linear on the left and quadratic on the right.

Finally, in Figure 2.4, we report the L^2 norm $\|u_h^n\|_{L_2(\Omega_{t^n})}$ of the solution computed by the BDF(2) scheme. This figure highlights the dissipation properties of this scheme and should be compared to Figures 2.1 and 2.2.

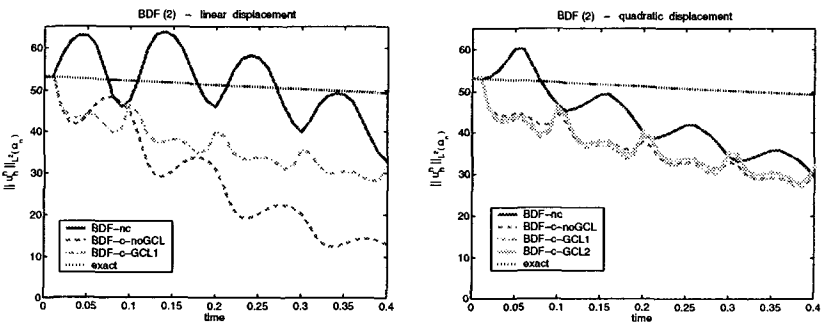

Figure 2.4: Test case 1 : L^2 norm of the computed and "exact" solution as a function of time for the BDF(2) scheme. Interpolation in time of the domain deformation : linear on the left and quadratic on the right.

Second test case - error analysis in time

We have considered again as reference configuration Ω_0 the unit 2D square. The domain deformation is given by

$$\mathbf{x} = \mathcal{A}_t(\mathbf{Y}): \quad \begin{cases} x_1 = Y_1[2 - \cos(10\pi t)] \\ x_2 = Y_2[2 - \cos(10\pi t)] \end{cases} \tag{2.3.7}$$

The problem we have considered is

$$\begin{cases} \dfrac{\partial u}{\partial t} - 0.1\Delta u = f, & \text{in } \Omega_t \\ u = 0, & \text{on } \partial\Omega_t \\ u(0) = 16Y_1(1-Y_1)Y_2(1-Y_2), & \text{in } \Omega_0. \end{cases} \tag{2.3.8}$$

The forcing term f has been chosen in such a way that the corresponding exact solution $u(\mathbf{Y}, t)$ is

$$u(\mathbf{Y}, t) = 16\left(1 + \frac{1}{2}\sin(5\pi t)\right) Y_1(1-Y_1)Y_2(1-Y_2)$$

Thus

$$f(\mathbf{Y}, t) = 40\pi\cos(5\pi t)Y_1(1-Y_1)Y_2(1-Y_2) + \frac{3.2(1+0.5\sin(5\pi t))}{(2-\cos(10\pi t))^2}(Y_1(1-Y_1)+Y_2(1-Y_2)) - \frac{160\pi(1+0.5\sin(5\pi t))\sin(5\pi t)}{2-\cos(10\pi t)}Y_1Y_2(2-3Y_1-3Y_2+4Y_1Y_2)$$

Problem (2.3.8) has been discretized in space with $\mathbb{P}_2$ isoparametric elements. Figure 2.5 shows the mesh used (on the left) and the initial solution (on the right). We have taken

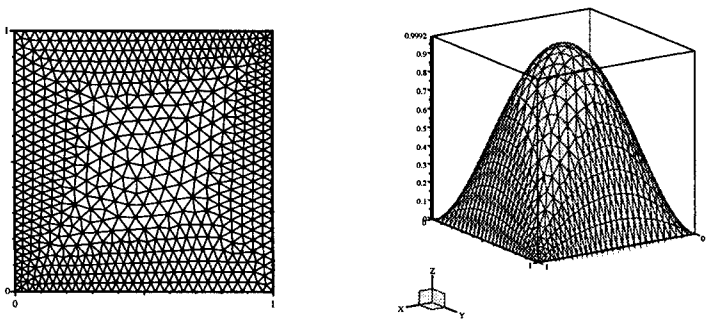

Figure 2.5: Mesh and initial solution of the problem illustrated in Test case 2

a sequence of decreasing time steps $\Delta t = 1/20, 1/40, \ldots, 1/320$ and we have computed the L^2 norm of the error at time $t = 0.3$ over the actual domain Ω_t. In all cases the error is

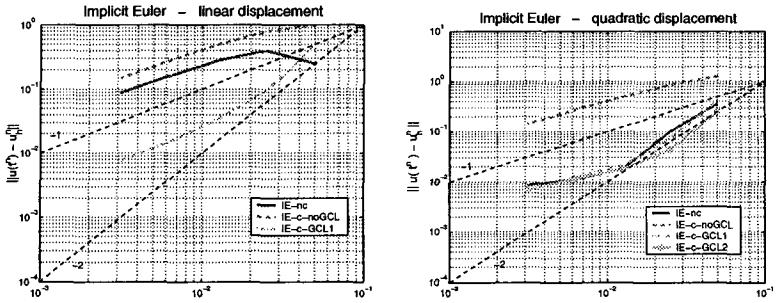

Figure 2.6: Test case 2 : error in the L^2 norm as a function of the time step Δt for the Implicit Euler scheme. Interpolation in time of the domain deformation : linear on the left and quadratic on the right.

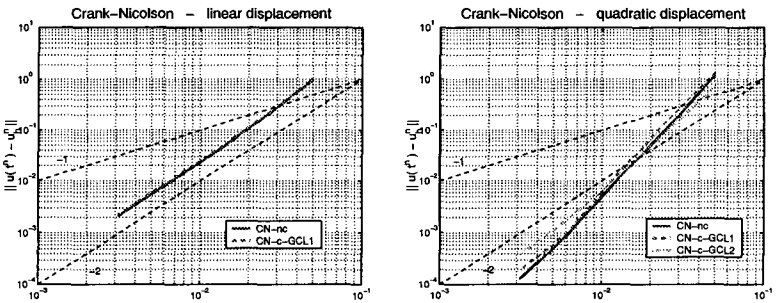

Figure 2.7: Test case 2 : error in the L^2 norm as a function of the time step Δt for the Crank-Nicolson scheme. Interpolation in time of the domain deformation : linear on the left and quadratic on the right.

dominated by the time discretisation. The results obtained are presented in figures 2.6, 2.7, 2.8 for the Implicit Euler, the Crank-Nicolson and the BDF(2) schemes, respectively.

We observe that all the different implementations of the Implicit Euler scheme are linearly convergent in time while all the Crank-Nicolson ones are quadratically convergent.

On the contrary, the BDF(2) scheme, applied to the non-conservative formulation or to the conservative one, without satisfying the GCL, is only linearly convergent when a linear in time interpolation of the domain deformation is considered. We recover a second order accuracy when employing a quadratic interpolation of the domain deformation. This result is not surprising; indeed, when a linear interpolation of the domain deformation is considered, expression (2.3.2) is only a linear approximation of the real domain velocity $\mathbf{w}_h(t^{n+1})$ which should be employed in both (2.2.12) and (2.2.24), whereas, when a quadratic interpolation is considered, th corresponding expression (2.3.4) provides a second order approximation of $\mathbf{w}_h(t^{n+1})$.

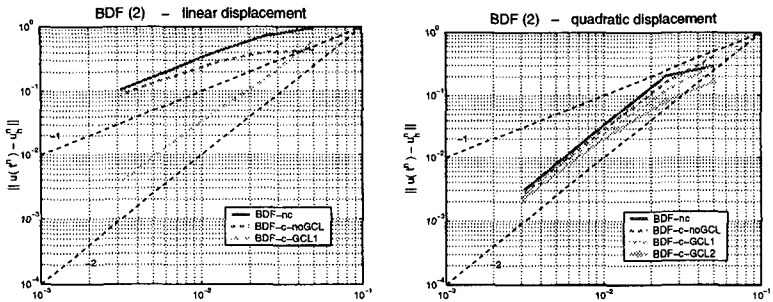

Figure 2.8: Test case 2 : error in the L^2 norm as a function of the time step Δt for the BDF(2). Interpolation in time of the domain deformation : linear on the left and quadratic on the right.

Finally, we remark that the BDF(2) scheme that satisfies the GCL, applied to the conservative formulation, preserves the second order accuracy even though the domain deformation is only linearly interpolated in time.

Chapter 3

Incompressible Navier-Stokes equations on moving domains

3.1 Introduction

In this chapter we will extend the Arbitrary Lagrangian Eulerian formulation to the Navier-Stokes equations for incompressible Newtonian fluids. The analysis that we are going to carry out will be used in Chapter 4 which deals with the fluid-structure interaction problem.
Let $\Omega_t \subset \mathbb{R}^d$ be a bounded domain, whose movement is described by a function $\mathbf{g} : \partial\Omega_0 \times I \to \mathbb{R}^{d-1}$ which identifies the position of the boundary $\partial\Omega_t$ at each $t \in I$ (i.e. $\partial\Omega_t = \mathbf{g}(\partial\Omega_0)$). We denote by $\mathbf{u}(\mathbf{x}, t)$, (with $\mathbf{x} \in \Omega_t,\ t \in I$), the fluid velocity and $p(\mathbf{x}, t)$ the fluid pressure. Then the Navier-Stokes equations read

$$\begin{cases} \rho\partial_t \mathbf{u} + \rho\mathbf{u} \cdot \nabla_{\mathbf{x}}\mathbf{u} - \mathrm{div}_{\mathbf{x}}(2\mu\mathbf{D}_{\mathbf{x}}(\mathbf{u}) - p\mathbf{I}) = \mathbf{f} \\ \mathrm{div}_{\mathbf{x}}\,\mathbf{u} = 0 \end{cases} \qquad \text{in } \Omega_t,\ t \in I \tag{3.1.1}$$

where $\mathbf{D}$ is the *strain tensor*

$$\mathbf{D}_{\mathbf{x}}(\mathbf{u}) = \frac{\nabla_{\mathbf{x}}\mathbf{u} + \nabla_{\mathbf{x}}^T\mathbf{u}}{2}, \tag{3.1.2}$$

$\mathbf{I}$ is the identity tensor, ρ the fluid density and μ the dynamic viscosity, which is here taken as a (positive) constant. Equations (3.1.1) must be supplied with initial conditions for the velocity field

$$\mathbf{u}(\mathbf{x}, 0) = \mathbf{u}_0, \qquad \text{in } \Omega_0 \tag{3.1.3}$$

and suitable boundary conditions.
Let the boundary $\partial\Omega_t$ be split into two non-overlapping parts $\partial\Omega_t = \Gamma_t^D \cup \Gamma_t^N$. In this Chapter we will consider the boundary conditions

$$\mathbf{u} = \mathbf{\Phi}, \qquad \text{on } \Gamma_t^D \tag{3.1.4}$$

$$-p\mathbf{n} + 2\mu\mathbf{D}_{\mathbf{x}}(\mathbf{u}) \cdot \mathbf{n} = \boldsymbol{\sigma} \qquad \text{on } \Gamma_t^N, \tag{3.1.5}$$

where $\mathbf{n}$ is the unit outward normal vector to $\partial\Omega_t$. A typical situation occurs when $\mathbf{\Phi} \circ \mathbf{g} = \partial_t \mathbf{g}$ on Γ_0^D, i.e. the fluid has the same velocity as the moving boundary on Γ_t^D. This will be always

the case when dealing with a fluid-structure interaction problem where Γ_t^D corresponds to the interface between fluid and structure. Other types of boundary conditions, more suited than (3.1.5) for hemodynamics applications, may be considered as well on Γ_t^N. An account will be given in Section 5.2.2 of Chapter 5.
Several theoretical results concerning equations (3.1.1) on moving domains can be found in the literature. In [33] existence of a weak solution for the non-homogeneous Dirichlet problem is proved by a penalty method, while in [49] equations (3.1.1) are recast on a cylindrical space-time domain introducing a suitable diffeomorphism. An result of existence of a weak solution is obtained also in [84, 85] through an elliptic regularization, under weaker hypotheses on the regularity of the domain boundary than in the previously cited papers. In those works a regularity result is presented as well.

3.2 Energy inequality for the Navier-Stokes equations on moving domains

We wish to point out that the fluid equations (3.1.1) defined on a moving domain maintain the same stability properties that they feature on a fixed domain. We derive here an energy inequality for the problem (3.1.1)÷(3.1.5) with homogeneous Dirichlet boundary conditions ($\mathbf{\Phi} = \mathbf{0}$). By standard techniques this result can be extended to the case of non-zero Dirichlet boundary data, by resorting to a suitable extension of the function $\mathbf{\Phi}$ to the interior of the domain Ω_t (see e.g. [87]).
We first recall the important inequality (see e.g. [14, Theorem 6.3-4]), which holds for all $\mathbf{u} \in [H^1(\Omega_t)]^d$ vanishing on a measurable portion Γ_t^D of the domain boundary :

$$\int_{\Omega_t} \mathbf{D_x(u)} : \mathbf{D_x(u)}\, d\Omega \geq C_0(\Omega_t) \|\nabla_{\mathbf{x}} \mathbf{u}\|^2_{L^2(\Omega_t)} \tag{3.2.1}$$

where $C_0(\Omega_t)$ is a positive constant, depending eventually on Ω_t. This inequality is a consequence of the well-known *Korn inequality*, whose demonstration can be foung e.g. in [21]. We here suppose that the domain deformation is such that $C_0(\Omega_t)$ is uniformly bounded from below with respect to t and we indicate with C_0 the more restrictive constant such that (3.2.1) holds for all $t \in I$.
We multiply the first of (3.1.1) by $\mathbf{u}$ and integrate over the current domain Ω_t. Proceeding as in Chapter 1 for the treatment of the time derivative, we have

$$\int_{\Omega_t} \frac{\partial \mathbf{u}}{\partial t} \cdot \mathbf{u}\, d\Omega = \frac{1}{2}\frac{d}{dt}\int_{\Omega_t} |\mathbf{u}|^2\, d\Omega - \frac{1}{2}\int_{\partial\Omega_t} |\mathbf{u}|^2\, \dot{\mathbf{g}} \cdot \mathbf{n}\, d\Gamma,$$

where we have noted $\dot{\mathbf{g}} = \partial_t \mathbf{g}$. After integration by parts of the convective, viscous and pressure terms, and observing that

$$\int_{\Omega_t} \mathbf{D_x(u)} : \nabla_{\mathbf{x}} \mathbf{u}\, d\Omega = \int_{\Omega_t} \mathbf{D_x(u)} : \mathbf{D_x(u)}\, d\Omega,$$

thanks to the symmetry of the strain tensor $\mathbf{D_x(u)}$, we obtain

$$\frac{\rho}{2}\frac{d}{dt}\int_{\Omega_t} |\mathbf{u}|^2\, d\Omega - \frac{\rho}{2}\int_{\Omega_t} \mathrm{div}_{\mathbf{x}}\, \mathbf{u}\, |\mathbf{u}|^2\, d\Omega + \frac{\rho}{2}\int_{\Gamma_t^N} |\mathbf{u}|^2\, (\mathbf{u} - \dot{\mathbf{g}}) \cdot \mathbf{n}\, d\Gamma + \kappa \int_{\Omega_t} |\nabla_{\mathbf{x}} \mathbf{u}|^2\, d\Omega$$
$$- \int_{\Omega_t} \mathrm{div}_{\mathbf{x}}\, \mathbf{u}\, p\, d\Omega = \int_{\Omega_t} \mathbf{f} \cdot \mathbf{u}\, d\Omega + \int_{\Gamma_t^N} \boldsymbol{\sigma} \cdot \mathbf{u}\, d\Gamma. \tag{3.2.2}$$

where we have used (3.2.1) and we have set $\kappa = 2\mu C_0$. Using the constraint $\mathrm{div}_{\mathbf{x}}\,\mathbf{u} = 0$, the previous equation simplifies in

$$\frac{\rho}{2}\frac{d}{dt}\|\mathbf{u}\|^2_{L_2(\Omega_t)} + \frac{\rho}{2}\int_{\Gamma_t^N}|\mathbf{u}|^2(\mathbf{u}-\dot{\mathbf{g}})\cdot\mathbf{n}\,d\Gamma + \kappa\|\boldsymbol{\nabla}_{\mathbf{x}}\mathbf{u}\|^2_{L_2(\Omega_t)} = \int_{\Omega_t}\mathbf{f}\cdot\mathbf{u}\,d\Omega + \int_{\Gamma_t^N}\boldsymbol{\sigma}\cdot\mathbf{u}\,d\Gamma. \tag{3.2.3}$$

The right hand side (r.h.s.) can be bounded as follows :

$$\begin{aligned}\text{r.h.s.} &\le \|\mathbf{f}\|_{H^{-1}(\Omega_t)}\|\mathbf{u}\|_{H^1(\Omega_t)} + \|\boldsymbol{\sigma}\|_{L^2(\Gamma_t^N)}\|\mathbf{u}\|_{L^2(\Gamma_t^N)}\\ &\le \sqrt{1+C_\Omega}\,\|\mathbf{f}\|_{H^{-1}(\Omega_t)}\,\|\boldsymbol{\nabla}_{\mathbf{x}}\mathbf{u}\|_{L_2(\Omega_t)} + \gamma\sqrt{1+C_\Omega}\|\boldsymbol{\sigma}\|_{L^2(\Gamma_t^N)}\,\|\boldsymbol{\nabla}_{\mathbf{x}}\mathbf{u}\|_{L_2(\Omega_t)}\\ &\le \frac{(1+C_\Omega)}{\kappa}\|\mathbf{f}\|^2_{H^{-1}(\Omega_t)} + \frac{\gamma^2(1+C_\Omega)}{\kappa}\|\boldsymbol{\sigma}\|^2_{L^2(\Gamma_t^N)} + \frac{\kappa}{2}\|\boldsymbol{\nabla}_{\mathbf{x}}\mathbf{u}\|^2_{L_2(\Omega_t)}\end{aligned}$$

where we have employed the Poincaré inequality (1.3.7) and a trace inequality $\|\mathbf{u}\|_{L^2(\Gamma_t^N)} \le \gamma\|\mathbf{u}\|_{H^1(\Omega_t)}$. Finally, by putting this estimate in (3.2.3) and integrating in time, we obtain

$$\begin{aligned}&\rho\|\mathbf{u}(t)\|^2_{L_2(\Omega_t)} + \rho\int_I\int_{\Gamma_s^N}|\mathbf{u}|^2(\mathbf{u}-\dot{\mathbf{g}})\cdot\mathbf{n}\,d\Gamma ds + \kappa\int_I\|\boldsymbol{\nabla}_{\mathbf{x}}\mathbf{u}(s)\|^2_{L_2(\Omega_s)}\,ds\\ &\qquad\le \rho\|\mathbf{u}_0\|^2_{L_2(\Omega_0)} + \frac{2(1+C_\Omega)}{\kappa}\int_I\left[\|\mathbf{f}(s)\|^2_{H^{-1}(\Omega_s)} + \gamma^2\|\boldsymbol{\sigma}(s)\|^2_{L^2(\Gamma_s^N)}\right]ds\end{aligned} \tag{3.2.4}$$

If $\Gamma_t^N = \emptyset$, the previous inequality provides an a-priori stability for the solution of the Navier-Stokes equations on a moving domain which is analogous to the one holding on a fixed domain. On the contrary, if $\Gamma_t^N \neq \emptyset$, the term $\rho\int_I\int_{\Gamma_s^N}|\mathbf{u}|^2(\mathbf{u}-\dot{\mathbf{g}})\cdot\mathbf{n}\,d\Gamma ds$ does not have a definite sign and does not allow to obtain the desired stability result. However, this drawback appears also on a fixed domain and it is not strictly related to the domain deformation. We remark, yet, that if $(\mathbf{u}-\dot{\mathbf{g}})\cdot\mathbf{n} \ge 0$, $\forall\mathbf{x}\in\Gamma_t^N$, this boundary term is positive and a global stability is thus recovered. This occurs when Γ_t^N is an *outflow section*; indeed, $\mathbf{u}-\dot{\mathbf{g}}$ represents the relative fluid velocity with respect to the moving boundary and if $(\mathbf{u}-\dot{\mathbf{g}})\cdot\mathbf{n} \ge 0$ the fluid actually exits the domain through Γ_t^N.
An existence and stability result for problem (3.1.1) with non-homogeneous Neumann boundary conditions on a fixed domain can be found in [46] under the hypotheses that $\boldsymbol{\sigma}$, $\mathbf{f}$ and $\mathbf{u}_0$ are small enough.

3.3 ALE formulation of Navier-Stokes equations

Let Ω_0 be the reference configuration. We introduce a family of ALE mappings

$$\mathcal{A}_t : \Omega_0 \subset \mathbb{R}^d \to \Omega_t, \qquad \mathbf{x}(\mathbf{Y},t) = \mathcal{A}_t(\mathbf{Y}), \quad \forall t\in I$$

as illustrated in Chapter 1. Then, equations (3.1.1) can be rewritten in ALE form as

$$\begin{cases}\rho\left.\dfrac{\partial\mathbf{u}}{\partial t}\right|_{\mathbf{Y}} + \rho(\mathbf{u}-\mathbf{w})\cdot\boldsymbol{\nabla}_{\mathbf{x}}\mathbf{u} - \mathrm{div}_{\mathbf{x}}(2\mu\mathbf{D}_{\mathbf{x}}(\mathbf{u}) - p\mathbf{I}) = \mathbf{f}\\ \mathrm{div}_{\mathbf{x}}\,\mathbf{u} = 0\end{cases} \qquad \text{in } \Omega_t,\ t\in I. \tag{3.3.1}$$

In order to write a weak formulation of (3.3.1), we introduce the following functional spaces :

$$\hat{\mathbf{V}}(\Omega_0) = \left[H^1(\Omega_0)\right]^d, \quad \hat{\mathbf{V}}_{\Gamma^D}(\Omega_0) = \left[H^1_{\Gamma^D}(\Omega_0)\right]^d \equiv \{\hat{\mathbf{v}} \in \hat{\mathbf{V}}(\Omega_0),\ \hat{\mathbf{v}} = 0 \text{ on } \Gamma_0^D\}, \tag{3.3.2}$$

$$\hat{Q}(\Omega_0) = L^2(\Omega_0), \qquad \hat{Q}_0(\Omega_0) \equiv \{\hat{q} \in \hat{Q}(\Omega_0), \quad \int_{\Omega_0} q\, d\Omega = 0\} \tag{3.3.3}$$

and

$$\mathbf{V}(\Omega_t) = \{\mathbf{v} : \Omega_t \times I \to \mathbb{R}^d, \quad \mathbf{v} = \hat{\mathbf{v}} \circ \mathcal{A}_t^{-1},\ \hat{\mathbf{v}} \in \hat{\mathbf{V}}(\Omega_0)\} \tag{3.3.4}$$

$$Q(\Omega_t) = \{q : \Omega_t \times I \to \mathbb{R}, \quad q = \hat{q} \circ \mathcal{A}_t^{-1},\ \hat{q} \in \hat{Q}(\Omega_0)\}. \tag{3.3.5}$$

Similar definitions hold for $\mathbf{V}_{\Gamma^D}(\Omega_t)$ and $Q_0(\Omega_t)$. As done in the previous Chapters, we can introduce either a non-conservative or a conservative formulation.

Non-conservative formulation

The non conservative formulation reads : *for almost every* $t \in I$ *find* $t \to \mathbf{u}(t) \in \mathbf{V}(\Omega_t)$, *with* $\mathbf{u}(t) = \mathbf{\Phi}(t)$ *on* Γ_t^D, $\mathbf{u}(0) = \mathbf{u}_0$ *in* Ω_0 *and* $t \to p(t) \in Q(\Omega_t)$ *such that*

$$\begin{cases} \rho \displaystyle\int_{\Omega_t} \left.\frac{\partial \mathbf{u}}{\partial t}\right|_{\mathbf{Y}} \cdot \mathbf{v}\, d\Omega + \rho \int_{\Omega_t} \left[(\mathbf{u} - \mathbf{w}) \cdot \boldsymbol{\nabla}_{\mathbf{x}}\right] \mathbf{u} \cdot \mathbf{v}\, d\Omega \\ \qquad +2\mu \displaystyle\int_{\Omega_t} \mathbf{D}_{\mathbf{x}}(\mathbf{u}) : \boldsymbol{\nabla}_{\mathbf{x}}\mathbf{v}\, d\Omega - \int_{\Omega_t} \mathrm{div}_{\mathbf{x}}\, \mathbf{v}\, p\, d\Omega = \int_{\Omega_t} \mathbf{f} \cdot \mathbf{v}\, d\Omega + \int_{\Gamma_t^N} \boldsymbol{\sigma} \cdot \mathbf{v}\, d\Gamma \qquad \forall \mathbf{v} \in \mathbf{V}_{\Gamma^D}(\Omega_t) \\ \displaystyle\int_{\Omega_t} \mathrm{div}_{\mathbf{x}}\, \mathbf{u}\, q\, d\Omega = 0 \qquad \forall q \in Q(\Omega_t) \end{cases} \tag{3.3.6}$$

If $\Gamma_t^N = \emptyset$, the space $\mathbf{V}_{\Gamma^D}(\Omega_t)$ coincides with $[H_0^1(\Omega_t)]^d$. In this case the functional space $Q(\Omega_t)$ in (3.3.6) should be replaced by $Q_0(\Omega_t)$ (i.e. the pressure is defined up to a constant) and the non-homogeneous Dirichlet boundary datum $\mathbf{\Phi}(t)$ must satisfy the compatibility condition

$$\int_{\partial\Omega_t} \mathbf{\Phi}(t) \cdot \mathbf{n}\, d\Gamma = 0, \qquad \forall t \in I.$$

Conservative formulation

In a very similar way as done in Chapter 1 for a generic conservation law, we can rewrite the weak problem (3.3.6) in conservative form

$$\begin{cases} \rho \dfrac{d}{dt} \displaystyle\int_{\Omega_t} \mathbf{u} \cdot \mathbf{v}\, d\Omega + \rho \int_{\Omega_t} \mathrm{div}_{\mathbf{x}} \left[(\mathbf{u} - \mathbf{w}) \otimes \mathbf{u}\right] \cdot \mathbf{v}\, d\Omega \\ \qquad +2\mu \displaystyle\int_{\Omega_t} \mathbf{D}_{\mathbf{x}}(\mathbf{u}) : \boldsymbol{\nabla}_{\mathbf{x}}\mathbf{v}\, d\Omega - \int_{\Omega_t} \mathrm{div}_{\mathbf{x}}\, \mathbf{v}\, p\, d\Omega = \int_{\Omega_t} \mathbf{f} \cdot \mathbf{v}\, d\Omega + \int_{\Gamma_t^N} \boldsymbol{\sigma} \cdot \mathbf{v}\, d\Gamma \qquad \forall \mathbf{v} \in \mathbf{V}_{\Gamma^D}(\Omega_t) \\ \displaystyle\int_{\Omega_t} \mathrm{div}_{\mathbf{x}}\, \mathbf{u}\, q\, d\Omega = 0 \qquad \forall q \in Q(\Omega_t) \end{cases} \tag{3.3.7}$$

where, we have coherently written also the convective term in conservative form.

3.4 Finite element discretisation

A finite element approximation of problem (3.3.6), or equivalently (3.3.7), involves at the same time the discretisation of the fluid equations and that of the domain movement, which can be chosen, for instance, as an harmonic extension of the boundary deformation $\mathbf{g}$ (see problem (1.4.2) in Chapter 1). As pointed out in section 1.5, the two discretisations are closely related.

Let us consider a triangulation $\mathcal{T}_{h,0}$ of the reference domain Ω_0 which, for simplicity, we suppose made up of elements with straight edges, and the space of Lagrangian finite elements $\mathcal{F}_{n,1}(\mathcal{T}_{h,0})$ of degree n and mapping of degree 1 (since we have taken a mesh of straight elements).

Whenever the fluid problem is defined on a fixed domain, say Ω_0, many finite element spaces $\hat{\mathbf{V}}_h(\Omega_0)$ and $\hat{Q}_h(\Omega_0)$, approximating $\hat{\mathbf{V}}(\Omega_0)$ and $\hat{Q}(\Omega_0)$ respectively, have been introduced in the literature, that satisfy the well known inf-sup (or LBB) condition (see e.g. [9]) :

$$\inf_{\hat{q}_h \in \hat{Q}_h(\Omega_0)} \sup_{\hat{\mathbf{v}}_h \in \hat{\mathbf{V}}_h(\Omega_0)} \frac{\int_{\Omega_0} \operatorname{div} \hat{\mathbf{v}}_h \, q_h \, d\Omega}{\|\hat{\mathbf{v}}_h\|_{H^1(\Omega_0)} \|\hat{q}_h\|_{L_2(\Omega_0)}} \geq \beta \tag{3.4.1}$$

where the constant $\beta > 0$ is independent of h. We remind that this property is necessary for the well posedness of the discrete problem.

We will focus here on continuous approximations of the pressure. Among the choices that satisfy (3.4.1) we mention the Taylor-Hood finite elements $\mathbb{P}_2 - \mathbb{P}_1$ or their generalisation to higher order polynomials $\mathbb{P}_k - \mathbb{P}_{k-1}$ introduced in [8] which corresponds to take

$$\hat{\mathbf{V}}_h(\Omega_0) = \mathcal{F}_{k,1}(\mathcal{T}_{h,0}), \qquad \hat{Q}_h(\Omega_0) = \mathcal{F}_{k-1,1}(\mathcal{T}_{h,0}), \quad k > 1,$$

and provides an optimal convergence rate for a Stokes problem, i.e.

$$\|\mathbf{u} - \mathbf{u}_h\|_{H^1(\Omega_0)} + \|p - p_h\|_{L_2(\Omega_0)} \leq C h^k \left(\|\mathbf{u}\|_{H^{k+1}(\Omega_0)} + \|p\|_{H^k(\Omega_0)} \right), \tag{3.4.2}$$

whenever the solution is regular enough.

Another admissible choice is $\mathbb{P}_1^b - \mathbb{P}_1$ where a piecewise linear approximation for the pressure is employed (i.e. $\hat{Q}_h(\Omega_0) = \mathcal{F}_{1,1}(\mathcal{T}_{h,0})$) while the velocity is approximated by piecewise linear functions suitably enriched with bubble functions which are element-based polynomials that vanish on the element boundary. These finite elements provide a linear convergence with respect to h for a Stokes problem, i.e.

$$\|\mathbf{u} - \mathbf{u}_h\|_{H^1(\Omega_0)} + \|p - p_h\|_{L_2(\Omega_0)} \leq C h \left(\|\mathbf{u}\|_{H^2(\Omega_0)} + \|p\|_{H^1(\Omega_0)} \right), \tag{3.4.3}$$

provided the solution is regular enough.

Finally we mention the so called $(\mathbb{P}_1 iso \mathbb{P}_2) - \mathbb{P}_1$ elements where, again, the pressure is piecewise linear, while the velocity has the same number of degrees of freedom as in the $\mathbb{P}_2$ case but it is piecewise linear over a suitable decomposition of each triangle K. In the 2D case the decomposition is shown in figure 3.1, while in 3D the decomposition consists of 8 tetrahedra. For these finite elements, error estimate (3.4.3) holds as well.

We consider now the case of a moving domain. The proper ALE extension of the finite element spaces for the velocity and the pressure to a moving domain are

$$\begin{aligned} \mathbf{V}_h(\Omega_{h,t}) &= \{\mathbf{v}_h : \Omega_{h,t} \times I \to \mathbb{R}^d, \quad \mathbf{v}_h = \hat{\mathbf{v}}_h \circ \mathcal{A}_{h,t}^{-1}, \ \hat{\mathbf{v}}_h \in \hat{\mathbf{V}}_h(\Omega_0)\} \\ Q_h(\Omega_{h,t}) &= \{q_h : \Omega_{h,t} \times I \to \mathbb{R}, \quad q_h = \hat{q}_h \circ \mathcal{A}_{h,t}^{-1}, \ \hat{q}_h \in \hat{Q}_h(\Omega_0)\} \end{aligned} \tag{3.4.4}$$

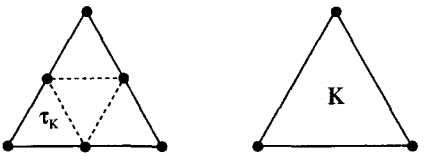

Figure 3.1: $(\mathbb{P}_1 iso\mathbb{P}_2) - \mathbb{P}_1$ elements: degrees of freedom for the velocity components (on the left) and for the pressure (on the right)

where $\Omega_{h,t} = \mathcal{A}_{h,t}(\Omega_0)$ and we have used the discrete ALE mapping $\mathcal{A}_{h,t}$ in the definition of the finite element spaces (3.4.4). In the sequel we will drop the subscript h to indicate the computational domain $\Omega_{h,t}$.

Whenever the mesh problem is solved using $\mathbb{P}_1$ finite elements, each triangle with straight edges in $\mathcal{T}_{h,0}$ is transformed in a triangle with straight edges in $\mathcal{T}_{h,t}$. It can thus be easily verified that if $\hat{\mathbf{V}}_h(\Omega_0)$ and $\hat{Q}_h(\Omega_0)$ are either $\mathbb{P}_1^b - \mathbb{P}_1$ or $(\mathbb{P}_1 iso\mathbb{P}_2) - \mathbb{P}_1$ finite element spaces on $\mathcal{T}_{h,0}$, then $\mathbf{V}_h(\Omega_t)$ and $Q_h(\Omega_t)$, as defined in (3.4.4), are finite element spaces of the same kind on the mesh $\mathcal{T}_{h,t}$. Moreover, using piecewise linear functions for the mesh problem, the boundary $\partial\Omega_t$ will be, in general, only linearly interpolated, which is enough, yet, to recover the error estimate (3.4.3).

When considering the Taylor-Hood elements, we can choose, a-priori, between solving the mesh problem with $\mathbb{P}_{k-1}$ or $\mathbb{P}_k$ finite elements.

In the former case, that means to take a discrete ALE mapping $\mathcal{A}_{h,t} \in \mathcal{F}_{k-1,1}$, which implies, thanks to Proposition 1.5.1, that the functional spaces $\mathbf{V}_h(\Omega_t)$ and $Q_h(\Omega_t)$ can be identified with

$$\mathbf{V}_h(\Omega_t) = \mathcal{F}_{k,k-1}, \qquad Q_h(\Omega_t) = \mathcal{F}_{k-1,k-1}.$$

In other words, pressure belongs to the isoparametric finite element space of degree $k-1$, while the velocity to the sub-parametric finite element space of degree k and mapping degree $k-1$. On the other hand, the boundary $\partial\Omega_t$ is interpolated only with polynomials of degree $k-1$ and this might cause a loss of accuracy with respect to the error estimate (3.4.2).

The second possibility consists in taking the discrete ALE mapping $\mathcal{A}_{h,t} \in \mathcal{F}_{k,1}$. We have in this case :

$$\mathbf{V}_h(\Omega_t) = \mathcal{F}_{k,k}, \qquad Q_h(\Omega_t) = \mathcal{F}_{k-1,k}.$$

In other words, the velocity belongs to the isoparametric finite element space of degree k, while the pressure to the super-parametric finite element space of degree $k-1$ and mapping degree k.

Whatever finite element spaces $\mathbf{V}_h(\Omega_t)$ and $Q_h(\Omega_t)$ we choose, the finite element semi-discretisation of the non-conservative problem (3.3.6) reads : *for almost every* $t \in I$ *find* $t \to \mathbf{u}_h(t) \in \mathbf{V}_h(\Omega_t)$, *with* $\mathbf{u}_h(t) = \mathbf{\Phi}_h(t)$ *on* Γ_t^D, $\mathbf{u}_h(0) = \mathbf{u}_{0h}$ *in* Ω_0 *and* $t \to p_h(t) \in Q_h(\Omega_t)$

such that

$$\begin{cases} \rho \displaystyle\int_{\Omega_t} \left.\frac{\partial \mathbf{u}_h}{\partial t}\right|_{\mathbf{Y}} \cdot \mathbf{v}_h \, d\Omega + \rho \int_{\Omega_t} [(\mathbf{u}_h - \mathbf{w}_h) \cdot \boldsymbol{\nabla}_{\mathbf{x}}] \, \mathbf{u}_h \cdot \mathbf{v}_h \, d\Omega + 2\mu \int_{\Omega_t} \mathbf{D}_{\mathbf{x}}(\mathbf{u}_h) : \boldsymbol{\nabla}_{\mathbf{x}} \mathbf{v}_h \, d\Omega \\ \quad - \displaystyle\int_{\Omega_t} \mathrm{div}_{\mathbf{x}} \, \mathbf{v}_h \, p_h \, d\Omega = \int_{\Omega_t} \mathbf{f} \cdot \mathbf{v}_h \, d\Omega + \int_{\Gamma_t^N} \boldsymbol{\sigma} \cdot \mathbf{v}_h \, d\Gamma \qquad \forall \mathbf{v}_h \in \mathbf{V}_h(\Omega_t) \cap \mathbf{V}_{\Gamma^D}(\Omega_t) \\ \displaystyle\int_{\Omega_t} \mathrm{div}_{\mathbf{x}} \, \mathbf{u}_h \, q_h \, d\Omega = 0 \qquad \forall q_h \in Q_h(\Omega_t) \end{cases} \tag{3.4.5}$$

where $\boldsymbol{\Phi}_h$ and $\mathbf{u}_{0h}$ are suitable approximations of $\boldsymbol{\Phi}$ and $\mathbf{u}_0$ respectively.
In the case $\Gamma_t^N = \emptyset$ and $\boldsymbol{\Phi} = 0$, as pointed out in section 3.2, the convective term $\int_{\Omega_t} (\mathbf{u} \cdot \boldsymbol{\nabla}_{\mathbf{x}}) \mathbf{u} \cdot \mathbf{v} \, d\Omega$ does not contribute to the energy of the system at the differential level in (3.3.6). Indeed, by taking $\mathbf{v} = \mathbf{u}$ we have

$$\int_{\Omega_t} (\mathbf{u} \cdot \boldsymbol{\nabla}_{\mathbf{x}}) \mathbf{u} \cdot \mathbf{u} \, d\Omega = \frac{1}{2} \int_{\Omega_t} \mathbf{u} \cdot \boldsymbol{\nabla}_{\mathbf{x}} |\mathbf{u}|^2 \, d\Omega = -\frac{1}{2} \int_{\Omega_t} \mathrm{div}_{\mathbf{x}} \, \mathbf{u} \, |\mathbf{u}|^2 \, d\Omega$$

Thanks to the second equation in (3.3.6) and the fact that $|\mathbf{u}|^2 \in Q(\Omega_t)$, the last term is zero. This property is not true anymore at the discrete level in (3.4.5); indeed, in this case, we have

$$\int_{\Omega_t} (\mathbf{u}_h \cdot \boldsymbol{\nabla}_{\mathbf{x}}) \mathbf{u}_h \cdot \mathbf{u}_h \, d\Omega = -\frac{1}{2} \int_{\Omega_t} \mathrm{div}_{\mathbf{x}} \, \mathbf{u}_h \, |\mathbf{u}_h|^2 \, d\Omega$$

and, in general, $|\mathbf{u}_h|^2 \notin Q_h(\Omega_t)$. Nonetheless, we can modify problem (3.4.5) in a consistent way, by adding to the first equation the term $\frac{1}{2} \int_{\Omega_t} \mathrm{div}_{\mathbf{x}} \, \mathbf{u}_h \, \mathbf{u}_h \mathbf{v} \, d\Omega$, so as to recover the same stability property featured at the differential level. We underline the fact that this modification is consistent since the exact solution satisfies $\mathrm{div}_{\mathbf{x}} \, \mathbf{u} = 0$.
In the sequel, we will consider always this modified problem that we rewrite hereafter for the sake of clarity :

non-conservative formulation

for almost every $t \in I$ find $t \to \mathbf{u}_h(t) \in \mathbf{V}_h(\Omega_t)$, with $\mathbf{u}_h(t) = \boldsymbol{\Phi}_h(t)$ on Γ_t^D, $\mathbf{u}_h(0) = \mathbf{u}_{0h}$ in Ω_0 and $t \to p_h(t) \in Q_h(\Omega_t)$ such that

$$\begin{cases} \rho \displaystyle\int_{\Omega_t} \left.\frac{\partial \mathbf{u}_h}{\partial t}\right|_{\mathbf{Y}} \cdot \mathbf{v}_h \, d\Omega + \rho \int_{\Omega_t} [(\mathbf{u}_h - \mathbf{w}_h) \cdot \boldsymbol{\nabla}_{\mathbf{x}}] \, \mathbf{u}_h \cdot \mathbf{v}_h \, d\Omega + \frac{\rho}{2} \int_{\Omega_t} \mathrm{div}_{\mathbf{x}} \, \mathbf{u}_h \, \mathbf{u}_h \cdot \mathbf{v}_h \, d\Omega \\ \qquad + 2\mu \displaystyle\int_{\Omega_t} \mathbf{D}_{\mathbf{x}}(\mathbf{u}_h) : \boldsymbol{\nabla}_{\mathbf{x}} \mathbf{v}_h \, d\Omega - \int_{\Omega_t} \mathrm{div}_{\mathbf{x}} \, \mathbf{v}_h \, p_h \, d\Omega = \int_{\Omega_t} \mathbf{f} \cdot \mathbf{v}_h \, d\Omega + \int_{\Gamma_t^N} \boldsymbol{\sigma} \cdot \mathbf{v}_h \, d\Gamma \\ \qquad\qquad \forall \mathbf{v}_h \in \mathbf{V}_h(\Omega_t) \cap \mathbf{V}_{\Gamma^D}(\Omega_t) \\ \displaystyle\int_{\Omega_t} \mathrm{div}_{\mathbf{x}} \, \mathbf{u}_h \, q_h \, d\Omega = 0 \qquad \forall q_h \in Q_h(\Omega_t) \end{cases} \tag{3.4.6}$$

Let, now, $\{\psi_i\}_{i=1}^{\mathcal{N}_p}$ be the Lagrange basis associated to the space $Q_h(\Omega_t)$ and $\{\boldsymbol{\varphi}_j\}_{j=1}^{\mathcal{N}_v}$ the one associated to $\mathbf{V}_h(\Omega_t) \cap \mathbf{V}_{\Gamma^D}(\Omega_t)$. Moreover, we denote $\{\boldsymbol{\varphi}_k^b\}_{k=1}^{\mathcal{N}_v^b}$ the set of basis functions corresponding to the nodes on Γ_t^D, such that $\{\boldsymbol{\varphi}_j\} \oplus \{\boldsymbol{\varphi}_k^b\}$ is a basis of $\mathbf{V}_h(\Omega_t)$.

We set

$$\mathbf{u}_h(\mathbf{x},t) = \sum_{j=1}^{\mathcal{N}_v} U_j(t)\boldsymbol{\varphi}_j(\mathbf{x},t) + \sum_{k=1}^{\mathcal{N}_v^b} U_k^b(t)\boldsymbol{\varphi}_k^b(\mathbf{x},t), \qquad p_h(\mathbf{x},t) = \sum_{i=1}^{\mathcal{N}_p} P_i(t)\psi_i(\mathbf{x},t).$$

The nodal values U_k^b are known form the boundary datum $\boldsymbol{\Phi}$, while the other values $\{U_j\}$ and $\{P_i\}$ are the unknowns of the problem.
We introduce the following matrices and vectors :

$$M_{ij}(t) = \int_{\Omega_t} \boldsymbol{\varphi}_i \cdot \boldsymbol{\varphi}_j \, d\Omega, \qquad 1 \le i,j \le \mathcal{N}_v,$$

$$K_{ij}(t) = \int_{\Omega_t} \mathbf{D}_{\mathbf{x}}(\boldsymbol{\varphi}_i) : \boldsymbol{\nabla}_{\mathbf{x}}\boldsymbol{\varphi}_j \, d\Omega = \int_{\Omega_t} \mathbf{D}_{\mathbf{x}}(\boldsymbol{\varphi}_i) : \mathbf{D}_{\mathbf{x}}(\boldsymbol{\varphi}_j) \, d\Omega, \qquad 1 \le i,j \le \mathcal{N}_v,$$

$$B_{ij}(t;\mathbf{w}_h,\mathbf{u}_h) = \int_{\Omega_t} [(\mathbf{u}_h - \mathbf{w}_h)\cdot\boldsymbol{\nabla}_{\mathbf{x}}]\,\boldsymbol{\varphi}_j \cdot \boldsymbol{\varphi}_i \, d\Omega + \frac{1}{2}\int_{\Omega_t} \mathrm{div}_{\mathbf{x}}\,\mathbf{u}_h\, \boldsymbol{\varphi}_j \cdot \boldsymbol{\varphi}_i \, d\Omega, \quad 1 \le i,j \le \mathcal{N}_v,$$

$$D_{ij}(t) = -\int_{\Omega_t} \mathrm{div}_{\mathbf{x}}\,\boldsymbol{\varphi}_j\,\psi_i \, d\Omega, \quad 1 \le j \le \mathcal{N}_p,\ 1 \le i \le \mathcal{N}_v$$

$$\mathbf{F}_i(t) = \int_{\Omega_t} \mathbf{f}\cdot\boldsymbol{\varphi}_i \, d\Omega + \int_{\Gamma_t^N} \boldsymbol{\sigma}\cdot\boldsymbol{\varphi}_i \, d\Gamma, \qquad 1 \le i \le \mathcal{N}_v.$$

Then, problem (3.4.6) can be written in algebraic form as :

$$\begin{cases} \rho M(t)\dfrac{d}{dt}\mathbf{U} + \rho B(t;\mathbf{w}_h;\mathbf{u}_h)\mathbf{U} + 2\mu K(t)\mathbf{U} + D^T(t)\mathbf{P} = \mathbf{F}(t) + \mathbf{b}_1(t), \\ D(t)\mathbf{U} = \mathbf{b}_2(t) \end{cases} \tag{3.4.7}$$

where $\mathbf{U} = [U_j]$ and $\mathbf{P} = [P_j]$ are the unknown vectors while $\mathbf{b}_1$ and $\mathbf{b}_2$ account for the non-homogeneous Dirichlet boundary condition.

The semi-discretisation of the conservative problem (3.3.7) reads instead :

conservative formulation

for almost every $t \in I$ *find* $t \to \mathbf{u}_h(t) \in \mathbf{V}_h(\Omega_t)$, *with* $\mathbf{u}_h(t) = \boldsymbol{\Phi}_h(t)$ *on* Γ_t^D, $\mathbf{u}_h(0) = \mathbf{u}_{0h}$ *in* Ω_0 *and* $t \to p_h(t) \in Q_h(\Omega_t)$ *such that*

$$\begin{cases} \rho\dfrac{d}{dt}\displaystyle\int_{\Omega_t} \mathbf{u}_h\cdot\mathbf{v}_h \, d\Omega + \rho\int_{\Omega_t} \mathrm{div}_{\mathbf{x}}\,[(\mathbf{u}_h - \mathbf{w}_h)\otimes\mathbf{u}_h]\cdot\mathbf{v}_h \, d\Omega - \dfrac{\rho}{2}\displaystyle\int_{\Omega_t} \mathrm{div}_{\mathbf{x}}\,\mathbf{u}_h\,\mathbf{u}_h\cdot\mathbf{v}_h \, d\Omega \\ \qquad +2\mu\displaystyle\int_{\Omega_t} \mathbf{D}_{\mathbf{x}}(\mathbf{u}_h) : \boldsymbol{\nabla}_{\mathbf{x}}\mathbf{v}_h \, d\Omega - \int_{\Omega_t} \mathrm{div}_{\mathbf{x}}\,\mathbf{v}_h\, p_h \, d\Omega = \int_{\Omega_t} \mathbf{f}\cdot\mathbf{v}_h \, d\Omega + \int_{\Gamma_t^N} \boldsymbol{\sigma}\cdot\mathbf{v}_h \, d\Gamma \\ \qquad\qquad \forall \mathbf{v}_h \in \mathbf{V}_h(\Omega_t) \cap \mathbf{V}_{\Gamma^D}(\Omega_t) \\ \displaystyle\int_{\Omega_t} \mathrm{div}_{\mathbf{x}}\,\mathbf{u}_h\, q_h \, d\Omega = 0 \qquad\qquad \forall q_h \in Q_h(\Omega_t) \end{cases} \tag{3.4.8}$$

where, as for the non-conservative formulation, the term $-\frac{\rho}{2}\int_{\Omega_t} \mathrm{div}_{\mathbf{x}}\,\mathbf{u}_h\,\mathbf{u}_h\cdot\mathbf{v}_h\,d\Omega$ has been added for stability purposes. We observe that

$$\int_{\Omega_t} \mathrm{div}_{\mathbf{x}}\left[(\mathbf{u}_h-\mathbf{w}_h)\otimes\mathbf{u}_h\right]\cdot\mathbf{v}_h\,d\Omega - \frac{1}{2}\int_{\Omega_t}\mathrm{div}_{\mathbf{x}}\,\mathbf{u}_h\,\mathbf{u}_h\cdot\mathbf{v}_h\,d\Omega =$$
$$\int_{\Omega_t}\mathrm{div}_{\mathbf{x}}(\mathbf{u}_h-\mathbf{w}_h)\,\mathbf{u}_h\cdot\mathbf{v}_h\,d\Omega+\int_{\Omega_t}\left[(\mathbf{u}_h-\mathbf{w}_h)\cdot\boldsymbol{\nabla}_{\mathbf{x}}\right]\mathbf{u}_h\cdot\mathbf{v}_h\,d\Omega-\frac{1}{2}\int_{\Omega_t}\mathrm{div}_{\mathbf{x}}\,\mathbf{u}_h\,\mathbf{u}_h\cdot\mathbf{v}_h\,d\Omega=$$
$$\int_{\Omega_t}\left[(\mathbf{u}_h-\mathbf{w}_h)\cdot\boldsymbol{\nabla}_{\mathbf{x}}\right]\mathbf{u}_h\cdot\mathbf{v}_h\,d\Omega+\frac{1}{2}\int_{\Omega_t}\mathrm{div}_{\mathbf{x}}\,\mathbf{u}_h\,\mathbf{u}_h\cdot\mathbf{v}_h\,d\Omega-\int_{\Omega_t}\mathrm{div}_{\mathbf{x}}\,\mathbf{w}_h\,\mathbf{u}_h\cdot\mathbf{v}_h\,d\Omega,$$

so that, the algebraic counterpart of (3.4.8) is

$$\begin{cases}\rho\dfrac{d}{dt}\left(M(t)\mathbf{U}\right)+\rho B(t;\mathbf{w}_h;\mathbf{u}_h)\mathbf{U}-\rho C(t;\mathbf{w}_h)\mathbf{U}+2\mu K(t)\mathbf{U}+D^T(t)\mathbf{P}=\mathbf{F}(t)+\mathbf{b}_1(t),\\ D(t)\mathbf{U}=\mathbf{b}_2(t)\end{cases}\tag{3.4.9}$$

where the matrix $C(t;\mathbf{w}_h)$ is defined as

$$C_{ij}(t;\mathbf{w}_h)=\int_{\Omega_t}\mathrm{div}_{\mathbf{x}}\,\mathbf{w}_h\,\boldsymbol{\varphi}_j\cdot\boldsymbol{\varphi}_i\,d\Omega,\qquad 1\le i,j\le\mathcal{N}_v.$$

3.5 Temporal discretisation

All the temporal schemes proposed in the previous Chapters can be easily extended to systems (3.4.7) and (3.4.9). Thus, for instance, the Implicit Euler scheme applied to the non-conservative formulation (3.4.5) will read

$$\begin{cases}\rho\displaystyle\int_{\Omega_{t_{n+1}}}\mathbf{u}_h^{n+1}\cdot\mathbf{v}_h\,d\Omega-\rho\int_{\Omega_{t_{n+1}}}\mathbf{u}_h^{n}\cdot\mathbf{v}_h\,d\Omega+\rho\Delta t\int_{\Omega_{t_{n+1}}}\left[(\mathbf{u}_h^{*}-\mathbf{w}_h^{n+1})\cdot\boldsymbol{\nabla}_{\mathbf{x}}\right]\mathbf{u}_h^{n+1}\cdot\mathbf{v}_h\,d\Omega\\ \quad+\dfrac{\rho\Delta t}{2}\displaystyle\int_{\Omega_{t_{n+1}}}\mathrm{div}_{\mathbf{x}}\,\mathbf{u}_h^{*}\,\mathbf{u}_h^{n+1}\cdot\mathbf{v}_h\,d\Omega+2\mu\Delta t\int_{\Omega_{t_{n+1}}}\mathbf{D}_{\mathbf{x}}(\mathbf{u}_h^{n+1}):\boldsymbol{\nabla}_{\mathbf{x}}\mathbf{v}_h\,d\Omega\\ \quad-\Delta t\displaystyle\int_{\Omega_{t_{n+1}}}\mathrm{div}_{\mathbf{x}}\,\mathbf{v}_h\,p_h^{n+1}\,d\Omega=\Delta t\int_{\Omega_{t_{n+1}}}\mathbf{f}^{n+1}\cdot\mathbf{v}_h\,d\Omega+\Delta t\int_{\Gamma^N_{t_{n+1}}}\boldsymbol{\sigma}^{n+1}\cdot\mathbf{v}_h\,d\Gamma\\ \qquad\qquad\qquad\qquad\qquad\qquad\qquad\qquad\qquad\qquad\qquad\qquad\forall\mathbf{v}_h\in\mathbf{V}_h(\Omega_t)\cap\mathbf{V}_{\Gamma^D}(\Omega_t)\\ \displaystyle\int_{\Omega_{t_{n+1}}}\mathrm{div}_{\mathbf{x}}\,\mathbf{u}_h^{n+1}\,q_h\,d\Omega=0\qquad\qquad\qquad\qquad\qquad\qquad\forall q_h\in Q_h(\Omega_t)\end{cases}\tag{3.5.1}$$

and in algebraic form :

$$\begin{cases}\dfrac{\rho}{\Delta t}M(t_{n+1})\mathbf{U}^{n+1}+\rho B(t_{n+1};\mathbf{w}_h^{n+1};\mathbf{u}_h^{*})\mathbf{U}^{n+1}+2\mu K(t_{n+1})\mathbf{U}^{n+1}+D^T(t_{n+1})\mathbf{P}^{n+1}\\ \qquad\qquad\qquad\qquad\qquad\qquad=\dfrac{\rho}{\Delta t}M(t_n)\mathbf{U}^{n}+\mathbf{F}(t_{n+1})+\mathbf{b}_1(t_{n+1}),\\ D(t_{n+1})\mathbf{U}^{n+1}=\mathbf{b}_2(t_{n+1}).\end{cases}\tag{3.5.2}$$

System (3.5.2) is fully implicit and non-linear when $\mathbf{u}_h^* = \mathbf{u}_h^{n+1}$. Otherwise, it can be linearized by taking $\mathbf{u}_h^* = \mathbf{u}_h^n$ which is an approximation of the same order as the Implicit Euler scheme. About the conservative formulation (3.4.9), we limit ourselves to a 2D domain and a linear in time interpolation of the domain deformation. Then, the Implicit Euler discretisation that satisfies the GCL reads

$$\begin{cases} \rho \displaystyle\int_{\Omega_{t_{n+1}}} \mathbf{u}_h^{n+1} \cdot \mathbf{v}_h \, d\Omega - \rho \int_{\Omega_{t_n}} \mathbf{u}_h^n \cdot \mathbf{v}_h \, d\Omega + \rho \Delta t \int_{\Omega_{t_{n+1/2}}} \operatorname{div}_{\mathbf{x}} \left[(\mathbf{u}_h^* - \mathbf{w}_h^{n+1/2}) \otimes \mathbf{u}_h^{n+1} \right] \cdot \mathbf{v}_h \, d\Omega \\ \qquad - \dfrac{\rho \Delta t}{2} \displaystyle\int_{\Omega_{t_{n+1/2}}} \operatorname{div}_{\mathbf{x}} \mathbf{u}_h^* \, \mathbf{u}_h^{n+1} \cdot \mathbf{v}_h \, d\Omega + 2\mu \Delta t \int_{\Omega_{t_{n+1/2}}} \mathbf{D}_{\mathbf{x}}(\mathbf{u}_h^{n+1}) : \boldsymbol{\nabla}_{\mathbf{x}} \mathbf{v}_h \, d\Omega \\ -\Delta t \displaystyle\int_{\Omega_{t_{n+1/2}}} \operatorname{div}_{\mathbf{x}} \mathbf{v}_h \, p_h^{n+1} \, d\Omega = \Delta t \int_{\Omega_{t_{n+1/2}}} \mathbf{f}^{n+1/2} \cdot \mathbf{v}_h \, d\Omega + \Delta t \int_{\Gamma^N_{t_{n+1/2}}} \boldsymbol{\sigma}^{n+1/2} \cdot \mathbf{v}_h \, d\Gamma \\ \qquad\qquad\qquad\qquad\qquad\qquad\qquad\qquad\qquad\qquad \forall \mathbf{v}_h \in \mathbf{V}_h(\Omega_t) \cap \mathbf{V}_{\Gamma^D}(\Omega_t) \\ \displaystyle\int_{\Omega_{t_{n+1/2}}} \operatorname{div}_{\mathbf{x}} \mathbf{u}_h^{n+1} \, q_h \, d\Omega = 0 \qquad\qquad\qquad\qquad\qquad\qquad \forall q_h \in Q_h(\Omega_t) \end{cases} \tag{3.5.3}$$

To be consistent with the chosen discretisation, we have taken both the constraint $\int_\Omega \operatorname{div}_{\mathbf{x}} \mathbf{u}_h^{n+1} \, q_h$ and the pressure term $\int_\Omega \operatorname{div}_{\mathbf{x}} \mathbf{v}_h \, p_h^{n+1}$ on the intermediate configuration $\Omega_{t_{n+1/2}}$.
By taking $\mathbf{v}_h = \mathbf{u}_h^{n+1}$ and $q_h = p_h^{n+1}$, it can be easily verified, by combining the derivation of the energy estimate presented in Section 3.2 with the stability analysis for the Implicit Euler scheme carried out in section 1.8.4, that for a fully homogeneous Dirichlet problem ($\Gamma_t^N = \emptyset$ and $\boldsymbol{\Phi} = \mathbf{0}$) scheme (3.5.3) is unconditionally stable whatever linearization $\mathbf{u}_h^*$ is employed. We summarise the result in the following

Lemma 3.5.1 *Scheme (3.5.3) applied to a fully homogeneous Dirichlet problem is unconditionally stable and the discrete solution $\mathbf{u}_h^n$ satisfies the inequality*

$$\rho \left\| \mathbf{u}_h^{n+1} \right\|^2_{L_2(\Omega_{t^{n+1}})} + \Delta t \kappa \sum_{i=0}^{n} \left\| \boldsymbol{\nabla}_{\mathbf{x}} \mathbf{u}_h^{i+1} \right\|^2_{L_2(\Omega_{t^{i+1/2}})} \leq \rho \left\| \mathbf{u}_{0h} \right\|^2_{L_2(\Omega_0)} + \Delta t \frac{(1 + C_\Omega)}{\kappa} \sum_{i=0}^{n} \left\| \mathbf{f}^{i+1/2} \right\|^2_{H^{-1}(\Omega_{t^{i+1/2}})} \tag{3.5.4}$$

Remark 3.5.1 *With that choice of test functions, the pressure term in the first equation of (3.5.3) is identically zero thanks to the second equation. It is thus important to compute those two terms on the same domain in order to recover the stability result of Lemma 3.5.1.*

System (3.5.3) can be equivalently written in algebraic form as

$$\begin{cases} \dfrac{\rho}{\Delta t} M(t_{n+1}) \mathbf{U}^{n+1} + \rho B(t_{n+1/2}; \mathbf{w}_h^{n+1/2}; \mathbf{u}_h^*) \mathbf{U}^{n+1} - \rho C(t_{n+1/2}; \mathbf{w}_h^{n+1/2}) \mathbf{U}^{n+1} \\ \qquad + 2\mu K(t_{n+1/2}) \mathbf{U}^{n+1} + D^T(t_{n+1/2}) \mathbf{P}^{n+1} = \dfrac{\rho}{\Delta t} M(t_n) \mathbf{U}^n + \mathbf{F}(t_{n+1/2}) + \mathbf{b}_1(t_{n+1/2}), \\ D(t_{n+1/2}) \mathbf{U}^{n+1} = \mathbf{b}_2(t_{n+1/2}). \end{cases} \tag{3.5.5}$$

A second order discretisation can be achieved, for instance, with the Crank-Nicolson scheme proposed in Section 2.2.1. We consider here only the conservative formulation in a 2D domain. Then, the Crank-Nicolson discretisation will read

$$\begin{cases} \rho \int_{\Omega_{t_{n+1}}} \mathbf{u}_h^{n+1} \cdot \mathbf{v}_h \, d\Omega - \rho \int_{\Omega_{t_n}} \mathbf{u}_h^n \cdot \mathbf{v}_h \, d\Omega + \rho \Delta t \int_{\Omega_{t_{n+1/2}}} \mathrm{div}_{\mathbf{x}} \left[(\mathbf{u}_h^* - \mathbf{w}_h^{n+\frac{1}{2}}) \otimes \dfrac{\mathbf{u}_h^n + \mathbf{u}_h^{n+1}}{2} \right] \cdot \mathbf{v}_h \, d\Omega \\ -\dfrac{\rho \Delta t}{2} \int_{\Omega_{t_{n+1/2}}} \mathrm{div}_{\mathbf{x}} \, \mathbf{u}_h^* \dfrac{\mathbf{u}_h^n + \mathbf{u}_h^{n+1}}{2} \cdot \mathbf{v}_h \, d\Omega + 2\mu \Delta t \int_{\Omega_{t_{n+1/2}}} \mathbf{D}_{\mathbf{x}}(\dfrac{\mathbf{u}_h^n + \mathbf{u}_h^{n+1}}{2}) : \boldsymbol{\nabla}_{\mathbf{x}} \mathbf{v}_h \, d\Omega \\ -\Delta t \int_{\Omega_{t_{n+1/2}}} \mathrm{div}_{\mathbf{x}} \, \mathbf{v}_h \dfrac{p_h^n + p_h^{n+1}}{2} \, d\Omega = \Delta t \int_{\Omega_{t_{n+1/2}}} \mathbf{f}^{n+1/2} \cdot \mathbf{v}_h \, d\Omega + \Delta t \int_{\Gamma^N_{t_{n+1/2}}} \boldsymbol{\sigma}^{n+1/2} \cdot \mathbf{v}_h \, d\Gamma \\ \qquad\qquad \forall \mathbf{v}_h \in \mathbf{V}_h(\Omega_t) \cap \mathbf{V}_{\Gamma^D}(\Omega_t) \\ \int_{\Omega_{t_{n+1/2}}} \mathrm{div}_{\mathbf{x}} \dfrac{\mathbf{u}_h^n + \mathbf{u}_h^{n+1}}{2} \, q_h \, d\Omega = 0 \qquad\qquad \forall q_h \in Q_h(\Omega_t) \end{cases} \tag{3.5.6}$$

Here $\mathbf{u}_h^*$ can be taken as $\frac{\mathbf{u}_h^n + \mathbf{u}_h^{n+1}}{2}$ for a fully implicit non-linear discretisation or as $\frac{3}{2}\mathbf{u}_h^n - \frac{1}{2}\mathbf{u}_h^{n-1}$ to obtain a second order linearisation of the equations.
For the same stability reasons as for the Implicit Euler scheme (3.5.3), we have discretised the continuity equation as $\int_{\Omega_{t_{n+1/2}}} \mathrm{div}_{\mathbf{x}} \frac{\mathbf{u}_h^n + \mathbf{u}_h^{n+1}}{2} \, q_h$. In this way, when taking $\mathbf{v}_h = \mathbf{u}_h^n + \mathbf{u}_h^{n+1}$ and $q_h = p_h^n + p_h^{n+1}$, the pressure term in the first equation is identically zero and a stability result analogous to the one obtained for an advection diffusion equation can be established. The following Lemma holds :

Lemma 3.5.2 *The discrete solution $\mathbf{u}_h^n$ of scheme (3.5.6) applied to a fully homogeneous Dirichlet problem, satisfies the inequality*

$$\begin{aligned} &\rho \left\| \mathbf{u}_h^{n+1} \right\|^2_{L_2(\Omega_{t^{n+1}})} + \frac{\Delta t}{4} \kappa \left\| \boldsymbol{\nabla}_{\mathbf{x}} (\mathbf{u}_h^n + \mathbf{u}_h^{n+1}) \right\|^2_{L_2(\Omega_{t^{n+1/2}})} \\ &-\frac{\Delta t}{4} \int_{\Omega_{t_{n+1/2}}} \mathrm{div}_{\mathbf{x}} \, \mathbf{w}_h^{n+1/2} |\mathbf{u}_h^{n+1} + \mathbf{u}_h^n|^2 \, d\Omega \leq \rho \left\| \mathbf{u}_h^n \right\|^2_{L_2(\Omega_{t^n})} + \Delta t \frac{(1 + C_\Omega)}{\kappa} \left\| \mathbf{f}^{n+1/2} \right\|^2_{H^{-1}(\Omega_{t^{n+1/2}})} \end{aligned} \tag{3.5.7}$$

We observe that we recover a global stability result only in the case $\mathrm{div}_{\mathbf{x}} \, \mathbf{w}_h^{n+1/2} \leq 0$ for all $n \geq 0$, while in the more general case only a conditional stability can be obtained.
The algebraic counterpart of (3.5.6) reads

$$\begin{cases} \dfrac{\rho}{\Delta t} M(t_{n+1}) \mathbf{U}^{n+1} + \rho B(t_{n+1/2}; \mathbf{w}_h^{n+1/2}; \mathbf{u}_h^*) \dfrac{\mathbf{U}^{n+1} + \mathbf{U}^n}{2} \\ -\rho C(t_{n+1/2}; \mathbf{w}_h^{n+1/2}) \dfrac{\mathbf{U}^{n+1} + \mathbf{U}^n}{2} + 2\mu K(t_{n+1/2}) \dfrac{\mathbf{U}^{n+1} + \mathbf{U}^n}{2} + D^T(t_{n+1/2}) \dfrac{\mathbf{P}^{n+1} + \mathbf{P}^n}{2} \\ \qquad = \dfrac{\rho}{\Delta t} M(t_n) \mathbf{U}^n + \mathbf{F}(t_{n+1/2}) + \mathbf{b}_1(t_{n+1/2}), \\ D(t_{n+1/2}) \dfrac{\mathbf{U}^{n+1} + \mathbf{U}^n}{2} = \mathbf{b}_2(t_{n+1/2}). \end{cases} \tag{3.5.8}$$

3.5.1 Inexact factorization schemes

Since the simultaneous computation of velocity and pressure is frequently unfeasible particularly in a 3D problem, several techniques have been developed to decouple the computation of the velocity field from that of the pressure. Here we focus on techniques based on an inexact factorisation of the problem matrix and particularly on the Yosida projection scheme proposed in [78] and analysed in [77] for a fixed domain problem.
At each time step t^n, both systems (3.5.2), (3.5.5) and (3.5.8) can be written in the general Stokes-like form

$$\begin{bmatrix} A & D^T \\ D & 0 \end{bmatrix} \begin{bmatrix} \mathbf{U}^{n+1} \\ \mathbf{P}^{n+1} \end{bmatrix} = \begin{bmatrix} \mathbf{f}_1 \\ \mathbf{f}_2 \end{bmatrix}. \tag{3.5.9}$$

In the case of the non-conservative formulation (3.4.7) we have

$$\begin{aligned} A &= \frac{\rho}{\Delta t} M(t_{n+1}) + \rho B(t_{n+1}; \mathbf{w}_h^{n+1}; \mathbf{u}_h^*) + 2\mu K(t_{n+1}), \\ \mathbf{f}_1 &= \frac{\rho}{\Delta t} M(t_{n+1})\mathbf{U}^n + \mathbf{F}(t_{n+1}) + \mathbf{b}_1(t_{n+1}), \\ \mathbf{f}_2 &= \mathbf{b}_2(t_{n+1}). \end{aligned}$$

For the conservative formulation (3.5.5) we have

$$\begin{aligned} A &= \frac{\rho}{\Delta t} M(t_{n+1}) + \rho B(t_{n+1/2}; \mathbf{w}_h^{n+1/2}; \mathbf{u}_h^*) - \rho C(t_{n+1/2}; \mathbf{w}_h^{n+1/2}) + 2\mu K(t_{n+1/2}), \\ \mathbf{f}_1 &= \frac{\rho}{\Delta t} M(t_n)\mathbf{U}^n + \mathbf{F}(t_{n+1/2}) + \mathbf{b}_1(t_{n+1/2}), \\ \mathbf{f}_2 &= \mathbf{b}_2(t_{n+1/2}). \end{aligned}$$

Finally, for the Crank-Nicolson scheme (3.5.8) we have

$$\begin{aligned} A &= \frac{2\rho}{\Delta t} M(t_{n+1}) + \rho B(t_{n+1/2}; \mathbf{w}_h^{n+1/2}; \mathbf{u}_h^*) - \rho C(t_{n+1/2}; \mathbf{w}_h^{n+1/2}) + 2\mu K(t_{n+1/2}), \\ \mathbf{f}_1 &= \left[\frac{2\rho}{\Delta t} M(t_n) - \rho B(t_{n+1/2}; \mathbf{w}_h^{n+1/2}; \mathbf{u}_h^*) + \rho C(t_{n+1/2}; \mathbf{w}_h^{n+1/2}) - 2\mu K(t_{n+1/2}) \right] \mathbf{U}^n \\ &\quad - D^T(t_{n+1/2})\mathbf{P}^n + 2\mathbf{F}(t_{n+1/2}) + 2\mathbf{b}_1(t_{n+1/2}), \\ \mathbf{f}_2 &= -D(t_{n+1/2})\mathbf{U}^n + 2\mathbf{b}_2(t_{n+1/2}). \end{aligned}$$

In the following of this section we will always suppose to have linearized the equations with $\mathbf{u}_h^* = \mathbf{u}_h^n$ and $\mathbf{u}_h^* = \frac{3}{2}\mathbf{u}_h^n - \frac{1}{2}\mathbf{u}_h^{n-1}$ for the implicit Euler and the Crank-Nicolson scheme,respectively.
The matrix $S = \left[\begin{smallmatrix} A & D^T \\ D & 0 \end{smallmatrix} \right]$ can be factorized as

$$S = \begin{bmatrix} A & D^T \\ D & 0 \end{bmatrix} = \begin{bmatrix} A & 0 \\ D & -DA^{-1}D^T \end{bmatrix} \begin{bmatrix} I & A^{-1}D^T \\ 0 & I \end{bmatrix},$$

hence, system (3.5.9) can be solved exactly by the following three step algorithm :

(i) $A\widetilde{\mathbf{U}}^{n+1} = \mathbf{f}_1$,

(ii) $DA^{-1}D^T\mathbf{P}^{n+1} = D\widetilde{\mathbf{U}}^{n+1} - \mathbf{f}_2$,

(iii) $\mathbf{U}^{n+1} = \widetilde{\mathbf{U}}^{n+1} - A^{-1}D^T\mathbf{P}^{n+1}$.

or, equivalently, by its *incremental* variant

(i) $A\widetilde{\mathbf{U}}^{n+1} = \mathbf{f}_1 - D^T\mathbf{P}^n$,

(ii) $DA^{-1}D^T\delta\mathbf{P} = D\widetilde{\mathbf{U}}^{n+1} - \mathbf{f}_2$,

(iii) $\mathbf{U}^{n+1} = \widetilde{\mathbf{U}}^{n+1} - A^{-1}D^T\delta\mathbf{P}$.

where we have set $\delta\mathbf{P} = \mathbf{P}^{n+1} - \mathbf{P}^n$.
Let, now, $H^{(1)}$ and $H^{(2)}$ denote two suitable approximations of A^{-1}. We can write an approximate factorization scheme as

(i) $A\widetilde{\mathbf{U}}^{n+1} = \mathbf{f}_1 - D^T\mathbf{P}^n$,

(ii) $DH^{(1)}D^T\delta\mathbf{P} = D\widetilde{\mathbf{U}}^{n+1} - \mathbf{f}_2$,

(iii) $\mathbf{U}^{n+1} = \widetilde{\mathbf{U}}^{n+1} - H^{(2)}D^T\delta\mathbf{P}$.

which correspond to the inexact factorization

$$\widetilde{S} = \begin{bmatrix} A & 0 \\ D & -DH^{(1)}D^T \end{bmatrix} \begin{bmatrix} I & H^{(2)}D^T \\ 0 & I \end{bmatrix} \tag{3.5.10}$$

of the matrix S in (3.5.9).
In this way we can recover many projection or quasi-compressibility methods for the Navier-Stokes equations (see [67, 78]). In particular, the *incremental Yosida projection scheme* consists in adopting $H^{(1)} = \Delta t M^{-1}/\rho$ for the Implicit Euler scheme (similarly, $H^{(1)} = \Delta t M^{-1}/2\rho$ for the Crank-Nicolson one), while no approximation is made in step *(iii)*, i.e. $H^{(2)} = A^{-1}$.
The matrix M^{-1} can be easily computed whenever the so-called *mass-lumping* technique is adopted.
We remark that the generalisation of those algorithms based on an inexact factorisation to the case of a moving domain is straightforward once the discrete system is written in the form (3.5.9).
In [77] it has been shown that, for a fixed domain problem, the incremental Yosida projection scheme is unconditionally stable and introduces a splitting error (with respect to the solution of system (3.5.9)) which is $O(\Delta t)$ both on velocity and pressure. This error is of the same order than the one introduced by the Implicit Euler discretisation. On the contrary, when considering the Crank-Nicolson scheme, the Yosida projection scheme might lead to a loss in the time accuracy. The problem of how to obtain second order accurate projection schemes based on inexact factorisations is still open.
In a recent paper [93], A. Venezziani suggested to use the inexact factorization (3.5.10) as a preconditioner for system (3.5.9). He showed that, for a linear symmetric problem, p Richardson iterations preconditioned with the Yosida inexact factorization are sufficient to recover a splitting error $O(\Delta t^p)$. In the non symmetric case, he verified numerically that three preconditioned iterations are sufficient to recover a second order accurate scheme. We give some more details on this algorithm hereafter. Let us consider a Richardson method,

with acceleration parameter equal to 1, to solve (3.5.9), preconditioned with the matrix $\widetilde{S}$. It may be written as follows : given the initial estimate $[\mathbf{U}_0^{n+1}, \mathbf{P}_0^{n+1}]^T$, solve for $k = 0, 1, \ldots$

$$\begin{bmatrix} A & 0 \\ D & -DH^{(1)}D^T \end{bmatrix} \begin{bmatrix} I & H^{(2)}D^T \\ 0 & I \end{bmatrix} \left(\begin{bmatrix} \mathbf{U}_{k+1}^{n+1} \\ \mathbf{P}_{k+1}^{n+1} \end{bmatrix} - \begin{bmatrix} \mathbf{U}_k^{n+1} \\ \mathbf{P}_k^{n+1} \end{bmatrix} \right) = \begin{bmatrix} \mathbf{f}_1 \\ \mathbf{f}_2 \end{bmatrix} - \begin{bmatrix} A & D^T \\ D & 0 \end{bmatrix} \begin{bmatrix} \mathbf{U}_k^{n+1} \\ \mathbf{P}_k^{n+1} \end{bmatrix} \tag{3.5.11}$$

We introduce the auxiliary variable

$$\begin{bmatrix} \delta\mathbf{W}_{k+1} \\ \delta\mathbf{P}_{k+1} \end{bmatrix} = \begin{bmatrix} I & H^{(2)}D^T \\ 0 & I \end{bmatrix} \left(\begin{bmatrix} \mathbf{U}_{k+1}^{n+1} \\ \mathbf{P}_{k+1}^{n+1} \end{bmatrix} - \begin{bmatrix} \mathbf{U}_k^{n+1} \\ \mathbf{P}_k^{n+1} \end{bmatrix} \right).$$

Then, algorithm (3.5.11) can be written as

(i) $A\delta\mathbf{W}_{k+1} = \mathbf{f}_1 - A\mathbf{U}_k^{n+1} - D^T\mathbf{P}_k^{n+1}$,

(ii) $DH^{(1)}D^T\delta\mathbf{P}_{k+1} = D\delta\mathbf{W}_{k+1} - \mathbf{f}_2 + D\mathbf{U}_k^{n+1}$,

(iii) $\mathbf{P}_{k+1}^{n+1} = \mathbf{P}_k^{n+1} + \delta\mathbf{P}_{k+1}$.

(iv) $\mathbf{U}_{k+1}^{n+1} = \mathbf{U}_k^{n+1} + \delta\mathbf{W}_{k+1} - H^{(2)}D^T\delta\mathbf{P}_k$.

We furtherly introduce the variable $\widetilde{\mathbf{U}}_{k+1}^{n+1} = \mathbf{U}_k^{n+1} + \delta\mathbf{W}_{k+1}$. Then, the previous algorithm can be written in the final form : given the initial estimate $[\mathbf{U}_0^{n+1}, \mathbf{P}_0^{n+1}]^T$

- solve for $k = 0, 1, \ldots$

  (i) $A\widetilde{\mathbf{U}}_{k+1}^{n+1} = \mathbf{f}_1 - D^T\mathbf{P}_k^{n+1}$,

  (ii) $DH^{(1)}D^T\delta\mathbf{P}_{k+1} = D\widetilde{\mathbf{U}}_{k+1}^{n+1} - \mathbf{f}_2$,

  (iii) $\mathbf{P}_{k+1}^{n+1} = \mathbf{P}_k^{n+1} + \delta\mathbf{P}_{k+1}$,

- compute $\mathbf{U}_{k+1}^{n+1} = \widetilde{\mathbf{U}}_{k+1}^{n+1} - H^{(2)}D^T\delta\mathbf{P}_{k+1}$.

Observe that the correction on the velocity field can be computed only at the end of the preconditioned iterations. Moreover, if we take as initial estimate $\mathbf{U}_0^{n+1} = \mathbf{U}^n$ and $\mathbf{P}_0^{n+1} = \mathbf{P}^n$, the first iteration of the preconditioned algorithm coincides exactly with the incremental Yosida projection scheme. It is natural to expect, then, that successive iterations of the preconditioned Richardson method will improve the accuracy with respect to the incremental Yosida scheme.

3.6 Numerical assessment

We have taken as a reference domain the 2D rectangle $\Omega_0 = \{(Y_1, Y_2) \in [0, 6] \times [0, 1]\}$ and a domain deformation defined by

$$\begin{cases} x_1 = Y_1, \\ x_2 = (1 - 0.4\sin(t\pi/5))\left(Y_2 - \frac{1}{2}\right) + \frac{1}{2} \end{cases} \tag{3.6.1}$$

i.e. the rectangle contracts and expands periodically in its shorter dimension, with a period $T = 10$.

We have considered the Navier-Stokes equations (3.1.1) with $\rho = 1$, $\mu = 1$ and forcing term $\mathbf{f} = 0$. An exact solution (valid in all $\mathbb{R}^2$) is given by

$$\begin{cases} u_1 = -\dfrac{2v}{1+2vt}(x_1 - 6), \\ u_2 = \dfrac{2v}{1+2vt}(x_2 - 1/2), \\ p = -\left(\dfrac{2v}{1+2vt}\right)^2 (x_1 - 6)^2. \end{cases} \tag{3.6.2}$$

We have taken $v = 0.2$ and we have imposed the exact velocity on the upper, lower and left edges of the rectangle and the exact Neumann condition associated to (3.6.2) on the right edge.

The Navier-Stokes equations have been discretised in space with $(\mathbb{P}_1 iso \mathbb{P}_2) - \mathbb{P}_1$ finite elements using a structured mesh of (61×21) $\mathbb{P}_1$ nodes (4961 $\mathbb{P}_2$ nodes); observe that in this case the velocity is interpolated exactly. To build the ALE mapping we have solved a Laplace equation at each time step with $\mathbb{P}_1$ finite elements in space and a linear interpolation in time. Observe that in this case the ALE mapping at each time instants t^n is computed exactly since the domain deformation is linear in space.

We have then compared the solutions obtained with the Implicit Euler (3.5.3) and Crank-Nicolson (3.5.6) schemes in conservative formulation and satisfying the GCL. In both cases, to solve system (3.5.9) at each time step, we have implemented the incremental Yosida projection scheme (indicated hereafter with the suffix *Yosida*) and the preconditioned Richardson algorithm with three iterations at each time step (indicated with *Yos3*). We have taken a sequence of decreasing time steps $\Delta t = 1/2,\ 1/4,\ 1/8,\ 1/16,\ 1/32$ and we have computed the velocity error at t^n as

$$e^n = \|\mathbf{u}_h^n - \mathbf{u}(t^n)\|_{L_2(\Omega_{t_n})}$$

and the pressure error as

$$\eta^n = \left(\sum_{i=0}^{n-1} \Delta t \left\|p_h^{i+1} - p(t^{i+1})\right\|^2_{L_2(\Omega_{t^{i+1}})}\right)^{\frac{1}{2}} \qquad \text{for the Implicit Euler scheme}$$

$$\eta^n = \left(\sum_{i=0}^{n-1} \Delta t \left\|\frac{p_h^{i+1} + p_h^i}{2} - p(t^{i+1/2})\right\|^2_{L_2(\Omega_{t^{i+1/2}})}\right)^{\frac{1}{2}} \qquad \text{for the Crank-Nicolson scheme}$$

Figures 3.2 and 3.3 show the velocity and pressure errors as a function of Δt at $t = 2$ and $t = 7$. We observe that the Implicit Euler scheme converges linearly in time no matter whether the Yosida factorisation is used as a solver or as a preconditioner. On the contrary, in this test case the Crank-Nicolson scheme features a second order accuracy both on the velocity and the pressure even if just the Yosida projection scheme is adopted. When the Yosida factorization is used as a preconditioner, the error reduces furtherly in absolute value, yet maintaining the same rate of convergence.

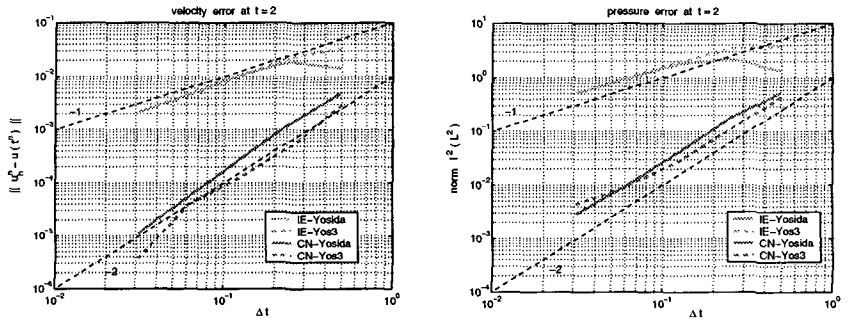

Figure 3.2: Velocity (on the left) and pressure (on the right) errors as a function of Δt for the Implicit Euler and Crank-Nicolson schemes at $t = 2$.

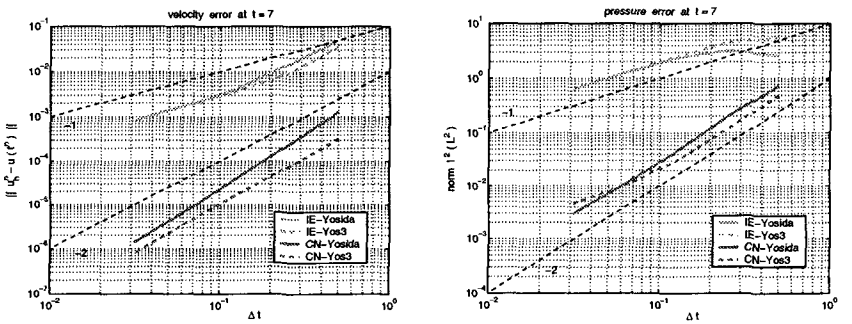

Figure 3.3: Velocity (on the left) and pressure (on the right) errors as a function of Δt for the Implicit Euler and Crank-Nicolson schemes at $t = 7$.

Part II

Incompressible fluids in compliant vessels

Chapter 4

The fluid-structure interaction problem

In this chapter, we consider the fluid-structure problem consisting of a thin elastic tube filled with an incompressible fluid. This is the typical situation arising in the modelling of blood flow in large arteries. However, many of the considerations carried out here may be applied to other fluid-structure applications as well.

We account for quite large deformations of the vessel wall; the fluid equations are, then, defined on a domain that changes in time and will be treated in ALE framework.

In Section 4.1 we will present the formulation for the 3D fluid-structure model. A simplified one-dimensional formulation for the structure is also addressed and used for the stability analysis of the coupled problem. The main result of the section is an energy inequality which, under a condition on the positivity of the kinetic energy flux at the outflow, provides a bound of the global energy of the coupled problem in terms of initial and boundary data. This result has already been published in the work by L. Formaggia, J-F. Gerbeau, F. Nobile and A. Quarteroni *On the Coupling of 3D and 1D Navier-Stokes equations for Flow Problems in Compliant Vessels* [29]. A simplified 2D problem will be introduced in Section 4.2 and used for the mathematical analysis carried out in the sequel and for the numerical simulations.

In Section 4.3 we will derive a global weak formulation for the coupled problem that accounts at the same time for the fluid and the structure equations. This formulation is well suited to devise fully implicit coupled algorithms as those proposed in Sections 4.7÷4.10. Then, in Section 4.4 we will show how the fluid and structure sub-problems may be recovered from the coupled weak formulation through a classical Domain Decomposition technique. The Finite Element approximation of the coupled problem will be discussed in Section 4.5, in the general case of a non conforming discretisation between fluid and structure. The algebraic formulation will be derived in Subsection 4.5.1 and detailed for a particular choice of conforming Finite Element spaces, which is indeed the one employed in the numerical simulations.

About time discretisation, we will focus on fully implicit coupled algorithms. Indeed, we have experienced that only implicit schemes allow to solve effectively the fluid structure problem arising in hemodynamic applications, when realistic physiological parameters are considered. In Sections 4.7÷4.10 we will propose three fully implicit coupled algorithms and we will analyse their stability properties. We will prove for the first two an unconditional stability result in the case of homogeneous Dirichlet boundary conditions and zero forcing terms. For the third one, that uses an explicit structure solver, we will obtain a conditional stability

result with a stability constant governed only by the structure discretisation (in other terms, the proposed coupled algorithm does not engender a further condition on the time step).
Since all the proposed coupled algorithms are implicit, at each time step we are faced with a coupled system, which is highly non-linear in those cases where the fluid domain is unknown. We need thus to introduce sub-iterations to solve such a system at each time step. In Section 4.9, we describe a simple substructuring algorithm which consists in subiterating between fluid and structure until the coupling conditions are satisfied within a fixed tolerance. This algorithm is the one used in our numerical simulations.
Finally, in Section 4.11 several numerical results will be presented. On a test case we will compare two coupled algorithms and we will carry out a numerical convergence analysis of the time discretisation error.

4.1 Model description

Let us consider a portion of a blood flow vessel (otherwise called *district*) that occupies at time t a region denoted by Ω_t, see Fig. 4.1. The vessel has a compliant wall denoted by Γ_t^w.

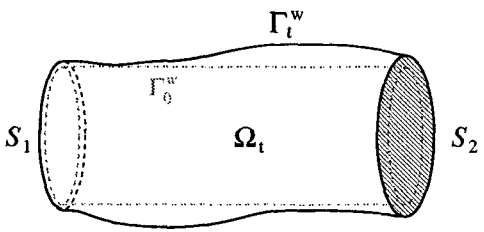

Figure 4.1: Simple compliant tube.

The boundary of the vessel is completed by the sections $\mathcal{S}_1$ and $\mathcal{S}_2$, connecting the district to the rest of the system. More precisely, $\mathcal{S}_1$ is the *upstream* section, $\mathcal{S}_2$ the *downstream* section, through which the fluid enters and leaves Ω_t respectively.

Remark 4.1.1 *In hemodynamic context, practitioners prefer to use the notation* proximal *and* distal *sections, to indicate the section nearest and farthest to the hearth, respectively.*

As usual, we will denote by $\mathbf{u}(\mathbf{x},t)$ (with $\mathbf{x} \in \Omega_t$, $t > 0$) the fluid velocity field, by $p(\mathbf{x},t)$ the pressure and by ρ the (constant) fluid density. We describe the fluid motion through the classical Navier-Stokes equations

$$\begin{cases} \rho\partial_t\mathbf{u} + \rho\mathbf{u}\cdot\boldsymbol{\nabla}\mathbf{u} - \text{div }\mathbf{T}(\mathbf{u},p) = 0 \\ \text{div }\mathbf{u} = 0 \end{cases} \quad \text{in } \Omega_t, \tag{4.1.1}$$

where $\mathbf{T}$ is the Cauchy stress tensor. Hereafter, we will consider the case of Newtonian fluids where we can use the following constitutive relation

$$\mathbf{T}(\mathbf{u},p) = -p\mathbf{I} + 2\mu\mathbf{D}(\mathbf{u}),$$

μ being the (constant) fluid viscosity.

Remark 4.1.2 *In large arteries (those whose diameter is roughly larger than 0.2 cm) blood can be assumed to behave as a Newtonian fluid ([60, 96]) while in small vessels and capillaries, its rheology is more complex. An account in given in [16, 65, 96].*

Whatever PDE model is considered for the vessel wall, it will provide the position of every point on Γ_t^w at any time $t > 0$, typically by means of the displacement $\boldsymbol{\eta}$ with respect to a reference position Γ_0^w (see for instance [13, 47]).
Then, matching conditions at Γ_t^w may be provided as follows:

$$\begin{cases} \mathbf{u} = \dot{\boldsymbol{\eta}} \\ \\ -\mathbf{T} \cdot \mathbf{n} - p_{ext}\mathbf{n} = \boldsymbol{\Phi} \end{cases} \quad \text{on } \Gamma_t^w, \tag{4.1.2}$$

where p_{ext} is a given external pressure, $\boldsymbol{\Phi}$ is the forcing term acting on the wall and $\mathbf{n}$ is the outward unit vector to Γ_t^w.
The first of (4.1.2) guarantees the perfect adherence of the fluid to the structure while the second one states the continuity of the stresses at the interface (according to the action and reaction principle).
Both fluid and structure equations must be supplied with initial conditions (resp. on Ω_0 and Γ_0^w) and boundary conditions (resp. on $\mathcal{S}_1, \mathcal{S}_2$ and $\partial\mathcal{S}_1, \partial\mathcal{S}_2$).

About the structure model, we will limit ourselves to consider a very simple model (the *generalised string* model; see [79]), derived for a cylindrical configuration . Let

$$\Gamma_0^w = \{(r, \theta, z) : \quad r = R_0,\, 0 \le z \le L,\, 0 \le \theta < 2\pi\}$$

be a cylindrical reference surface of radius R_0; we neglect the longitudinal and angular displacement while the radial displacement $\eta_r = \eta_r(t, \theta, z)$ is given by

$$\rho_w h \frac{\partial^2 \eta_r}{\partial t^2} - kGh\frac{\partial^2 \eta_r}{\partial z^2} + \frac{Eh}{1-\nu^2}\frac{\eta_r}{R_0^2} - \gamma\frac{\partial^3 \eta_r}{\partial z^2 \partial t} = f(t, \theta, z) \tag{4.1.3}$$

Here, h is the wall thickness, R_0 is the arterial reference radius at rest; k is the so called *Timoshenko shear correction factor*; G the *shear modulus*; E the Young modulus, ν the Poisson ratio (which for an incompressible material is equal to $1/2$); ρ_w the wall volumetric mass, γ is a viscoelastic parameter and, finally f is an external forcing term.
Model (4.1.3) is basically derived from the equations of linear elasticity for a cylindrical tube with small thickness, under the hypotheses of plane stresses and membrane deformations (i.e negligible elastic bending terms). The term $kGh\dfrac{\partial^2 \eta_r}{\partial z^2}$ accounts for shear deformations ([82]) while the term $\gamma\dfrac{\partial^3 \eta_r}{\partial z^2 \partial t}$ introduces a viscoelastic behaviour.

Remark 4.1.3 *We can give also another meaning to a term of the form $\alpha\dfrac{\partial^2 \eta_r}{\partial z^2}$, in equation (4.1.3), namely, it is a term that accounts for longitudinal pre-stress in the arterial wall at the equilibrium position. In that case, the coefficient α represent the longitudinal tension at rest. In physiological conditions, arteries experience a longitudinal pre-stress.*

Remark 4.1.4 *Other, even simpler, wall models, which can be derived from (4.1.3) by neglecting some other terms, have been employed in cardiovascular simulations as well.*
In particular, by neglecting the viscoelastic term and the term with second derivative in z, we obtain the so called independent ring *model*

$$\rho_w h \frac{\partial^2 \eta_r}{\partial t^2} + \frac{Eh}{1-\nu^2}\frac{\eta_r}{R_0^2} = p - p_{ext} \tag{4.1.4}$$

where p is the fluid pressure. This model has been adopted, for instance in [63, 66, 50].
If we further neglect the inertia term, we obtain the simple algebraic relation

$$\frac{Eh}{1-\nu^2}\frac{\eta_r}{R_0^2} = p - p_{ext} \tag{4.1.5}$$

which is widely used in deriving simplified monodimensional or lumped models for the circulatory system (see e.g. [95, 83]; see also Chapter 5 for a brief account of a monodimensional model of the circulatory system).
On the other hand, also shell models have been considered to simulate blood flow in complex districts such as bifurcations. See e.g. [64, 3].

4.1.1 Energy inequality for the coupled fluid-structure problem

Let us consider the 3D Navier-Stokes equations coupled with the structure model (4.1.3) through the matching conditions (4.1.2). In eq. (4.1.3), the forcing term $f(t,\theta,z)$ is given by the radial component Φ_r of the normal stress exerted by the fluid, recast in the reference configuration Γ_0^w, that is

$$f(t,\theta,z) = \Phi_r \frac{R}{R_0}\sqrt{1+\left(\frac{\partial \eta_r}{\partial z}\right)^2 + \left(\frac{1}{R}\frac{\partial \eta_r}{\partial \theta}\right)^2} \qquad \text{on } \Gamma_0^w. \tag{4.1.6}$$

Here we have noted $R = R_0 + \eta_r$, while the term under square root accounts for the change in the surface measure passing from Γ_t^w to Γ_0^w. Clearly, with such a right hand side, eq. (4.1.3) becomes non-linear and difficult to handle with. However, as we will show in Sec. 4.9, at the numerical level we will decouple the fluid and structure problems, and the right hand side will be computed at a previous step of the iterative algorithm.

Remark 4.1.5 *Since, from (4.1.2), we have* $\Phi_r = -(\mathbf{T} + p_{ext}\mathbf{I})\cdot\mathbf{n}\cdot\mathbf{e}_r$ *where* $\mathbf{T}$ *is the Cauchy stress tensor field, we may note that*

$$\mathbf{n} = \frac{\mathbf{N}}{|\mathbf{N}|} \qquad \text{with } \mathbf{N} = R\mathbf{e}_r - \frac{\partial \eta_r}{\partial \theta}\mathbf{e}_\theta - R\frac{\partial \eta_r}{\partial z}\mathbf{e}_z$$

and the right hand side of (4.1.3) becomes

$$\Phi_r \frac{R}{R_0}\sqrt{1+\left(\frac{\partial \eta_r}{\partial z}\right)^2 + \left(\frac{1}{R}\frac{\partial \eta_r}{\partial \theta}\right)^2} = -\frac{1}{R_0}(\mathbf{T} + p_{ext}\mathbf{I})\cdot\mathbf{N}\cdot\mathbf{e}_r = \left(-T_{rr} - p_{ext} + T_{r\theta}\frac{1}{R}\frac{\partial \eta_r}{\partial \theta} + T_{rz}\frac{\partial \eta_r}{\partial z}\right)\frac{R}{R_0},$$

which is now linear in η_r *provided we approximate R by* R_0*. Moreover, under the same approximation, if* $\mathbf{T}$ *is an isotropic tensor field, i.e.* $\mathbf{T} = -p\mathbf{I}$*, we have* $(-\mathbf{T} - p_{ext}\mathbf{I})\cdot\mathbf{N}\cdot\mathbf{e}_r/R_0 = p - p_{ext}$ *and the right hand side reduces simply to the pressure difference* $p - p_{ext}$*.*

We now analyse in more detail the coupled fluid-structure problem with the following initial and boundary conditions:

for the fluid

$$\begin{array}{ll} \mathbf{u} = \mathbf{u}_0 & \text{for } t = 0, \text{ in } \Omega_0 \\ \mathbf{u} = 0 & \text{on } \mathcal{S}_1 \\ \mathbf{T} \cdot \mathbf{n} = 0 & \text{on } \mathcal{S}_2 \end{array} \tag{4.1.7}$$

for the structure

$$\begin{array}{ll} \eta_r = \eta_0,\ \dot{\eta}_r \mathbf{e}_r = \mathbf{u}_0 & \text{for } t = 0, \text{ on } \Gamma_0^w \\ \eta_r = 0 & \text{for } z = 0,\ z = L \end{array} \tag{4.1.8}$$

For the sake of simplicity, and without loss of generality, we will put $p_{ext} = 0$. Let us rewrite equation (4.1.3) in the general form

$$\tilde{\rho}_w \frac{\partial^2 \eta_r}{\partial t^2} - a\frac{\partial^2 \eta_r}{\partial z^2} + b\eta_r - c\frac{\partial^3 \eta_r}{\partial^2 z \partial t} = \Phi_r \frac{R}{R_0}\sqrt{1 + \left(\frac{\partial \eta_r}{\partial z}\right)^2 + \left(\frac{1}{R}\frac{\partial \eta_r}{\partial \theta}\right)^2} \tag{4.1.9}$$

on Γ_0^w and for $t > 0$, where all the coefficients $\tilde{\rho}_w$, a, b, and c are positive quantities. We wish to derive an energy inequality for the coupled problem. The following Lemma holds

Lemma 4.1.1 *Should a solution to the coupled problem (4.1.1), (4.1.9) with matching conditions (4.1.2) and initial and boundary conditions (4.1.7) and (4.1.8) exist, then it would satisfy the following energy equality*

$$\frac{1}{2}\frac{d}{dt}\left\{\rho\|\mathbf{u}\|^2_{L^2(\Omega_t)} + \tilde{\rho}_w\|\frac{\partial \eta_r}{\partial t}\|^2_{L^2(\Gamma_0^w)} + a\|\frac{\partial \eta_r}{\partial z}\|^2_{L^2(\Gamma_0^w)} + b\|\eta_r\|^2_{L^2(\Gamma_0^w)}\right\} + \kappa\|\nabla \mathbf{u}\|^2_{L^2(\Omega_t)} + c\|\frac{\partial^2 \eta_r}{\partial z \partial t}\|^2_{L^2(\Gamma_0^w)} + \frac{1}{2}\rho\int_{\mathcal{S}_2}|\mathbf{u}|^2\mathbf{u}\cdot\mathbf{n}d\gamma = 0 \tag{4.1.10}$$

Moreover, if

$$\int_{\mathcal{S}_2}|\mathbf{u}|^2\mathbf{u}\cdot\mathbf{n}d\gamma > 0, \quad \forall t > 0, \tag{4.1.11}$$

we obtain the a-priori *energy estimate*

$$\rho\|\mathbf{u}(T)\|^2_{L^2(\Omega_t)} + \tilde{\rho}_w\|\frac{\partial \eta_r}{\partial t}(T)\|^2_{L^2(\Gamma_0^w)} + a\|\frac{\partial \eta_r}{\partial z}(T)\|^2_{L^2(\Gamma_0^w)} + b\|\eta_r(T)\|^2_{L^2(\Gamma_0^w)} + 2\kappa\int_0^T \|\nabla \mathbf{u}\|^2_{L^2(\Omega_t)}dt + 2\int_0^T c\|\frac{\partial^2 \eta_r}{\partial z \partial t}\|^2_{L^2(\Gamma_0^w)}dt \le C, \tag{4.1.12}$$

where C is a constant which depends on the initial conditions $\mathbf{u}_0$ and η_0 and κ is defined as in Section 3.2.

Proof. We first multiply eq. (4.1.9) by $\dfrac{\partial \eta_r}{\partial t}$ and integrate on the cylindrical surface Γ_0^w, obtaining

$$\frac{1}{2}\frac{d}{dt}\left\{\tilde{\rho}_w\|\frac{\partial\eta_r}{\partial t}\|^2_{L^2(\Gamma_0^w)}+a\|\frac{\partial\eta_r}{\partial z}\|^2_{L^2(\Gamma_0^w)}+b\|\eta_r\|^2_{L^2(\Gamma_0^w)}\right\}+$$
$$c\|\frac{\partial^2\eta_r}{\partial z\partial t}\|^2_{L^2(\Gamma_0^w)}-\left(a\frac{\partial\eta_r}{\partial z}\frac{\partial\eta_r}{\partial t}+c\frac{\partial^2\eta_r}{\partial z\partial t}\frac{\partial\eta_r}{\partial t}\right)\Big|_{z=0}^{z=L}=$$
$$\int_{\Gamma_0^w}\Phi_r\frac{R}{R_0}\sqrt{1+\left(\frac{\partial\eta_r}{\partial z}\right)^2+\left(\frac{1}{R}\frac{\partial\eta_r}{\partial\theta}\right)^2}\frac{\partial\eta_r}{\partial t}R_0\,d\theta\,dz \quad (4.1.13)$$

Thanks to the specific boundary conditions, the last term on the left side is identically zero, while the right hand side, if computed on the actual configuration Γ_t^w, becomes

$$\int_{\Gamma_0^w}\Phi_r\sqrt{1+\left(\frac{\partial\eta_r}{\partial z}\right)^2+\left(\frac{1}{R}\frac{\partial\eta_r}{\partial\theta}\right)^2}\frac{\partial\eta_r}{\partial t}R\,d\theta\,dz=\int_{\Gamma_t^w}\Phi_r\frac{\partial\eta_r}{\partial t}d\gamma=\int_{\Gamma_t^w}(-\mathbf{T}\cdot\mathbf{n})\cdot\mathbf{u}d\gamma$$

where in the last equality we have exploited the coupling conditions (4.1.2). Then, the following energy equality holds for the structure problem

$$\frac{1}{2}\frac{d}{dt}\left\{\tilde{\rho}_w\|\frac{\partial\eta_r}{\partial t}\|^2_{L^2(\Gamma_0^w)}+a\|\frac{\partial\eta_r}{\partial z}\|^2_{L^2(\Gamma_0^w)}+b\|\eta_r\|^2_{L^2(\Gamma_0^w)}\right\}+$$
$$c\|\frac{\partial^2\eta_r}{\partial z\partial t}\|^2_{L^2(\Gamma_0^w)}=\int_{\Gamma_t^w}(-\mathbf{T}\cdot\mathbf{n})\cdot\mathbf{u}d\gamma \quad (4.1.14)$$

Similarly, by multiplying the first of (4.1.1) by $\mathbf{u}$ and integrating over Ω_t we can derive the following energy estimate (see Section 3.2, Chapter 3)

$$\frac{1}{2}\rho\frac{d}{dt}\|\mathbf{u}\|^2_{L^2(\Omega_t)}+\kappa\|\boldsymbol{\nabla}\mathbf{u}\|^2_{L^2(\Omega_t)}-\int_{\mathcal{S}_1\cup\mathcal{S}_2}\left(\mathbf{T}\cdot\mathbf{n}-\frac{1}{2}\rho|\mathbf{u}|^2\mathbf{n}\right)\cdot\mathbf{u}d\gamma=\int_{\Gamma_t^w}(\mathbf{T}\cdot\mathbf{n})\cdot\mathbf{u}d\gamma$$

and, exploiting the boundary conditions, we have

$$\frac{1}{2}\rho\frac{d}{dt}\|\mathbf{u}\|^2_{L^2(\Omega_t)}+\kappa\|\boldsymbol{\nabla}\mathbf{u}\|^2_{L^2(\Omega_t)}+\int_{\mathcal{S}_2}\frac{1}{2}\rho|\mathbf{u}|^2\mathbf{n}\cdot\mathbf{u}d\gamma=\int_{\Gamma_t^w}(\mathbf{T}\cdot\mathbf{n})\cdot\mathbf{u}d\gamma. \quad (4.1.15)$$

By summing equalities (4.1.14) and (4.1.15) the term $\int_{\Gamma_t^w}(\mathbf{T}\cdot\mathbf{n})\cdot\mathbf{u}d\gamma$ cancels out and we obtain (4.1.10).
Finally, integrating (4.1.10) in time between 0 and T, under the hypothesis (4.1.11), we obtain the desired inequality (4.1.12).

■

The hypothesis (4.1.11) is actually satisfied if $\mathcal{S}_2$ is an *outflow section*, i.e. $\mathbf{u}\cdot\mathbf{n}>0$ for all $\mathbf{x}\in\mathcal{S}_2$. However, in vascular problems, this assumption is seldom true because the pulsating nature of blood flow might induce a flow reversal along portions of an artery during the cardiac beat.

We may observe that the "viscoelastic term" in (4.1.3) allows to obtain the appropriate regularity of the velocity field $\mathbf{u}$ on the boundary (see [79]).

In the derivation of energy inequality (4.1.12), we have considered homogeneous boundary conditions both for the fluid and the structure. However, the conditions $\eta = 0$ at $z = 0$ and $z = L$, which correspond to hold the wall ends fixed, are not realistic in the blood flow context. Since the model (4.1.3) for the structure is of propagative type, first order absorbing boundary conditions are a better choice, i.e.

$$\frac{\partial \eta_r}{\partial t} - \sqrt{\frac{a}{\tilde{\rho}_w}}\frac{\partial \eta_r}{\partial z} = 0 \qquad \text{at } z = 0 \tag{4.1.16}$$

$$\frac{\partial \eta_r}{\partial t} + \sqrt{\frac{a}{\tilde{\rho}_w}}\frac{\partial \eta_r}{\partial z} = 0 \qquad \text{at } z = L. \tag{4.1.17}$$

In this case, the final estimate (4.1.12) is still valid. Indeed the boundary term which appears in (4.1.13) now should read

$$-\left(a\frac{\partial \eta_r}{\partial z}\frac{\partial \eta_r}{\partial t} + c\frac{\partial^2 \eta_r}{\partial z \partial t}\frac{\partial \eta_r}{\partial t}\right)\Big|_{z=0}^{z=L} =$$
$$\sqrt{\tilde{\rho}_w a}\left[\left(\frac{\partial \eta_r}{\partial t}\Big|_{z=0}\right)^2 + \left(\frac{\partial \eta_r}{\partial t}\Big|_{z=L}\right)^2\right] + \frac{c}{2}\sqrt{\frac{\tilde{\rho}_w}{a}}\frac{d}{dt}\left[\left(\frac{\partial \eta_r}{\partial t}\Big|_{z=0}\right)^2 + \left(\frac{\partial \eta_r}{\partial t}\Big|_{z=L}\right)^2\right].$$

This term, integrated in time, would eventually appear on the left hand side of inequality (4.1.12) and the latter becomes

$$\rho\|\mathbf{u}(T)\|^2_{L^2(\Omega_t)} + \tilde{\rho}_w\|\frac{\partial \eta_r}{\partial t}(T)\|^2_{L^2(\Gamma_0^w)} + a\|\frac{\partial \eta_r}{\partial z}(T)\|^2_{L^2(\Gamma_0^w)} + b\|\eta_r(T)\|^2_{L^2(\Gamma_0^w)}$$
$$+2\kappa\int_0^T \|\nabla \mathbf{u}\|^2_{L^2(\Omega_t)}dt + 2\int_0^T c\|\frac{\partial^2 \eta_r}{\partial z \partial t}\|^2_{L^2(\Gamma_0^w)}dt + \frac{c}{2}\sqrt{\frac{\tilde{\rho}_w}{a}}\left[\left(\frac{\partial \eta_r}{\partial t}(T)\Big|_{z=0}\right)^2 + \left(\frac{\partial \eta_r}{\partial t}(T)\Big|_{z=L}\right)^2\right]$$
$$+\sqrt{\tilde{\rho}_w a}\int_0^T\left[\left(\frac{\partial \eta_r}{\partial t}(\tau)\Big|_{z=0}\right)^2 + \left(\frac{\partial \eta_r}{\partial t}(\tau)\Big|_{z=L}\right)^2\right]d\tau \le C.$$

Therefore, this additional term is positive and it depends only on the initial conditions.
Yet, conditions (4.1.16) and (4.1.17) are not compatible with the homogeneous Dirichlet boundary conditions for the fluid; indeed, if $\eta|_{z=0} \neq 0$ and $\mathbf{u} = 0$ on $\mathcal{S}_1$, the trace of $\mathbf{u}(\mathbf{x}, t)$ on the boundary is discontinuous and thus not compatible with the regularity required on the solution of (4.1.1) (see. e.g. [80]).
A possible remedy consists in changing the condition $\mathbf{u} = 0$ on $\mathcal{S}_1$ into

$$\begin{aligned} &\mathbf{u}\cdot\mathbf{e}_z = g \\ &\mathbf{T}\cdot\mathbf{n} - (\mathbf{T}\cdot\mathbf{n})\cdot\mathbf{e}_z = 0 \end{aligned} \qquad \text{on } \mathcal{S}_1$$

with $g = 0$ on $\partial\mathcal{S}_1$. An energy inequality for the coupled problem can be derived also in this case with standard calculations, taking a suitable harmonic extension $\tilde{g}$ of the non homogeneous data g such that

$$\tilde{g}|_{\mathcal{S}_1} = g \quad \text{and} \quad \tilde{g}|_{\Gamma_t^w} = 0.$$

The calculations are here omitted for the sake of brevity.

4.2 A 2D simplified problem

For the purpose of the mathematical analysis, we will consider a 2D model obtained by intersecting the tube Ω_t of figure 4.1 with a plane $\theta = \bar{\theta}$ (see fig. 4.2). Correspondingly, we will consider the 2D problem arising from the combination of the 2D Navier-Stokes equations for the fluid with eq. (4.1.3) to describe the motion of the upper and lower boundary (with a frozen value of the angle θ). This model will be adopted in Section 4.11 to obtain some numerical results.

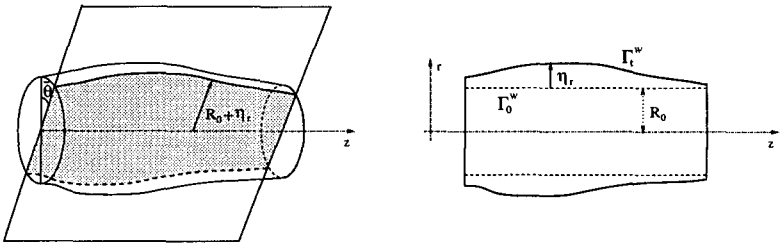

Figure 4.2: Intersecting the cylinder with the plane $\theta = \bar{\theta}$ we obtain a 2D geometry with a 1D compliant wall

Remark 4.2.1 *Although not completely realistic for blood flow problems, this simplified 2D analysis maintains all the mathematical aspects peculiar to the original coupled fluid-structure problem and will therefore be adopted to test the numerical coupling algorithms we will present in the next sections.*

A more realistic two dimensional representation of the fluid structure model in hemodynamic applications may be obtained from the 3D problem by supposing an axial symmetry. In this case, we should consider the combination of the Navier-Stokes equations written in cylindrical coordinates with the structure model (4.1.3). If we suppose that the data and the solution of the coupled problem do not depend on the angular coordinate θ, the 3D problem can be reduced to a 2D one. We will not investigate this axial symmetric model in the present work.

In order to analyse the finite element discretisation and the stability of some implicit coupling algorithms, we furtherly simplify the problem by taking the lower boundary fixed. Thus, the situation we will consider from now on consists of the 2D geometry depicted in figure 4.3 : let Ω_0 be the rectangle $(0, L) \times (0, D) \subset \mathbb{R}^2$; the upper edge is identified by

$$\Gamma_0^w = \{(z, r) \in \mathbb{R}^2 \ : \ r = D \text{ and } 0 \leq z \leq L\}$$

In the following we will drop the subscript r from η_r. Thus, we indicate with $\eta(z,t) : [0, L] \times \mathbb{R}_+ \to \mathbb{R}$ the vertical displacement of Γ_0^w. We introduce the transformation

$$\varphi_\eta(z,t) \ : \ [0, L] \times \mathbb{R}_+ \to \mathbb{R}^2, \qquad \varphi_\eta(z,t) = (z, D + \eta(z,t)) \in \mathbb{R}^2 \tag{4.2.1}$$

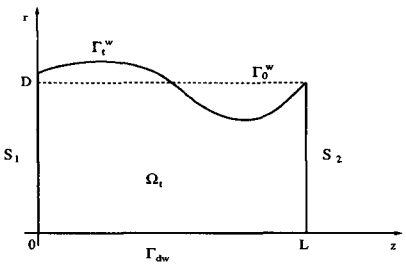

Figure 4.3: 2D geometry considered for the mathematical analysis

which identifies the position of the actual boundary Γ_t^w, i.e. $\forall t \geq 0$, $\Gamma_t^w = \{(z,r) = \varphi_\eta(z,t),\ 0 \leq z \leq L\}$. On the contrary, $\mathcal{S}_1$, $\mathcal{S}_2$ and Γ_{dw} are kept fixed[1]. The fluid domain is then delimited by the four boundary segments $\mathcal{S}_1$, $\mathcal{S}_2$, Γ_{dw} and Γ_t^w. The fluid-structure problem we are going to analyze reads

$$\begin{cases} \rho\partial_t \mathbf{u} + \rho\mathbf{u}\cdot\nabla\mathbf{u} - \operatorname{div}(2\mu\mathbf{D}(\mathbf{u}) - p\mathbf{I}) = \mathbf{f}, & \text{in } \Omega_t \\ \operatorname{div}\mathbf{u} = 0, & \\ \tilde{\rho}_w \dfrac{\partial^2\eta}{\partial t^2} - a\dfrac{\partial^2\eta}{\partial z^2} + b\eta - c\dfrac{\partial^3\eta}{\partial^2 z\partial t} = \Phi_r\sqrt{1+\left(\dfrac{\partial\eta}{\partial z}\right)^2}, & z\in(0,L) \\ \mathbf{u}\big|_{\Gamma_t^w}\circ\varphi_\eta = \dot{\eta}\mathbf{e}_r, & \text{on } \Gamma_0^w \\ \Phi_r = -\left[\left(\mathbf{T}\big|_{\Gamma_t^w} + p_{ext}\mathbf{I}\right)\cdot\mathbf{n}\cdot\mathbf{e}_r\right]\circ\varphi_\eta, & \end{cases} \tag{4.2.2}$$

supplied with initial conditions

$$\begin{cases} \mathbf{u} = \mathbf{u}_0 & \text{for } t = 0, \text{ in } \Omega_0 \\ \eta = \eta_0,\ \dot{\eta}\mathbf{e}_r = \mathbf{u}_0 & \text{for } t = 0, \text{ on } \Gamma_0^w \end{cases} \tag{4.2.3}$$

We will introduce two different boundary value problems: the former is the one used for the numerical simulations that will be presented in Section 4.11 while the latter will be considered in Sections 4.7÷4.10 to study the stability of some implicit coupled algorithms.

Problem 4.2.1 (Neumann) *We consider system (4.2.2) with initial conditions (4.2.3) and boundary conditions*

$$\textit{(fluid)}\ \begin{cases} \mathbf{u} = 0 & \text{on } \Gamma_{dw}, \\ \mathbf{T}\cdot\mathbf{n} = \boldsymbol{\sigma}_1 & \text{on } \mathcal{S}_1, \\ \mathbf{T}\cdot\mathbf{n} = \boldsymbol{\sigma}_2 & \text{on } \mathcal{S}_2, \end{cases} \qquad \textit{(structure)}\ \begin{cases} \dfrac{\partial\eta}{\partial t} - \sqrt{\dfrac{a}{\tilde{\rho}_w}}\dfrac{\partial\eta}{\partial z} = 0 & \text{at } z = 0, \\ \dfrac{\partial\eta}{\partial t} + \sqrt{\dfrac{a}{\tilde{\rho}_w}}\dfrac{\partial\eta}{\partial z} = 0 & \text{at } z = L. \end{cases} \tag{4.2.4}$$

[1]When $\eta(0) \neq 0$ (resp. $\eta(L) \neq 0$), section $\mathcal{S}_1$ (resp. $\mathcal{S}_2$) is not really fixed since its upper end follows the wall motion. Yet, section $\mathcal{S}_1$ is kept vertical and its movement is not determined by a dynamic law but is a mere consequence of the motion of Γ_t^w.

Problem 4.2.2 (Dirichlet) *We consider system (4.2.2) with initial conditions (4.2.3) and boundary conditions*

$$\textit{(fluid)} \begin{cases} \mathbf{u} = 0 & \text{on } \Gamma_{dw}, \\ \mathbf{u} = \mathbf{\Phi}_1 & \text{on } \mathcal{S}_1, \\ \mathbf{u} = \mathbf{\Phi}_2 & \text{on } \mathcal{S}_2, \end{cases} \qquad \textit{(structure)} \begin{cases} \eta = \alpha_1 & \text{at } z = 0, \\ \eta = \alpha_2 & \text{at } z = L, \end{cases} \tag{4.2.5}$$

where the non-homogeneous Dirichlet data must satisfy the compatibility relations

$$\mathbf{\Phi}_i\big|_{\Gamma_t^w} \circ \boldsymbol{\varphi}_\eta = \dot{\alpha}_i \cdot \mathbf{e}_r, \qquad i = 1, 2.$$

Observe that, due to the incompressibility constraint div $\mathbf{u} = 0$, we have for Problem 4.2.2 :

$$0 = \int_{\Omega_t} \operatorname{div} \mathbf{u}\, d\Omega = \int_{\partial\Omega_t} \mathbf{u} \cdot \mathbf{n}\, d\Gamma = \int_{\Gamma_t^w} \mathbf{u} \cdot \mathbf{n}\, d\Gamma + \int_{\mathcal{S}_1} \mathbf{\Phi}_1 \cdot \mathbf{n}\, d\Gamma + \int_{\mathcal{S}_2} \mathbf{\Phi}_2 \cdot \mathbf{n}\, d\Gamma.$$

On the other hand,

$$\begin{aligned} \int_{\Gamma_t^w} \mathbf{u} \cdot \mathbf{n}\, d\Gamma &= \int_{\Gamma_0^w} \left[(u_r \mathbf{e}_r + u_z \mathbf{e}_z) \cdot \mathbf{n} \right]\big|_{\Gamma_t^w} \circ \boldsymbol{\varphi}_\eta \sqrt{1 + \left(\frac{\partial \eta}{\partial z}\right)^2}\, d\Gamma \\ &= \int_{\Gamma_0^w} \left(u_r - u_z \frac{\partial \eta}{\partial z} \right)\Big|_{\Gamma_t^w} \circ \boldsymbol{\varphi}_\eta\, d\Gamma = \int_{\Gamma_0^w} \dot{\eta}\, d\Gamma \end{aligned}$$

where we have exploited the fact that $\mathbf{n} = \mathbf{N}/|\mathbf{N}|$, with $\mathbf{N} = \mathbf{e}_r - \dfrac{\partial \eta}{\partial z}\mathbf{e}_z$. Hence, we conclude that in Problem 4.2.2, the displacement η satisfies the supplementary relation

$$\frac{d}{dt} \int_{\Gamma_0^w} \eta\, d\Gamma = - \int_{\mathcal{S}_1} \mathbf{\Phi}_1 \cdot \mathbf{n}\, d\Gamma - \int_{\mathcal{S}_2} \mathbf{\Phi}_2 \cdot \mathbf{n}\, d\Gamma \tag{4.2.6}$$

In particular, when $\mathbf{\Phi}_1 = \mathbf{\Phi}_2 = \mathbf{0}$, relation (4.2.6), integrated in time between 0 and T, becomes

$$\int_{\Gamma_0^w} \eta(T)\, d\Gamma = \int_{\Gamma_0^w} \eta_0\, d\Gamma$$

which is equivalent to require that the initial volume $|\Omega_0|$ is preserved in time.
In order to write the fluid equations in ALE form, we introduce an ALE mapping $\mathcal{A}_t : \Omega_0 \to \Omega_t$. Let $\mathbf{Y} = (Y_1, Y_2)$ be the reference coordinates in Ω_0. The boundary position, identified by the function $\mathbf{g}_\eta : \partial\Omega_0 \to \partial\Omega_t$, depends on the wall displacement η and is given by

$$\mathbf{g}_\eta = \begin{cases} \mathbf{Y} + \eta \mathbf{e}_r = \boldsymbol{\varphi}_\eta & \text{on } \Gamma_0^w \\ \mathbf{Y}, & \text{on } \Gamma_{dw}, \end{cases}$$

and, on the fixed sections $\mathcal{S}_1$ and $\mathcal{S}_2$

$$\mathbf{g}_\eta = \mathbf{Y}, \qquad \text{if } \eta(0,t) = \eta(L,t) = 0.$$

Otherwise we may impose (arbitrarily) a linear deformation

$$\text{on } \mathcal{S}_1 \quad \mathbf{g}_\eta = \mathbf{Y} + Y_2 \frac{\eta(0,t)}{D}\mathbf{e}_r,$$
$$\text{on } \mathcal{S}_2 \quad \mathbf{g}_\eta = \mathbf{Y} + Y_2 \frac{\eta(L,t)}{D}\mathbf{e}_r.$$

The ALE mapping may, now, be determined, for instance, by solving at each $t > 0$ the Laplace problem (harmonic extension)

$$(z,r) = \mathcal{A}_t(\mathbf{Y}), \qquad \begin{cases} \Delta \mathcal{A}_t = 0, & \text{in } \Omega_0, \\ \mathcal{A}_t = \mathbf{g}_\eta, & \text{on } \partial\Omega_0. \end{cases} \tag{4.2.7}$$

As pointed out in Chapter 1, other problems different than the Laplace one may be considered as well.

Remark 4.2.2 *In this particular case we observe that we can build an ALE mapping directly, by considering the transformation*

$$\mathcal{A}_t(\mathbf{Y}) : \begin{cases} z = Y_1, \\ r = Y_2 \left(1 + \dfrac{\eta(z,t)}{D}\right), \end{cases} \qquad \forall (Y_1, Y_2) \in \Omega_0. \tag{4.2.8}$$

This mapping is invertible provided $\eta(z,t) > -D$, for all $z \in [0,L]$ and $t > 0$.

The fluid-structure system (4.2.2) written in ALE form reads then

$$\begin{cases} \rho \left.\dfrac{\partial \mathbf{u}}{\partial t}\right|_{\mathbf{Y}} + \rho(\mathbf{u} - \mathbf{w}) \cdot \boldsymbol{\nabla}_{\mathbf{x}} \mathbf{u} - \operatorname{div}_{\mathbf{x}}(2\mu \mathbf{D}_{\mathbf{x}}(\mathbf{u}) - p\mathbf{I}) = \mathbf{f}, & \text{in } \Omega_t \\ \operatorname{div}_{\mathbf{x}} \mathbf{u} = 0, & \text{"} \\ \tilde{\rho}_w \dfrac{\partial^2 \eta}{\partial t^2} - a\dfrac{\partial^2 \eta}{\partial z^2} + b\eta - c\dfrac{\partial^3 \eta}{\partial^2 z \partial t} = \Phi_r \sqrt{1 + \left(\dfrac{\partial \eta}{\partial z}\right)^2}, & z \in (0,L) \\ \mathbf{u}|_{\Gamma_t^w} \circ \boldsymbol{\varphi}_\eta = \dot{\eta}\mathbf{e}_r, & \text{on } \Gamma_0^w \\ \Phi_r = -\left[(\mathbf{T}|_{\Gamma_t^w} + p_{ext}\mathbf{I}) \cdot \mathbf{n} \cdot \mathbf{e}_r\right] \circ \boldsymbol{\varphi}_\eta, & \text{"} \\ \Delta \mathcal{A}_t = 0 & \text{in } \Omega_0, \ \forall t > 0 \\ \mathcal{A}_t = \mathbf{g}_\eta & \text{on } \partial\Omega_0, \ \forall t > 0 \end{cases} \tag{4.2.9}$$

4.3 Global weak formulation

Following the approach proposed by Le Tallec and Mouro in [55] we will consider a global weak formulation for the fluid-structure problem that accounts at the same time for the fluid and the structure part. This formulation is well suited to devise and analyze fully implicit coupled algorithms. For the structure equation, we introduce the following spaces :

$$V^S(\Gamma_0^w) = H^1(0,L), \qquad V_0^S(\Gamma_0^w) = H_0^1(0,L),$$

while for the fluid equations we proceed as in Chapter 3 by introducing the spaces

$$\hat{\mathbf{V}}^F(\Omega_0) = \left\{\hat{\mathbf{v}} \in \left[H^1(\Omega_0)\right]^d,\ \hat{\mathbf{v}} = \mathbf{0} \text{ on } \Gamma_{dw}\right\}$$
$$\hat{\mathbf{V}}^F_{\mathcal{S}_{1,2}}(\Omega_0) = \left\{\hat{\mathbf{v}} \in \left[H^1(\Omega_0)\right]^d,\ \hat{\mathbf{v}} = \mathbf{0} \text{ on } \Gamma_{dw} \cup \mathcal{S}_1 \cup \mathcal{S}_2\right\}$$

and

$$\mathbf{V}^F(\Omega_t) = \{\mathbf{v} : \Omega_t \times I \to \mathbb{R}^d, \quad \mathbf{v} = \hat{\mathbf{v}} \circ \mathcal{A}_t^{-1},\ \hat{\mathbf{v}} \in \hat{\mathbf{V}}^F(\Omega_0)\}.$$

An analogous definition holds for $\mathbf{V}^F_{\mathcal{S}_{1,2}}(\Omega_t)$. The spaces $Q(\Omega_t)$ and $Q_0(\Omega_t)$ are defined as in (3.3.3) and (3.3.5). Finally, let

$$\mathbf{V}(t) = \{(\mathbf{v}, \xi) \in \mathbf{V}^F(\Omega_t) \times V^S(\Gamma_0^w),\ \text{s.t. } \mathbf{v} \circ \mathcal{A}_t\big|_{\Gamma_0^w} = \xi \mathbf{e}_r\}. \tag{4.3.1}$$

and $\mathbf{V}_0(t) = \mathbf{V}(t) \cap \left(\mathbf{V}^F_{\mathcal{S}_{1,2}}(\Omega_t) \times V_0^S(\Gamma_0^w)\right)$ be the spaces of test functions for the fluid/structure problem. In (4.3.1) we are requiring that the fluid and structure functions match exactly on Γ_0^w.

In the following of this Chapter, we will consider only the conservative formulation of the fluid equations in ALE framework. Moreover, we will indicate the problem used to determine the ALE mapping in the general form

$$\mathcal{P}_{\mathcal{A}}(\mathcal{A}_t, \mathbf{z}) = 0, \qquad \forall \mathbf{z} \in [H_0^1(\Omega_0)]^d. \tag{4.3.2}$$

If we employ system (4.2.7) to build the ALE mapping, the form $\mathcal{P}_{\mathcal{A}}(\cdot,\cdot)$ reads simply

$$\mathcal{P}_{\mathcal{A}}(\mathcal{A}_t, \mathbf{z}) = \int_{\Omega_0} \nabla \mathcal{A}_t : \nabla \mathbf{z}\, d\Omega.$$

Then, the weak formulation of the Neumann Problem 4.2.1 reads :

Problem 4.3.1 (weak-Neumann) *for almost every $t \in I$, find $t \to \mathbf{u}(t) \in \mathbf{V}^F(\Omega_t)$, $t \to p(t) \in Q(\Omega_t)$ and $t \to \eta(t) \in V^S(\Gamma_0^w) \cap W^{1,\infty}(0, L)$ such that*

$$\begin{cases} \displaystyle\int_{\Gamma_0^w} \tilde{\rho}_w \frac{\partial^2 \eta}{\partial t^2} \xi\, dz + \int_{\Gamma_0^w} b\eta\xi\, dz + \int_{\Gamma_0^w} \left(a\frac{\partial \eta}{\partial z} + c\frac{\partial^2 \eta}{\partial z \partial t}\right)\frac{\partial \xi}{\partial z}\, dz + \sqrt{\frac{\tilde{\rho}_w}{a}}\left(a\frac{\partial \eta}{\partial t} + c\frac{\partial^2 \eta}{\partial t^2}\right)\xi\Big|_{z=0,z=L} \\ \quad + \rho\frac{d}{dt}\displaystyle\int_{\Omega_t} \mathbf{u}\cdot\mathbf{v}\, d\Omega + \rho\int_{\Omega_t} \mathrm{div}_{\mathbf{x}}\left[(\mathbf{u}-\mathbf{w})\otimes\mathbf{u}\right]\cdot\mathbf{v}\, d\Omega + 2\mu\int_{\Omega_t} \mathbf{D}_{\mathbf{x}}(\mathbf{u}) : \nabla_{\mathbf{x}}\mathbf{v}\, d\Omega \\ \quad - \displaystyle\int_{\Omega_t} \mathrm{div}_{\mathbf{x}}\,\mathbf{v}\, p\, d\Omega = \int_{\Omega_t} \mathbf{f}\cdot\mathbf{v}\, d\Omega + \sum_{i=1,2}\int_{\mathcal{S}_i} \boldsymbol{\sigma}_i\cdot\mathbf{v}\, d\Gamma - \int_{\Gamma_0^w} p_{ext}\xi\, dz \qquad \forall (\mathbf{v},\xi) \in \mathbf{V}(t) \\ \displaystyle\int_{\Omega_t} \mathrm{div}_{\mathbf{x}}\,\mathbf{u}\, q\, d\Omega = 0 \qquad \forall q \in Q(\Omega_t) \end{cases}$$

(P-FS)

$$\mathbf{u} \circ \mathcal{A}_t = \dot{\eta}\mathbf{e}_r, \qquad \text{on } \Gamma_0^w \tag{ICC}$$

$$\begin{cases} \mathcal{P}_{\mathcal{A}}(\mathcal{A}_t, \mathbf{z}) = 0 & \forall \mathbf{z} \in [H_0^1(\Omega_0)]^d,\ \forall t > 0 \\ \mathcal{A}_t = \mathbf{g}_\eta & \text{on } \partial\Omega_0,\ \forall t > 0 \end{cases} \qquad \text{and } \mathbf{w} = \frac{\partial \mathcal{A}_t}{\partial t} \circ \mathcal{A}_t^{-1} \quad \text{in } \Omega_t \tag{P-ALE}$$

where $\mathbf{u}(t)$ and $\eta(t)$ satisfy the initial conditions (4.2.3).

In Problem 4.3.1 we have highlighted the fluid/structure equations (P-FS), the interface coupling condition (ICC) stating the continuity of the velocity between fluid and structure, and the problem used to determine the ALE mapping (P-ALE). The second coupling condition, stating the continuity of the stresses at the interface is hidden in the fluid structure problem (P-FS) because of the choice of matching test functions on Γ_0^w. This point will be clarified later on in Proposition 4.3.1.
Similarly, the weak formulation of the Dirichlet Problem (4.2.2) reads :

Problem 4.3.2 (weak-Dirichlet) *for almost every $t \in I$, find $t \to \mathbf{u}(t) \in \mathbf{V}^F(\Omega_t)$, $t \to p(t) \in Q(\Omega_t)$ and $t \to \eta(t) \in V^S(\Gamma_0^w) \cap W^{1,\infty}(0,L)$ that satisfy system*

$$\begin{cases} \displaystyle\int_{\Gamma_0^w} \tilde{\rho}_w \frac{\partial^2 \eta}{\partial t^2} \xi \, dz + \int_{\Gamma_0^w} b\eta\xi \, dz + \int_{\Gamma_0^w} \left(a\frac{\partial \eta}{\partial z} + c\frac{\partial^2 \eta}{\partial z \partial t} \right) \frac{\partial \xi}{\partial z} \, dz \\ \quad + \rho \frac{d}{dt} \displaystyle\int_{\Omega_t} \mathbf{u} \cdot \mathbf{v} \, d\Omega + \rho \int_{\Omega_t} \mathrm{div}_{\mathbf{x}} \left[(\mathbf{u} - \mathbf{w}) \otimes \mathbf{u} \right] \cdot \mathbf{v} \, d\Omega + 2\mu \int_{\Omega_t} \mathbf{D}_{\mathbf{x}}(\mathbf{u}) : \nabla_{\mathbf{x}} \mathbf{v} \, d\Omega \\ \quad - \displaystyle\int_{\Omega_t} \mathrm{div}_{\mathbf{x}} \mathbf{v} \, p \, d\Omega = \int_{\Omega_t} \mathbf{f} \cdot \mathbf{v} \, d\Omega - \int_{\Gamma_0^w} p_{ext} \xi \, dz \qquad \forall (\mathbf{v}, \xi) \in \mathbf{V}_0(t) \\ \displaystyle\int_{\Omega_t} \mathrm{div}_{\mathbf{x}} \mathbf{u} \, q \, d\Omega = 0 \qquad \forall q \in Q(\Omega_t) \end{cases} \tag{P-FS}$$

supplied with the same interface coupling condition (ICC) and ALE mapping problem (P-ALE) as in the weak-Neumann Problem 4.3.1, and initial and boundary conditions given by (4.2.3) and (4.2.5), respectively.

Some remarks are in order. In the weak formulations here presented, we look for a displacement $\eta(t) \in W^{1,\infty}(0,L)$ which is a necessary condition to construct an ALE mapping that belongs to $[W^{1,\infty}(\Omega_0)]^2$ as well, and provide a correct weak formulation for the fluid equations. On the other hand, the natural space in which to look for the solution $\eta(t)$ should be $L^\infty(0,T;H^1(0,L))$ with time derivative $\dfrac{\partial \eta}{\partial t} \in L^\infty(0,T;L^2(0,L)) \cap L^2(0,T;H^1(0,L))$ as we can infer from the a-priori energy inequality (4.1.12). The well-posedness of both Problems 4.3.1 and 4.3.2 is still an open question.
Until now, at our knowledge, only a few and partial results are available for fluid structure interaction problems. A framework similar to the one considered in this section has been studied in [43]; on the same geometry as in fig. 4.3, existence and uniqueness of weak solutions has been proven for the stationary problem consisting of the coupling between Stokes equations and a fourth order structural equation under the hypothesis of small data. Other available results concern the motion in a fluid of rigid bodies or deformable ones, whose deformations are described by a linear combination of a finite number of elastic eigenmodes. Existence of weak solutions has been proven in [18, 19] for all $T > 0$ provided there isn't any collision between the bodies. In [17] an alternative proof is given resorting to a penalization technique, valid only for one rigid body.
Existence of strong solutions of the motion of a rigid body in a viscous incompressible fluid, at least for a short time interval, has instead been proven in [40] under the hypothesis that the mass and the inertia of the body is sufficiently large.
For a review of results concerning fluid structure interaction problems see also [41].

In the following Proposition, we will show that a smooth solution of the weak problem is also a solution of the strong coupled problem. This result will be presented only for the Dirichlet Problem for the sake of brevity, yet it is valid for the Neumann Problem as well.

Proposition 4.3.1 *Any smooth solution of Problem 4.3.2 is also a solution of Problem 4.2.2.*

Proof. We will show the equivalence between the weak Problem 4.3.2 and the strong Problem 4.2.2 written in ALE form, which is given by system (4.2.9) supplied with boundary conditions (4.2.5) and initial conditions (4.2.3). The latter is, on its turn, equivalent to Problem 4.2.2 in Eulerian form.
Let us firstly introduce a linear continuous extension operator $\tilde{\mathcal{R}} : V_0^S(\Gamma_0^w) \to \hat{\mathbf{V}}^F_{S_{1,2}}(\Omega_0)$, such that $\forall \xi \in V_0^S(\Gamma_0^w), \quad \tilde{\mathcal{R}}(\xi)|_{\Gamma_0^w} = \xi \mathbf{e}_r$; such an operator exists since the boundary datum ξ extended by zero in $\partial\Omega_0 \setminus \Gamma_0^w$ belongs to $H^{1/2}(\partial\Omega_0)$ (see e.g. [76])[2]. Let, moreover $\mathcal{R} : V_0^S(\Gamma_0^w) \to \mathbf{V}^F_{S_{1,2}}(\Omega_t)$ be defined as

$$\forall \xi \in V_0^S(\Gamma_0^w),\ t > 0, \quad \mathcal{R}(\xi) = \tilde{\mathcal{R}}(\xi) \circ \mathcal{A}_t^{-1}. \tag{4.3.3}$$

If we take in system (P-FS) of Problem 4.3.2 the test function as $(\mathbf{v}, 0)$ we obtain the system

$$\begin{cases} \rho \dfrac{d}{dt} \displaystyle\int_{\Omega_t} \mathbf{u} \cdot \mathbf{v}\, d\Omega + \rho \int_{\Omega_t} \mathrm{div}_{\mathbf{x}} \left[(\mathbf{u} - \mathbf{w}) \otimes \mathbf{u} \right] \cdot \mathbf{v}\, d\Omega + 2\mu \int_{\Omega_t} \mathbf{D}_{\mathbf{x}}(\mathbf{u}) : \boldsymbol{\nabla}_{\mathbf{x}} \mathbf{v}\, d\Omega \\ \quad - \displaystyle\int_{\Omega_t} \mathrm{div}_{\mathbf{x}}\, \mathbf{v}\, p\, d\Omega = \int_{\Omega_t} \mathbf{f} \cdot \mathbf{v}\, d\Omega \qquad \forall (\mathbf{v}, 0) \in \mathbf{V}_0(t) \\ \displaystyle\int_{\Omega_t} \mathrm{div}_{\mathbf{x}}\, \mathbf{u}\, q\, d\Omega = 0 \qquad \forall q \in Q(\Omega_t) \end{cases} \tag{4.3.4}$$

Then, integrating by parts the first equation and exploiting relation (1.2.8) we have

$$\begin{cases} < \rho \left. \dfrac{\partial \mathbf{u}}{\partial t} \right|_{\mathbf{Y}} + \rho(\mathbf{u} - \mathbf{w}) \cdot \boldsymbol{\nabla}_{\mathbf{x}} \mathbf{u} - \mathrm{div}_{\mathbf{x}}(2\mu \mathbf{D}_{\mathbf{x}}(\mathbf{u}) - p\mathbf{I}), \mathbf{v} > = < \mathbf{f}, \mathbf{v} > \quad \forall (\mathbf{v}, 0) \in \mathbf{V}_0(t) \\ < \mathrm{div}_{\mathbf{x}}\, \mathbf{u}, q > = 0 \qquad \forall q \in Q(\Omega_t) \end{cases} \tag{4.3.5}$$

Thus, the first two equations of (4.2.9) are satisfied almost everywhere in Ω_t, provided the solution is sufficiently smooth.
Now, by taking the test function in the first equation of (P-FS) as $(\mathcal{R}(\xi), \xi)$ and integrating by parts the structure terms we have

$$< \tilde{\rho}_w \frac{\partial^2 \eta}{\partial t^2} - a \frac{\partial^2 \eta}{\partial z^2} + b\eta - c \frac{\partial^3 \eta}{\partial^2 z \partial t}, \xi > = - < p_{ext}, \xi > + < \tilde{\Phi}(\mathbf{u}, p), \xi >, \qquad \forall \xi \in V_0^S(\Gamma_0^w)$$

where the functional $\tilde{\Phi}(\mathbf{u}, p) \in \left(V_0^S(\Gamma_0^w)\right)'$ is defined as

$$< \tilde{\Phi}(\mathbf{u}, p), \xi > = < \Phi(\mathbf{u}, p), \mathcal{R}(\xi) >, \qquad \forall \xi \in V_0^S(\Gamma_0^w) \tag{4.3.6}$$

[2]For the Neumann Problem the operator $\tilde{\mathcal{R}}$ should be defined as $\tilde{\mathcal{R}} : V^S(\Gamma_0^w) \to \mathbf{V}^F(\Omega_t)$.

and the functional $\Phi(\mathbf{u},p) \in \left(\mathbf{V}^F_{S_{1,2}}(\Omega_t)\right)'$ is the residual of the first equation in (4.3.4) for all fluid test functions $\mathbf{v} \in \mathbf{V}^F_{S_{1,2}}(\Omega_t)$ non vanishing on Γ^w_t, i.e.

$$< \Phi(\mathbf{u},p), \mathbf{v} >= \int_{\Omega_t} \mathbf{f}\cdot\mathbf{v}\, d\Omega - \rho\frac{d}{dt}\int_{\Omega_t}\mathbf{u}\cdot\mathbf{v}\, d\Omega$$
$$- \rho\int_{\Omega_t} \mathrm{div}_{\mathbf{x}}\left[(\mathbf{u}-\mathbf{w})\otimes\mathbf{u}\right]\cdot\mathbf{v}\, d\Omega - 2\mu\int_{\Omega_t}\mathbf{D}_{\mathbf{x}}(\mathbf{u}) : \boldsymbol{\nabla}_{\mathbf{x}}\mathbf{v}\, d\Omega + \int_{\Omega_t}\mathrm{div}_{\mathbf{x}}\,\mathbf{v}\, p\, d\Omega \quad (4.3.7)$$

Then, the equation

$$\tilde{\rho}_w\frac{\partial^2\eta}{\partial t^2} - a\frac{\partial^2\eta}{\partial z^2} + b\eta - c\frac{\partial^3\eta}{\partial^2 z\partial t} = -p_{ext} + \tilde{\Phi}(\mathbf{u},p) \quad (4.3.8)$$

is satisfied in the sense of $V_0^S(\Gamma_0^w)'$. We are going now to show that right hand side in (4.3.8) is noting else that

$$-p_{ext} + \tilde{\Phi}(\mathbf{u},p) = -\left[(\mathbf{T}|_{\Gamma^w_t} + p_{ext}\mathbf{I})\cdot\mathbf{n}\cdot\mathbf{e}_r\right]\circ\boldsymbol{\varphi}_\eta\sqrt{1+\left(\frac{\partial\eta}{\partial z}\right)^2} \quad (4.3.9)$$

and this will conclude the proof. Indeed, by integrating by part the right hand side in (4.3.7) for $\mathbf{v} = \mathcal{R}(\xi)$ and exploiting (4.3.5) we obtain

$$< -p_{ext} + \tilde{\Phi}(\mathbf{u},p), \xi >=< \mathbf{f} - \rho\left.\frac{\partial\mathbf{u}}{\partial t}\right|_{\mathbf{Y}} - \rho(\mathbf{u}-\mathbf{w})\boldsymbol{\nabla}_{\mathbf{x}}\mathbf{u} + \mathrm{div}_{\mathbf{x}}(2\mu\mathbf{D}_{\mathbf{x}}(\mathbf{u}) - p\mathbf{I}), \mathcal{R}(\xi) >$$
$$- < p_{ext}, \xi > + \int_{\Gamma^w_t}(p\mathbf{n} - 2\mu\mathbf{D}_{\mathbf{x}}(\mathbf{u})\cdot\mathbf{n})\cdot\mathcal{R}(\xi)\, d\Gamma$$
$$= - < p_{ext}, \xi > + \int_{\Gamma^w_0}\left[(\mathbf{T}\cdot\mathbf{n})\circ\mathcal{A}_t\right]\cdot\left[\mathcal{R}(\xi)\circ\mathcal{A}_t\right]\sqrt{1+\left(\frac{\partial\eta}{\partial z}\right)^2}\, d\Gamma$$
$$= \int_{\Gamma^w_0}\left[(\mathbf{T} - p_{ext}\mathbf{I})\cdot\mathbf{n}\circ\boldsymbol{\varphi}_\eta\right]\cdot\xi\mathbf{e}_r\sqrt{1+\left(\frac{\partial\eta}{\partial z}\right)^2}\, d\Gamma$$

which gives exactly relation (4.3.9).

■

We may observe that the normal stress exerted by the fluid on the structure, in Problem 4.3.2, can be recovered in a weak form from the first equation of system (P-FS) as the residual of the fluid equation for any test function non vanishing on Γ^w_t. This is exactly what will be done at numerical level.

4.4 Two sub-problems decomposition

In practical applications it is useful to solve separately the fluid and the structure part. Typically, this is the case, when one disposes of two different codes solving the fluid and the structure equations, respectively, and the objective is to couple them effectively in order to carry out a fluid-structure simulation.

By a standard Domain Decomposition technique (see e.g. [76]) we will show in this section that both weak coupled Problems 4.3.1 and 4.3.2 can be split equivalently into two subproblems associated to the fluid and the structure part, respectively. Starting from this splitting, different iterative algorithms can be set up which allow to solve the two subproblems, separately. We first prove the following Lemma

Lemma 4.4.1 *The space* $\mathbf{V}(t)$ *can be written as* $\mathbf{V}(t) = \mathbf{V}_{int}(t) \oplus \mathbf{V}_{\Gamma_w}(t)$ *(direct sum), where*

$$\mathbf{V}_{int}(t) = \{(\mathbf{v}, \xi) \in \mathbf{V}(t) : \quad \xi = 0\} \tag{4.4.1}$$

$$\mathbf{V}_{\Gamma_w}(t) = \{(\mathbf{v}, \xi) \in \mathbf{V}(t) : \quad \mathbf{v} = \mathcal{R}(\xi)\}, \tag{4.4.2}$$

the operator $\mathcal{R} : V^S(\Gamma_0^w) \to \mathbf{V}^F(\Omega_t)$ *being defined as in (4.3.3).*

Proof The inclusion $\mathbf{V}_{int}(t) \oplus \mathbf{V}_{\Gamma_w}(t) \subset \mathbf{V}(t)$ is evident since both $\mathbf{V}_{int}(t) \subset \mathbf{V}(t)$ and $\mathbf{V}_{\Gamma_w}(t) \subset \mathbf{V}(t)$. Conversely, $\forall \mathbf{w} = (\mathbf{v}, \xi) \in \mathbf{V}(t)$, we can always define $\mathbf{w}_{\Gamma_w} = (\mathcal{R}(\xi), \xi) \in \mathbf{V}_{\Gamma_w}(t)$. It follows immediately that $\mathbf{w} - \mathbf{w}_{\Gamma_w} \in \mathbf{V}_{int}(t)$ and we conclude that $\mathbf{V}_{int}(t) \oplus \mathbf{V}_{\Gamma_w}(t) \equiv \mathbf{V}(t)$. Finally, $\mathbf{V}_{int}(t)$ and $\mathbf{V}_{\Gamma_w}(t)$ are clearly disjoint since, $(\mathbf{v}, \xi) \in \mathbf{V}_{int}(t) \cap \mathbf{V}_{\Gamma_w}(t) \Rightarrow \xi = 0$ and then $\mathcal{R}(\xi) = 0$. ■

Keeping in mind this Lemma, the weak Neumann Problem can be easily split into two subproblems by taking either test functions $\mathbf{w} \in \mathbf{V}_{int}(t)$ or $\mathbf{w} \in \mathbf{V}_{\Gamma_w}(t)$. We have then the following result :

Proposition 4.4.1 *Problem 4.3.1 can be equivalently reformulated as :*

fluid sub-problem *: find* $t \to \mathbf{u}(t) \in \mathbf{V}^F(\Omega_t)$, $t \to p(t) \in Q(\Omega_t)$ *such that*

$$\begin{cases} \rho \dfrac{d}{dt} \displaystyle\int_{\Omega_t} \mathbf{u} \cdot \mathbf{v} \, d\Omega + \rho \int_{\Omega_t} \mathrm{div}_{\mathbf{x}} \left[(\mathbf{u} - \mathbf{w}) \otimes \mathbf{u} \right] \cdot \mathbf{v} \, d\Omega + 2\mu \int_{\Omega_t} \mathbf{D}_{\mathbf{x}}(\mathbf{u}) : \nabla_{\mathbf{x}} \mathbf{v} \, d\Omega \\ \qquad - \displaystyle\int_{\Omega_t} \mathrm{div}_{\mathbf{x}} \, \mathbf{v} \, p \, d\Omega = \int_{\Omega_t} \mathbf{f} \cdot \mathbf{v} \, d\Omega + \sum_{i=1,2} \int_{S_i} \boldsymbol{\sigma_i} \cdot \mathbf{v} \, d\Gamma \qquad \forall (\mathbf{v}, 0) \in \mathbf{V}_{int}(t) \\ \displaystyle\int_{\Omega_t} \mathrm{div}_{\mathbf{x}} \, \mathbf{u} \, q \, d\Omega = 0 \qquad \forall q \in Q(\Omega_t) \end{cases} \tag{4.4.3}$$

$$\mathbf{u} \circ \mathcal{A}_t = \dot{\eta} \mathbf{e}_r, \qquad \text{on } \Gamma_0^w \tag{4.4.4}$$

and ALE mapping problem (P-ALE) as in Problem 4.3.1,

structure sub-problem *: find* $t \to \eta(t) \in V^S(\Gamma_0^w) \cap W^{1,\infty}(0, L)$ *such that*

$$\begin{aligned} &\int_{\Gamma_0^w} \tilde{\rho}_w \frac{\partial^2 \eta}{\partial t^2} \xi \, dz + \int_{\Gamma_0^w} b \eta \xi \, dz + \int_{\Gamma_0^w} \left(a \frac{\partial \eta}{\partial z} + c \frac{\partial^2 \eta}{\partial z \partial t} \right) \frac{\partial \xi}{\partial z} \, dz \\ &+ \sqrt{\frac{\tilde{\rho}_w}{a}} \left(a \frac{\partial \eta}{\partial t} + c \frac{\partial^2 \eta}{\partial t^2} \right) \xi \Big|_{z=0, z=L} = < -p_{ext} + \tilde{\Phi}(\mathbf{u}, p), \xi > \qquad \forall (\mathcal{R}(\xi), \xi) \in \mathbf{V}_{\Gamma_w}(t) \end{aligned} \tag{4.4.5}$$

where the operator $\tilde{\Phi}$ *is defined as in (4.3.6)-(4.3.7).*

Observe that, given a wall displacement $\eta(t)$ the fluid sub-problem is well defined and can thus be solved; symmetrically, the structure displacement can be computed, if the fluid solution $(\mathbf{u}, p)$ is available. This is the underlying idea of iterative algorithms.
When considering the weak Dirichlet Problem 4.3.2, it is a little more complex to devise a good splitting from which iterative algorithms can be derived. Indeed, in this case, as we have seen in Section 4.2 the displacement $\eta(t)$ must satisfy the supplementary constraint (4.2.6). Thus, when we split the coupled problem, we have to add this constraint to the structure equation, for instance by means of a Lagrange multiplier. On the other hand, when considering the fluid sub-problem on its own, since we are prescribing the velocity field on all the boundary, we obtain a pressure defined only up to a constant while in the coupled problem it is not so. As already pointed out in [43], this constant is related to the Lagrange multiplier introduced in the structure equation. We formalize this aspect in the next

Proposition 4.4.2 *Let us consider the following two sub-problem splitting for the weak-Dirichlet Problem 4.3.2*

fluid sub-problem *: find $t \to \mathbf{u}(t) \in \mathbf{V}^F(\Omega_t)$, with $\mathbf{u} = \mathbf{\Phi}_i$ on $\mathcal{S}_i$, $i = 1, 2$, and $t \to p(t) \in Q_0(\Omega_t)$, such that*

$$\begin{cases} \rho \dfrac{d}{dt} \displaystyle\int_{\Omega_t} \mathbf{u} \cdot \mathbf{v} \, d\Omega + \rho \int_{\Omega_t} \mathrm{div}_{\mathbf{x}} \left[(\mathbf{u} - \mathbf{w}) \otimes \mathbf{u} \right] \cdot \mathbf{v} \, d\Omega + 2\mu \int_{\Omega_t} \mathbf{D}_{\mathbf{x}}(\mathbf{u}) : \boldsymbol{\nabla}_{\mathbf{x}} \mathbf{v} \, d\Omega \\ \qquad - \displaystyle\int_{\Omega_t} \mathrm{div}_{\mathbf{x}} \mathbf{v} \, p \, d\Omega = \int_{\Omega_t} \mathbf{f} \cdot \mathbf{v} \, d\Omega \qquad \forall (\mathbf{v}, 0) \in \mathbf{V}_{int}(t) \cap \mathbf{V}_0(t) \\ \displaystyle\int_{\Omega_t} \mathrm{div}_{\mathbf{x}} \mathbf{u} \, q \, d\Omega = 0 \qquad \forall q \in Q_0(\Omega_t) \end{cases} \tag{4.4.6}$$

$$\mathbf{u} \circ \mathcal{A}_t = \dot{\eta} \mathbf{e}_r, \qquad \text{on } \Gamma_0^w \tag{4.4.7}$$

and ALE mapping problem (P-ALE) as in Problem 4.3.2,

structure sub-problem *: find $t \to \eta(t) \in V^S(\Gamma_0^w) \cap W^{1,\infty}(0, L)$, with $\eta = \alpha_1$ at $z = 0$ and $\eta = \alpha_2$ at $z = L$, and $t \to \lambda(t) \in \mathbb{R}$ such that*

$$\begin{cases} \displaystyle\int_{\Gamma_0^w} \tilde{\rho}_w \frac{\partial^2 \eta}{\partial t^2} \xi \, dz + \int_{\Gamma_0^w} b \eta \xi \, dz + \int_{\Gamma_0^w} \left(a \frac{\partial \eta}{\partial z} + c \frac{\partial^2 \eta}{\partial z \partial t} \right) \frac{\partial \xi}{\partial z} \, dz + \lambda \int_{\Gamma_0^w} \xi \, dz \\ \qquad = < -p_{ext} + \tilde{\Phi}(\mathbf{u}, p), \xi > \qquad \forall (\mathcal{R}(\xi), \xi) \in \mathbf{V}_{\Gamma_w}(t) \cap \mathbf{V}_0(t) \\ \displaystyle\int_{\Gamma_0^w} \eta \, dz = - \int_0^t \left(\int_{\mathcal{S}_1} \mathbf{\Phi}_1(s) \cdot \mathbf{n} \, d\Gamma + \int_{\mathcal{S}_2} \mathbf{\Phi}_2(s) \cdot \mathbf{n} \, d\Gamma \right) ds. \end{cases} \tag{4.4.8}$$

If $(\mathbf{u}, p)$, (η, λ) is a solution of the two sub-problems, then $(\mathbf{u}, p - \lambda, \eta)$ is a solution of the weak-Dirichlet Problem 4.3.2. Conversely, given a solution $(\mathbf{u}, p, \eta)$ of Problem 4.3.2, then $(\mathbf{u}, p - p_0)$ and $(\eta, -p_0)$, with $p_0 = \frac{1}{\mathrm{meas}\, \Omega_t} \int_{\Omega_t} p \, d\Omega$, are the solutions of the fluid and structure subproblems, respectively.

Proof. Let $(\mathbf{u}, p)$ and (η, λ) be the solutions of the fluid and structure sub-problem, respectively. Observe that we can write

$$\lambda \int_{\Gamma_0^w} \xi \, dz = \int_{\Omega_t} \mathrm{div}_{\mathbf{x}} \mathcal{R}(\xi) \, \lambda \, d\Omega, \qquad \forall \xi \in V_0^S(\Gamma_0^w)$$

so that the first equation of the structure sub-problem can be rewritten equivalently as

$$\int_{\Gamma_0^w} \tilde{\rho}_w \frac{\partial^2 \eta}{\partial t^2} \xi \, dz + \int_{\Gamma_0^w} b\eta\xi \, dz + \int_{\Gamma_0^w} \left(a\frac{\partial \eta}{\partial z} + c\frac{\partial^2 \eta}{\partial z \partial t} \right) \frac{\partial \xi}{\partial z} \, dz = < -p_{ext} + \tilde{\Phi}(\mathbf{u}, p - \lambda), \xi >$$
$$\forall (\mathcal{R}(\xi), \xi) \in \mathbf{V}_{\Gamma_w}(t) \cap \mathbf{V}_0(t).$$

Hence, the solution $(\mathbf{u}, p - \lambda, \eta)$ satisfies the first equation of (P-FS) in Problem 4.3.2 for all $(\mathbf{v}, \xi) \in \mathbf{V}_{\Gamma_w}(t) \cap \mathbf{V}_0(t)$. Moreover, since in the fluid sub-problem the pressure is defined up to a constant, $(\mathbf{u}, p - \lambda)$ is still a solution of the fluid sub-problem and $(\mathbf{u}, p - \lambda, \eta)$ satisfies the first equation of (P-FS) also for all $(\mathbf{v}, \xi) \in \mathbf{V}_{int}(t) \cap \mathbf{V}_0(t)$. Finally, we remind that the constraint in the structure sub-problem comes out from condition

$$\int_{\Omega_t} \mathrm{div}_{\mathbf{x}} \, \mathbf{u} = 0.$$

We have then

$$\int_{\Omega_t} \mathrm{div}_{\mathbf{x}} \, \mathbf{u} \, q = 0 \quad \forall q \in Q_0(\Omega_t) \text{ and } q = 1 \qquad \Longrightarrow \qquad \int_{\Omega_t} \mathrm{div}_{\mathbf{x}} \, \mathbf{u} \, q = 0 \quad \forall q \in Q(\Omega_t)$$

and this concludes the first part of the proof.
We consider, now, the inverse implication. If $(\mathbf{u}, p, \eta)$ is a solution of the weak-Dirichlet Problem 4.3.2, then by taking $(\mathbf{v}, \xi) \in \mathbf{V}_{int}(t) \cap \mathbf{V}_0(t)$, clearly $(\mathbf{u}, p)$ satisfies both equations in (4.4.6). Yet, p does not belongs, in general, to $Q_0(\Omega_t)$. Nevertheless, if we take $(\mathbf{u}, p - p_0)$, then, $p - p_0 \in Q_0(\Omega_t)$ and the fluid sub-problem is still satisfied since

$$\int_{\Omega_t} \mathrm{div}_{\mathbf{x}} \, \mathbf{v} p_0 \, d\Omega = \int_{\partial\Omega_t} p_0 \mathbf{v} \cdot \mathbf{n} \, d\Gamma = 0, \qquad \forall (\mathbf{v}, \xi) \in \mathbf{V}_{int}(t) \cap \mathbf{V}_0(t)$$

Moreover, it is clear from the previous considerations that the equation

$$\int_{\Gamma_0^w} \tilde{\rho}_w \frac{\partial^2 \eta}{\partial t^2} \xi \, dz + \int_{\Gamma_0^w} b\eta\xi \, dz + \int_{\Gamma_0^w} \left(a\frac{\partial \eta}{\partial z} + c\frac{\partial^2 \eta}{\partial z \partial t} \right) \frac{\partial \xi}{\partial z} \, dz - p_0 \int_{\Gamma_0^w} \xi \, dz$$
$$= < -p_{ext} + \tilde{\Phi}(\mathbf{u}, p - p_0), \xi >$$

is satisfied for all $(\mathcal{R}(\xi), \xi) \in \mathbf{V}_{\Gamma_w}(t) \cap \mathbf{V}_0(t)$ and that the displacement η satisfies the supplementary constraint (4.2.6), since it is a solution of the weak-Dirichlet Problem. We conclude that $(\eta, -p_0)$ is a solution of the structure sub-problem (4.4.8) and this concludes the proof. ■

Remark 4.4.1 *In Section 5.2.2 of Chapter 5, we will introduce other kinds of boundary conditions for the fluid problem, which we will call* defective *since they provide information only on averaged (and not pointwise) quantities on the boundary. Among the others, we will consider the following condition that prescribes the flux on a portion $\mathcal{S}$ of the boundary:*

$$\int_{\mathcal{S}} \mathbf{u} \cdot \mathbf{n} \, d\Gamma = Q.$$

Whenever a flux condition is imposed on both $\mathcal{S}_1$ and $\mathcal{S}_2$, let's say

$$\int_{\mathcal{S}_i} \mathbf{u} \cdot \mathbf{n} \, d\Gamma = Q_i, \qquad i = 1, 2,$$

the structure displacement η satisfies a supplementary constraint analogous to (4.2.6); precisely

$$\frac{d}{dt}\int_{\Gamma_0^w}\eta\, d\Gamma = -(Q_1+Q_2).$$

The technique presented in Proposition 4.4.2, to split the coupled problem into two subproblems, extends immediately to that case as well.

4.5 Conforming and non-conforming finite element discretisation

Let us introduce a triangulation $\mathcal{T}_{h,0}$ of the reference configuration Ω_0. This triangulation induces a partition $\mathcal{I}_h$ on Γ_0^w. Let $\mathcal{I}_H$ be an independent partition of Γ_0^w. In the case where $\mathcal{I}_h \equiv \mathcal{I}_H$, we will speak of *geometric conforming* meshes while the more general case will be addressed to as *geometric non-conforming* discretisation.
Let

$$V_H^S(\Gamma_0^w)\subset V^S(\Gamma_0^w),\qquad \hat{\mathbf{V}}_h^F(\Omega_0)\subset\hat{\mathbf{V}}^F(\Omega_0),\qquad \hat{Q}_h(\Omega_0)\subset\hat{Q}(\Omega_0)$$

be the finite element spaces approximating the corresponding continuous ones. The fluid finite element spaces may be chosen as in Chapter 3. The structural space, instead, may be taken as the space of $\mathbb{P}_r$ continuous finite elements.
In the general case of non-conforming meshes at the fluid-structure interface, we have to devise a strategy to impose the continuity of displacement and velocity on the moving boundary. As it will be shown in Sections 4.7÷4.10, it is important for stability purposes to preserve, at the same time, the two constraints

$$\mathbf{u}\big|_{\Gamma_t^w}\circ\boldsymbol{\varphi}_\eta = \dot{\eta}\mathbf{e}_r,\qquad \text{and}\qquad \mathbf{u}\big|_{\Gamma_t^w}=\mathbf{w}\big|_{\Gamma_t^w}$$

where $\mathbf{w}$ denotes, as usual, the mesh velocity, also at the discrete level. To this aim, we introduce an operator

$$\Pi_h^H:\ V_H^S(\Gamma_0^w)\to\hat{V}_h^F(\Gamma_0^w) \tag{4.5.1}$$

which associates to each $\xi_H\in V_H^S(\Gamma_0^w)$ a function $\Pi_h^H\xi_H:\ \Gamma_0^w\to\mathbb{R}$, approximating ξ_H, that is an admissible trace for the radial component of a function $\hat{\mathbf{v}}_h\in\hat{\mathbf{V}}_h^F(\Omega_0)$.
The best choice to preserve the accuracy of the fluid discretisation, consists in computing the discrete ALE mapping $\mathcal{A}_{h,t}$ with finite elements in $\hat{\mathbf{V}}_h^F(\Omega_0)$ and imposing the coupling conditions

$$\mathbf{u}_h\big|_{\Gamma_t^w}\circ\mathcal{A}_{h,t} = \Pi_h^H\dot{\eta}_H\mathbf{e}_r \tag{4.5.2}$$

$$\mathcal{A}_{h,t}\big|_{\Gamma_0^w} = \mathbf{Y}+\Pi_h^H\eta_H\mathbf{e}_r \tag{4.5.3}$$

In the particular case where the fluid finite element spaces are chosen either as $\mathbb{P}_1^b-\mathbb{P}_1$ or $\mathbb{P}_1 iso\mathbb{P}_2-\mathbb{P}_1$, the ALE mapping can be computed with $\mathbb{P}_1$ finite elements without loss of

accuracy, as pointed out in section 3.4. Consequently, the ALE finite element space coincides with $[\hat{Q}_h(\Omega_0)]^d$. The operator Π_h^H should then be defined as

$$\Pi_h^H : V_H^S(\Gamma_0^w) \to \hat{Q}_h(\Gamma_0^w)$$

and, since $\hat{Q}_h(\Gamma_0^w) \subset \hat{V}_h^F(\Gamma_0^w)$, the two relations (4.5.2) and (4.5.3) are still meaningful. Typical choices for the operator Π_h^H are

- **interpolation operator**

$$\Pi_h^H \xi_H(\mathbf{x}_i) = \xi_H(\mathbf{x}_i) \qquad \text{for all the nodes } \mathbf{x}_i \text{ of } \mathcal{I}_h. \tag{4.5.4}$$

- L^2 **projection operator** (*mortar method*)

$$\begin{cases} \displaystyle\int_{\Gamma_0^w} \left(\Pi_h^H \xi_H - \xi_H\right) \psi_h \, d\Gamma = 0, \quad \forall \psi_h \in \widetilde{\hat{V}_h^F(\Gamma_0^w)}, \qquad \text{and} \\ \Pi_h^H \xi_H(0) = \xi_H(0), \quad \Pi_h^H \xi_H(L) = \xi_H(L), \end{cases} \tag{4.5.5}$$

  where $\widetilde{\hat{V}_h^F(\Gamma_0^w)}$ is a sub-space of codimension 2 of $\hat{V}_h^F(\Gamma_0^w)$. For more details on the mortar method see e.g. [6, 4, 1, 5].

In [43] it has been shown, on a very simple coupled problem, that the mortar method is optimal[3] for any degree of the polynomials used for the discretisation of the fluid equations. On the contrary, for a coupled problem with a second order differential structural equation (as it is in our case, indeed), the interpolation operator is optimal only when piecewise linear finite elements are employed for the fluid.

Once introduced the operator Π_h^H and the ALE mapping discretisation, the finite element spaces for the fluid equations will read, as usual

$$\begin{aligned} \mathbf{V}_h^F(\Omega_t) &= \{\mathbf{v}_h : \Omega_t \times I \to \mathbb{R}^d, \quad \mathbf{v}_h = \hat{\mathbf{v}}_h \circ \mathcal{A}_{h,t}^{-1}, \ \hat{\mathbf{v}}_h \in \hat{\mathbf{V}}_h^F(\Omega_0)\}, \\ Q_h(\Omega_t) &= \{q_h : \Omega_t \times I \to \mathbb{R}, \quad q_h = \hat{q}_h \circ \mathcal{A}_{h,t}^{-1}, \ \hat{q}_h \in \hat{Q}_h(\Omega_0)\} \end{aligned}$$

and the space for the fluid-structure coupled problem is

$$\mathbf{V}_{h,H}(t) = \{(\mathbf{v}_h, \xi_H) \in \mathbf{V}_h^F(\Omega_t) \times V_H^S(\Gamma_0^w), \ \text{s.t.} \ \mathbf{v}_h \circ \mathcal{A}_{h,t}\big|_{\Gamma_0^w} = \Pi_h^H \xi_H \mathbf{e}_r\}. \tag{4.5.6}$$

Observe that this space is not contained in $\mathbf{V}(t)$ because of the non-conformity of the meshes. We are now in the position to introduce the semi-discrete coupled problem. We will detail only the discretisation of the Neumann weak Problem 4.3.1, the extension to the Dirichlet one being straightforward.

[3] in the sense that it does not degenerate the rate of convergence featured by the fluid and the structure discretisation when taken separately.

Problem 4.5.1 (semi-discrete Neumann) *for almost every* $t \in I$, *find* $t \to \mathbf{u}_h(t) \in \mathbf{V}_h^F(\Omega_t)$, $t \to p_h(t) \in Q_h(\Omega_t)$ *and* $t \to \eta_H(t) \in V_H^S(\Gamma_0^w)$ *such that*

$$
\begin{cases}
\displaystyle\int_{\Gamma_0^w} \tilde{\rho}_w \frac{\partial^2 \eta_H}{\partial t^2} \xi_H \, dz + \int_{\Gamma_0^w} b\eta_H \xi_H \, dz + \int_{\Gamma_0^w} \left(a \frac{\partial \eta_H}{\partial z} + c \frac{\partial^2 \eta_H}{\partial z \partial t} \right) \frac{\partial \xi_H}{\partial z} \, dz \\
\displaystyle + \sqrt{\frac{\tilde{\rho}_w}{a}} \left(a \frac{\partial \eta_H}{\partial t} + c \frac{\partial^2 \eta_H}{\partial t^2} \right) \xi_H \Big|_{z=0,L} + \rho \frac{d}{dt} \int_{\Omega_t} \mathbf{u}_h \cdot \mathbf{v}_h \, d\Omega + \rho \int_{\Omega_t} \mathrm{div}_{\mathbf{x}} \left[(\mathbf{u}_h - \mathbf{w}_h) \otimes \mathbf{u}_h \right] \cdot \mathbf{v}_h \, d\Omega \\
\displaystyle \quad - \frac{\rho}{2} \int_{\Omega_t} \mathrm{div}_{\mathbf{x}} \mathbf{u}_h \, \mathbf{u}_h \cdot \mathbf{v}_h \, d\Omega + 2\mu \int_{\Omega_t} \mathbf{D}_{\mathbf{x}}(\mathbf{u}_h) : \nabla_{\mathbf{x}} \mathbf{v}_h \, d\Omega - \int_{\Omega_t} \mathrm{div}_{\mathbf{x}} \mathbf{v}_h \, p_h \, d\Omega \\
\displaystyle \quad = \int_{\Omega_t} \mathbf{f} \cdot \mathbf{v}_h \, d\Omega + \sum_{i=1,2} \int_{S_i} \boldsymbol{\sigma}_i \cdot \mathbf{v}_h \, d\Gamma - \int_{\Gamma_0^w} p_{ext} \xi_H \, dz \qquad \forall (\mathbf{v}_h, \xi_H) \in \mathbf{V}_{h,H}(t) \\
\displaystyle \int_{\Omega_t} \mathrm{div}_{\mathbf{x}} \mathbf{u}_h \, q_h \, d\Omega = 0 \qquad \forall q_h \in Q_h(\Omega_t)
\end{cases}
\tag{Ph-FS}
$$

$$
\mathbf{u}_h \circ \mathcal{A}_{h,t} = \Pi_h^H \dot{\eta}_H \mathbf{e}_r, \qquad \text{on } \Gamma_0^w, \tag{ICCh}
$$

$$
\begin{cases}
\mathcal{P}_{\mathcal{A}} \left(\mathcal{A}_{h,t}, \mathbf{z}_h \right) = 0 \qquad \forall \mathbf{z}_h \in \hat{\mathbf{V}}_h^F(\Omega_0), \ \mathbf{z}_h = \mathbf{0} \quad \text{on } \partial\Omega_0, \ \forall t > 0 \\
\mathcal{A}_{h,t} = \mathbf{Y} + \Pi_h^H \eta_H \mathbf{e}_r \quad \Gamma_0^w, \qquad \mathcal{A}_{h,t} = \mathbf{g}_\eta \quad \text{on } \partial\Omega_0 \setminus \Gamma_0^w, \ \forall t > 0.
\end{cases}
\tag{Ph-ALE}
$$

where $\mathbf{u}_h(t)$ *and* $\eta_H(t)$ *satisfy suitable finite element approximations of the initial conditions (4.2.3).*

In system (Ph-FS) we have added the consistent stabilizing term $-\frac{\rho}{2} \int_{\Omega_t} \mathrm{div}_{\mathbf{x}} \mathbf{u}_h \, \mathbf{u}_h \cdot \mathbf{v}_h \, d\Omega$ as in formulation (3.4.8) proposed in Chapter 3.
The two sub-problem splitting of Problem 4.5.1 is straightforward once we introduce the following decomposition of $\mathbf{V}_{h,H}(t)$:

$$
\mathbf{V}_{h,H}(t) = \mathbf{V}_{h,H}^{int}(t) \oplus \mathbf{V}_{h,H}^{\Gamma_w}(t), \qquad
\begin{cases}
\mathbf{V}_{h,H}^{int}(t) = \{ (\mathbf{v}_h, \xi_H) \in \mathbf{V}_{h,H}(t), \ \xi_H = 0 \} \\
\mathbf{V}_{h,H}^{\Gamma_w}(t) = \{ (\mathbf{v}_h, \xi_H) \in \mathbf{V}_{h,H}(t), \ \mathbf{v}_h = \mathcal{R}_h(\xi_H) \}
\end{cases}
$$

and the discrete extension $\mathcal{R}_h$ is defined as

$$
\mathcal{R}_h : \ V_H^S(\Gamma_0^w) \to \mathbf{V}_h^F(\Omega_t), \qquad \mathcal{R}_h(\xi_H) \Big|_{\Gamma_t^w} \circ \mathcal{A}_{h,t} = \Pi_h^H \xi_H \mathbf{e}_r. \tag{4.5.7}
$$

The most natural extension consists in taking the finite element function $\mathbf{v}_h = \mathcal{R}_h(\xi_H)$ which is zero on all the interior nodes of Ω_t and satisfies condition (4.5.7) on Γ_t^w.

4.5.1 Algebraic formulation of the semi-discrete problem

We adopt here the same notations as in Chapter 3. For the fluid equations we introduce the Lagrange basis $\{\psi_i\}_{i=1}^{\mathcal{N}_p}$ and $\{\varphi_j\}_{j=1}^{\mathcal{N}_v} \oplus \{\varphi_k^b\}_{k=1}^{\mathcal{N}_v^b}$ associated, respectively, to $Q_h(\Omega_t)$ and

$\mathbf{V}_h^F(\Omega_t)$. In particular $\{\boldsymbol{\varphi}_k^b\}$ is the set of basis functions of $\mathbf{V}_h^F(\Omega_t)$ corresponding to the nodes on Γ_t^w. We set

$$\mathbf{u}_h(\mathbf{x},t) = \sum_{j=1}^{\mathcal{N}_v} U_j(t)\boldsymbol{\varphi}_j(\mathbf{x},t) + \sum_{k=1}^{\mathcal{N}_v^b} U_k^b(t)\boldsymbol{\varphi}_k^b(\mathbf{x},t), \qquad p_h(\mathbf{x},t) = \sum_{i=1}^{\mathcal{N}_p} P_i(t)\psi_i(\mathbf{x},t).$$

The nodal values U_k^b depend, clearly, on the structure velocity $\dot{\eta}_H$. The matrices $M(t)$, $B(t;\mathbf{w}_h;\mathbf{u}_h)$, $K(t)$, $D(t)$ and $C(t;\mathbf{w}_h)$ are defined as in Section 3.4 while the vector $\mathbf{F}$ is now given by

$$\mathbf{F}_i(t) = \int_{\Omega_t} \mathbf{f}\cdot\boldsymbol{\varphi}_i\, d\Omega + \sum_{i=1,2}\int_{\mathcal{S}_i} \boldsymbol{\sigma_i}\cdot\boldsymbol{\varphi}_i\, d\Gamma.$$

Concerning the structure equation, let $\{\chi_l\}_{l=1}^{\mathcal{N}_\eta}$ be the set of Lagrange basis functions associated to $V_H^S(\Gamma_0^w)$; we set

$$\eta_H = \sum_{l=1}^{\mathcal{N}_\eta} \Upsilon_l\chi_l,$$

and we indicate with $\boldsymbol{\Upsilon}$ the vector of nodal values; moreover, we define the matrices

$$\tilde{M}_{ij} = \int_{\Gamma_0^w} \chi_j\chi_i\, d\Gamma, \quad 1\le i,j\le\mathcal{N}_\eta \qquad \tilde{K}_{ij} = \int_{\Gamma_0^w} \frac{\partial\chi_j}{\partial z}\frac{\partial\chi_i}{\partial z}\, d\Gamma, \quad 1\le i,j\le\mathcal{N}_\eta$$
$$\tilde{B}c_{ij} = \chi_j\chi_i\Big|_{z=0,z=L}, \quad 1\le i,j\le\mathcal{N}_\eta$$

and the vector $\mathbf{P}_{ext} = \left[-\int_{\Gamma_0^w} p_{ext}\chi_i\, d\Gamma\right]_{i=1,\dots\mathcal{N}_\eta}$.
The coupling condition (4.5.2) can be written in algebraic form in the following way : the trace $\mathbf{u}_h|_{\Gamma_t^w}$ depends only on the boundary values and can thus be expressed only as a function of the basis $\{\boldsymbol{\varphi}_k^b\}$

$$\mathbf{u}_h\big|_{\Gamma_t^w} = \sum_{k=1}^{\mathcal{N}_v^b} U_k^b\boldsymbol{\varphi}_k^b\big|_{\Gamma_t^w}.$$

Similarly, for each structure base function χ_l, the function $\Pi_h^H\chi_l\,\mathbf{e}_r$ belongs to $\hat{\mathbf{V}}_h^F(\Gamma_0^w)$ and can thus be developed on the same basis $\{\hat{\boldsymbol{\varphi}}_k^b\}$ expressed on the reference configuration. We have then

$$\Pi_h^H\chi_l\,\mathbf{e}_r = \sum_{k=1}^{\mathcal{N}_v^b} \Xi_{kl}\,\hat{\boldsymbol{\varphi}}_k^b\big|_{\Gamma_0^w}. \tag{4.5.8}$$

Thus, the matching condition (4.5.2) becomes

$$\mathbf{u}_h\big|_{\Gamma_t^w}\circ\mathcal{A}_{h,t} = \sum_{k=1}^{\mathcal{N}_v^b} U_k^b\hat{\boldsymbol{\varphi}}_k^b\big|_{\Gamma_0^w} = \Pi_h^H\sum_{l=1}^{\mathcal{N}_\eta}\Upsilon_l\chi_l\,\mathbf{e}_r = \sum_{l=1}^{\mathcal{N}_\eta}\Upsilon_l\left(\Pi_h^H\chi_l\,\mathbf{e}_r\right) = \sum_{k=1}^{\mathcal{N}_v^b}\left(\sum_{l=1}^{\mathcal{N}_\eta}\Upsilon_l\Xi_{kl}\right)\hat{\boldsymbol{\varphi}}_k^b\big|_{\Gamma_0^w}$$

which can be written in algebraic form as

$$\mathbf{U}^b = Q\boldsymbol{\Upsilon}, \qquad \text{where } Q = [\Xi_{kl}]. \tag{4.5.9}$$

Observe that the matrix Q does not depend on time since the matching condition is always imposed on the fixed configuration Γ_0^w. A similar derivation holds for the imposition at the algebraic level of the coupling condition (4.5.3).
The **fluid sub-problem** is then given by

$$\begin{cases} \mathbf{U}^b = Q\boldsymbol{\Upsilon} \\ \rho\dfrac{d}{dt}\left(M(t)\mathbf{U}\right) + \rho B(t;\mathbf{w}_h;\mathbf{u}_h)\mathbf{U} - \rho C(t;\mathbf{w}_h)\mathbf{U} + 2\mu K(t)\mathbf{U} + D^T(t)\mathbf{P} = \mathbf{F}(t) + \mathbf{b}_1(t), \\ D(t)\mathbf{U} = \mathbf{b}_2(t) \end{cases} \tag{4.5.10}$$

together with the computation of the ALE mapping. The vectors $\mathbf{b}_1$ and $\mathbf{b}_2$ depend on $\mathbf{U}^b$ and ultimately on $\boldsymbol{\Upsilon}$.
Let's now come to the structure sub-problem. Its algebraic counterpart reads

$$\left(\tilde{\rho}_w\tilde{M} + c\sqrt{\frac{\tilde{\rho}_w}{a}}\widetilde{Bc}\right)\ddot{\boldsymbol{\Upsilon}} + \left(c\tilde{K} + \sqrt{a\tilde{\rho}_w}\widetilde{Bc}\right)\dot{\boldsymbol{\Upsilon}} + \left(b\tilde{M} + a\tilde{K}\right)\boldsymbol{\Upsilon} = \mathbf{P}_{ext} + \tilde{\boldsymbol{\Phi}}. \tag{4.5.11}$$

The vector $\tilde{\boldsymbol{\Phi}}$ is given by

$$\tilde{\Phi}_i = < \tilde{\Phi}_{\Pi}(\mathbf{u}_h, p_h), \chi_i > = < \Phi(\mathbf{u}_h, p_h), \mathcal{R}_h(\chi_i) >, \qquad 1 \le i \le \mathcal{N}_\eta \tag{4.5.12}$$

where $< \Phi(\mathbf{u}_h, p_h), \mathbf{v}_h >$ is defined as in (4.3.7).
Whenever we consider a discrete extension $\mathcal{R}_h(\xi_{\Pi})$, $\forall \xi_{\Pi} \in V_{\Pi}^S(\Gamma_0^w)$, which vanishes on all the internal fluid nodes, we can write the extension of a basis function χ_l as

$$\mathcal{R}_h(\chi_l) = \sum_{k=1}^{\mathcal{N}_v^b} \Xi_{kl}\,\varphi_k^b.$$

where the Ξ_{kl} are the same of (4.5.8). Thus, we have

$$< \Phi(\mathbf{u}_h, p_h), \mathcal{R}_h(\chi_i) > = < \Phi(\mathbf{u}_h, p_h), \sum_{k=1}^{\mathcal{N}_v^b} \Xi_{kl}\,\varphi_k^b > = \sum_{k=1}^{\mathcal{N}_v^b} \Xi_{kl} < \Phi(\mathbf{u}_h, p_h), \varphi_k^b >$$

and relation (4.5.12) can be written in algebraic form as

$$\tilde{\boldsymbol{\Phi}} = Q^T\boldsymbol{\Phi}, \qquad \text{where } \Phi_k = < \Phi(\mathbf{u}_h, p_h), \varphi_k^b >, \quad k = 1, \ldots \mathcal{N}_v^b$$

In other words, once the fluid solution is computed, we have to evaluate the residual of the fluid equations tested on all functions φ_k^b. Then, by multiplying the vector $\boldsymbol{\Phi}$ by Q^T we obtain the right hand side for the structure equation.
This approach to exchange information between the fluid and the structure solver has already been proposed in [25], with Π_h^H taken as the interpolation operator. It was shown that the

coupled scheme thus obtained conserves the energy at discrete level. The scheme has been applied to several large scale numerical simulations (see e.g. [23] and other related works).
In the last part of this section, we detail the discretisation we have adopted in our numerical simulations. We have taken a conforming discretisation between fluid and structure. We have used $\mathbb{P}_1 iso \mathbb{P}_2 - \mathbb{P}_1$ finite elements for the fluid sub-problem and $\mathbb{P}_1$ finite elements to compute the ALE mapping. In this way, the fluid mesh $\mathcal{T}_{h,t}$ at each time $t > 0$ is made up of triangles with straight edges. The structure equation has been discretised with $\mathbb{P}_1$ finite elements as well. In such a case, we have $V_H^S(\Gamma_0^w) \subseteq \hat{Q}_h(\Gamma_0^w) \subset \hat{V}_h^F(\Gamma_0^w)$ and the discretisation is completely conforming in both the geometry and the polynomial degree. A possible evolution of the interface configuration and of the adjacent fluid elements is shown in figure 4.4.

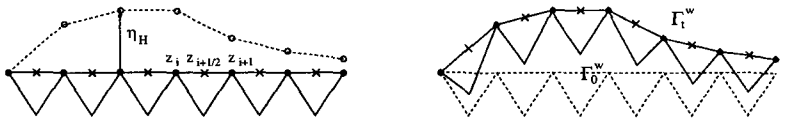

Figure 4.4: On the left: $\mathbb{P}_1$ displacement of the structure; on the right: new domain configuration computed with $\mathbb{P}_1$ finite elements. The bullets • denote the $\mathbb{P}_1$ nodes while the crosses $\times$ denote the $\mathbb{P}_2$ nodes on Γ_t^w.

The operator Π_h^H has thus been taken as the identity operator, i.e. the coupling conditions (4.5.2) and (4.5.3) simply read

$$\mathbf{u}_h|_{\Gamma_t^w} \circ \mathcal{A}_{h,t} = \dot{\eta}_H \mathbf{e}_r \qquad\qquad \mathcal{A}_{h,t}|_{\Gamma_0^w} = \mathbf{Y} + \eta_H \mathbf{e}_r.$$

If we number the nodes on the interface as shown in fig. 4.4 (on the left), then the first coupling condition is equivalent to

$$\left(\mathbf{u}_h|_{\Gamma_t^w} \circ \mathcal{A}_{h,t}\right)(z_i) = \dot{\eta}_H(z_i)\mathbf{e}_r, \qquad \text{for each } \mathbb{P}_1 \text{ node } z_i$$

$$\left(\mathbf{u}_h|_{\Gamma_t^w} \circ \mathcal{A}_{h,t}\right)(z_{i+1/2}) = \frac{\dot{\eta}_H(z_i) + \dot{\eta}_H(z_{i+1})}{2}\mathbf{e}_r \qquad \text{for each } \mathbb{P}_2 \text{ node } z_{i+1/2}$$

Conversely, let $\hat{\varphi}_i^b = [0, \hat{\varphi}_i^b]$ be a fluid Lagrange radial basis function associated to the node z_i. Observe that a structure Lagrange basis function χ_i can be written as (see figure 4.5)

$$\chi_i = \left(\frac{1}{2}\hat{\varphi}_{i-1/2}^b + \hat{\varphi}_i^b + \frac{1}{2}\hat{\varphi}_{i+1/2}^b\right)\Big|_{\Gamma_0^w} \mathbf{e}_r.$$

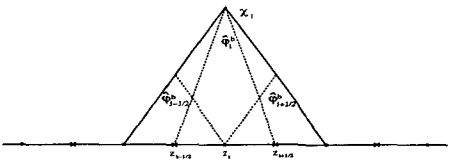

Figure 4.5: Lagrangian basis function χ_i written as a linear combination of fluid Lagrangian radial basis functions $\hat{\varphi}_j^b$.

It follows that, once computed the vector Φ of the stresses exerted by the fluid on the structure, the right hand side of the structure equation is obtained simply as

$$\tilde{\Phi}_i = \left(\frac{1}{2} < \Phi(\mathbf{u}_h, p_h), \boldsymbol{\varphi}^b_{i-1/2} > + < \Phi(\mathbf{u}_h, p_h), \boldsymbol{\varphi}^b_i > + \frac{1}{2} < \Phi(\mathbf{u}_h, p_h), \boldsymbol{\varphi}^b_{i+1/2} > \right).$$

4.6 Temporal discretisation and coupled algorithms

Many different strategies can be devised to discretise in time the coupled fluid structure problem. A wide class of algorithms can be derived by taking an explicit temporal scheme for the fluid (resp. the structure) and an implicit one for the structure (resp. the fluid). In this way, at each time step, the solution of the fluid can be computed directly starting from the solution at the previous time step and, once the fluid pressure and velocity have been computed, the structure can be advanced in time providing the new position of the interface. This simple iterative algorithm is often referred to as *conventional serial staggered (CSS) procedure* (see e.g. [26, 24]). Many improvements have been proposed to the CSS procedure such as sub-cycling the explicit solver in each time interval and/or introducing a structure predictor. In the presence of sub-cycling, different strategies to exchange data between fluid and structure solvers have been considered as well [26, 71]. These ideas have been furtherly generalized to implicit/implicit coupled schemes. This family of algorithms, known also as *staggered* or *partitioned procedures* or *loosely coupled algorithms*, have been adopted for instance in [24, 23] and their stability properties have been investigated in [72, 73]. A scheme of a possible staggered algorithm is presented in fig. 4.6.

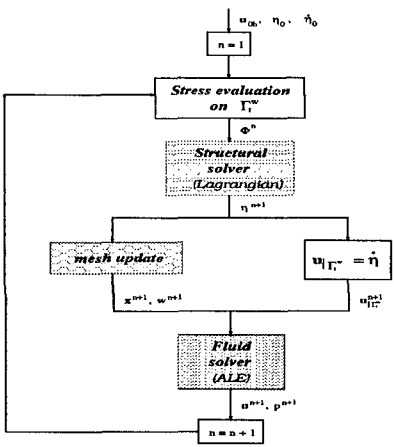

Figure 4.6: Example of staggered algorithm : at each time step we solve first the structure equation, with forcing term given by the fluid solution at the previous time step, then the fluid equation on the updated geometry and with a boundary velocity given by the recently computed structure solution.

However, we have verified numerically that these loosely coupled algorithms are unstable when the structure is light, in particular when its density is comparable to that of the fluid, as it happens in our application.
In the following part of this chapter we will focus on fully coupled implicit algorithms. In particular, we will propose three coupling strategies which are unconditionally stable. Clearly, at each time step, we have to solve a highly non-linear coupled system, since the fluid domain is unknown and depends on the structure solution. The most simple strategy to solve such a non-linear system consists in sub-iterating between fluid and structure, adding eventually a relaxation step on the structure displacement. We will refer to this iterative solver as a *block Gauss-Seidel method.* A representation of this algorithm is given in fig. 4.7.

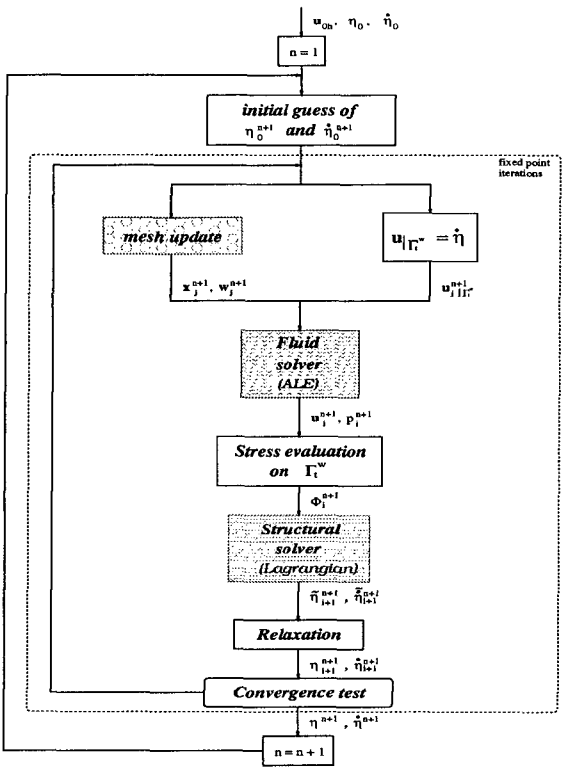

Figure 4.7: Example of fully implicit coupled algorithm : at each time step we need to subiterate between fluid and structure until the coupling conditions are satisfied within a fixed tolerance. A relaxation step may be added on the structure displacement

As it will be shown in section 4.11, in those cases where the loosely coupled procedure is

unstable, the block Gauss-Seidel method needs, in general, a small relaxation parameter and features a slow convergence rate. The problem of how to accelerate subiteration convergence is the subject of current research and will not be investigated in the present work. In our numerical simulations we have limited ourselves to apply the simple block Gauss-Seidel method.

In order to lighten the presentation of the coupled algorithms we introduce some additional notations. For the semi-discrete structure sub-problem we introduce the forms

$$\mathcal{E}(\varphi,\psi)_{\Gamma_0^w} = b\int_{\Gamma_0^w}\varphi\,\psi\,dz + a\int_{\Gamma_0^w}\frac{\partial\varphi}{\partial z}\frac{\partial\psi}{\partial z}\,dz, \qquad \forall\varphi,\psi\in V^S(\Gamma_0^w) \tag{4.6.1}$$

$$\mathcal{V}(\varphi,\psi)_{\Gamma_0^w} = c\int_{\Gamma_0^w}\frac{\partial\varphi}{\partial z}\frac{\partial\psi}{\partial z}\,dz, \qquad \forall\varphi,\psi\in V^S(\Gamma_0^w). \tag{4.6.2}$$

The first form groups the elastic terms of the structure equation, is bilinear and coercive and can be taken as a scalar product on $V^S(\Gamma_0^w)$ with associated norm

$$\|\varphi\|_{\mathcal{E}} = \left(b\,\|\varphi\|^2_{L^2(\Gamma_0^w)} + a\left\|\frac{\partial\varphi}{\partial z}\right\|^2_{L^2(\Gamma_0^w)}\right)^{\frac{1}{2}}.$$

Similarly, the second form represents the viscoelastic structural term and is bilinear and monotone, i.e.

$$\mathcal{V}(\varphi,\varphi)_{\Gamma_0^w} = c\left\|\frac{\partial\varphi}{\partial z}\right\|^2_{L^2(\Gamma_0^w)} \geq 0, \qquad \forall\varphi\in V^S(\Gamma_0^w).$$

Finally, we will denote by $(\cdot,\cdot)_{\Gamma_0^w}$ the L^2 scalar product on Γ_0^w.
For the fluid equation we introduce the linear and continuous forms

$$\mathcal{D}(\mathbf{v},q)_{\Omega_t} = -\int_{\Omega_t}\mathrm{div}_{\mathbf{x}}\,\mathbf{v}\,q\,d\Omega, \qquad \forall\mathbf{v}\in\mathbf{V}^F(\Omega_t),\ q\in Q(\Omega_t) \tag{4.6.3}$$

$$\begin{aligned}\mathcal{B}(\mathbf{w},\mathbf{u}^*,\mathbf{u},\mathbf{v})_{\Omega_t} &= \rho\int_{\Omega_t}\mathrm{div}_{\mathbf{x}}\left[(\mathbf{u}^*-\mathbf{w})\otimes\mathbf{u}\right]\cdot\mathbf{v}\,d\Omega\\ &\quad-\frac{\rho}{2}\int_{\Omega_t}\mathrm{div}_{\mathbf{x}}\,\mathbf{u}^*\,\mathbf{u}\cdot\mathbf{v}\,d\Omega + 2\mu\int_{\Omega_t}\mathbf{D}_{\mathbf{x}}(\mathbf{u}):\nabla_{\mathbf{x}}\mathbf{v}\,d\Omega \qquad \forall\mathbf{w},\mathbf{u}^*,\mathbf{u},\mathbf{v}\in\mathbf{V}^F(\Omega_t).\end{aligned} \tag{4.6.4}$$

Observe that, given a function $\mathbf{u}^*$ such that $\mathbf{u}^*=\mathbf{w}$ on Γ_t^w, we have for any $\mathbf{u}\in\mathbf{V}^F_{\mathcal{S}_{1,2}}(\Omega_t)$

$$\mathcal{B}(\mathbf{w},\mathbf{u}^*,\mathbf{u},\mathbf{u})_{\Omega_t} = \kappa\,\|\nabla_{\mathbf{x}}\mathbf{u}\|^2_{L_2(\Omega_t)} - \frac{\rho}{2}\int_{\Omega_t}\mathrm{div}_{\mathbf{x}}\,\mathbf{w}|\mathbf{u}|^2\,d\Omega. \tag{4.6.5}$$

This relation will be useful for the stability analysis carried out in the next sections on the coupled algorithms.
Thus, system (Ph-FS) in the semi-discrete Neumann Problem 4.5.1 can be rewritten in a

more compact form as

$$\begin{cases} \tilde{\rho}_w(\dfrac{\partial^2\eta_H}{\partial t^2},\xi_H)_{\Gamma_0^w} + \mathcal{E}(\eta_H,\xi_H)_{\Gamma_0^w} + \mathcal{V}(\dfrac{\partial\eta_H}{\partial t},\xi_H)_{\Gamma_0^w} + \sqrt{\dfrac{\tilde{\rho}_w}{a}}\left(a\dfrac{\partial\eta_H}{\partial t} + c\dfrac{\partial^2\eta_H}{\partial t^2}\right)\xi_H\Big|_{z=0,L} \\ \quad +\rho\dfrac{d}{dt}\displaystyle\int_{\Omega_t}\mathbf{u}_h\cdot\mathbf{v}_h\,d\Omega + \mathcal{B}(\mathbf{w}_h,\mathbf{u}_h,\mathbf{u}_h,\mathbf{v}_h)_{\Omega_t} + \mathcal{D}(\mathbf{v}_h,p_h)_{\Omega_t} \\ \quad = \displaystyle\int_{\Omega_t}\mathbf{f}\cdot\mathbf{v}_h\,d\Omega + \sum_{i=1,2}\int_{\mathcal{S}_i}\boldsymbol{\sigma_i}\cdot\mathbf{v}_h\,d\Gamma - \int_{\Gamma_0^w}p_{ext}\xi_H\,dz \qquad \forall(\mathbf{v}_h,\xi_H)\in\mathbf{V}_{h,H}(t) \\ \mathcal{D}(\mathbf{u}_h,q_h)_{\Omega_t} = 0 \qquad \forall q_h\in Q_h(\Omega_t) \end{cases} \tag{4.6.6}$$

In the following Sections, we will present the coupled algorithms for the Dirichlet Problem 4.2.2 since this allows us to obtain unconditional stability results. Indeed, as we have seen in Chapter 3 and in Section 4.1.1, we are not able to get an a-priori energy estimate when Neumann conditions are imposed in some parts of the boundary. As we have already observed, this is not due to the fluid-structure interaction mechanism but is related uniquely to the convective term in the Navier-Stokes equations. On the contrary, the Dirichlet Problem allows to obtain unconditionally stable discretisations of the fluid and structure sub-problems when taken separately and is well suited to focus on the stability properties of the coupled algorithms.

4.7 A first order implicit coupled algorithm

We discretise the structure by a first order backward finite difference scheme and the fluid by the Implicit Euler scheme which satisfies the GCL. Furthermore, the ALE mapping will be computed at each t_n by solving a suitable mesh problem $\mathcal{P}_{\mathcal{A}}(\mathcal{A}_{h,t},\mathbf{z}_h)=0$ and will be linearly interpolated in time in each time slab $[t_n,t_{n+1}]$. Thus, in order to satisfy the GCL, we integrate the fluid terms on the middle configuration. Let us denote by $\mathbf{u}_h^n$, p_h^n and η_H^n the approximations of $\mathbf{u}_h(t^n)$, $p_h(t^n)$ and $\eta_H(t^n)$, respectively. The interface coupling condition between fluid and structure velocities will be discretised as follows

$$\mathbf{u}_h^{n+1}\circ\mathcal{A}_{h,t_{n+1}}\big|_{\Gamma_0^w} = \Pi_h^H\frac{\eta_H^{n+1}-\eta_H^n}{\Delta t}\mathbf{e}_r.$$

The coupled problem reads then

Problem 4.7.1 (BDF1/Implicit Euler) *Given the initial solution* $\mathbf{u}_{h0}$, η_{H0} *and* $\dot{\eta}_{H0}$, *set*

$$\eta_H^{-1} = \eta_H^1 - 2\Delta t\dot{\eta}_{H0},$$

and find $\mathbf{u}_h^{n+1}\in\mathbf{V}_h^F(\Omega_t)$, $p_h^{n+1}\in Q_h(\Omega_t)$ *and* $\eta_H^{n+1}\in V_H^S(\Gamma_0^w)$ *with*

$$\begin{aligned} &\mathbf{u}_h^{n+1} = \boldsymbol{\Phi}_i^{n+1} \quad \text{on } \mathcal{S}_i,\ i=1,2, \qquad \text{and} \\ &\eta_H^{n+1} = \alpha_1^{n+1} \quad \text{at } z=0, \qquad \eta_H^{n+1} = \alpha_2^{n+1} \quad \text{at } z=L, \end{aligned}$$

such that

$$\begin{cases} \tilde{\rho}_w(\dfrac{\eta_H^{n+1}-2\eta_H^n+\eta_H^{n-1}}{\Delta t^2},\xi_H)_{\Gamma_0^w}+\mathcal{E}(\eta_H^{n+1},\xi_H)_{\Gamma_0^w}+\mathcal{V}(\dfrac{\eta_H^{n+1}-\eta_H^n}{\Delta t},\xi_H)_{\Gamma_0^w} \\ \quad +\dfrac{\rho}{\Delta t}\displaystyle\int_{\Omega_{t_{n+1}}}\mathbf{u}_h^{n+1}\cdot\mathbf{v}_h\,d\Omega-\dfrac{\rho}{\Delta t}\int_{\Omega_{t_n}}\mathbf{u}_h^n\cdot\mathbf{v}_h\,d\Omega+\mathcal{B}(\mathbf{w}_h^{n+1/2},\mathbf{u}_h^{n+1},\mathbf{u}_h^{n+1},\mathbf{v}_h)_{\Omega_{t_{n+1/2}}} \\ \quad +\mathcal{D}(\mathbf{v}_h,p_h^{n+1})_{\Omega_{t_{n+1/2}}}=\displaystyle\int_{\Omega_{t_{n+1/2}}}\mathbf{f}^{n+1/2}\cdot\mathbf{v}_h\,d\Omega-\int_{\Gamma_0^w}p_{ext}^{n+1}\xi_H\,dz \\ \qquad\qquad\qquad\qquad\qquad\qquad\qquad\qquad\qquad\qquad\qquad\qquad \forall(\mathbf{v}_h,\xi_H)\in\mathbf{V}_{h,H}(t)\cap\mathbf{V}_0(t) \\ \mathcal{D}(\mathbf{u}_h^{n+1},q_h)_{\Omega_{t_{n+1/2}}}=0 \qquad\qquad\qquad\qquad\qquad\qquad\qquad\qquad \forall q_h\in Q_h(\Omega_t) \end{cases} \tag{Ph-FS}$$

$$\mathbf{u}_h^{n+1}\circ\mathcal{A}_{h,t_{n+1}}=\Pi_h^H\frac{\eta_H^{n+1}-\eta_H^n}{\Delta t}\mathbf{e}_r,\qquad on\ \Gamma_0^w \tag{ICCh}$$

$$\begin{cases} \mathcal{P}_{\mathcal{A}}\left(\mathcal{A}_{h,t_{n+1}},\mathbf{z}_h\right)=0 \qquad\qquad \forall\mathbf{z}_h\in\hat{\mathbf{V}}_h^F(\Omega_0),\quad \mathbf{z}_h=\mathbf{0}\ on\ \partial\Omega_0, \\ \mathcal{A}_{h,t_{n+1}}=\mathbf{Y}+\Pi_h^H\eta_H^{n+1}\mathbf{e}_r\quad on\ \Gamma_0^w,\qquad \mathcal{A}_{h,t_{n+1}}=\mathbf{g}_\eta\quad on\ \partial\Omega_0\setminus\Gamma_0^w, \\ \mathcal{A}_{h,t}=\dfrac{t-t_n}{\Delta t}\mathcal{A}_{h,t_{n+1}}+\dfrac{t_{n+1}-t}{\Delta t}\mathcal{A}_{h,t_n}, \qquad\qquad t\in[t_n,t_{n+1}]. \end{cases} \tag{Ph-ALE}$$

for all $n\geq 0$.

Since we are taking a piecewise linear in time ALE mapping, the mesh velocity is constant in each time slab $[t_n,t_{n+1}]$. Moreover, thanks to the chosen coupling conditions, we have on Γ_0^w

$$\mathbf{w}_h\circ\mathcal{A}_{h,t}=\mathbf{u}_h^{n+1}\circ\mathcal{A}_{h,t_{n+1}}=\Pi_h^H\frac{\eta_H^{n+1}-\eta_H^n}{\Delta t}\mathbf{e}_r,\qquad \forall t\in(t_n,t_{n+1}] \tag{4.7.1}$$

and this is an important condition in order to obtain an energy conservative scheme.

4.7.1 Stability analysis of the coupled algorithm with zero forcing terms

We investigate now the stability of the coupled scheme, described in Problem 4.7.1, in the case of homogeneous Dirichlet data and zero forcing terms. We begin with analysing the stability properties of the discretisation of the structural equation for a given forcing term f_S, while the main result is postponed in Proposition 4.7.1.

Lemma 4.7.1 *For any given forcing term* $f_S\in C^0(0,T;\left(V_0^S(\Gamma_0^w)\right)')$, *the following discretisation of the structure equation*

$$\begin{cases} \tilde{\rho}_w(\dfrac{\eta_H^{n+1}-2\eta_H^n+\eta_H^{n-1}}{\Delta t^2},\xi_H)_{\Gamma_0^w}+\mathcal{E}(\eta_H^{n+1},\xi_H)_{\Gamma_0^w}+\mathcal{V}(\dfrac{\eta_H^{n+1}-\eta_H^n}{\Delta t},\xi_H)_{\Gamma_0^w}=<f_S^{n+1},\xi_H>, \\ \qquad\qquad\qquad\qquad\qquad\qquad\qquad\qquad \forall\xi_H\in V_H^S(\Gamma_0^w)\cap V_0^S(\Gamma_0^w) \\ \eta_H^0=\eta_{H0},\quad \eta_H^{-1}=\eta_H^1-2\Delta t\dot{\eta}_{H0} \end{cases} \tag{4.7.2}$$

is unconditionally stable and the following inequality holds

$$\tilde{\rho}_w \left\| \frac{\eta_H^{n+1} - \eta_H^n}{\Delta t} \right\|^2_{L^2(\Gamma_0^w)} + \left\| \eta_H^{n+1} \right\|^2_{\mathcal{E}} + c\Delta t \sum_{i=0}^{n} \left\| \frac{\partial}{\partial z} \left(\frac{\eta_H^{i+1} - \eta_H^i}{\Delta t} \right) \right\|^2_{L^2(\Gamma_0^w)}$$
$$\leq 2\tilde{\rho}_w \left\| \dot{\eta}_{H0} \right\|^2_{L^2(\Gamma_0^w)} + \left\| \eta_{H0} \right\|^2_{\mathcal{E}} + \frac{\Delta t(1 + C_{\Gamma_0^w})}{c} \sum_{i=0}^{n} \left\| f_S^{i+1} \right\|^2_{H^{-1}(\Gamma_0^w)} \quad (4.7.3)$$

for all $n \geq 0$.

Proof. We take in (4.7.2) $\xi_H = \eta_H^{n+1} - \eta_H^n$. Then,

- $\tilde{\rho}_w (\frac{\eta_H^{n+1} - 2\eta_H^n + \eta_H^{n-1}}{\Delta t^2}, \eta_H^{n+1} - \eta_H^n)_{\Gamma_0^w} =$
$$= \frac{\tilde{\rho}_w}{2} \left[\left\| \frac{\eta_H^{n+1} - \eta_H^n}{\Delta t} \right\|^2_{L^2(\Gamma_0^w)} - \left\| \frac{\eta_H^n - \eta_H^{n-1}}{\Delta t} \right\|^2_{L^2(\Gamma_0^w)} + \left\| \frac{\eta_H^{n+1} - 2\eta_H^n + \eta_H^{n-1}}{\Delta t} \right\|^2_{L^2(\Gamma_0^w)} \right]$$
- $\mathcal{E}(\eta_H^{n+1}, \eta_H^{n+1} - \eta_H^n)_{\Gamma_0^w} = \frac{1}{2} \left[\left\| \eta_H^{n+1} \right\|^2_{\mathcal{E}} - \left\| \eta_H^n \right\|^2_{\mathcal{E}} + \left\| \eta_H^{n+1} - \eta_H^n \right\|^2_{\mathcal{E}} \right]$
- $\mathcal{V}(\frac{\eta_H^{n+1} - \eta_H^n}{\Delta t}, \eta_H^{n+1} - \eta_H^n)_{\Gamma_0^w} = c\Delta t \left\| \frac{\partial}{\partial z} \left(\frac{\eta_H^{n+1} - \eta_H^n}{\Delta t} \right) \right\|^2_{L^2(\Gamma_0^w)}$
- $< f_S^{n+1}, \eta_H^{n+1} - \eta_H^n > \leq \Delta t \left\| f_S^{n+1} \right\|_{H^{-1}(\Gamma_0^w)} \left\| \frac{\eta_H^{n+1} - \eta_H^n}{\Delta t} \right\|_{H^1(\Gamma_0^w)}$
$$\leq \frac{\Delta t(1 + C_{\Gamma_0^w})}{2c} \left\| f_S^{n+1} \right\|^2_{H^{-1}(\Gamma_0^w)} + \frac{c\Delta t}{2} \left\| \frac{\partial}{\partial z} \left(\frac{\eta_H^{n+1} - \eta_H^n}{\Delta t} \right) \right\|^2_{L^2(\Gamma_0^w)}.$$

where $C_{\Gamma_0^w}$ is the Poincaré constant on Γ_0^w. The terms $\frac{\tilde{\rho}_w}{2} \left\| \frac{\eta_H^{n+1} - 2\eta_H^n + \eta_H^{n-1}}{\Delta t} \right\|^2_{L^2(\Gamma_0^w)}$ and $\frac{1}{2} \left\| \eta_H^{n+1} - \eta_H^n \right\|^2_{\mathcal{E}}$ highlight the dissipation of the scheme. By putting together the previous expressions we obtain for $n \geq 1$

$$\tilde{\rho}_w \left\| \frac{\eta_H^{n+1} - \eta_H^n}{\Delta t} \right\|^2_{L^2(\Gamma_0^w)} + \left\| \eta_H^{n+1} \right\|^2_{\mathcal{E}} + c\Delta t \left\| \frac{\partial}{\partial z} \left(\frac{\eta_H^{n+1} - \eta_H^n}{\Delta t} \right) \right\|^2_{L^2(\Gamma_0^w)}$$
$$\leq \tilde{\rho}_w \left\| \frac{\eta_H^n - \eta_H^{n-1}}{\Delta t} \right\|^2_{L^2(\Gamma_0^w)} + \left\| \eta_H^n \right\|^2_{\mathcal{E}} + \frac{\Delta t(1 + C_{\Gamma_0^w})}{c} \left\| f_S^{n+1} \right\|^2_{H^{-1}(\Gamma_0^w)} \quad (4.7.4)$$

For n=0 we have, instead, for the first term

$$\tilde{\rho}_w(\frac{\eta_H^1 - 2\eta_H^0 + \eta_H^{-1}}{\Delta t^2}, \eta_H^1 - \eta_H^0)_{\Gamma_0^w} = 2\tilde{\rho}_w(\frac{\eta_H^1 - \eta_{H0} - \Delta t\dot{\eta}_{H0}}{\Delta t^2}, \eta_H^1 - \eta_H^0)_{\Gamma_0^w}$$

$$= \tilde{\rho}_w \left[\left\| \frac{\eta_H^1 - \eta_H^0}{\Delta t} \right\|^2_{L^2(\Gamma_0^w)} - \|\dot{\eta}_{H0}\|^2_{L^2(\Gamma_0^w)} + \left\| \frac{\eta_H^1 - \eta_H^0}{\Delta t} - \dot{\eta}_{H0} \right\|^2_{L^2(\Gamma_0^w)} \right]$$

$$\geq \frac{\tilde{\rho}_w}{2} \left\| \frac{\eta_H^1 - \eta_H^0}{\Delta t} \right\|^2_{L^2(\Gamma_0^w)} - \tilde{\rho}_w \|\dot{\eta}_{H0}\|^2_{L^2(\Gamma_0^w)}$$

while the other terms can be treated as before. Then, for $n = 0$ we obtain

$$\tilde{\rho}_w \left\| \frac{\eta_H^1 - \eta_H^0}{\Delta t} \right\|^2_{L^2(\Gamma_0^w)} + \|\eta_H^1\|^2_{\mathcal{E}} + c\Delta t \left\| \frac{\partial}{\partial z} \left(\frac{\eta_H^1 - \eta_H^0}{\Delta t} \right) \right\|^2_{L^2(\Gamma_0^w)}$$

$$\leq 2\tilde{\rho}_w \|\dot{\eta}_{H0}\|^2_{L^2(\Gamma_0^w)} + \|\eta_{H0}\|^2_{\mathcal{E}} + \frac{\Delta t(1 + C_{\Gamma_0^w})}{c} \|f_S^1\|^2_{H^{-1}(\Gamma_0^w)} \quad (4.7.5)$$

By summing inequalities (4.7.4) over n, for $n \geq 1$, and inequality (4.7.5) we obtain the final estimate (4.7.3).

■

We come back, now, to the coupled Problem 4.7.1 and we prove the following result :

Proposition 4.7.1 *The solution of the coupled Problem 4.7.1 with homogeneous Dirichlet boundary conditions and zero forcing terms (i.e.* $\mathbf{f}^{n-1/2} = \mathbf{0}$ *and* $p_{ext}^n = 0$ *for all* $n > 0$*), provided it exists, is uniformly bounded with respect to n, and the following a-priori estimate holds*

$$\tilde{\rho}_w \left\| \frac{\eta_H^{n+1} - \eta_H^n}{\Delta t} \right\|^2_{L^2(\Gamma_0^w)} + \|\eta_H^{n+1}\|^2_{\mathcal{E}} + 2c\Delta t \sum_{i=0}^{n} \left\| \frac{\partial}{\partial z} \left(\frac{\eta_H^{i+1} - \eta_H^i}{\Delta t} \right) \right\|^2_{L^2(\Gamma_0^w)} + \rho \left\| \mathbf{u}_h^{n+1} \right\|^2_{L_2(\Omega_{t_{n+1}})}$$

$$+ 2\kappa\Delta t \sum_{i=0}^{n} \left\| \nabla_{\mathbf{x}} \mathbf{u}_h^{i+1} \right\|^2_{L_2(\Omega_{t_{i+1/2}})} \leq 2\tilde{\rho}_w \|\dot{\eta}_{H0}\|^2_{L^2(\Gamma_0^w)} + \|\eta_{H0}\|^2_{\mathcal{E}} + \rho \|\mathbf{u}_{h0}\|^2_{L_2(\Omega_0)} \quad (4.7.6)$$

for all $n \geq 0$.

Proof. We take in (Ph-FS) as a test function $(\mathbf{v}_h, \xi_H) = (\Delta t\mathbf{u}_h^{n+1}, \eta_H^{n+1} - \eta_H^n)$. Observe that, thanks to the coupling condition (ICCh), this is an admissible test function. As pointed out in (4.7.1), $\mathbf{w}_h \circ \mathcal{A}_{h,t} = \mathbf{u}_h^{n+1} \circ \mathcal{A}_{h,t_{n+1}}$ on Γ_0^w and then also on $\Gamma_{t_{n+1/2}}^w$ since both quantities are transported on each configuration Ω_t by the same mapping. Thanks to relation (4.6.5) we have

$$\mathcal{B}(\mathbf{w}_h^{n+1/2}, \mathbf{u}_h^{n+1}, \mathbf{u}_h^{n+1}, \Delta t\mathbf{u}_h^{n+1})_{\Omega_{t_{n+1/2}}}$$

$$= \kappa\Delta t \left\| \nabla_{\mathbf{x}} \mathbf{u}_h^{n+1} \right\|^2_{L_2(\Omega_{t_{n+1/2}})} - \frac{\rho\Delta t}{2} \int_{\Omega_{t_{n+1/2}}} \mathrm{div}_{\mathbf{x}}\, \mathbf{w}_h^{n+1/2} |\mathbf{u}_h^{n+1}|^2 \, d\Omega.$$

On the other hand, the other fluid terms can be elaborated as in Section 1.8.4. We have

$$\frac{\rho}{\Delta t}\int_{\Omega_{t_{n+1}}} \mathbf{u}_h^{n+1}\cdot\Delta t\mathbf{u}_h^{n+1}\,d\Omega - \frac{\rho}{\Delta t}\int_{\Omega_{t_n}} \mathbf{u}_h^{n}\cdot\Delta t\mathbf{u}_h^{n+1}\,d\Omega$$
$$\geq \frac{\rho}{2}\left\|\mathbf{u}_h^{n+1}\right\|^2_{L_2(\Omega_{t_{n+1}})} - \frac{\rho}{2}\left\|\mathbf{u}_h^{n}\right\|^2_{L_2(\Omega_{t_n})} + \frac{\rho\Delta t}{2}\int_{\Omega_{t_{n+1/2}}} \mathrm{div}_{\mathbf{x}}\,\mathbf{w}_h^{n+1/2}|\mathbf{u}_h^{n+1}|^2\,d\Omega.$$

The structure terms can be treated as in the proof of Lemma 4.7.1. Thus we obtain the inequality

$$\tilde{\rho}_w\left\|\frac{\eta_H^{n+1}-\eta_H^n}{\Delta t}\right\|^2_{L^2(\Gamma_0^w)} + \left\|\eta_H^{n+1}\right\|^2_{\mathcal{E}} + 2c\Delta t\left\|\frac{\partial}{\partial z}\left(\frac{\eta_H^{n+1}-\eta_H^n}{\Delta t}\right)\right\|^2_{L^2(\Gamma_0^w)} + \rho\left\|\mathbf{u}_h^{n+1}\right\|^2_{L_2(\Omega_{t_{n+1}})}$$
$$+ 2\kappa\Delta t\left\|\nabla_{\mathbf{x}}\mathbf{u}_h^{n+1}\right\|^2_{L_2(\Omega_{t_{n+1/2}})} \leq \tilde{\rho}_w\left\|\frac{\eta_H^{n}-\eta_H^{n-1}}{\Delta t}\right\|^2_{L^2(\Gamma_0^w)} + \left\|\eta_H^{n}\right\|^2_{\mathcal{E}} + \rho\left\|\mathbf{u}_h^{n}\right\|^2_{L_2(\Omega_{t_n})} \quad (4.7.7)$$

for $n > 0$ and the modification as in (4.7.5) for $n = 0$. Finally, by summing over n the previous inequality we obtain the desired result.

■

Remark 4.7.1 *In [42] a similar time discretisation is employed on a monodimensional fluid-structure problem. More precisely, the structure terms are discretised as in (4.7.2); on the contrary, the fluid equations are written in non-conservative form and solved on the previous configuration instead of on the new (unknown) one. For this coupled problem, discretised in time but not in space, the authors proved a stability result similar to the one presented in Proposition 4.7.1.*

Remark 4.7.2 *A similar algorithm as in Problem 4.7.1 is proposed also in [54] for fluid-structure problems in two or three dimensions, accounting both for compressible an incompressible fluids. Yet, in this work, the authors do not introduce the Geometric Conservation Law as we did; they rather propose a different discretisation of the mass conservation equation for the fluid. Precisely, they write also the mass equation in ALE conservative form, i.e.*

$$\left.\frac{\partial J_{\mathcal{A}_t}\rho}{\partial t}\right|_{\mathbf{Y}} + J_{\mathcal{A}_t}\,\mathrm{div}_{\mathbf{x}}\left(\rho(\mathbf{u}-\mathbf{w})\right) = 0 \quad (4.7.8)$$

and they discretise both the momentum equation and (4.7.8) by a standard Implicit Euler scheme. In particular that means for (4.7.8)

$$\int_{\Omega_{t_{n+1}}} \rho_h^{n+1}\,q_h\,d\Omega - \int_{\Omega_{t_n}} \rho_h^{n}\,q_h\,d\Omega + \Delta t\int_{\Omega_{t_{n+1}}} \mathrm{div}_{\mathbf{x}}\left(\rho_h^{n+1}(\mathbf{u}_h^{n+1}-\mathbf{w}_h^{n+1})\right)\,q_h\,d\Omega = 0, \quad (4.7.9)$$

$\forall q_h \in Q_h(\Omega_t)$. *In the case of incompressible fluids, the density ρ is constant in time (it is not an unknown of the problem) and (4.7.9) is equivalent to the following constraint on the fluid velocity*

$$\rho\int_{\Omega_{t_{n+1}}} \mathrm{div}_{\mathbf{x}}\,\mathbf{u}_h^{n+1}\,q_h\,d\Omega = -\frac{\rho}{\Delta t}\int_{\Omega_{t_{n+1}}} q_h\,d\Omega + \frac{\rho}{\Delta t}\int_{\Omega_{t_n}} q_h\,d\Omega + \rho\int_{\Omega_{t_{n+1}}} \mathrm{div}_{\mathbf{x}}\,\mathbf{w}_h^{n+1}\,q_h\,d\Omega \quad (4.7.10)$$

Observe that the velocity field $\mathbf{u}_h^{n+1}$ is not forced to be exactly divergence free at t_{n+1} and the right hand side in (4.7.10) is precisely the error in representing the domain deformation. For this numerical scheme the authors obtained a stability result very similar to the one presented in Proposition 4.7.1.

4.7.2 Some remarks on the stability of the coupled algorithm with non-zero forcing terms

When considering non zero forcing terms $\mathbf{f}^n \neq 0$ and $p_{ext} \neq 0$, $n > 0$, the following inequality, that generalizes (4.7.7), can be easily obtained, following the same procedure as in the proof of Proposition 4.7.1 :

$$\tilde{\rho}_w \left\| \frac{\eta_H^{n+1} - \eta_H^n}{\Delta t} \right\|^2_{L^2(\Gamma_0^w)} + \left\| \eta_H^{n+1} \right\|^2_{\mathcal{E}} + c\Delta t \left\| \frac{\partial}{\partial z} \left(\frac{\eta_H^{n+1} - \eta_H^n}{\Delta t} \right) \right\|^2_{L^2(\Gamma_0^w)} + \rho \left\| \mathbf{u}_h^{n+1} \right\|^2_{L_2(\Omega_{t_{n+1}})}$$
$$+ \kappa\Delta t \left\| \nabla_{\mathbf{x}} \mathbf{u}_h^{n+1} \right\|^2_{L_2(\Omega_{t_{n+1/2}})} \leq \tilde{\rho}_w \left\| \frac{\eta_H^n - \eta_H^{n-1}}{\Delta t} \right\|^2_{L^2(\Gamma_0^w)} + \left\| \eta_H^n \right\|^2_{\mathcal{E}} + \rho \left\| \mathbf{u}_h^n \right\|^2_{L_2(\Omega_{t_n})}$$
$$+ \frac{\Delta t(1 + C_\Omega^{n+1})}{\kappa} \left\| \mathbf{f}^{n+1/2} \right\|^2_{H^{-1}(\Omega_{t_{n+1/2}})} + \frac{\Delta t(1 + C_{\Gamma_0^w})}{c} \left\| p_{ext}^{n+1/2} \right\|^2_{H^{-1}(\Gamma_0^w)} \quad (4.7.11)$$

Observe that the Poincaré constant appearing in the term that contains the fluid force $\mathbf{f}^{n+1/2}$ depends on the domain $\Omega_{t_{n+1/2}}$ and eventually on the structure displacement η_H^{n+1}; that is the reason why we denoted it C_Ω^{n+1} instead of simply C_Ω. Hence, we cannot derive straightforwardly from (4.7.11) an a-priori estimate by simply summing over n. In the geometry considered up to now (see figure 4.3), the relation between the Poincaré constant and the structure displacement can be easily found. The following Lemma fixes this point

Lemma 4.7.2 *Given a displacement of the structure $\eta \in V_0^S(\Gamma_0^w)$, with $\eta(z) > -D$, $\forall z \in (0, L)$, that identifies a domain configuration $\Omega_\eta \equiv \{(z,r) : \ 0 < z < L, \ \text{and} \ 0 < r < D + \eta(z)\}$, then, for any function $f \in H^1(\Omega_\eta)$ such that $f = 0$ on Γ_{dw}, the Poincaré constant can be taken as*

$$C_{\Omega_\eta} = 8 \left(D^2 + L \left\| \frac{\partial \eta}{\partial z} \right\|^2_{L^2(\Gamma_0^w)} \right) \quad (4.7.12)$$

Proof. For any given $f \in C^1(\Omega_\eta)$ such that $f = 0$ on Γ_{dw}, we have

$$f^2(z,r) = \int_0^r 2 \frac{\partial f}{\partial s}(z,s) f(z,s)\, ds \leq \int_0^{D+\eta(z)} 2 \left| \frac{\partial f}{\partial s}(z,s) \right| |f(z,s)|\, ds.$$

Hence,

$$\|f\|^2_{L_2(\Omega_\eta)} \leq \int_0^L \int_0^{D+\eta(z)} \left(\int_0^{D+\eta(z)} 2 \left| \frac{\partial f}{\partial s}(z,s) \right| |f(z,s)|\, ds \right) dr dz$$
$$\leq \int_0^L 2(D + \eta(z)) \int_0^{D+\eta(z)} \left| \frac{\partial f}{\partial s}(z,s) \right| |f(z,s)|\, ds dz$$
$$\leq 2 \left(D + \|\eta(z)\|_{L^\infty(\Gamma_0^w)} \right) \|f\|_{L_2(\Omega_\eta)} \|\nabla f\|_{L_2(\Omega_\eta)}$$

Moreover, since $V_0^S(\Gamma_0^w)$ is continuously embedded in $L^\infty(\Gamma_0^w)$, we have also

$$\|\eta(z)\|_{L^\infty(\Gamma_0^w)} \leq \sqrt{L}\left\|\frac{\partial\eta}{\partial z}\right\|_{L^2(\Gamma_0^w)}$$

and finally

$$\|f\|^2_{L_2(\Omega_\eta)} \leq 4\left(D+\sqrt{L}\left\|\frac{\partial\eta}{\partial z}\right\|_{L^2(\Gamma_0^w)}\right)^2\|\nabla f\|^2_{L_2(\Omega_\eta)} \leq 8\left(D^2+L\left\|\frac{\partial\eta}{\partial z}\right\|^2_{L^2(\Gamma_0^w)}\right)\|\nabla f\|^2_{L_2(\Omega_\eta)} \tag{4.7.13}$$

Since the space of functions $\{v \in C^1(\Omega_\eta),\ v=0 \text{ on } \Gamma_{dw}\}$ is dense in $H^1_{\Gamma_{dw}}(\Omega_\eta) \equiv \{f \in H^1(\Omega_\eta),\ f=0 \text{ on } \Gamma_{dw}\}$, relation (4.7.13) can be extended to all $H^1_{\Gamma_{dw}}(\Omega_\eta)$ and this concludes the proof.

■

The domain $\Omega_{t_{n+1/2}}$, in inequality (4.7.11), is identified by the structure displacement $\Pi_h^H \frac{\eta_H^{n+1}+\eta_H^n}{2}$ and the critical term can be developed as

$$\begin{aligned}
&\frac{\Delta t(1+C_\Omega^{n+1})}{\kappa}\left\|\mathbf{f}^{n+1/2}\right\|^2_{H^{-1}(\Omega_{t_{n+1/2}})} \\
&\quad=\frac{\Delta t}{\kappa}\left(1+8D^2+8L\left\|\frac{\partial}{\partial z}\left(\Pi_h^H\frac{\eta_H^{n+1}+\eta_H^n}{2}\right)\right\|^2_{L^2(\Gamma_0^w)}\right)\left\|\mathbf{f}^{n+1/2}\right\|^2_{H^{-1}(\Omega_{t_{n+1/2}})} \\
&\quad\leq\frac{\Delta t}{\kappa}(1+8D^2)\left\|\mathbf{f}^{n+1/2}\right\|^2_{H^{-1}(\Omega_{t_{n+1/2}})}+\frac{2L\Delta t}{\kappa}CH^{-2}\|\Pi_h^H\|^2\left\|\eta_H^{n+1}+\eta_H^n\right\|^2_{L^2(\Gamma_0^w)} \\
&\leq\frac{\Delta t}{\kappa}(1+8D^2)\left\|\mathbf{f}^{n+1/2}\right\|^2_{H^{-1}(\Omega_{t_{n+1/2}})}+\frac{4L\Delta t}{b\kappa}CH^{-2}\|\Pi_h^H\|^2\left(\left\|\eta_H^{n+1}\right\|^2_{\mathcal{E}}+\left\|\eta_H^n\right\|^2_{\mathcal{E}}\right)\left\|\mathbf{f}^{n+1/2}\right\|^2_{H^{-1}(\Omega_{t_{n+1/2}})}
\end{aligned}$$

where C is the constant of the inverse inequality $\left\|\frac{\partial\eta_H}{\partial z}\right\|^2_{L^2(\Gamma_0^w)} \leq CH^{-2}\|\eta_H\|^2_{L^2(\Gamma_0^w)}$. Then, inequality (4.7.11) can be rewritten as

$$\begin{aligned}
&\tilde{\rho}_w\left\|\frac{\eta_H^{n+1}-\eta_H^n}{\Delta t}\right\|^2_{L^2(\Gamma_0^w)}+(1-\gamma^{n+1})\left\|\eta_H^{n+1}\right\|^2_{\mathcal{E}}+c\Delta t\left\|\frac{\partial}{\partial z}\left(\frac{\eta_H^{n+1}-\eta_H^n}{\Delta t}\right)\right\|^2_{L^2(\Gamma_0^w)} \\
&+\rho\left\|\mathbf{u}_h^{n+1}\right\|^2_{L_2(\Omega_{t_{n+1}})}+\kappa\Delta t\left\|\nabla_{\mathbf{x}}\mathbf{u}_h^{n+1}\right\|^2_{L_2(\Omega_{t_{n+1/2}})}\leq\tilde{\rho}_w\left\|\frac{\eta_H^n-\eta_H^{n-1}}{\Delta t}\right\|^2_{L^2(\Gamma_0^w)}+(1+\gamma^{n+1})\left\|\eta_H^n\right\|^2_{\mathcal{E}} \\
&\quad+\rho\left\|\mathbf{u}_h^n\right\|^2_{L_2(\Omega_{t_n})}+\frac{\Delta t(1+8D^2)}{\kappa}\left\|\mathbf{f}^{n+1/2}\right\|^2_{H^{-1}(\Omega_{t_{n+1/2}})}+\frac{\Delta t(1+C_{\Gamma_0^w})}{c}\left\|p_{ext}^{n+1/2}\right\|^2_{H^{-1}(\Gamma_0^w)}
\end{aligned} \tag{4.7.14}$$

where we have set

$$\gamma^{n+1}=\frac{4L\Delta t}{b\kappa}CH^{-2}\|\Pi_h^H\|^2\left\|\mathbf{f}^{n+1/2}\right\|^2_{H^{-1}(\Omega_{t_{n+1/2}})}.$$

Then, by applying the discrete Gronwall lemma, we can obtain an a-priori estimate under the stability condition

$$\Delta t < \frac{b\kappa H^2}{4LC\|\Pi_h^H\|^2 \left\|\mathbf{f}^{i+1/2}\right\|^2_{H^{-1}(\Omega_{t_{i+1/2}})}}, \qquad \forall i > 0.$$

This estimate might not be optimal; surely, if $\mathbf{f} \in C^0(0,T;L^2(\Omega_t))$, other estimates can be obtained that avoid the use of the Poincaré inequality. What we wanted to point out here, is that whenever we need to use the Poincaré inequality in the fluid domain, this might induce restrictions on the time step and/or the spatial discretisation to have a stable scheme. Similar considerations hold when considering the coupled Problem 4.7.1 with non-homogeneous Dirichlet boundary conditions.

4.8 Second order discretisation of the structure

An improvement to the previous coupled algorithm can be obtained by considering a better and less dissipative discretisation of the structural equation. We focus, here, on the so called *mid-point* scheme which can be seen as a particular case of the Newmark discretisation (see also Remark 4.8.1 later on). Applied to the structure equation it reads as follows. Let us denote by η_H^n an approximation of $\eta_H(t^n)$ and by $\dot{\eta}_H^n$ an approximation of $\dot{\eta}_H(t^n)$. Then, given at each time $t^{n+1/2}$ a forcing term $f_S^{n+1/2}$ on the structure, we solve for all $n > 0$

$$\begin{cases} (\dfrac{\eta_H^{n+1} - \eta_H^n}{\Delta t}, \xi_H)_{\Gamma_0^w} = (\dfrac{\dot{\eta}_H^{n+1} + \dot{\eta}_H^n}{2}, \xi_H)_{\Gamma_0^w}, & \forall \xi_H \in V_H^S(\Gamma_0^w) \cap V_0^S(\Gamma_0^w) \\ \tilde{\rho}_w(\dfrac{\dot{\eta}_H^{n+1} - \dot{\eta}_H^n}{\Delta t}, \xi_H)_{\Gamma_0^w} + \mathcal{E}(\dfrac{\eta_H^{n+1} + \eta_H^n}{2}, \xi_H)_{\Gamma_0^w} + \mathcal{V}(\dfrac{\dot{\eta}_H^{n+1} + \dot{\eta}_H^n}{2}, \xi_H)_{\Gamma_0^w} = < f_S^{n+1/2}, \xi_H >, & \\ \qquad\qquad \forall \xi_H \in V_H^S(\Gamma_0^w) \cap V_0^S(\Gamma_0^w) \\ \eta_H^0 = \eta_{H0}, \quad \dot{\eta}_H^0 = \dot{\eta}_{H0} \end{cases} \tag{4.8.1}$$

This scheme is second order accurate in time. We will show that this structural solver coupled with the Implicit Euler scheme for the fluid equations gives an unconditionally stable algorithm. Clearly, in doing so, the fluid discretisation is only first order accurate. In a second step, we will instead consider a Crank-Nicolson solver for the fluid. The coupled algorithm thus obtained is "potentially" second order accurate since both the fluid and the structure solvers feature a quadratic convergence rate when taken separately. Yet, this does not guarantee that the coupled algorithm is really second order accurate and a complete convergence analysis should be carried out. At our knowledge, such an analysis is still missing though it is very important for the future developments in this field. We do not dwell on this aspect in the present work, but it is the subject of an ongoing research. Yet, in Section 4.11 we will carry out a numerical analysis of the accuracy of this scheme and we will show on a test case that this algorithms is indeed second order accurate.

4.8.1 Coupling with an Implicit Euler discretisation for the fluid equations

We consider now the coupling algorithm obtained by employing the mid-point scheme (4.8.1) for the structure and the same discretisation as in Problem 4.7.1, for the fluid and ALE mapping problems and the interface coupling condition. The formulation obtained reads

Problem 4.8.1 (Mid-point/Implicit Euler) *Given the initial solution* $\mathbf{u}_{h0}$, η_{H0} *and* $\dot{\eta}_{H0}$ *find* $\mathbf{u}_h^{n+1} \in \mathbf{V}_h^F(\Omega_t)$, $p_h^{n+1} \in Q_h(\Omega_t)$, $\eta_H^{n+1} \in V_H^S(\Gamma_0^w)$, *and* $\dot{\eta}_H^{n+1} \in V_H^S(\Gamma_0^w)$, *with*

$$\begin{aligned} &\mathbf{u}_h^{n+1} = \mathbf{\Phi}_i^{n+1} \quad \text{on } \mathcal{S}_i,\ i=1,2, \quad \text{and} \\ &\eta_H^{n+1} = \alpha_1^{n+1} \quad \text{at } z=0, \qquad \eta_H^{n+1} = \alpha_2^{n+1} \quad \text{at } z=L, \\ &\dot{\eta}_H^{n+1} = \dot{\alpha}_1^{n+1} \quad \text{at } z=0, \qquad \dot{\eta}_H^{n+1} = \dot{\alpha}_2^{n+1} \quad \text{at } z=L, \end{aligned}$$

that satisfy, for all $n \geq 0$,

$$\left\{ \begin{aligned} &(\frac{\eta_H^{n+1}-\eta_H^n}{\Delta t}, \xi_H)_{\Gamma_0^w} = (\frac{\dot{\eta}_H^{n+1}+\dot{\eta}_H^n}{2}, \xi_H)_{\Gamma_0^w} && \forall \xi_H \in V_H^S(\Gamma_0^w) \cap V_0^S(\Gamma_0^w) \\ &\tilde{\rho}_w(\frac{\dot{\eta}_H^{n+1}-\dot{\eta}_H^n}{\Delta t}, \xi_H)_{\Gamma_0^w} + \mathcal{E}(\frac{\eta_H^{n+1}+\eta_H^n}{2}, \xi_H)_{\Gamma_0^w} + \mathcal{V}(\frac{\dot{\eta}_H^{n+1}+\dot{\eta}_H^n}{2}, \xi_H)_{\Gamma_0^w} \\ &\quad + \frac{\rho}{\Delta t}\int_{\Omega_{t_{n+1}}} \mathbf{u}_h^{n+1}\cdot\mathbf{v}_h\, d\Omega - \frac{\rho}{\Delta t}\int_{\Omega_{t_n}} \mathbf{u}_h^n \cdot \mathbf{v}_h\, d\Omega + \mathcal{B}(\mathbf{w}_h^{n+1/2}, \mathbf{u}_h^{n+1}, \mathbf{u}_h^{n+1}, \mathbf{v}_h)_{\Omega_{t_{n+1/2}}} \\ &\quad + \mathcal{D}(\mathbf{v}_h, p_h^{n+1})_{\Omega_{t_{n+1/2}}} = \int_{\Omega_{t_{n+1/2}}} \mathbf{f}^{n+1/2}\cdot\mathbf{v}_h\, d\Omega - \int_{\Gamma_0^w} p_{ext}^{n+1/2}\xi_H\, dz \\ &\qquad\qquad && \forall (\mathbf{v}_h, \xi_H) \in \mathbf{V}_{h,H}(t) \cap \mathbf{V}_0(t) \\ &\mathcal{D}(\mathbf{u}_h^{n+1}, q_h)_{\Omega_{t_{n+1/2}}} = 0 && \forall q_h \in Q_h(\Omega_t) \end{aligned} \right. \qquad \text{(Ph-FS)}$$

and interface coupling condition (ICCh) and ALE mapping problem (Ph-ALE) as in Problem 4.7.1.

Observe that, for this algorithm, relation (4.7.1) is still valid since we have not changed the ALE mapping problem and the interface coupling condition between fluid and structure velocity.

The structure discretisation requires the forcing term at time $t^{n+1/2}$. In the coupled problem, this term is obtained as the residual of the fluid equation by taking as a test function $(\mathbf{v}_h, \xi_H) = (\mathcal{R}_h(\xi_H), \xi_H)$, i.e.

$$< f_S^{n+1/2}, \xi_H >= -\int_{\Gamma_0^w} p_{ext}^{n+1/2}\xi_H\, dz + < \Phi(\mathbf{u}_h^{n+1}, p_h^{n+1}), \mathcal{R}_h(\xi_H) >, \qquad \text{and} \tag{4.8.2}$$

$$\begin{aligned} &< \Phi(\mathbf{u}_h^{n+1}, p_h^{n+1}), \mathcal{R}_h(\xi_H) > \\ &= \int_{\Omega_{t_{n+1/2}}} \mathbf{f}^{n+1/2}\cdot\mathcal{R}_h(\xi_H)\, d\Omega - \frac{\rho}{\Delta t}\int_{\Omega_{t_{n+1}}} \mathbf{u}_h^{n+1}\cdot\mathcal{R}_h(\xi_H)\, d\Omega + \frac{\rho}{\Delta t}\int_{\Omega_{t_n}} \mathbf{u}_h^n\cdot\mathcal{R}_h(\xi_H)\, d\Omega \\ &- \mathcal{B}(\mathbf{w}_h^{n+1/2}, \mathbf{u}_h^{n+1}, \mathbf{u}_h^{n+1}, \mathcal{R}_h(\xi_H))_{\Omega_{t_{n+1/2}}} - \mathcal{D}(\mathcal{R}_h(\xi_H), p_h^{n+1})_{\Omega_{t_{n+1/2}}}. \end{aligned} \tag{4.8.3}$$

Observe that the term in (4.8.3) can be seen as a first order approximation of the fluid stress on the structure at time $t^{n+1/2}$.

4.8.2 Stability analysis of the coupled algorithm

We are going now to study the stability of this coupled scheme. As in the Section 4.7.1, we investigate first the stability of the structure discretisation while the main result is postponed in Proposition 4.8.1.

Lemma 4.8.1 *For any given forcing term $f_S \in C^0(0,T;(V_0^S(\Gamma_0^w))')$, the mid-point discretisation (4.8.1) of the structure equation is unconditionally stable and the following inequality holds :*

$$\tilde{\rho}_w \left\|\dot{\eta}_H^{n+1}\right\|^2_{L^2(\Gamma_0^w)} + \left\|\eta_H^{n+1}\right\|^2_{\mathcal{E}} + c\Delta t \sum_{i=0}^{n} \left\| \frac{\partial}{\partial z}\left(\frac{\dot{\eta}_H^{i+1}+\dot{\eta}_H^{i}}{2}\right)\right\|^2_{L^2(\Gamma_0^w)}$$
$$\leq \tilde{\rho}_w \left\|\dot{\eta}_{H0}\right\|^2_{L^2(\Gamma_0^w)} + \left\|\eta_{H0}\right\|^2_{\mathcal{E}} + \frac{\Delta t(1+C_{\Gamma_0^w})}{c} \sum_{i=0}^{n} \left\| f_S^{i+1/2}\right\|^2_{H^{-1}(\Gamma_0^w)} \quad (4.8.4)$$

for all $n \geq 0$.

Proof. We take in the second equation of (4.8.1) $\xi_H = \Delta t \frac{\dot{\eta}_H^{n+1}+\dot{\eta}_H^n}{2}$. Bearing in mind the first relation in (4.8.1), we have

$$\frac{\tilde{\rho}_w}{2}\left(\left\|\eta_H^{n+1}\right\|^2_{L^2(\Gamma_0^w)} - \left\|\dot{\eta}_H^{n}\right\|^2_{L^2(\Gamma_0^w)}\right) + \frac{1}{2}\left(\left\|\eta_H^{n+1}\right\|^2_{\mathcal{E}} - \left\|\eta_H^{n}\right\|^2_{\mathcal{E}}\right) + c\Delta t \left\| \frac{\partial}{\partial z}\left(\frac{\dot{\eta}_H^{n+1}+\dot{\eta}_H^{n}}{2}\right)\right\|^2_{L^2(\Gamma_0^w)}$$
$$\leq \frac{c\Delta t}{2}\left\| \frac{\partial}{\partial z}\left(\frac{\dot{\eta}_H^{n+1}+\dot{\eta}_H^{n}}{2}\right)\right\|^2_{L^2(\Gamma_0^w)} + \frac{\Delta t(1+C_{\Gamma_0^w})}{2c}\left\| f_S^{n+1/2}\right\|^2_{H^{-1}(\Gamma_0^w)}$$

and thus

$$\tilde{\rho}_w \left\|\dot{\eta}_H^{n+1}\right\|^2_{L^2(\Gamma_0^w)} + \left\|\eta_H^{n+1}\right\|^2_{\mathcal{E}} + c\Delta t \left\| \frac{\partial}{\partial z}\left(\frac{\dot{\eta}_H^{n+1}+\dot{\eta}_H^{n}}{2}\right)\right\|^2_{L^2(\Gamma_0^w)}$$
$$\leq \tilde{\rho}_w \left\|\dot{\eta}_H^{n}\right\|^2_{L^2(\Gamma_0^w)} + \left\|\eta_H^{n}\right\|^2_{\mathcal{E}} + \frac{\Delta t(1+C_{\Gamma_0^w})}{c}\left\| f_S^{n+1/2}\right\|^2_{H^{-1}(\Gamma_0^w)}$$

Finally, by summing over n we obtain the desired result.

■

The main result of this section is given in the following

Proposition 4.8.1 *The solution of the coupled Problem 4.8.1 with homogeneous Dirichlet boundary conditions and zero forcing terms (i.e. $\mathbf{f}^{n+1/2} = \mathbf{0}$ and $p_{ext}^{n+1/2} = 0$ for all $n \geq 0$), provided it exists, is uniformly bounded with respect to n and the following a-priori estimate holds*

$$\tilde{\rho}_w \left\|\dot{\eta}_H^{n+1}\right\|^2_{L^2(\Gamma_0^w)} + \left\|\eta_H^{n+1}\right\|^2_{\mathcal{E}} + 2c\Delta t \sum_{i=0}^{n} \left\| \frac{\partial}{\partial z}\left(\frac{\dot{\eta}_H^{i+1}+\dot{\eta}_H^{i}}{2}\right)\right\|^2_{L^2(\Gamma_0^w)} + \rho \left\|\mathbf{u}_h^{n+1}\right\|^2_{L_2(\Omega_{t_{n+1}})}$$
$$+ 2\kappa\Delta t \sum_{i=0}^{n} \left\|\boldsymbol{\nabla}_{\mathbf{x}}\mathbf{u}_h^{i+1}\right\|^2_{L_2(\Omega_{t_{i+1/2}})} \leq \tilde{\rho}_w \left\|\dot{\eta}_{H0}\right\|^2_{L^2(\Gamma_0^w)} + \left\|\eta_{H0}\right\|^2_{\mathcal{E}} + \rho \left\|\mathbf{u}_{h0}\right\|^2_{L_2(\Omega_0)} \quad (4.8.5)$$

for all $n \geq 0$.

Proof. We proceed as in the proof of Proposition 4.7.1, by taking as a test function $(\mathbf{v}_h, \xi_H) = (\Delta t \mathbf{u}_h^{n+1}, \eta_H^{n+1} - \eta_H^n)$, which is an admissible test function. Observe that $(\Delta t \mathbf{u}_h^{n+1}, \eta_H^{n+1} - \eta_H^n) =$

$(\Delta t \mathbf{u}_h^{n+1}, \Delta t \frac{\ddot{\eta}_H^{n+1}+\dot{\eta}_H^n}{2})$. Thus, the fluid terms can be manipulated as in Proposition 4.7.1 while the structure terms as in Lemma 4.8.1, and we obtain the inequality

$$\tilde{\rho}_w \left\|\dot{\eta}_H^{n+1}\right\|^2_{L^2(\Gamma_0^w)} + \left\|\eta_H^{n+1}\right\|^2_{\mathcal{E}} + 2c\Delta t \left\| \frac{\partial}{\partial z}\left(\frac{\dot{\eta}_H^{n+1}+\dot{\eta}_H^n}{2}\right)\right\|^2_{L^2(\Gamma_0^w)} + \rho \left\|\mathbf{u}_h^{n+1}\right\|^2_{L_2(\Omega_{t_{n+1}})}$$
$$+ 2\kappa\Delta t \left\|\nabla_{\mathbf{x}} \mathbf{u}_h^{n+1}\right\|^2_{L_2(\Omega_{t_{n+1/2}})} \leq \tilde{\rho}_w \left\|\dot{\eta}_H^n\right\|^2_{L^2(\Gamma_0^w)} + \left\|\eta_H^n\right\|^2_{\mathcal{E}} + \rho \left\|\mathbf{u}_h^n\right\|^2_{L_2(\Omega_{t_n})}$$

Finally, by summing over n we obtain inequality (4.8.5) and this concludes the proof. ■

Remark 4.8.1 *The Newmark scheme applied to the scalar second order differential equation*

$$\ddot{y}(t) = f(t, y(t), \dot{y}(t)), \quad t > 0, \qquad y(0) = y_0, \quad \dot{y}(0) = \dot{y}_0$$

reads

$$\begin{cases} y^{n+1} = y^n + \Delta t \dot{y}^n + \Delta t^2 \left[\beta f(t^{n+1}, y^{n+1}, \dot{y}^{n+1}) + \left(\frac{1}{2} - \beta\right) f(t^n, y^n, \dot{y}^n)\right], \\ \dot{y}^{n+1} = \dot{y}^n + \Delta t \left[\gamma f(t^{n+1}, y^{n+1}, \dot{y}^{n+1}) + (1-\gamma) f(t^n, y^n, \dot{y}^n)\right]. \end{cases} \tag{4.8.6}$$

It can be shown (see e.g. [81]) that this scheme is second order accurate for $\gamma = 1/2$ and first order accurate for $\gamma \neq 1/2$. A typical choice consists in taking $\beta = 1/4$ and $\gamma = 1/2$. In this case, if we subtract the second equation in (4.8.6) multiplied by $\Delta t/2$ to the first equation, we obtain the relation

$$y^{n+1} - \frac{\Delta t}{2}\dot{y}^{n+1} = y^n + \frac{\Delta t}{2}\dot{y}^n$$

and the Newmark scheme can be rewritten in the more familiar form

$$\begin{cases} \dfrac{y^{n+1} - y^n}{\Delta t} = \dfrac{\dot{y}^{n+1} + \dot{y}^n}{2} \\ \dot{y}^{n+1} = \dot{y}^n + \frac{\Delta t}{2}\left[f(t^{n+1}, y^{n+1}, \dot{y}^{n+1}) + f(t^n, y^n, \dot{y}^n)\right]. \end{cases} \tag{4.8.7}$$

This last formulation, applied to the structure equation gives the following scheme

$$\begin{cases} (\dfrac{\eta_H^{n+1} - \eta_H^n}{\Delta t}, \xi_H)_{\Gamma_0^w} = (\dfrac{\dot{\eta}_H^{n+1} + \dot{\eta}_H^n}{2}, \xi_H)_{\Gamma_0^w}, & \forall \xi_H \in V_H^S(\Gamma_0^w) \cap V_0^S(\Gamma_0^w) \\ \tilde{\rho}_w (\dfrac{\dot{\eta}_H^{n+1} - \dot{\eta}_H^n}{\Delta t}, \xi_H)_{\Gamma_0^w} + \mathcal{E}(\dfrac{\eta_H^{n+1} + \eta_H^n}{2}, \xi_H)_{\Gamma_0^w} + \mathcal{V}(\dfrac{\dot{\eta}_H^{n+1} + \dot{\eta}_H^n}{2}, \xi_H)_{\Gamma_0^w} \\ \qquad = < \dfrac{f_S^{n+1} + f_S^n}{2}, \xi_H >, & \forall \xi_H \in V_H^S(\Gamma_0^w) \cap V_0^S(\Gamma_0^w) \end{cases} \tag{4.8.8}$$

which is basically the same as (4.8.1) apart from the forcing term in the second equation that, here, is computed as $< \frac{f_S^{n+1}+f_S^n}{2}, \xi_H >$ while in (4.8.1) is given by $< f_S^{n+1/2}, \xi_H >$. Scheme (4.8.6) is widely used in structural analysis and fluid structure interaction problems. Yet, the choice of (4.8.1) instead of (4.8.8) in the coupled Problem 4.8.1 allows to obtain the stability result presented in Proposition 4.8.1, while no similar results can be obtained with (4.8.8).

4.8.3 Coupling with a Crank-Nicolson discretisation for the fluid equations

We present, now, the coupled algorithm obtained by taking the mid-point scheme for the structure and the Crank-Nicolson discretisation (3.5.6), proposed in Chapter 3, for the fluid. The ALE mapping is constructed as in Problems 4.7.1 and 4.8.1. Finally, the interface coupling condition between the fluid and the structure velocity is taken as

$$\mathbf{u}_h^{n+1} \circ \mathcal{A}_{h,t_{n+1}} = \Pi_h^H \dot{\eta}_H^{n+1} \mathbf{e}_r$$

Then, the coupled problem reads

Problem 4.8.2 (Mid-point/Crank-Nicolson) *Given the initial solution* $\mathbf{u}_{h0}$, p_h^0, η_{H0} *and* $\dot{\eta}_{H0}$ *find* $\mathbf{u}_h^{n+1} \in \mathbf{V}_h^F(\Omega_t)$, $p_h^{n+1} \in Q_h(\Omega_t)$, $\eta_H^{n+1} \in V_H^S(\Gamma_0^w)$, *and* $\dot{\eta}_H^{n+1} \in V_H^S(\Gamma_0^w)$, *with boundary conditions as in Problem 4.8.1, that safisfy, for all* $n \geq 0$,

$$\begin{cases}
(\dfrac{\eta_H^{n+1} - \eta_H^n}{\Delta t}, \xi_H)_{\Gamma_0^w} = (\dfrac{\dot{\eta}_H^{n+1} + \dot{\eta}_H^n}{2}, \xi_H)_{\Gamma_0^w} & \forall \xi_H \in V_H^S(\Gamma_0^w) \cap V_0^S(\Gamma_0^w) \\
\tilde{\rho}_w(\dfrac{\dot{\eta}_H^{n+1} - \dot{\eta}_H^n}{\Delta t}, \xi_H)_{\Gamma_0^w} + \mathcal{E}(\dfrac{\eta_H^{n+1} + \eta_H^n}{2}, \xi_H)_{\Gamma_0^w} + \mathcal{V}(\dfrac{\dot{\eta}_H^{n+1} + \dot{\eta}_H^n}{2}, \xi_H)_{\Gamma_0^w} & \\
\quad + \dfrac{\rho}{\Delta t} \displaystyle\int_{\Omega_{t_{n+1}}} \mathbf{u}_h^{n+1} \cdot \mathbf{v}_h \, d\Omega - \dfrac{\rho}{\Delta t} \int_{\Omega_{t_n}} \mathbf{u}_h^n \cdot \mathbf{v}_h \, d\Omega & \\
\quad + \mathcal{B}(\mathbf{w}_h^{n+1/2}, \dfrac{\mathbf{u}_h^{n+1} + \mathbf{u}_h^n}{2}, \dfrac{\mathbf{u}_h^{n+1} + \mathbf{u}_h^n}{2}, \mathbf{v}_h)_{\Omega_{t_{n+1/2}}} + \mathcal{D}(\mathbf{v}_h, \dfrac{p_h^{n+1} + p_h^n}{2})_{\Omega_{t_{n+1/2}}} & \\
\quad = \displaystyle\int_{\Omega_{t_{n+1/2}}} \mathbf{f}^{n+1/2} \cdot \mathbf{v}_h \, d\Omega - \int_{\Gamma_0^w} p_{ext}^{n+1/2} \xi_H \, dz & \forall (\mathbf{v}_h, \xi_H) \in \mathbf{V}_{h,H}(t) \cap \mathbf{V}_0(t) \\
\mathcal{D}(\dfrac{\mathbf{u}_h^{n+1} + \mathbf{u}_h^n}{2}, q_h)_{\Omega_{t_{n+1/2}}} = 0 & \forall q_h \in Q_h(\Omega_t),
\end{cases} \tag{Ph-FS}$$

interface coupling condition

$$\mathbf{u}_h^{n+1} \circ \mathcal{A}_{h,t_{n+1}} = \Pi_h^H \dot{\eta}_H^{n+1} \mathbf{e}_r, \qquad \text{on } \Gamma_0^w \tag{ICCh}$$

and ALE mapping problem (Ph-ALE) as in Problem 4.7.1.

Observe that both the fluid and the structure schemes can be seen as an approximation of the corresponding differential equations at $t^{n+1/2}$. Consequently, the global coupled algorithm, as well, is an approximation of the coupled problem at time $t^{n+1/2}$ and the two subproblems are perfectly compatible (there is not any temporal mismatch discretisation between fluid and structure).

Besides, with the chosen coupling conditions, we have that

$$\frac{\mathbf{u}_h^{n+1} \circ \mathcal{A}_{h,t_{n+1}} + \mathbf{u}_h^n \circ \mathcal{A}_{h,t_n}}{2} = \Pi_h^H \frac{\dot{\eta}_H^{n+1} + \dot{\eta}_H^n}{2} = \Pi_h^H \frac{\eta_H^{n+1} - \eta_H^n}{\Delta t} = \mathbf{w}_h \circ \mathcal{A}_{h,t}, \qquad t \in (t_n, t_{n+1}].$$

which implies that also on $\Gamma_{t_{n+1/2}}^w$ we have $\mathbf{w}_h^{n+1/2} = \frac{\mathbf{u}_h^{n+1} + \mathbf{u}_h^n}{2}$. Thus, the kinetic energy flux across the interface

$$\int_{\Gamma_{t_{n+1/2}}^w} \left(\frac{\mathbf{u}_h^{n+1} + \mathbf{u}_h^n}{2} - \mathbf{w}_h^{n+1/2} \right) \left| \frac{\mathbf{u}_h^{n+1} + \mathbf{u}_h^n}{2} \right|^2 d\Gamma$$

obtained from the integration by parts of the term $\mathcal{B}(\mathbf{w}_h^{n+1/2}, \frac{\mathbf{u}_h^{n+1}+\mathbf{u}_h^n}{2}, \frac{\mathbf{u}_h^{n+1}+\mathbf{u}_h^n}{2}, \frac{\mathbf{u}_h^{n+1}+\mathbf{u}_h^n}{2})_{\Omega_{t_{n+1/2}}}$, is identically zero and this contributes to the stability of the coupled scheme. Moreover, by taking as a test function $(\mathbf{v}_h, \xi_H) = (\Delta t \frac{\mathbf{u}_h^{n+1}+\mathbf{u}_h^n}{2}, \Delta t \frac{\dot{\eta}_H^{n+1}+\dot{\eta}_H^n}{2})$, which is an admissible test function, the most of the fluid and structure terms can be estimated as in Lemmas 4.8.1 (for the structure) and 3.5.2 (for the fluid). However, as pointed out in Lemma 3.5.2, the Crank-Nicolson scheme (3.5.6) is not unconditionally stable and we were not able to obtain, for this coupled algorithm, an result analogous to the one stated in Proposition 4.7.1 or 4.8.1.

4.9 Substructuring iterations

All the coupling algorithms presented until now are fully implicit. As already mentioned in Section 4.6, they should be solved at each time step by an iterative method. We detail here the Block Gauss-Seidel strategy applied to Problem 4.8.1 since it is indeed the one actually employed in the numerical simulations presented in Section 4.11. Furthermore, we will consider Problem 4.8.1 with Neumann boundary conditions instead of the Dirichlet ones, since it is more interesting for our application. The generalisation of this strategy to the other two implicit coupled Problems 4.7.1 and 4.8.2 is straightforward.

Given the solution $\mathbf{u}_h^n$, p_h^n, η_H^n and $\dot{\eta}_H^n$ of Problem 4.8.1 at time step t_n, we denote with $\mathbf{u}_h^{n+1,k}$, $p_h^{n+1,k}$, $\eta_H^{n+1,k}$ and $\dot{\eta}_H^{n+1,k}$ the solutions obtained at the $k-$th subiteration at time step t_{n+1}. With $\mathcal{A}_{h,t}^k$ we will indicate the ALE mapping computed at the $k-$th subiteration. Keeping in mind the decomposition into two sub-problems of the coupled problem, the block Gauss-Seidel iterative method reads as follows :

compute a suitable extrapolation $\eta_H^{n+1,0}$ and $\dot{\eta}_H^{n+1,0}$ of the structure displacement at t_{n+1}, for instance by taking

$$\eta_H^{n+1,0} = \eta_H^n + \Delta t \dot{\eta}_H^n, \qquad \dot{\eta}_H^{n+1,0} = \dot{\eta}_H^n. \tag{4.9.1}$$

then, for $k = 1, 2, \ldots$

1. *compute the ALE mapping $\mathcal{A}_{h,t}^k$ in $[t_n, t_{n+1}]$ by*

$$\begin{cases} \mathcal{P}_{\mathcal{A}}\left(\mathcal{A}_{h,t_{n+1}}^k, \mathbf{z}_h\right) = 0 & \forall \mathbf{z}_h \in \hat{\mathbf{V}}_h^F(\Omega_0), \quad \mathbf{z}_h = \mathbf{0} \text{ on } \partial\Omega_0, \\ \mathcal{A}_{h,t_{n+1}}^k = \mathbf{Y} + \Pi_h^H \eta_H^{n+1,k-1} \mathbf{e}_r \quad \text{on } \Gamma_0^w, & \mathcal{A}_{h,t_{n+1}}^k = \mathbf{g}_\eta \quad \text{on } \partial\Omega_0 \setminus \Gamma_0^w, \\ \mathcal{A}_{h,t}^k = \dfrac{t-t_n}{\Delta t}\mathcal{A}_{h,t_{n+1}}^k + \dfrac{t_{n+1}-t}{\Delta t}\mathcal{A}_{h,t_n}, & t \in [t_n, t_{n+1}]. \end{cases} \tag{4.9.2}$$

2. *compute the fluid solution* $\mathbf{u}_h^{n+1,k}$ *and* $p_h^{n+1,k}$ *by solving the fluid sub-problem*

$$\begin{cases} \dfrac{\rho}{\Delta t}\displaystyle\int_{\Omega_{t_{n+1}}} \mathbf{u}_h^{n+1,k}\cdot\mathbf{v}_h\,d\Omega - \dfrac{\rho}{\Delta t}\int_{\Omega_{t_n}} \mathbf{u}_h^{n}\cdot\mathbf{v}_h\,d\Omega + \mathcal{B}(\mathbf{w}_h^{n+1/2,k},\mathbf{u}_h^{*},\mathbf{u}_h^{n+1,k},\mathbf{v}_h)_{\Omega_{t_{n+1/2}}} \\ \qquad +\mathcal{D}(\mathbf{v}_h,p_h^{n+1,k})_{\Omega_{t_{n+1/2}}} = \displaystyle\int_{\Omega_{t_{n+1/2}}} \mathbf{f}^{n+1/2}\cdot\mathbf{v}_h\,d\Omega + \sum_{i=1,2}\int_{S_i}\boldsymbol{\sigma}_i^{n+1/2}\cdot\mathbf{v}_h\,d\Gamma \\ \qquad\qquad\qquad\qquad\qquad\qquad\qquad\qquad \forall(\mathbf{v}_h,\xi_H)\in\mathbf{V}_{h,H}^{int}(t) \\ \mathcal{D}(\mathbf{u}_h^{n+1,k},q_h)_{\Omega_{t_{n+1/2}}} = 0 \qquad\qquad \forall q_h\in Q_h(\Omega_t) \\ \mathbf{u}_h^{n+1,k}\circ\mathcal{A}_{h,t_{n+1}}^{k} = \Pi_h^H\dfrac{\eta_H^{n+1,k-1}-\eta_H^n}{\Delta t}\mathbf{e}_r, \qquad \text{on } \Gamma_0^w \end{cases} \tag{4.9.3}$$

3. *compute the structure solution* $\tilde{\eta}_H^{n+1,k}$, $\tilde{\dot{\eta}}_H^{n+1,k}$ *by solving the structure sub-problem*

$$\begin{cases} (\dfrac{\tilde{\eta}_H^{n+1,k}-\eta_H^n}{\Delta t},\xi_H)_{\Gamma_0^w} = (\dfrac{\tilde{\dot{\eta}}_H^{n+1,k}+\dot{\eta}_H^n}{2},\xi_H)_{\Gamma_0^w} \qquad \forall\xi_H\in V_H^S(\Gamma_0^w) \\ \tilde{\rho}_w(\dfrac{\tilde{\dot{\eta}}_H^{n+1,k}-\dot{\eta}_H^n}{\Delta t},\xi_H)_{\Gamma_0^w} + \mathcal{E}(\dfrac{\tilde{\eta}_H^{n+1,k}+\eta_H^n}{2},\xi_H)_{\Gamma_0^w} \\ \quad +\mathcal{V}(\dfrac{\tilde{\dot{\eta}}_H^{n+1,k}+\dot{\eta}_H^n}{2},\xi_H)_{\Gamma_0^w} + \sqrt{\dfrac{\tilde{\rho}_w}{a}}\left(a\dfrac{\tilde{\dot{\eta}}_H^{n+1,k}+\dot{\eta}_H^n}{2} + c\dfrac{\tilde{\eta}_H^{n+1,k}-\dot{\eta}_H^n}{\Delta t}\right)\xi_H\Big|_{z=0,L} \\ \quad = -\displaystyle\int_{\Gamma_0^w} p_{ext}^{n+1/2}\xi_H\,dz + <\Phi(\mathbf{u}_h^{n+1,k},p_h^{n+1,k}),\mathcal{R}_h(\xi_H)> \qquad \forall\xi_H\in V_H^S(\Gamma_0^w) \end{cases} \tag{4.9.4}$$

where the forcing term $<\Phi(\mathbf{u}_h^{n+1,k},p_h^{n+1,k}),\mathcal{R}_h(\xi_H)>$ *is defined as in (4.8.3)*

4. *relax the structure displacement and velocity by*

$$\begin{cases} \eta_H^{n+1,k} = \omega\tilde{\eta}_H^{n+1,k} + (1-\omega)\eta_H^{n+1,k-1}, \\ \dot{\eta}_H^{n+1,k} = \omega\tilde{\dot{\eta}}_H^{n+1,k} + (1-\omega)\dot{\eta}_H^{n+1,k-1} \end{cases} \tag{4.9.5}$$

5. *go back to 1. and iterate until convergence of* $\eta_H^{n+1,k}$, $\dot{\eta}_H^{n+1,k}$, $\mathbf{u}_h^{n+1,k}$ *and* $p_h^{n+1,k}$.

The fluid equations in step 2. of the algorithm can be taken *fully implicit* if $\mathbf{u}_h^{*}=\mathbf{u}_h^{n+1,k}$ or they can be linearised with $\mathbf{u}_h^{*}=\mathbf{u}_h^{n+1,k-1}$. In both cases, once convergence is reached, the final solution $\mathbf{u}_h^{n+1}$, p_h^{n+1}, η_H^{n+1} and $\dot{\eta}_H^{n+1}$ satisfies the coupled Problem 4.8.1. Observe that, if we linearise (4.9.3) with $\mathbf{u}_h^{*}=\mathbf{u}_h^{n}$ as suggested in Chapter 3, we do not recover the solution of the coupled Problem 4.8.1 and thus the stability result of the Proposition 4.8.1.
This iterative strategy is very costly since at each sub-iteration the matrices corresponding to the fluid discretisation (4.9.3) have to be recomputed on the new configuration and for the new convective term $\mathbf{w}_h^{n+1/2,k}$ and $\mathbf{u}_h^{*}$ if taken equal to $\mathbf{u}_h^{n+1,k-1}$.
For the start up of the algorithm we can consider other extrapolations than the one proposed in (4.9.1). We have verified numerically that the following strategy

- take $\eta_H^{n+1,0}$ and $\dot{\eta}_H^{n+1,0}$ as the solution of the structural equation with forcing term $< \Phi(\mathbf{u}_h^n, p_h^n), \mathcal{R}_h(\xi_H) >$, i.e.

$$\begin{cases} (\dfrac{\eta_H^{n+1,0} - \eta_H^n}{\Delta t}, \xi_H)_{\Gamma_0^w} = (\dfrac{\dot{\eta}_H^{n+1,0} + \dot{\eta}_H^n}{2}, \xi_H)_{\Gamma_0^w} & \forall \xi_H \in V_H^S(\Gamma_0^w) \\ \tilde{\rho}_w(\dfrac{\dot{\eta}_H^{n+1,0} - \dot{\eta}_H^n}{\Delta t}, \xi_H)_{\Gamma_0^w} + \mathcal{E}(\dfrac{\eta_H^{n+1,0} + \eta_H^n}{2}, \xi_H)_{\Gamma_0^w} \\ \quad + \mathcal{V}(\dfrac{\dot{\eta}_H^{n+1,0} + \dot{\eta}_H^n}{2}, \xi_H)_{\Gamma_0^w} + \sqrt{\dfrac{\tilde{\rho}_w}{a}} \left(a \dfrac{\dot{\eta}_H^{n+1,0} + \dot{\eta}_H^n}{2} + c \dfrac{\dot{\eta}_H^{n+1,0} - \dot{\eta}_H^n}{\Delta t} \right) \xi_H \Big|_{z=0,L} \\ \quad = - \displaystyle\int_{\Gamma_0^w} p_{ext}^{n+1/2} \xi_H \, dz + < \Phi(\mathbf{u}_h^n, p_h^n), \mathcal{R}_h(\xi_H) > & \forall \xi_H \in V_H^S(\Gamma_0^w) \end{cases} \tag{4.9.6}$$

provide a much better initial guess than (4.9.1) and allows to reduce by about a factor two the number of sub-iterations.

4.10 A "semi-implicit" coupled algorithm

The last coupled algorithm that we present is obtained by taking a Leap-Frog discretisation for the structure and an Implicit Euler (or a Crank-Nicolson) discretisation for the fluid. The Leap-Frog scheme, applied to the structural equation with a given forcing term f_S^n at each time step t_n, reads

$$\begin{cases} \tilde{\rho}_w(\dfrac{\eta_H^{n+1} - 2\eta_H^n + \eta_H^{n-1}}{\Delta t^2}, \xi_H)_{\Gamma_0^w} + \mathcal{E}(\eta_H^n, \xi_H)_{\Gamma_0^w} + \mathcal{V}(\dfrac{\eta_H^{n+1} - \eta_H^{n-1}}{2\Delta t}, \xi_H)_{\Gamma_0^w} = < f_S^n, \xi_H >, \\ \qquad\qquad \forall \xi_H \in V_H^S(\Gamma_0^w) \cap V_0^S(\Gamma_0^w), \quad n \geq 1 \\ \eta_H^0 = \eta_{H0}, \quad \eta_H^1 = \eta_{H0} + \Delta t \dot{\eta}_{H0} \end{cases} \tag{4.10.1}$$

Scheme (4.10.1) is explicit and second order accurate. The stability condition associated to this discretisation will be derived in Lemma 4.10.1. If we consider an implicit discretisation for the fluid equation with interface coupling condition as in Problems 4.7.1 or 4.8.1, i.e.

$$\mathbf{u}_h^n \circ \mathcal{A}_{h,t_n}\big|_{\Gamma_0^w} = \Pi_h^H \frac{\eta_H^n - \eta_H^{n-1}}{\Delta t} \mathbf{e}_r, \tag{4.10.2}$$

we obtain a staggered algorithm. Indeed, given the structure displacement η_H^n at time step t_n, we compute first the fluid solution $\mathbf{u}_h^n$, p_h^n at time step t_n with coupling condition (4.10.2), then we advance in time and we compute the new structure solution η_H^{n+1} at t_{n+1} (see also fig. 4.6). Unfortunately, as already mentioned in Section 4.6, such a staggered algorithm is unstable when applied to our fluid-structure interaction problem with realistic physiological parameters. A possible remedy consists in making the coupling condition (4.10.2) implicit by taking

$$\mathbf{u}_h^n \circ \mathcal{A}_{h,t_n}\big|_{\Gamma_0^w} = \Pi_h^H \frac{\eta_H^{n+1} - \eta_H^{n-1}}{2\Delta t} \mathbf{e}_r. \tag{4.10.3}$$

We thus obtain the coupled algorithm

Problem 4.10.1 (Leap-Frog/Implicit Euler) *Given the initial solution* $\mathbf{u}_{h0}$, η_{H0} *and* $\dot{\eta}_{H0}$, *set*

$$\eta_H^1 = \eta_{H0} + \Delta t \dot{\eta}_{H0},$$

and find $\mathbf{u}_h^n \in \mathbf{V}_h^F(\Omega_t)$, $p_h^n \in Q_h(\Omega_t)$ *and* $\eta_H^{n+1} \in V_H^S(\Gamma_0^w)$ *with*

$$\mathbf{u}_h^n = \mathbf{\Phi}_i^n \quad \text{on } \mathcal{S}_i,\ i = 1,2, \qquad \text{and}$$
$$\eta_H^{n+1} = \alpha_1^{n+1} \quad \text{at } z = 0, \qquad \eta_H^{n+1} = \alpha_2^{n+1} \quad \text{at } z = L,$$

such that

$$\begin{cases} \mathcal{P}_{\mathcal{A}}(\mathcal{A}_{h,t_n}, \mathbf{z}_h) = 0 & \forall \mathbf{z}_h \in \hat{\mathbf{V}}_h^F(\Omega_0), \quad \mathbf{z}_h = \mathbf{0} \text{ on } \partial\Omega_0, \\ \mathcal{A}_{h,t_n} = \mathbf{Y} + \Pi_h^H \eta_H^n \mathbf{e}_r \quad \text{on } \Gamma_0^w, \qquad \mathcal{A}_{h,t_n} = \mathbf{g}_\eta \quad \text{on } \partial\Omega_0 \setminus \Gamma_0^w, & \text{(Ph-ALE)} \\ \mathcal{A}_{h,t} = \dfrac{t - t_{n-1}}{\Delta t}\mathcal{A}_{h,t_n} + \dfrac{t_n - t}{\Delta t}\mathcal{A}_{h,t_{n-1}}, & t \in [t_{n-1}, t_n] \end{cases}$$

and

$$\begin{cases} \tilde{\rho}_w\Big(\dfrac{\eta_H^{n+1} - 2\eta_H^n + \eta_H^{n-1}}{\Delta t^2}, \xi_H\Big)_{\Gamma_0^w} + \mathcal{E}(\eta_H^n, \xi_H)_{\Gamma_0^w} + \mathcal{V}\Big(\dfrac{\eta_H^{n+1} - \eta_H^{n-1}}{2\Delta t}, \xi_H\Big)_{\Gamma_0^w} \\ \quad + \dfrac{\rho}{\Delta t}\displaystyle\int_{\Omega_{t_n}} \mathbf{u}_h^n \cdot \mathbf{v}_h \, d\Omega - \dfrac{\rho}{\Delta t}\int_{\Omega_{t_{n-1}}} \mathbf{u}_h^{n-1} \cdot \mathbf{v}_h \, d\Omega + \mathcal{B}(\mathbf{w}_h^{n-1/2}, \mathbf{u}_h^*, \mathbf{u}_h^n, \mathbf{v}_h)_{\Omega_{t_{n-1/2}}} \\ \quad + \mathcal{D}(\mathbf{v}_h, p_h^n)_{\Omega_{t_{n-1/2}}} = \displaystyle\int_{\Omega_{t_{n-1/2}}} \mathbf{f}^{n-1/2} \cdot \mathbf{v}_h \, d\Omega - \int_{\Gamma_0^w} p_{ext}^n \xi_H \, dz \\ \qquad\qquad \forall (\mathbf{v}_h, \xi_H) \in \mathbf{V}_{h,H}(t) \cap \mathbf{V}_0(t) \\ \mathcal{D}(\mathbf{u}_h^n, q_h)_{\Omega_{t_{n-1/2}}} = 0 \qquad\qquad \forall q_h \in Q_h(\Omega_t) \end{cases} \quad \text{(Ph-FS)}$$

$$\mathbf{u}_h^n \circ \mathcal{A}_{h,t_n} = \Pi_h^H \frac{\eta_H^{n+1} - \eta_H^{n-1}}{2\Delta t}\mathbf{e}_r, \qquad \text{on } \Gamma_0^w \qquad \text{(ICCh)}$$

for all $n \geq 1$.

In the first equation of (Ph-FS) we have let the possibility to linearise the fluid terms with an extrapolated velocity $\mathbf{u}_h^*$.

Observe that, once the structure displacement η_H^n at time step t^n is available, the ALE mapping problem (Ph-ALE) can be solved, providing the ALE mapping $\mathcal{A}_{h,t}$ in the time interval $[t_{n-1}, t_n]$. Hence, at each time step, the computation of the ALE mapping is decoupled from that of $\mathbf{u}_h^n$, p_h^n and η_H^{n+1}. This implies that, once computed the mapping $\mathcal{A}_{h,t}$, the fluid domain configuration is no more an unknown in the sub-problem (Ph-FS). For this reason we have addressed to Problem 4.10.1 as a "semi-implicit" algorithm, since we treat explicitly the geometry and implicitly the interface velocity.

Moreover, if we linearise the fluid terms with a suitable velocity $\mathbf{u}_h^*$, system (Ph-FS) turns out to be *linear*. It can be solved, for instance, by Block Gauss-Seidel subiterations of the

type shown in Section 4.9 with the great advantage that, at each subiteration, the fluid sub-problem is solved on the same domain, thus avoiding the recomputation of all fluid matrices. Moreover, we can apply in this case all the techniques to accelerate convergence that are well suited for linear problems.
In the case where the linearised velocity $\mathbf{u}_h^*$ is taken in such a way that

$$\mathbf{u}_h^* = \mathbf{w}_h \qquad \text{on } \Gamma_t^w, \qquad \text{i.e.} \quad \mathbf{u}_h^* \circ \mathcal{A}_{h,t_n} = \Pi_h^H \frac{\eta_H^n - \eta_H^{n-1}}{\Delta t}, \tag{4.10.4}$$

we can prove, (see Proposition 4.10.1) a conditional stability result, for this coupled scheme, similar to that holding for the implicit Problems 4.7.1 and 4.8.1, with a stability condition governed only by the structure solver. In other terms, the fluid-structure coupling proposed in Problem 4.10.1 does not engender a further condition on the time step.
This scheme is very attractive since it is linear and (conditionally) stable. Its investigation is in progress. We will not present in this work any numerical result.

Remark 4.10.1 *A linearised velocity $\mathbf{u}_h^*$ that satisfies condition (4.10.4) can be obtained, for instance, by solving a supplementary fluid-problem with (4.10.4) as boundary condition; i.e. we take $\mathbf{u}_h^*$ that satisfies*

$$\begin{cases} \dfrac{\rho}{\Delta t}\displaystyle\int_{\Omega_{t_n}} \mathbf{u}_h^* \cdot \mathbf{v}_h \, d\Omega - \dfrac{\rho}{\Delta t}\int_{\Omega_{t_{n-1}}} \mathbf{u}_h^{n-1} \cdot \mathbf{v}_h \, d\Omega + \mathcal{B}(\mathbf{w}_h^{n-1/2}, \mathbf{u}_h^{n-1}, \mathbf{u}_h^*, \mathbf{v}_h)_{\Omega_{t_{n-1/2}}} \\ \qquad + \mathcal{D}(\mathbf{v}_h, p_h^*)_{\Omega_{t_{n-1/2}}} = \displaystyle\int_{\Omega_{t_{n-1/2}}} \mathbf{f}^{n-1/2} \cdot \mathbf{v}_h \, d\Omega \qquad \forall (\mathbf{v}_h, \xi_H) \in \mathbf{V}_{h,H}^{int}(t) \cap \mathbf{V}_0(t) \\ \mathcal{D}(\mathbf{u}_h^*, q_h)_{\Omega_{t_{n-1/2}}} = 0 \qquad \forall q_h \in Q_h(\Omega_t) \cap Q_0(\Omega_t) \\ \mathbf{u}_h^* \circ \mathcal{A}_{h,t_n} = \Pi_h^H \dfrac{\eta_H^n - \eta_H^{n-1}}{\Delta t} \mathbf{e}_r, \qquad \text{on } \Gamma_0^w \end{cases} \tag{4.10.5}$$

and $\mathbf{u}_h^* = \mathbf{\Phi}_i^n$ on $\mathcal{S}_i$ as for the velocity $\mathbf{u}_h^n$.

Remark 4.10.2 *We will derive in Lemma 4.10.1 the stability condition for the Leap-Frog discretisation (4.10.1). In hemodynamics applications, this condition might be too restrictive, since the elasticity coefficient b of the arterial wall is much larger than the wall mass $\tilde{\rho}_w$. In physiological applications the condition on the time step is normally of the order of $\Delta t \approx 10^{-4}$ but it may be much more restrictive whenever we want to simulate the presence in arteries of stents or prostheses which may have a high Young modulus (see e.g. [31]).*
In these cases, an implicit solver should be preferred for the structure as, for instance, the mid-point one. Following the same philosophy which led us to build Problem 4.10.1, we can easily obtain a "semi-implicit" version of coupled Problem 4.8.1 (which employs an implicit structure solver) by taking a suitable extrapolation $\tilde{\eta}_H^{n+1}$ of the structure displacement η_H^{n+1} at time step t^{n+1}. Then we solve the fluid equations on the configuration identified by $\tilde{\eta}_H^{n+1}$ and with a linearised velocity $\mathbf{u}_h^*$ computed as in (4.10.5) while keeping implicit coupling conditions between fluid and structure velocity at the interface.

4.10.1 Stability analysis of the coupled algorithm

We present, now, the results concerning the stability of coupled Problem 4.10.1. We first prove the following

Lemma 4.10.1 *For any given forcing term $f_S \in C^0(0,T;\left(V_0^S(\Gamma_0^w)\right)')$, the Leap-Frog discretisation (4.10.1) of the structure equation is stable under the condition*

$$\Delta t \leq \sqrt{\frac{2\tilde{\rho}_w}{aCH^{-2}+b}} \tag{4.10.6}$$

where C is the constant of the inverse inequality $\|\frac{\partial \eta_H}{\partial z}\|_{\Gamma_0^w} \leq CH^{-2}\|\eta_H\|_{\Gamma_0^w}$. Moreover, the following a-priori estimate holds

$$\left(\tilde{\rho}_w - \frac{\Delta t^2(aCH^{-2}+b)}{2}\right)\left\|\frac{\eta_H^{n+1}-\eta_H^n}{\Delta t}\right\|^2_{L^2(\Gamma_0^w)} + \frac{1}{2}\left[\left\|\eta_H^{n+1}\right\|^2_{\mathcal{E}} + \left\|\eta_H^n\right\|^2_{\mathcal{E}}\right]$$
$$+ c\Delta t\sum_{i=1}^{n}\left\|\frac{\partial}{\partial z}\left(\frac{\eta_H^{n+1}-\eta_H^{n-1}}{2\Delta t}\right)\right\|^2_{L^2(\Gamma_0^w)} \leq \tilde{\rho}_w\left\|\dot{\eta}_{H0}\right\|^2_{L^2(\Gamma_0^w)} + \frac{1}{2}\left\|\eta_{H0}\right\|^2_{\mathcal{E}} + \frac{1}{2}\left\|\Delta t\dot{\eta}_{H0}\right\|^2_{\mathcal{E}}$$
$$+ \frac{1}{2}\left\|\eta_{H0}+\Delta t\dot{\eta}_{H0}\right\|^2_{\mathcal{E}} + \frac{\Delta t(1+C_{\Gamma_0^w})}{c}\sum_{i=1}^{n}\left\|f_S^n\right\|^2_{H^{-1}(\Gamma_0^w)} \tag{4.10.7}$$

for all $n \geq 1$.

Proof. We take in (4.10.1) $\xi_H = \eta_H^{n+1} - \eta_H^n$. Then,

- $$(\frac{\eta_H^{n+1}-2\eta_H^n+\eta_H^{n-1}}{\Delta t^2}, \eta_H^{n+1}-\eta_H^{n-1})_{\Gamma_0^w}$$
$$= (\frac{(\eta_H^{n+1}-\eta_H^n)-(\eta_H^n-\eta_H^{n-1})}{\Delta t^2}, (\eta_H^{n+1}-\eta_H^n)+(\eta_H^n-\eta_H^{n-1}))_{\Gamma_0^w}$$
$$= \left\|\frac{\eta_H^{n+1}-\eta_H^n}{\Delta t}\right\|^2_{L^2(\Gamma_0^w)} - \left\|\frac{\eta_H^n-\eta_H^{n-1}}{\Delta t}\right\|^2_{L^2(\Gamma_0^w)}$$
- $$\mathcal{V}(\frac{\eta_H^{n+1}-\eta_H^{n-1}}{2\Delta t}, \eta_H^{n+1}-\eta_H^{n-1})_{\Gamma_0^w} = 2c\Delta t\left\|\frac{\partial}{\partial z}\left(\frac{\eta_H^{n+1}-\eta_H^{n-1}}{2\Delta t}\right)\right\|^2_{L^2(\Gamma_0^w)}$$
- $$< f_S^n, \eta_H^{n+1}-\eta_H^{n-1} > \leq c\Delta t\left\|\frac{\partial}{\partial z}\left(\frac{\eta_H^{n+1}-\eta_H^{n-1}}{2\Delta t}\right)\right\|^2_{L^2(\Gamma_0^w)} + \frac{\Delta t(1+C_{\Gamma_0^w})}{c}\left\|f_S^n\right\|^2_{H^{-1}(\Gamma_0^w)}$$

Putting together these estimates we obtain

$$\tilde{\rho}_w\left\|\frac{\eta_H^{n+1}-\eta_H^n}{\Delta t}\right\|^2_{L^2(\Gamma_0^w)} + \mathcal{E}(\eta_H^n, \eta_H^{n+1})_{\Gamma_0^w} + c\Delta t\left\|\frac{\partial}{\partial z}\left(\frac{\eta_H^{n+1}-\eta_H^{n-1}}{2\Delta t}\right)\right\|^2_{L^2(\Gamma_0^w)}$$
$$\leq \tilde{\rho}_w\left\|\frac{\eta_H^n-\eta_H^{n-1}}{\Delta t}\right\|^2_{L^2(\Gamma_0^w)} + \mathcal{E}(\eta_H^n, \eta_H^{n-1})_{\Gamma_0^w} + \frac{\Delta t(1+C_{\Gamma_0^w})}{c}\left\|f_S^n\right\|^2_{H^{-1}(\Gamma_0^w)}.$$

Since the form $\mathcal{E}(\cdot,\cdot)_{\Gamma_0^w}$ is symmetric, by summing over $n = 1, 2, \ldots$ we have

$$\tilde{\rho}_w \left\| \frac{\eta_H^{n+1} - \eta_H^n}{\Delta t} \right\|^2_{L^2(\Gamma_0^w)} + \mathcal{E}(\eta_H^n, \eta_H^{n+1})_{\Gamma_0^w} + c\Delta t \sum_{i=1}^{n} \left\| \frac{\partial}{\partial z} \left(\frac{\eta_H^{n+1} - \eta_H^{n-1}}{2\Delta t} \right) \right\|^2_{L^2(\Gamma_0^w)}$$
$$\leq \tilde{\rho}_w \left\| \dot{\eta}_{H0} \right\|^2_{L^2(\Gamma_0^w)} + \mathcal{E}(\eta_{H0} + \Delta t \dot{\eta}_{H0}, \eta_{H0})_{\Gamma_0^w} + \frac{\Delta t(1 + C_{\Gamma_0^w})}{c} \sum_{i=1}^{n} \left\| f_S^n \right\|^2_{H^{-1}(\Gamma_0^w)} \quad (4.10.8)$$

The elastic term $\mathcal{E}(\eta_H^n, \eta_H^{n+1})_{\Gamma_0^w}$ can be manipulated as

- $\mathcal{E}(\eta_H^n, \eta_H^{n+1})_{\Gamma_0^w} = \mathcal{E}(\eta_H^n, \eta_H^{n+1} - \eta_H^n)_{\Gamma_0^w} + \left\| \eta_H^n \right\|^2_{\mathcal{E}} = \frac{1}{2} \left[\left\| \eta_H^{n+1} \right\|^2_{\mathcal{E}} + \left\| \eta_H^n \right\|^2_{\mathcal{E}} - \left\| \eta_H^{n+1} - \eta_H^n \right\|^2_{\mathcal{E}} \right]$
- $\mathcal{E}(\eta_{H0} + \Delta t \dot{\eta}_{H0}, \eta_{H0})_{\Gamma_0^w} \leq \frac{1}{2} \left[\left\| \eta_{H0} \right\|^2_{\mathcal{E}} + \left\| \Delta t \dot{\eta}_{H0} \right\|^2_{\mathcal{E}} + \left\| \eta_{H0} + \Delta t \dot{\eta}_{H0} \right\|^2_{\mathcal{E}} \right]$

and (4.10.8) becomes

$$\tilde{\rho}_w \left\| \frac{\eta_H^{n+1} - \eta_H^n}{\Delta t} \right\|^2_{L^2(\Gamma_0^w)} + \frac{1}{2} \left[\left\| \eta_H^{n+1} \right\|^2_{\mathcal{E}} + \left\| \eta_H^n \right\|^2_{\mathcal{E}} \right] - \frac{1}{2} \left\| \eta_H^{n+1} - \eta_H^n \right\|^2_{\mathcal{E}}$$
$$+ c\Delta t \sum_{i=1}^{n} \left\| \frac{\partial}{\partial z} \left(\frac{\eta_H^{n+1} - \eta_H^{n-1}}{2\Delta t} \right) \right\|^2_{L^2(\Gamma_0^w)} \leq \tilde{\rho}_w \left\| \dot{\eta}_{H0} \right\|^2_{L^2(\Gamma_0^w)} + \frac{1}{2} \left\| \eta_{H0} \right\|^2_{\mathcal{E}} + \frac{1}{2} \left\| \Delta t \dot{\eta}_{H0} \right\|^2_{\mathcal{E}}$$
$$+ \frac{1}{2} \left\| \eta_{H0} + \Delta t \dot{\eta}_{H0} \right\|^2_{\mathcal{E}} + \frac{\Delta t(1 + C_{\Gamma_0^w})}{c} \sum_{i=1}^{n} \left\| f_S^n \right\|^2_{H^{-1}(\Gamma_0^w)} \quad (4.10.9)$$

Finally, by applying the inverse inequality we have

$$- \left\| \eta_H^{n+1} - \eta_H^n \right\|^2_{\mathcal{E}} = -a \left\| \frac{\partial}{\partial z} (\eta_H^{n+1} - \eta_H^n) \right\|^2_{L^2(\Gamma_0^w)} - b \left\| \eta_H^{n+1} - \eta_H^n \right\|^2_{L^2(\Gamma_0^w)}$$
$$\geq -\Delta t^2 (aCH^{-2} + b) \left\| \frac{\eta_H^{n+1} - \eta_H^n}{\Delta t} \right\|^2_{L^2(\Gamma_0^w)}$$

and the final inequality (4.10.7) is thus obtained.

■

We present now, the main result on the stability of Problem 4.10.1

Proposition 4.10.1 *Let us consider a linearised velocity* $\mathbf{u}_h^*$ *in the first equation of (Ph-FS), in Problem 4.10.1, that satisfies condition (4.10.4). Then, the solution of the coupled Problem 4.10.1 with homogeneous Dirichlet boundary conditions and zero forcing terms (i.e.* $\mathbf{f}^{n-1/2} = \mathbf{0}$ *and* $p_{ext}^n = 0$ *for all* $n \geq 1$*) is uniformly bounded with respect to* n*, under the*

stability condition (4.10.6), and the following a-priori estimate holds

$$\left(\tilde{\rho}_w - \frac{\Delta t^2(aCH^{-2}+b)}{2}\right)\left\|\frac{\eta_H^{n+1}-\eta_H^n}{\Delta t}\right\|^2_{L^2(\Gamma_0^w)} + \frac{1}{2}\left[\|\eta_H^{n+1}\|^2_{\mathcal{E}} + \|\eta_H^n\|^2_{\mathcal{E}}\right]$$
$$+ 2c\Delta t\sum_{i=1}^{n}\left\|\frac{\partial}{\partial z}\left(\frac{\eta_H^{n+1}-\eta_H^{n-1}}{2\Delta t}\right)\right\|^2_{L^2(\Gamma_0^w)} + \rho\|\mathbf{u}_h^n\|^2_{L_2(\Omega_{t_n})} + 2\kappa\Delta t\sum_{i=1}^{n}\|\nabla_{\mathbf{x}}\mathbf{u}_h^n\|^2_{L_2(\Omega_{t_{n-1/2}})}$$
$$\leq \tilde{\rho}_w\|\dot{\eta}_{H0}\|^2_{L^2(\Gamma_0^w)} + \frac{1}{2}\|\eta_{H0}\|^2_{\mathcal{E}} + \frac{1}{2}\|\Delta t\dot{\eta}_{H0}\|^2_{\mathcal{E}} + \frac{1}{2}\|\eta_{H0}+\Delta t\dot{\eta}_{H0}\|^2_{\mathcal{E}} + \rho\|\mathbf{u}_{h0}\|^2_{L_2(\Omega_0)} \quad (4.10.10)$$

for all $n \geq 1$.

Proof. We take as a test function in the first equation of (Ph-FS) $(\mathbf{v}_h, \xi_H) = (2\Delta t\mathbf{u}_h^n, \eta_H^{n+1} - \eta_H^{n-1})$. Observe that, thanks to the interface coupling condition (ICCh), this is an admissible test function. Since we are considering a linearisation velocity $\mathbf{u}_h^*$ that satisfies (4.10.4), relation (4.6.5) is still applicable to the term $\mathcal{B}(\mathbf{w}_h^{n-1/2}, \mathbf{u}_h^*, \mathbf{u}_h^n, \mathbf{v}_h)_{\Omega_{t_{n-1/2}}}$. Manipulating the other fluid terms as in the proof of Proposition 4.7.1 and the structure terms as in Lemma 4.10.1, we obtain the inequality

$$\tilde{\rho}_w\left\|\frac{\eta_H^{n+1}-\eta_H^n}{\Delta t}\right\|^2_{L^2(\Gamma_0^w)} + \mathcal{E}(\eta_H^n, \eta_H^{n+1})_{\Gamma_0^w} + 2c\Delta t\left\|\frac{\partial}{\partial z}\left(\frac{\eta_H^{n+1}-\eta_H^{n-1}}{2\Delta t}\right)\right\|^2_{L^2(\Gamma_0^w)} + \rho\|\mathbf{u}_h^n\|^2_{L_2(\Omega_{t_n})}$$
$$+ 2\kappa\Delta t\|\nabla_{\mathbf{x}}\mathbf{u}_h^n\|^2_{L_2(\Omega_{t_{n-1/2}})} \leq \tilde{\rho}_w\left\|\frac{\eta_H^n-\eta_H^{n-1}}{\Delta t}\right\|^2_{L^2(\Gamma_0^w)} + \mathcal{E}(\eta_H^n, \eta_H^{n-1})_{\Gamma_0^w} + \rho\|\mathbf{u}_h^{n-1}\|^2_{L_2(\Omega_{t_{n-1}})} \quad (4.10.11)$$

Then, by summing over n ($n = 1, 2, \ldots$) and applying the inverse inequality as in Lemma 4.10.1, we obtain inequality (4.10.10).

■

4.11 Numerical results

We have considered the Neumann fluid-structure Problem 4.2.1 with zero forcing terms $\mathbf{f}$ and p_{ext}. The initial domain is a 2D rectangle of height $D = 1\,cm$ and length $L = 6\,cm$ whose upper and the lower edges are deformable in the vertical direction as shown in the picture on the right of figure 4.2. The fluid and the structure are initially at rest and Neumann boundary conditions have been imposed on the inflow and outflow sections; namely :

$$\mathbf{T}\cdot\mathbf{n} = \boldsymbol{\sigma}_1 = -\frac{P_{in}}{2}\left[1 - cos\left(\frac{\pi t}{2.5\,ms}\right)\right]\mathbf{n} \qquad \text{on } \mathcal{S}_1,$$
$$\mathbf{T}\cdot\mathbf{n} = \boldsymbol{\sigma}_2 = \mathbf{0} \qquad \text{on } \mathcal{S}_2$$

We have used the following parameters:

- **Fluid** : viscosity $\mu = 0.035\,poise$, density $\rho = 1\,gr/cm^3$.

- **Structure** : density $\rho_w = 1.1\, gr/cm^3$, thickness $h = 0.1\, cm$, Young modulus $E = 0.75 \cdot 10^6\, dyne/cm^2$ and Poisson coefficient $\nu = 0.5$.

  Thus, the coefficients appearing in the structure equation (4.1.9) are : $\tilde{\rho}_w = 0.11\, gr/cm^2$ and $b = 4 \cdot 10^5\, dyne/cm^3$. The other two coefficients have been taken as $a = 2.5 \cdot 10^4\, dyne$ and $c = 10^{-2}\, dyne \cdot sec$.

This simulation would represent the propagation, in a straight artery of length L, of a pressure pulse coming from the heart and traveling towards the peripheral vessels. The parameters chosen for the fluid and structure models have been taken in the physiological range for a human body. The amplitude P_{in} of the pressure pulse has been taken equal to $P_{in} = 2 \cdot 10^4\, dynes/cm^2$ ($\approx 15\, mmHg$) which is about 1/8 of the real amplitude in a cardiac beat. On the contrary the time duration of the pulse ($T = 5\, ms$) is much smaller than the one of a cardiac beat (systolic phase: about $0.3\, sec$). The input profile $\boldsymbol{\sigma}_1 \cdot \mathbf{n}$ is shown in figure 4.8. This choice has been made to amplify the propagative phenomena engendered by the fluid-

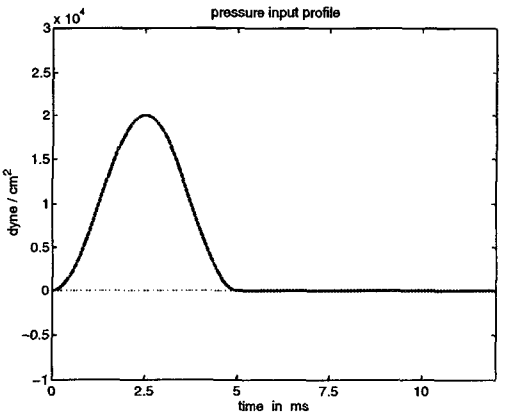

Figure 4.8: Input profile of the inflow Neumann boundary condition $\boldsymbol{\sigma}_1 \cdot \mathbf{n}$.

structure coupling and it allows to highlight many interesting aspects both in the modelling and in the numerical approximation of the coupled problem.

We have considered a conforming space discretisation between fluid and structure, consisting of $(\mathbb{P}_1 iso \mathbb{P}_2) - \mathbb{P}_1$ finite elements for the fluid and $\mathbb{P}_1$ finite elements for the structure.

First test case. We have investigated first the stability/instability of some coupled algorithms. In particular, we have considered an explicit staggered coupled algorithm obtained by employing a Leap-Frog discretisation for the structure equation, an Implicit Euler for the fluid and the explicit interface coupling condition (4.10.2). This algorithm revealed to be unstable for the chosen set of parameters regardless of the time step employed (provided the stability condition (4.10.6) for the explicit structure discretisation is satisfied) . We have verified that the stability condition depends substantially on the ratio between the structure and

Table 4.1: Stability/Instability of the explicit coupled algorithm for different choices of $\tilde{\rho}_w/\rho$ and L/D. Here we have taken $\rho = 1$ and $D = 1$

	$L = 2$	$L = 6$	$L = 10$
$\tilde{\rho}_w = 50$	stable	stable	stable
$\tilde{\rho}_w = 10$	stable	stable	**unstab.**
$\tilde{\rho}_w = 5$	stable	**unstab.**	**unstab.**
$\tilde{\rho}_w = 1$	stable	**unstab.**	**unstab.**
$\tilde{\rho}_w = 0.5$	**unstab.**	**unstab.**	**unstab.**
$\tilde{\rho}_w = 0.1$	**unstab.**	**unstab.**	**unstab.**

fluid densities $\tilde{\rho}_w/\rho$ and on the aspect ratio of the tube L/D but it seems almost independent of all the other parameter and (surprisingly) on Δt. Table 4.1 summarizes these results.
We have considered then the implicit *Mid-point/Implicit Euler* coupled algorithm presented in Problem 4.8.1 (in the following indicated briefly with *MP/IE*). We have solved the non-linear system arising at each time step by the iterative algorithm proposed in Section 4.9. We have verified that in those cases where the explicit Leap-Frog/Implicit Euler algorithm is unstable, a relaxation parameter ω strictly less then 1 is needed for the substructuring iterations to converge. The parameter ω can be taken in this case as an index of the "stiffness" of the fluid/structure coupling.
Table 4.2 shows the highest value of ω under which we have convergence of the substructuring iterations, as a function of the wall mass $\tilde{\rho}_w = \rho_w h$ and the length L of the tube. Again this value seems independent of the elastic constants of the structural model and of Δt.

Table 4.2: Values of ω which guarantee convergence of the implicit *MP/IE* algorithm.

	$L = 2$	$L = 6$	$L = 10$
$\tilde{\rho}_w = 50$	$\omega \leq 1$	$\omega \leq 1$	$\omega \leq 1$
$\tilde{\rho}_w = 10$	$\omega \leq 1$	$\omega \leq 1$	$\omega \leq \mathbf{0.9}$
$\tilde{\rho}_w = 5$	$\omega \leq 1$	$\omega \leq 1$	$\omega \leq \mathbf{0.6}$
$\tilde{\rho}_w = 1$	$\omega \leq 1$	$\omega \leq \mathbf{0.4}$	$\omega \leq \mathbf{0.1}$
$\tilde{\rho}_w = 0.5$	$\omega \leq \mathbf{0.9}$	$\omega \leq \mathbf{0.2}$	$\omega \leq \mathbf{0.09}$
$\tilde{\rho}_w = 0.1$	$\omega \leq \mathbf{0.4}$	$\omega \leq \mathbf{0.05}$	$\omega \leq \mathbf{0.01}$

Finally, we have tested the *Mid-Point/Crank-Nicolson* algorithm presented in Problem 4.8.2 (in the following indicated briefly with *MP/CN*). In this case the relaxation parameter should be chosen a little smaller than the one needed for the *MP/IE* algorithm.

Second test case. We have solved the problem with the two algorithms *MP/IE* and *MP/CN* on the structured mesh of 11×31 $\mathbb{P}_1$ fluid nodes (1281 $\mathbb{P}_1 iso \mathbb{P}_2$ nodes) shown in fig. 4.9 and with a time step $\Delta t = 10^{-4}$. In both cases we have solved the non-linear system arising at each time step through the fluid/structure substructuring algorithm presented in Section 4.9 with a first extrapolation of the structure displacement and velocity as in (4.9.6). The

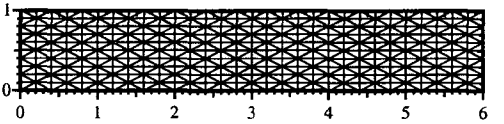

Figure 4.9: Structured mesh employed

stopping criterion adopted is

$$\max\left\{\frac{\|\eta_H^{n,k+1}-\eta_H^{n,k}\|_{L^\infty}}{\|\eta_H^{n,k+1}\|_{L^\infty}},\frac{\|\dot\eta_H^{n,k+1}-\dot\eta_H^{n,k}\|_{L^\infty}}{\|\dot\eta_H^{n,k+1}\|_{L^\infty}}\right\}\le 10^{-4},\qquad n=1,2,\dots \tag{4.11.1}$$

Moreover, for the *MP/IE* algorithm we have solver the Navier-Stokes equations at each time step with the Yosida projection scheme while for the *MP/CN* one we have employed three Richardson iterations preconditioned with the Yosida inexact factorisation as detailed in Chapter 3.

The results obtained with the *MP/CN* algorithm are reported in figures 4.10 and 4.11. In particular, figure 4.10 shows the fluid pressure together with the tube deformation every $2\,ms$. Observe that the structure displacement is not negligible (it has not been magnified in the figure!). Figure 4.11, instead, shows the axial fluid velocity inside the tube. The propagation of the pressure pulse inside the tube is evident. Associated to the pressure pulse we can observe also a wave of deformation of the vessel wall and a wave of flow rate. Quite surprisingly, even if the fluid model consists of incompressible Navier-Stokes equations, the coupled fluid/structure model behave like a propagative system. This is due to the compliance of the vessel wall. We will address again this phenomenon when discussing a reduced 1D model for fluid flows in compliant vessels (see Chapter 5).

To better highlight the propagative phenomena and the performances of the numerical schemes in capturing the wave velocity and shape, we have computed averaged quantities on each vertical line $\mathcal{S}_i$ of the mesh, corresponding to the position $z_i = ih$, $i = 0,\dots,30$ and $h = 0.2\,cm$, on the axis (see fig. 4.9). In particular, we have computed the diameter of the tube, the averaged pressure and the flux at each time step :

$$A^n(z_i)=\mathrm{meas}(\mathcal{S}_i^n),\qquad \bar p^n(z_i)=\frac{1}{\mathcal{S}_i^n}\int_{\mathcal{S}_i} p_h^n\,dr,\qquad Q^n(z_i)=\int_{\mathcal{S}_i}\mathbf{u}_h^n\cdot\mathbf{e}_z\,dr$$

Figures 4.12 and 4.13 show these three quantities at different instants. We have compared the solutions computed by the two algorithms with a solution obtained on the same mesh with a mush smaller time step ($\Delta t = 10^{-6}$).

It is clear from these plots that a propagating pulse is associated to all these three quantities. Moreover, the solution obtained with the *MP/CN* algorithm with $\Delta t = 10^{-4}$ is not distinguishable from that computed with a much smaller time step. On the contrary, the *MP/IE* algorithm turns out to be quite dissipative.

Figure 4.14 shows the number of substructuring iterations needed by the two coupled algorithms at each time step to satisfy the stopping criterion (4.11.1). As it can be seen in the figure, the number of subiterations is dramatically high. We remind that we have not investigated any accelerating technique for the substructuring iterations; yet, this aspect becomes

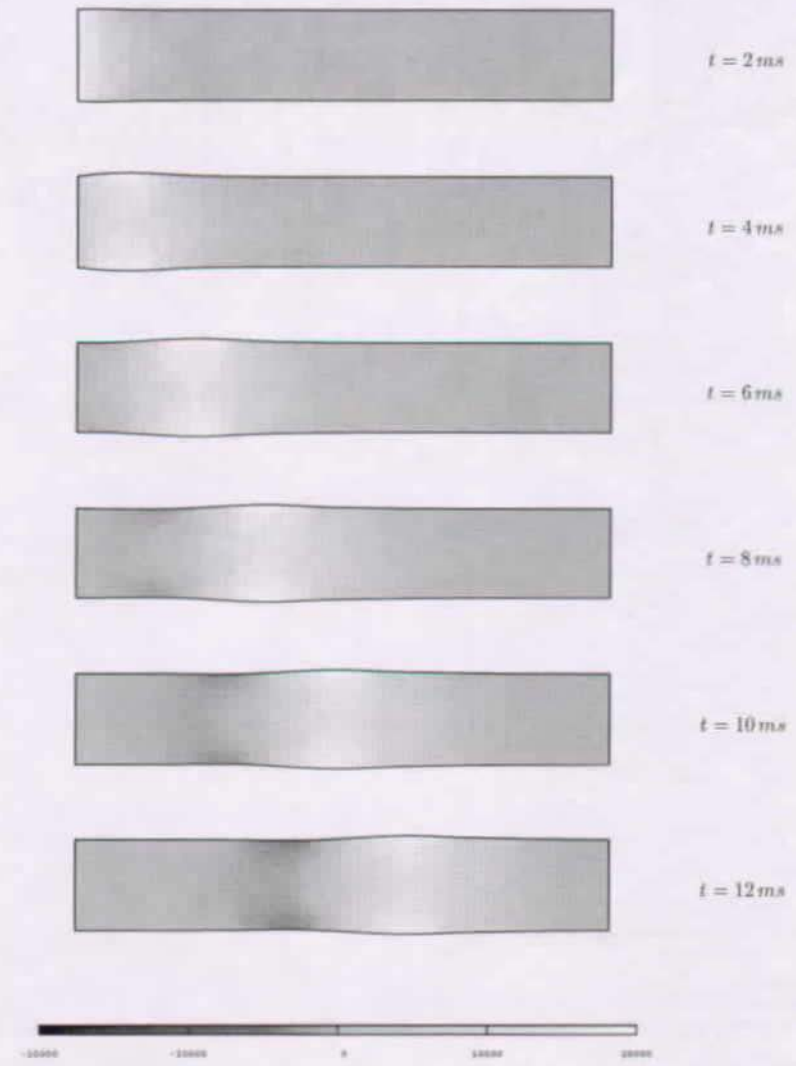

Figure 4.10: Pressure pulse entering at the *inflow* and homogeneous Neumann conditions at the *outflow*. Solutions every $2\,ms$. Note how the pressure pulse propagates inside the tube.

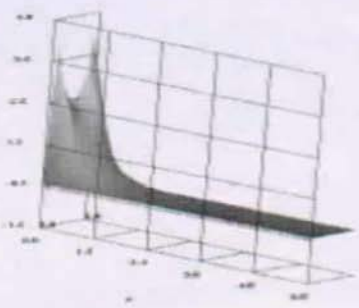

$t = 2\,ms$

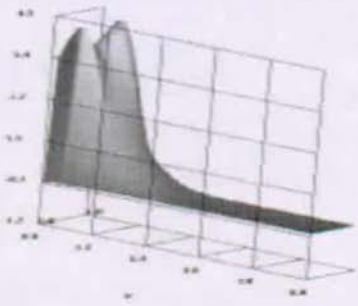

$t = 4\,ms$

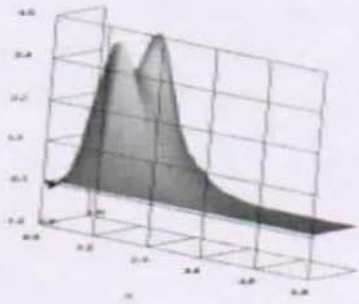

$t = 6\,ms$

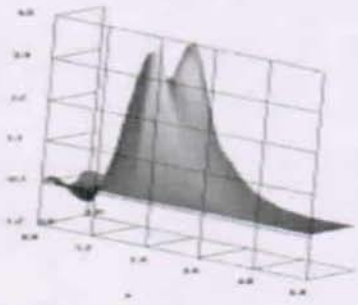

$t = 8\,ms$

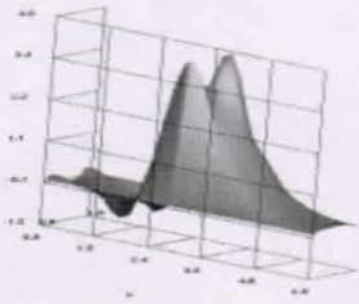

$t = 10\,ms$

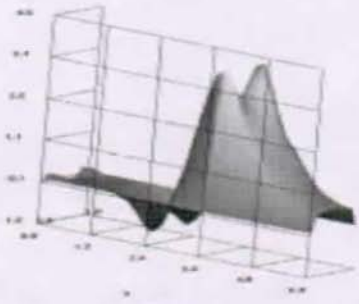

$t = 12\,ms$

Figure 4.11: Profile of the axial fluid velocity along the tube, every $2\,ms$. Observe the presence of a wave inside the tube. The actual velocity values, measured in cm/sec, are 10 times greater than the ones reported in the plots.

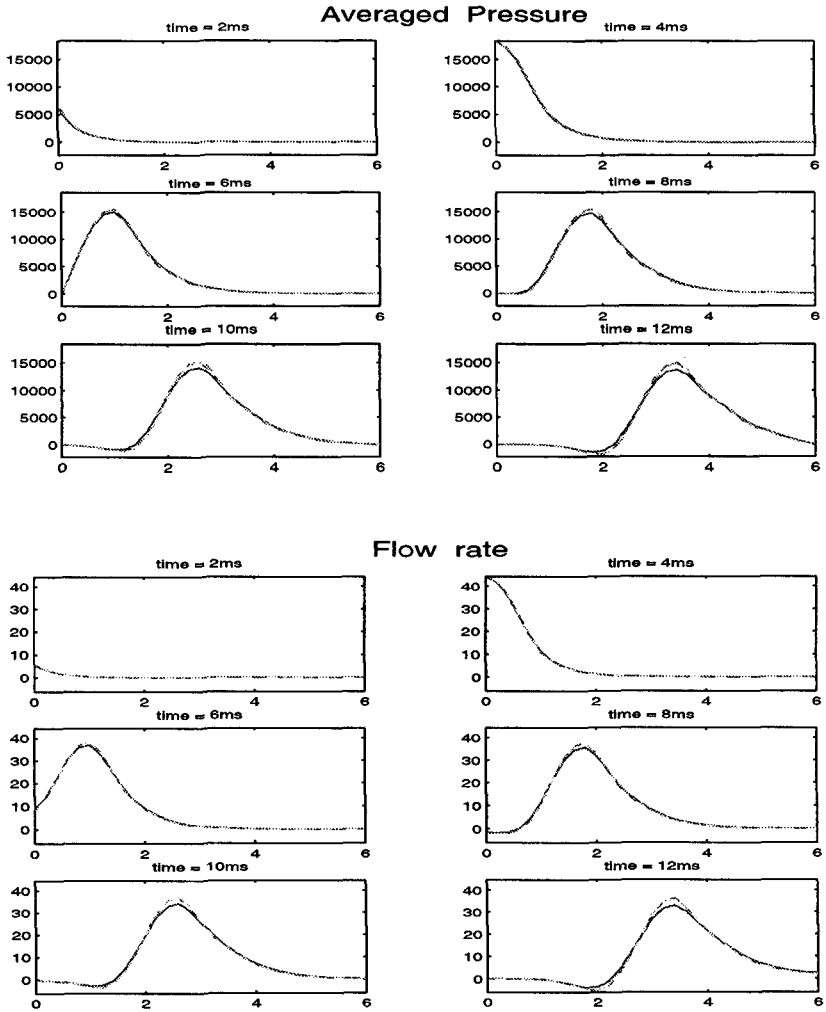

Figure 4.12: Averaged pressure (on the top) and flow rate (on the bottom) at different time instants; comparison between the solutions computed by the *MP/IE* (blue/solid line) and the *MP/CN* (red/dashed) algorithms with a time step $\Delta t = 10^{-4}$ and a solution obtained with a much smaller Δt (green/dash-dotted). The red and the green lines are almost indistinguishable.

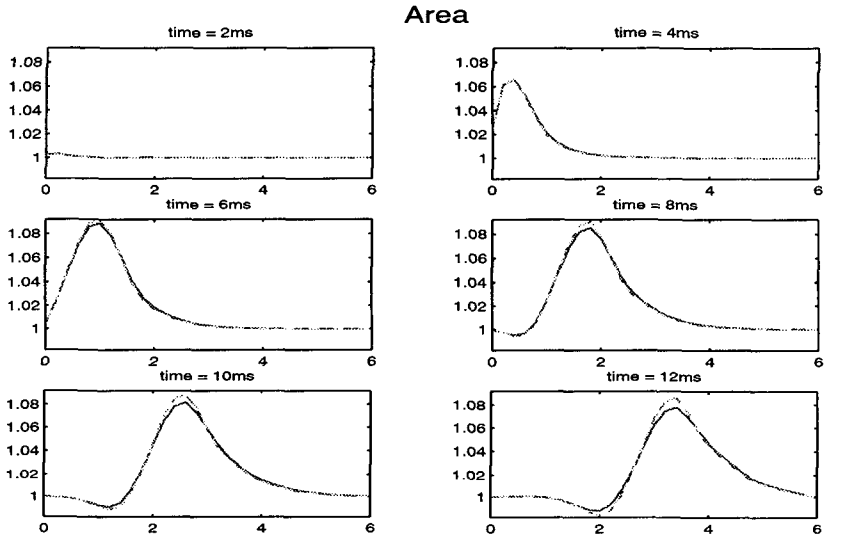

Figure 4.13: Area of each section $\mathcal{S}_i$ at different time instants; comparison between the solutions computed by the *MP/IE* (blue/solid line) and the *MP/CN* (red/dashed) algorithm with a time step $\Delta t = 10^{-4}$ and a solution obtained with a much smaller Δt (green/dash-dotted). The red and the green lines are almost indistinguishable.

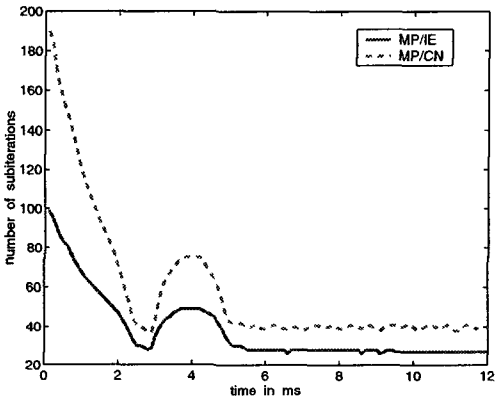

Figure 4.14: Number of substructuring iterations needed at each time step to satisfy criterion (4.11.1).

mandatory to make these algorithms employable for real applications. The start up of the simulation seems to be very critical and demands for a high number of subiterations. The second peak in the number of subiterations, at about $t = 4ms$, corresponds to the instant of the steepest decrease of the pressure pulse at the inflow. Yet, even once the pulse has completely entered the tube, the number of subiterations is not negligible : about 28 for the *MP/IE* algorithm and 40 for the *MP/CN* one.
Finally, to highlight the influence of the spatial discretisation on the numerical solution, we have computed the solution on a finer mesh; precisely we have used a structured mesh of 21×61 $\mathbb{P}_1$ fluid nodes (4961 $\mathbb{P}_1 iso \mathbb{P}_2$ nodes). Figure 4.15 shows the averaged pressure obtained with the *MP/CN* algorithm on the coarse and fine mesh and with a very small time step of $\Delta t = 10^{-6}$. The behaviour of solution is essentially the same in both case. The

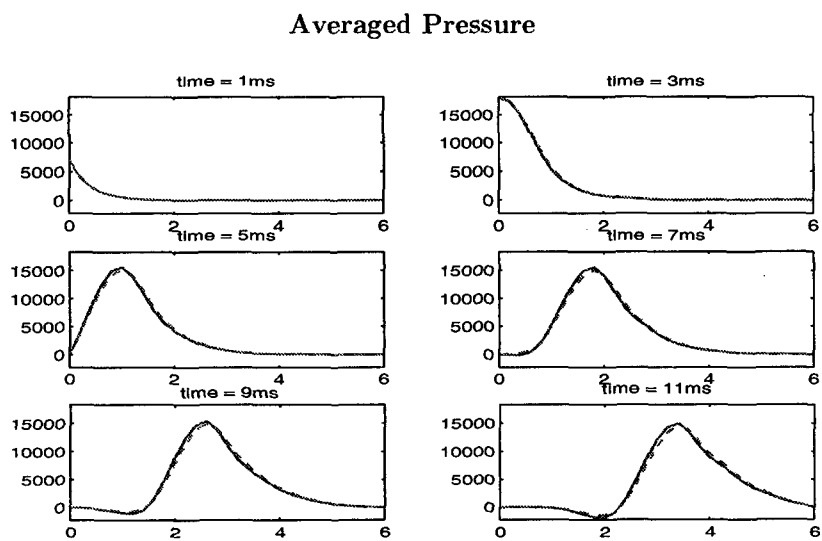

Figure 4.15: Averaged pressure : comparison between the solution computed on the coarse mesh of 11×31 $\mathbb{P}_1$ nodes (blue/solid line) and the one computed on the finer mesh of 21×61 $\mathbb{P}_1$ nodes (red/dashed line). In both cases the time step used is $\Delta t = 10^{-6}$.

solution computed on the fine grid seems to be slightly faster than the one computed on the coarse grid.

Third test case. We aim at verifying the time accuracy of the two algorithms *MP/IE* and *MP/CN*. To do that, we have taken a sequence of decreasing time steps : $\Delta t = 2 \cdot 10^{-4}, 10^{-4}, 5 \cdot 10^{-5}, 2.5 \cdot 10^{-5}$ and we have solved the problem on the mesh of figure 4.9 and for the aforementioned time steps. Moreover we have taken a tolerance of 10^{-6} in the stopping criterion (4.11.1). We have then compared the solutions computed by the two algorithms *MP/IE* and *MP/CN* at the different time steps, with those obtained using the same two algorithms on the same mesh, but with a time step $\Delta t = 10^{-6}$. We will address to these last

solutions as the "exact" solutions. No remarkable difference has been observed in taking as "exact" solution the one computed with the *MP/IE* algorithm rather then the *MP/CN* one. Figure 4.16 shows the error on the fluid velocity field at the end of the simulation (i.e. for $t = 12\,ms$), evaluated in the L^2 norm. Figure 4.17, on the other hand, shows the errors on

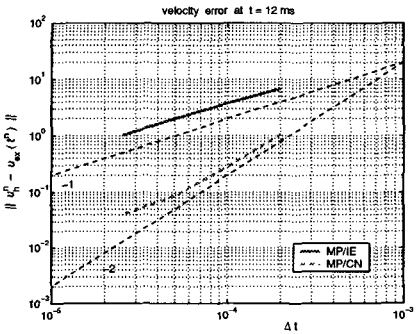

Figure 4.16: Error on the fluid velocity field in the L^2 norm at $t = 12\,ms$: difference between the solutions computed by algorithms *MP/IE* and *MP/CN* and the "exact" solution computed with $\Delta t = 10^{-6}$.

the displacement η_H and the velocity $\dot{\eta}_H$ of the structure, always at time $t = 12\,ms$. The error on the structure displacement has been computed in the norm $\|\cdot\|_{\mathcal{E}}$ while the error on the velocity in the L^2 norm. As it was expected, we recover a quadratic convergence

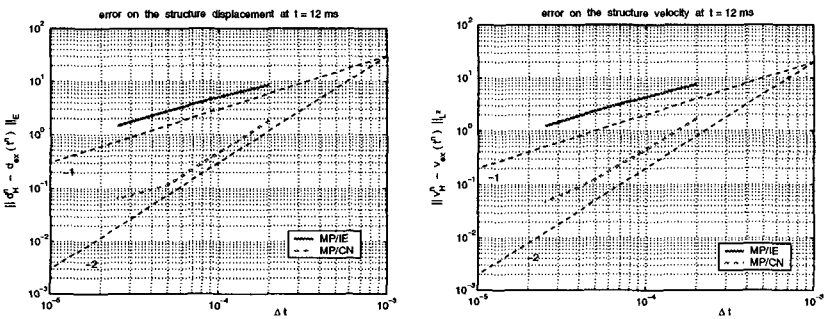

Figure 4.17: Error at time $t = 12\,ms$ on the structure displacement in norm $\|\cdot\|_{\mathcal{E}}$ (on the left) and on the structure velocity in norm L^2.

for the *MP/CN* algorithm while algorithm *MP/IE* converges linearly. Moreover, at a given time step, the *MP/CN* scheme is much more accurate than *MP/IE*. Clearly, it requires more subiterations to converge and thus demands for a larger CPU time. Since the number of subiterations slightly decreases by decreasing the time step Δt, we may wonder whether it is better, from the point of view of CPU time, to employ the second order algorithm *MP/CN*

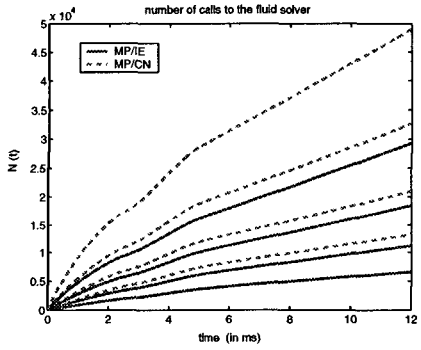

Figure 4.18: Function $N(t)$: number of times the fluid equations are solved until time t. For each of the two algorithms (blue/solid or red/dashed lines) from the bottom to the top: simulations at $\Delta t = 2 \cdot 10^{-4}, 10^{-4}, 5 \cdot 10^{-5}, 2.5 \cdot 10^{-5}$.

with a larger time step or the first order algorithm *MP/IE* with a smaller time step to achieve the same accuracy level. For each simulation which has been used in the convergence analysis of figures 4.16 and 4.17, we have computed the total number of times the fluid equations are solved until time t is reached. Let us call this quantity $N(t)$. Since the computational cost to solve the structure problem is negligible with respect to that of the fluid, this quantity provides a quite accurate estimate of the computational cost of each simulation. Figure 4.18 shows the quantity $N(t)$ associated to each simulation which has been used for the convergence test (i.e. 4 simulations for algorithm *MP/IE* and as many for *MP/CN*) We may observe that a simulation with algorithm *MP/CN* at time step $\Delta t = 2 \cdot 10^{-4}$ is more expensive than a simulation with *MP/IE* at $\Delta t = 10^{-4}$ and cheaper than the one at $\Delta t = 5 \cdot 10^{-5}$. On the other hand, the solution obtained with algorithm *MP/CN* at $\Delta t = 2 \cdot 10^{-4}$ is still slightly more accurate than that obtained with *MP/IE* at $\Delta t = 5 \cdot 10^{-5}$. Hence, at the moment, we can conclude that the *MP/CN* solver is a little more efficient than the *MP/IE* one. Clearly, these considerations might change greatly if a good accelerating technique will be devised.

Fourth test case. We have carried out again the simulation presented in the second test case on a longer time interval; precisely until $t = 24\,ms$. Figure 4.19 shows the pressure and the tube deformation at different instants between $t = 12\,ms$ and $t = 24\,ms$.
It is evident that the pressure pulse is reflected on the outflow section because of the homogeneous Neumann boundary conditions imposed. This poses another problem of how to devise suitable boundary conditions capable of absorbing the outgoing waves. This problem will be tackled in next chapter where the coupling between a fluid-structure model and a reduced monodimensional model of fluid flows in a distensible tube is investigated. We propose to use the reduced model as a far field condition for the 2D or 3D fluid-structure problem and we will show the effectiveness of such a technique.

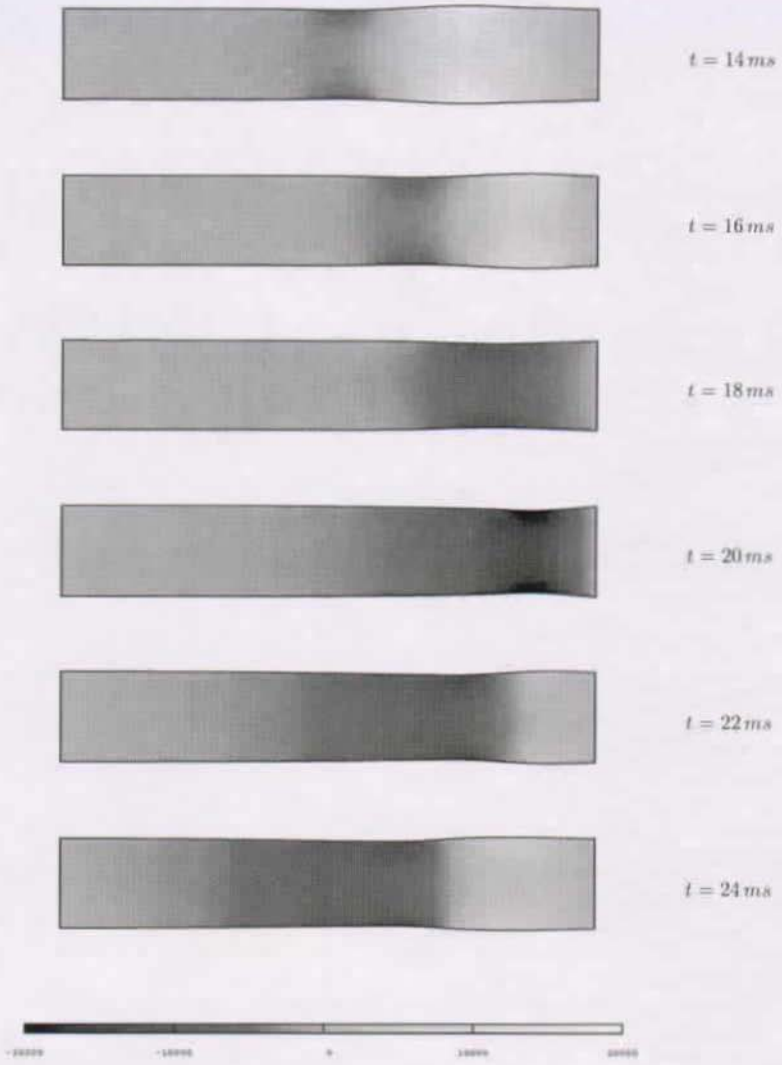

Figure 4.19: Sequel of the simulation presented in figure 4.10. Observe how the pressure pulse reflects on the outflow section because of the homogeneous Neumann boundary conditions imposed.

Chapter 5

Boundary treatment through the coupling with reduced models

One of the peculiar features of the fluid-structure problem considered in the previous chapter, is the appearance of traveling pressure waves along the vessel, as it has been focused in the numerical simulations of Section 4.11.

In this chapter we tackle the problem of devising suitable "absorbing" boundary conditions by coupling the 2D/3D fluid-structure model with a reduced one-dimensional model, which acts as an "absorbing" device for the waves exiting the computational domain. This reduced model is obtained by integrating the fluid equations over each section normal to the axis of the vessel and describes the coupled system in terms of *transversally averaged* flow rate and pressure.

We will first present in Section 5.1 the 1D model for a fluid flow inside a straight compliant vessel. Under suitable approximations, we derive a hyperbolic system of equations with source term. A proper set of boundary conditions is derived by means of standard characteristics analysis. Then the stability of the system is analysed for the sub-critical case, which is the most relevant for our target applications. A bound on the energy of the system is found in terms of the initial and boundary data, stating the stability of the 1D model. Finally, in section 5.1.4, we detail the adopted numerical discretisation based on a finite element Lax-Wendroff scheme.

Next, in section 5.2, we present several strategies for coupling the two models and possible related algorithms based on sub-domain iterations. A brief account of the possibility to impose averaged quantities, such as the mean pressure of the flux, as boundary conditions for the Navier-Stokes equations is given in Section 5.2.2. For a more detailed presentation we refer to the work by L. Formaggia, J.F. Gerbeau, F. Nobile and A. Quarteroni *Numerical treatment of defective boundary conditions for the Navier-Stokes equations* [28].

Finally, numerical results are provided for the 2D-1D models coupling. We compare the solution behaviour when a homogeneous Neumann boundary condition on the velocity is prescribed at the outlet with the solution obtained by the coupling. The latter shows a greatly reduced level of spurious reflections. A quantitative analysis on the error is also provided by comparing the results with those obtained on a vessel of double length.

The ideas presented in this chapter have already been published in a paper by L. Formaggia, J-F. Gerbeau, F. Nobile and A. Quarteroni *On the Coupling of 3D and 1D Navier-Stokes equations for Flow Problems in Compliant Vessels* [29].

5.1 The 1D model

We refer, in this section, to the situation depicted in figure 4.1 of Chapter 4, which we reproduce hereafter for the sake of clarity. In the case where the boundary Γ_0^w of the reference

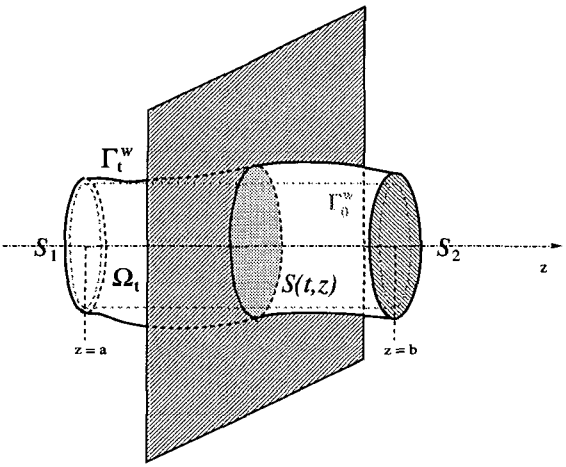

Figure 5.1: A straight deformable pipe.

configuration Ω_0 is a cylinder of radius R_0, a simplified 1D model can be obtained by integrating, at each time $t > 0$, the Navier-Stokes equations (4.1.1) over each section $\mathcal{S}(t,z)$ normal to the axis z of the cylinder. In the sequel, $A(t,z)$ denotes the area of $\mathcal{S}(t,z)$ and $u_z(t,z)$ the axial velocity, while $Q(t,z)$ and $\overline{p}(t,z)$ are the flow rate (or flux) and the mean pressure in every section, given by

$$Q(t,z) = \int_{\mathcal{S}(t,z)} u_z(t,z)d\sigma, \qquad \overline{p}(t,z) = \frac{1}{A(t,z)} \int_{\mathcal{S}(t,z)} p(t,z)d\sigma.$$

Finally $\overline{u} = Q/A$ denotes the mean axial velocity.
The 1D model which is obtained reads

$$\begin{cases} \dfrac{\partial A}{\partial t} + \dfrac{\partial Q}{\partial z} = 0 \\ \dfrac{\partial Q}{\partial t} + \dfrac{\partial}{\partial z}\left(\alpha \dfrac{Q^2}{A}\right) + \dfrac{A}{\rho}\dfrac{\partial \overline{p}}{\partial z} + K_R \dfrac{Q}{A} = 0. \end{cases} \tag{5.1.1}$$

Its derivation may be found in [75] (see also [32])
The constant K_R is a resistance parameter which accounts for fluid viscosity, while α, some-

times indicated *Coriolis* coefficient, is defined as

$$\alpha = A\left(\int_S u_z^2 d\sigma\right)\left(\int_S u_z d\sigma\right)^{-2}.$$

and accounts for the fact that the flux of momentum computed with the averaged quantities (i.e. Q^2/A) is in general different from the actual one. Even if, in general, α is function of z and t, we have taken it constant and equal to one, which corresponds to assume a *flat* velocity profile.

System (5.1.1) is a system of two equations in three unknowns ($\overline{p}$, A and Q). For its closure, a third equation is provided by a suitable wall model relating the radial displacement (and henceforth the area A) to the mean pressure $\overline{p}$.

Here we consider a simple algebraic relation between pressure and area of the type

$$\overline{p} = p_{ext} + \psi(A), \quad \text{with } \frac{d\psi}{dA} > 0 \quad \text{and} \quad \psi(A_0) = 0, \tag{5.1.2}$$

where p_{ext} is a constant external pressure and $A_0 = \pi R_0^2$ is the reference area. Then, by setting

$$c_1^2(A) = \frac{A}{\rho}\frac{\partial \psi(A)}{\partial A}, \tag{5.1.3}$$

system (5.1.1) can be written in conservative form as :

$$\frac{\partial \mathbf{U}}{\partial t} + \frac{\partial}{\partial z}\mathbf{F}(\mathbf{U}) = \mathbf{B}(\mathbf{U}), \tag{5.1.4}$$

where

$$\mathbf{U} = \begin{bmatrix} A \\ Q \end{bmatrix}, \qquad \mathbf{F}(\mathbf{U}) = \begin{bmatrix} Q \\ \alpha\dfrac{Q^2}{A} + \displaystyle\int_{A_0}^{A} c_1^2(y)dy \end{bmatrix}, \qquad \mathbf{B}(\mathbf{U}) = \begin{bmatrix} 0 \\ -K_R\dfrac{Q}{A} \end{bmatrix},$$

Alternative one-dimensional models for blood flow in arteries, which adopt the non-conservative variables $\overline{p}$ and Q (or $\overline{p}$ and $\overline{u}$) as unknowns, have been used in the literature as well (see e.g. [70, 74]).

System (5.1.4) may be written in *quasi linear* form

$$\frac{\partial \mathbf{U}}{\partial t} + \mathbf{H}\frac{\partial \mathbf{U}}{\partial z} = \mathbf{B}(\mathbf{U}), \qquad \text{with } \mathbf{H} = \begin{bmatrix} 0 & 1 \\ -\alpha\left(\dfrac{Q}{A}\right)^2 + c_1^2(A) & 2\alpha\dfrac{Q}{A} \end{bmatrix} \tag{5.1.5}$$

and it turns out to be hyperbolic since it possesses two real distinct eigenvalues which, for $\alpha = 1$, read simply

$$\lambda_{1,2} = \overline{u} \pm c_1. \tag{5.1.6}$$

and a complete set of eigenvectors. We now indicate by $\mathbf{L}$ and $\mathbf{\Lambda} = \mathrm{diag}(\lambda_1, \lambda_2)$ the matrix of left eigenvectors and that of the eigenvalues of $\mathbf{H}$, respectively. Then, relation (5.1.5) may be written as

$$\mathbf{L}\frac{\partial \mathbf{U}}{\partial t} + \mathbf{\Lambda}\mathbf{L}\frac{\partial \mathbf{U}}{\partial z} = \mathbf{L}\mathbf{B}(\mathbf{U}). \tag{5.1.7}$$

At least for $\alpha = 1$, it is possible to find a vector function $\mathbf{W} = \mathbf{W}(\mathbf{U}) = [W_1(\mathbf{U}), W_2(\mathbf{U})]$ such that $\frac{\partial \mathbf{W}}{\partial \mathbf{U}} = \mathbf{L}$. The quantities W_1 and W_2 are the *characteristic variables* of problem (5.1.1) and their expression may be given as function of the average velocity $\overline{u}$ and the area A (and eventually of A and Q) as follows

$$W_{1,2} = \overline{u} \pm \int_{A_0}^{A} \frac{c_1(\tau)}{\tau} d\tau = \boldsymbol{\mathcal{H}}(Q, A). \tag{5.1.8}$$

They are not constant along the characteristic curves $dz_i/dt = \lambda_i$, $i = 1, 2$ because of the presence of a source term. By inverting relation (5.1.8) we may express the conserved variables in terms of W_1 and W_2:

$$\mathbf{U} = \boldsymbol{\mathcal{H}}^{-1}(\mathbf{W}). \tag{5.1.9}$$

In the case $\mathbf{B} = \mathbf{0}$, equations (5.1.7) decouple and may be written component-wise as

$$\begin{cases} \dfrac{\partial}{\partial t} W_1 + \lambda_1 \dfrac{\partial W_1}{\partial z} = 0, \\ \dfrac{\partial}{\partial t} W_2 + \lambda_2 \dfrac{\partial W_2}{\partial z} = 0. \end{cases} \tag{5.1.10}$$

System (5.1.4) must be supplemented by appropriate boundary conditions at the two ends of the interval (let's say $z = a$ and $z = b$).
In hemodynamics applications, the values attained by the mechanical parameters and blood velocities in physiological conditions are such that $c_1 > |\overline{u}|$ (i.e. the eigenvalues have opposite sign). Hence, a single boundary condition must be specified at both ends. In particular, we may impose the entering characteristic variable, i.e., $\forall t > 0$

$$W_1(t) = g_1(t) \text{ at } z = a, \quad \text{and} \quad W_2(t) = g_2(t) \text{ at } z = b, \tag{5.1.11}$$

where g_1 and g_2 are given functions of t. Alternative boundary conditions applied to the primary variables Q and A (or $\overline{p}$) can be devised as well, under suitable restrictions [39]. For the numerical discretisation of (5.1.4), the two boundary conditions above need to be supplemented by two additional equations, one at each side, in order to allow the computation of two vector unknowns $\mathbf{U}(a)$ and $\mathbf{U}(b)$. We will address this issue in more detail in Section 5.1.5.

5.1.1 Wall laws

An example of algebraic relation of type (5.1.2) has been given in equation (4.1.5) of Chapter 4. In such a case, we have

$$\overline{p} - p_{ext} = \frac{Eh}{1 - \nu^2} \frac{\eta_r}{R_0^2}.$$

Since $A = \pi(R_0 + \eta_r)^2$, we obtain

$$\overline{p} - p_{ext} = \beta\sqrt{A} - p^*, \qquad \text{where } \begin{cases} \beta = \frac{\sqrt{\pi} h E}{(1-\nu^2)A_0} \\ p^* = \beta\sqrt{A_0} \end{cases} \tag{5.1.12}$$

Henceforth, in view of (5.1.2), we have that

$$\psi(A) = \beta\sqrt{A} - p^* \tag{5.1.13}$$

The characteristic variables now are

$$W_{1,2} = \overline{u} \pm 2\sqrt{\frac{2}{\rho}}\left(\sqrt{\overline{p} - p_{ext} + p^*} - \sqrt{p^*}\right). \tag{5.1.14}$$

and this relation can be inverted as

$$A = \frac{1}{\beta^2}\left[\sqrt{\frac{\rho}{32}}(W_1 - W_2) + \sqrt{p^*}\right]^4, \qquad Q = A\frac{W_1 + W_2}{2} \tag{5.1.15}$$

In our simulations we have adopted this algebraic model. A presentation of other models that make use of differential laws linking $\overline{p}$ to A and its time derivatives is reported in the already published article by L. Formaggia, F. Nobile, A. Quarteroni and A. Veneziani *Multiscale Modelling of the Circulatory System: a Preliminary Analysis* [32]. Another example can be found in [74].

Remark 5.1.1 *In the blood flow context, other algebraic relationships between $\overline{p}$ and A, possibly featuring a better accordance with experiments, can be found in [45], [59] and [91].*

When considering a 2D geometry like the one shown in Fig. 4.2 of Chapter 4, equations (5.1.1) are still valid provided we now take $A = 2(R_0 + \eta_r)$. The algebraic relation (5.1.13) becomes

$$\psi(A) = \beta A - p^* \qquad \text{where } \begin{cases} \beta = \frac{hE}{2(1-\nu^2)R_0^2} \\ p^* = \beta A_0 \end{cases} \tag{5.1.16}$$

and the characteristic variables are $W_{1,2} = \overline{u} \pm 2\sqrt{\frac{1}{\rho}}\,(\sqrt{\overline{p} - p_{ext} + p^*} - \sqrt{p^*})$.

The 1D model considered until now is valid for a straight pipe and constant elastic properties of the wall. In the paper by L. Formaggia, F. Nobile and A. Quarteroni *A One Dimensional Model for Blood Flow: Application to Vascular Prosthesis* we have generalized this model to the case of a varying elastic Young's modulus E of the arterial wall in order to simulate the presence of a vascular prosthesis or a stent. Numerous numerical results are also provided. The methodology adopted therein allows only for smooth variations of the elastic parameter. Further improvements of the 1D model accounting for instance for discontinuous coefficients, more complex wall laws, tapering, curved pipes or branching are the subject of current research.

5.1.2 Energy conservation for the 1D model

Here we derive an *a priori* estimate for the solution of system (5.1.1) in the interval $I = [a, b]$ under the hypotheses that $\forall t > 0$, $\lambda_1 > 0$, $\lambda_2 < 0$ (sub-critical flow regime) and the area A maintains positive.

We will consider the following initial and boundary conditions

$$\text{initial conditions} \qquad A(0,z) = A^0, \quad Q(0,z) = Q^0 \qquad a \le z \le b \tag{5.1.17}$$

$$\text{boundary conditions} \qquad \begin{array}{l} W_1 = g_1 \quad \text{at } z = a \\ W_2 = g_2 \quad \text{at } z = b \end{array} \tag{5.1.18}$$

We define the energy of the 1D model, for each $t > 0$, as

$$\mathcal{E}(t) = \frac{1}{2}\rho \int_a^b A(t,z)\overline{u}^2(t,z)dz + \int_a^b \Psi(A(t,z))dz \tag{5.1.19}$$

where

$$\Psi(A) = \int_{A_0}^{A} \psi(\zeta)d\zeta \tag{5.1.20}$$

Owing to (5.1.2) we may observe that

$$\Psi(A_0) = \Psi'(A_0) = 0 \qquad \text{and } \Psi''(A) > 0 \quad \forall A > 0.$$

Therefore $\Psi(A)$ is always positive and $\mathcal{E}(t)$ is a positive function for all Q and $A > 0$ at each $t > 0$. The following Lemma holds

Lemma 5.1.1 *In the case $\alpha = 1$, system (5.1.1), supplied with an algebraic pressure-area relationship like in (5.1.2), satisfies the following conservation property*

$$\mathcal{E}(T) + \rho K_R \int_0^T \int_a^b \overline{u}^2 dz dt + \int_0^T Q\left(\overline{p} - p_{ext} + \frac{1}{2}\rho\overline{u}^2\right)\Big|_a^b dt = \mathcal{E}(0). \tag{5.1.21}$$

Obviously, $\mathcal{E}(0)$ depends only on the initial data A^0 and Q^0.

Proof.
Let's multiply the second equation of (5.1.1) by $\overline{u}$ and integrate over I. We will analyse separately the four terms.

- First term

$$I_1 = \int_a^b \frac{\partial(A\overline{u})}{\partial t}\overline{u}dz = \frac{1}{2}\int_a^b A\frac{\partial\overline{u}^2}{\partial t}dz + \int_a^b \frac{\partial A}{\partial t}\overline{u}^2 dz = \frac{1}{2}\frac{d}{dt}\int_a^b A\overline{u}^2 dz + \frac{1}{2}\int_a^b \overline{u}^2\frac{\partial A}{\partial t}dz \tag{5.1.22}$$

- Second term

$$I_2 = \alpha\int_a^b \frac{\partial(A\overline{u}^2)}{\partial z}\overline{u}dz = \alpha\left[\int_a^b \frac{\partial(A\overline{u})}{\partial z}\overline{u}^2 dz + \int_a^b A\overline{u}^2\frac{\partial\overline{u}}{\partial z}dz\right] = \alpha\left[\frac{1}{2}\int_a^b \frac{\partial(A\overline{u})}{\partial z}\overline{u}^2 dz + \frac{1}{2}\int_a^b \frac{\partial A}{\partial z}\overline{u}^3 dz + \frac{3}{2}\int_a^b A\overline{u}^2\frac{\partial\overline{u}}{\partial z}dz\right] = \alpha\left[\frac{1}{2}\int_a^b \frac{\partial Q}{\partial z}\overline{u}^2 dz + \frac{1}{2}\int_a^b \frac{\partial(A\overline{u}^3)}{\partial z}dz\right] \tag{5.1.23}$$

Now, using the first equation in (5.1.1) we obtain

$$I_2 = \frac{\alpha}{2}\left[-\int_a^b \frac{\partial A}{\partial t}\overline{u}^2 dz + (A\overline{u}^3)\Big|_a^b\right] \tag{5.1.24}$$

- Third term. Using (5.1.2) and the fact that p_{ext} is independent of z we have

$$I_3 = \int_a^b \frac{A}{\rho}\frac{\partial \overline{p}}{\partial z}\overline{u}dz = \frac{1}{\rho}\int_a^b A\frac{\partial}{\partial z}(\overline{p}-p_{ext})\overline{u}dz = \frac{1}{\rho}\left[-\int_a^b \frac{\partial Q}{\partial z}\psi(A)dz + (\overline{p}-p_{ext})Q\Big|_a^b\right] \quad (5.1.25)$$

Again, using the first of (5.1.1) we have

$$I_3 = \frac{1}{\rho}\left[\int_a^b \frac{\partial A}{\partial t}\psi(A)dz + (\overline{p}-p_{ext})Q\Big|_a^b\right] = \frac{1}{\rho}\left[\frac{d}{dt}\int_a^b \Psi(A)dz + (\overline{p}-p_{ext})Q\Big|_a^b\right] \quad (5.1.26)$$

- Fourth term

$$I_4 = \int_a^b K_R\frac{Q}{A}\overline{u}dz = K_R\int_a^b \overline{u}^2dz \quad (5.1.27)$$

In the case $\alpha = 1$, by summing the four terms we obtain the following equality

$$\frac{1}{2}\rho\frac{d}{dt}\int_a^b A\overline{u}^2dz + \frac{d}{dt}\int_a^b \Psi(A)dz + \rho K_R\int_a^b \overline{u}^2dz + Q\left(\overline{p}-p_{ext}+\frac{1}{2}\rho\overline{u}^2\right)\Big|_a^b = 0 \quad (5.1.28)$$

Integrating equation (5.1.28) in time between 0 and T we obtain the desired result.
■

In order to draw an energy inequality from (5.1.21), we need to investigate the sign of the different terms. The first two of them are clearly positive. Concerning the third one let us analyse the homogeneous case (i.e. the case where $g_1 = g_2 = 0$).

We will rewrite the boundary term in (5.1.21) as a function of A, $\psi(A)$ and c_1 (which, in its turn, depends on A and $\psi(A)$, see (5.1.6)).
If $g_1 = g_2 = 0$ in (5.1.18), then

$$\text{at z = a} \qquad W_1 = \overline{u} + \int_{A_0}^{A}\frac{c_1(\zeta)}{\zeta}d\zeta = 0 \qquad \Longrightarrow \qquad \overline{u}(t,a) = -\int_{A_0}^{A}\frac{c_1(\zeta)}{\zeta}d\zeta$$

$$\text{at z = b} \qquad W_2 = \overline{u} - \int_{A_0}^{A}\frac{c_1(\zeta)}{\zeta}d\zeta = 0 \qquad \Longrightarrow \qquad \overline{u}(t,b) = \int_{A_0}^{A}\frac{c_1(\zeta)}{\zeta}d\zeta$$

Then, using (5.1.2)

$$Q\left(\overline{p}-p_{ext}+\frac{1}{2}\rho\overline{u}^2\right)\Big|_a^b = F(A(t,a)) + F(A(t,b)) \quad (5.1.29)$$

where

$$F(A) = A\int_{A_0}^{A}\frac{c_1(\zeta)}{\zeta}d\zeta\left[\psi(A) + \frac{1}{2}\rho\left(\int_{A_0}^{A}\frac{c_1(\zeta)}{\zeta}d\zeta\right)^2\right] \quad (5.1.30)$$

We recall that we *are assuming* $\lambda_1 > 0$ and $\lambda_2 < 0$ (sub-critical flow regime). Then, from (5.1.6), we have $|\overline{u}| < c_1$ which implies at both $z = a$ and $z = b$

$$\left| \int_{A_0}^{A} \frac{c_1(\zeta)}{\zeta} d\zeta \right| < c_1(A) \tag{5.1.31}$$

We are now in the position to conclude with the following result

Lemma 5.1.2 *If the function $\psi(A)$ is chosen in such a way that $F(A) > 0$, for all $A > 0$ which satisfy (5.1.31), then the energy inequality*

$$\mathcal{E}(T) + \rho K_R \int_0^T \int_a^b \overline{u}^2 dz dt \leq \mathcal{E}(0) \tag{5.1.32}$$

holds for system (5.1.1).

The pressure-area relationship given in (5.1.13) satisfies the hypotheses of Lemma 5.1.2. In fact, in this case

$$\Psi(A) = \beta(\sqrt{A} - \sqrt{A_0}), \qquad c_1^2 = \frac{\beta}{2\rho}\sqrt{A}$$

and

$$\int_{A_0}^{A} \frac{c_1(\zeta)}{\zeta} d\zeta = \int_{A_0}^{A} \sqrt{\frac{\beta}{2\rho}} \zeta^{-\frac{3}{4}} d\zeta = 4\sqrt{\frac{\beta}{2\rho}} (A^{\frac{1}{4}} - A_0^{\frac{1}{4}}).$$

Condition (5.1.31) becomes

$$\left| 4\sqrt{\frac{\beta}{2\rho}} (A^{\frac{1}{4}} - A_0^{\frac{1}{4}}) \right| < \sqrt{\frac{\beta}{2\rho}} A^{\frac{1}{4}} \qquad \text{and then} \qquad \frac{4}{5} A_0^{\frac{1}{4}} < A^{\frac{1}{4}} < \frac{4}{3} A_0^{\frac{1}{4}} \tag{5.1.33}$$

On the other hand we have

$$F(A) = A4\sqrt{\frac{\beta}{2\rho}} (A^{\frac{1}{4}} - A_0^{\frac{1}{4}}) \left[\beta(A^{\frac{1}{2}} - A_0^{\frac{1}{2}}) + \frac{\rho}{2} 16 \frac{\beta}{2\rho} (A^{\frac{1}{4}} - A_0^{\frac{1}{4}})^2 \right] =$$

$$4\beta\sqrt{\frac{\beta}{2\rho}} A (A^{\frac{1}{4}} - A_0^{\frac{1}{4}}) \left[(A^{\frac{1}{4}} - A_0^{\frac{1}{4}})(A^{\frac{1}{4}} + A_0^{\frac{1}{4}}) + 4(A^{\frac{1}{4}} - A_0^{\frac{1}{4}})^2 \right] =$$

$$4\beta\sqrt{\frac{\beta}{2\rho}} A (A^{\frac{1}{4}} - A_0^{\frac{1}{4}})^2 (5A^{\frac{1}{4}} - 3A_0^{\frac{1}{4}})$$

Then, condition $F(A) > 0$ gives

$$A^{\frac{1}{4}} > \frac{3}{5} A_0^{\frac{1}{4}},$$

whose satisfaction is a consequence of (5.1.33). Therefore, in that case the 1D model is stable.

More generally, under the same relation (5.1.13), we can prove an energy estimate also in the case of non homogeneous boundary conditions. We have the following result

Lemma 5.1.3 *If the pressure-area relationship is given by (5.1.13), and the boundary data satisfy*

$$g_1(t) > -4\sqrt{\frac{p^*}{2\rho}} \quad \text{and} \quad g_2(t) < 4\sqrt{\frac{p^*}{2\rho}} \qquad \forall t > 0, \tag{5.1.34}$$

then there exists a positive function $G = G(g_1, g_2, p^*)$ such that

$$\mathcal{E}(T) + \rho K_R \int_0^T \int_a^b \overline{u}^2 dz dt \leq \mathcal{E}(0) + \int_0^T G(g_1(t), g_2(t), p^*) dt. \tag{5.1.35}$$

Proof.
We will consider only the case where $g_1 \neq 0$ and $g_2 = 0$, since the most general case may be derived in a similar fashion. We recall that relationship (5.1.13) satisfies the hypotheses on $F(A)$ of Lemma 5.1.2. Then from (5.1.28) we obtain the following inequality

$$\frac{\rho}{2}\frac{d}{dt}\int_a^b A\overline{u}^2 dz + \frac{d}{dt}\int_a^b \Psi(A) dz + \rho K_R \int_a^b \overline{u}^2 dz \leq$$
$$Q\left(\overline{p} - p_{ext} + \frac{1}{2}\rho\overline{u}^2\right)\Big|_{z=a} \leq \left(A|\overline{u}||\psi(A)| + \frac{1}{2}\rho A|\overline{u}|^3\right)\Big|_{z=a} \tag{5.1.36}$$

We have then at $z = a$ (from (5.1.14) and (5.1.18))

$$\overline{u} + 2\sqrt{\frac{2}{\rho}}\left(\sqrt{\overline{p} - p_{ext} + p^*} - \sqrt{p^*}\right) = g_1$$

thus, from (5.1.2)

$$\overline{u} = g_1 - 2\sqrt{\frac{2}{\rho}}\left(\sqrt{\psi(A) + p^*} - \sqrt{p^*}\right). \tag{5.1.37}$$

On the other hand, $\lambda_1 = \overline{u} + \frac{1}{\sqrt{2\rho}}\sqrt{\overline{p} - p_{ext} + p^*} > 0$, and then

$$\overline{u} > -\frac{1}{\sqrt{2\rho}}\sqrt{\psi(A) + p^*} \tag{5.1.38}$$

Combining (5.1.37) and (5.1.38) we have

$$-\frac{1}{\sqrt{2\rho}}\sqrt{\psi(A) + p^*} < g_1 - 2\sqrt{\frac{2}{\rho}}\left(\sqrt{\psi(A) + p^*} - \sqrt{p^*}\right)$$

and then

$$\sqrt{\psi(A) + p^*} < f_1(g_1, p^*) \tag{5.1.39}$$

where

$$f_1(g_1, p^*) = \frac{\sqrt{2\rho}}{3}g_1 + \frac{4}{3}\sqrt{p^*}.$$

The assumptions (5.1.34) are necessary conditions for the eigenvalues of system (5.1.1) being of opposite sign.

Furthermore, we deduce from (5.1.13) that $\psi(A) > -p^*$. The following inequalities thus hold at $z = a$

$$|\psi(A)| \leq \max\left\{p^*, |f_1^2(g_1, p^*) - p^*|\right\}$$
$$|\overline{u}| = \left|g_1 - 2\sqrt{\frac{2}{\rho}}\left(\sqrt{\psi(A) + p^*} - \sqrt{p^*}\right)\right| \leq |g_1| + 2\sqrt{\frac{2}{\rho}}(\sqrt{p^*} + f_1(g_1, p^*))$$
$$A = \frac{1}{\beta^2}(\psi(A) + p^*)^2 \leq \frac{1}{\beta^2} f_1^4(g_1, p^*)$$

and the right hand side in (5.1.36) may thus be expressed by a positive function of the boundary data g_1 and the reference pressure at rest $p^* = \beta\sqrt{A_0}$, which we have indicate by $G(g_1, p^*)$. We obtain then the desired stability inequality.

■

5.1.3 Entropy function for the 1D model

If we take again the differential problem (5.1.1) and we carry out derivations similar to those illustrated in (5.1.22)-(5.1.28), considering now the integrals over an arbitrary interval $[z, z + dz] \subset [a, b]$, we may derive a relation analogous to (5.1.28). Then, passing to the limit as $dz \to 0$, the following pointwise differential relation may be deduced

$$\frac{\partial}{\partial t}\left(\frac{1}{2}\rho A\overline{u}^2 + \Psi(A)\right) + \frac{\partial}{\partial z}\left[Q\left(\psi(A) + \frac{1}{2}\rho\overline{u}^2\right)\right] = -\rho K_R \overline{u}^2 \tag{5.1.40}$$

which can be interpreted as an entropy balance equation for the hyperbolic system. Indeed, the function

$$s(A, Q) = \frac{1}{2}\rho A\overline{u}^2 + \Psi(A) \tag{5.1.41}$$

is an entropy for system (5.1.1), with an associated flux

$$F_s(A, Q) = Q\left(\psi(A) + \frac{1}{2}\rho\overline{u}^2\right) \tag{5.1.42}$$

The term $\rho K_R \overline{u}^2$ may be recognised as a dissipative term.

5.1.4 Numerical discretisation

The equations in conservation form (5.1.4) have been discretised by adopting a second order Taylor-Galerkin scheme, which is the finite element counterpart of the well known Lax-Wendroff scheme. We recall here, briefly, its derivation. We will use the abridged notation

$$\mathbf{H} = \frac{\partial \mathbf{F}}{\partial \mathbf{U}}, \quad \mathbf{J_B} = \frac{\partial \mathbf{B}}{\partial \mathbf{U}}.$$

By following the usual route to derive the Lax-Wendroff scheme, we write

- $$\frac{\partial \mathbf{U}}{\partial t} = \mathbf{B} - \frac{\partial \mathbf{F}}{\partial z} \tag{5.1.43}$$

- $$\frac{\partial^2 \mathbf{U}}{\partial t^2} = \frac{\partial \mathbf{B}}{\partial t} - \frac{\partial^2 \mathbf{F}}{\partial t \partial z} = \mathbf{J_B}\frac{\partial \mathbf{U}}{\partial t} - \frac{\partial}{\partial z}\left(\mathbf{H}\frac{\partial \mathbf{U}}{\partial t}\right) \tag{5.1.44}$$
$$= \mathbf{J_B}\left(\mathbf{B} - \frac{\partial \mathbf{F}}{\partial z}\right) - \frac{\partial(\mathbf{HB})}{\partial z} + \frac{\partial}{\partial z}\left(\mathbf{H}\frac{\partial \mathbf{F}}{\partial z}\right).$$

We note that, in contrast with what is usually done for the derivation of a Lax-Wendroff scheme in standard cases, here we have not further developed the z derivative of the fluxes. In this way, the discretisation presented hereafter is compatible with a variable coefficient β in the wall law (5.1.13). Indeed, if β is not constant, the relation

$$\frac{\partial \mathbf{F}}{\partial z} = \mathbf{H}\frac{\partial \mathbf{U}}{\partial z},$$

is not anymore true because of the dependence of $\mathbf{F}$ on z through β.
For the time discretisation, we consider a time step Δt and indicate with the superscript n quantities computed at time $t^n = n\Delta t$. Using, as in a standard Lax-Wendroff procedure, a truncated Taylor expansion in time around t^n and exploiting (5.1.43) and (5.1.44) we finally obtain the following time-marching scheme

$$\mathbf{U}^{n+1} = \mathbf{U}^n - \Delta t\frac{\partial}{\partial z}\left[\mathbf{F}^n + \frac{\Delta t}{2}\mathbf{H}^n\mathbf{B}^n\right] - \frac{\Delta t^2}{2}\left[\mathbf{J}_{\mathbf{B}}^n\frac{\partial \mathbf{F}^n}{\partial z} - \frac{\partial}{\partial z}\left(\mathbf{H}^n\frac{\partial \mathbf{F}^n}{\partial z}\right)\right] + \Delta t\left(\mathbf{I} + \frac{\Delta t}{2}\mathbf{J}_{\mathbf{B}}^n\right)\mathbf{B}^n. \quad (5.1.45)$$

Space discretisation is carried out by using linear finite elements. To that purpose, let us subdivide the interval $[a, b]$ into N finite elements $[z_i, z_{i+1}]$, with $i = 0, \cdots, N$ and $z_i = ih$ being h the constant element size. We indicate by $\mathbf{V}_h = [V_h]^2$ the space of continuous vector functions defined on $[a, b]$, linear on each element, and with $\mathbf{V}_h^0$ the set formed by functions of $\mathbf{V}_h$ which are zero at $z = a$ and $z = b$. Furthermore, we indicate by $(\mathbf{u}, \mathbf{v}) = \int_a^b \mathbf{u}\cdot\mathbf{v}\,dz$ the L^2 vector product.
Let us put

$$\mathbf{F}_{LW} = \mathbf{F} + (\Delta t/2)\mathbf{H}\mathbf{B} \quad \text{and}$$

$$\mathbf{B}_{LW} = [\mathbf{I} + (\Delta t/2)\mathbf{J}_{\mathbf{B}}]\,\mathbf{B}.$$

A finite element formulation of (5.1.45) is: for $n \geq 0$, find $\mathbf{U}_h^{n+1} \in \mathbf{V}_h$ which satisfies

$$(\mathbf{U}_h^{n+1}, \boldsymbol{\psi}_h) = (\mathbf{U}_h^n, \boldsymbol{\psi}_h) + \Delta t(\mathbf{F}_{LW}^n, \frac{\partial \boldsymbol{\psi}_h}{\partial z}) - \frac{\Delta t^2}{2}(\mathbf{J}_{\mathbf{B}}^n\frac{\partial \mathbf{F}^n}{\partial z}, \boldsymbol{\psi}_h) - \frac{\Delta t^2}{2}(\mathbf{H}^n\frac{\partial \mathbf{F}^n}{\partial z}, \frac{\partial \boldsymbol{\psi}_h}{\partial z}) + \Delta t(\mathbf{B}_{LW}^n, \boldsymbol{\psi}_h), \quad \forall \boldsymbol{\psi}_h \in \mathbf{V}_h^0. \quad (5.1.46)$$

The boundary values of $\mathbf{U}_h^{n+1}$ will be calculated using the prescribed boundary conditions and following the technique described in Section 5.1.5. $\mathbf{U}_h^0$ will be taken as the finite element interpolant of the given initial data $\mathbf{U}_0$.
A Von Neumann linear stability analysis for the proposed finite element scheme on a grid with uniform spacing h, gives a stability condition of the type

$$\frac{\Delta t \sup_{a<z<b}(\max_{i=1,2}|\lambda_i|)}{h} < \frac{1}{\sqrt{3}},$$

which is more restrictive than the classical CFL condition for finite difference or finite volume Lax Wendroff schemes. This has been confirmed by our numerical experiments.
In (5.1.46) there is the need of integrating numerically the terms containing the fluxes and the sources, i.e. $\mathbf{F}^n$, $\mathbf{H}^n$, $\mathbf{B}^n$ and $\mathbf{J}_{\mathbf{B}}^n$. We have used the technique of projecting each component of these terms on the finite element function space V_h by interpolation.

5.1.5 Computing the boundary data for the numerical scheme

In this section we detail two different choices of boundary conditions for the differential problem (5.1.4) :

$$\text{a.} \quad W_1(t) = g_1(t) \quad \text{at } z = a, \qquad W_2(t) = g_2(t) \quad \text{at } z = b; \tag{5.1.47}$$

$$\text{b.} \quad A(t) = a_1(t) \quad \text{at } z = a, \qquad A(t) = a_2(t) \quad \text{at } z = b; \tag{5.1.48}$$

The numerical scheme (5.1.46) needs to have a complete boundary data $\mathbf{U}^{n+1}$ at the boundary nodes. However, for the well posedness of the differential problem only one condition at each end, for instance either (5.1.47) or (5.1.48), has to be assigned.
In order to compute the complete boundary data we need an additional equation, which must be compatible with the original differential problem. Here, we have adopted a technique based on the extrapolation of the outgoing characteristics. The term $K_R(Q/A)$ is normally of small size, so that we feel legitimated to assume that the flow is essentially governed by equations (5.1.10). Let us consider now the first end $z = a$ (the case for $z = b$ will be treated similarly), and a generic time step of our numerical procedure. We assume that $\mathbf{U}^n$ is known and we linearise λ_2 in the second equation in (5.1.10) by taking its value at time t^n and at $z = a$. The solution corresponding to this linearised problem at the time level t^{n+1} gives

$$W_2^{n+1}(a) = W_2^n(-\lambda_2^n(a)\Delta t) \ ,$$

and is in fact a first order extrapolation of the outgoing characteristic variable W_2 from the previous time level; we will denote this value with $W_{2,extr}^{n+1}$. Higher order extrapolations can be used as well.

In the case of boundary conditions (5.1.47), by combining the extrapolated value $W_{2,extr}^{n+1}$ with the value of W_1 provided by the boundary condition, $W_1^{n+1} = g_1(t^{n+1})$, we are able to compute, the required boundary data $\mathbf{U}^{n+1}(a) = \boldsymbol{\mathcal{H}}^{-1}(g_1(t^{n+1}), W_{2,extr}^{n+1})$.

If boundary conditions (5.1.48) are considered, should we be able to express W_1 as a function of A and W_2 ($W_1 = W_1(A, W_2)$), the required boundary data $\mathbf{U}^{n+1}$ would be given, at $z = a$, by

$$\mathbf{U}^{n+1}(a) = \boldsymbol{\mathcal{H}}^{-1}\left(W_1\left(a_1(t^{n+1}), W_{2,extr}^{n+1}\right) \ , \ W_{2,extr}^{n+1}\right) \tag{5.1.49}$$

Indeed, relation (5.1.49) guarantees that $A^{n+1}(a) = a_1(t^{n+1})$ while $Q^{n+1}(a)$ is determined as a function of $a_1(t^{n+1})$ and $W_{2,extr}^{n+1}$. At $z = b$, we need to express W_2 as a function of A and W_1 ($W_2 = W_2(A, W_1)$); then we compute $\mathbf{U}^{n+1}(b)$ as $\mathbf{U}^{n+1}(b) = \boldsymbol{\mathcal{H}}^{-1}(W_{1,extr}^{n+1}, W_2(a_2(t^{n+1}), W_{1,extr}^{n+1}))$.
In the case where we employ algebraic relation 5.1.13 for the vessel wall, relation $W_1 = W_1(A, W_2)$ is given by

$$W_1 = W_2 + 4\sqrt{\frac{2}{\rho}}\left(\sqrt{\beta\sqrt{A}} - \sqrt{p^*}\right).$$

A similar relation holds for $W_2 = W_2(A, W_1)$.

Remark 5.1.2 *The methodology just illustrated is not the only possibility to provide boundary data for the discrete problem. Another possible approach is to adopt the so-called compatibility*

conditions [39, 76], namely

$$\begin{aligned} \mathbf{l}_2^T \left(\frac{\partial \mathbf{U}}{\partial t} + \mathbf{H}\frac{\partial \mathbf{U}}{\partial z} - \mathbf{B}(\mathbf{U}) \right) = 0, \quad z = a,\, t > 0 \ , \\ \mathbf{l}_1^T \left(\frac{\partial \mathbf{U}}{\partial t} + \mathbf{H}\frac{\partial \mathbf{U}}{\partial z} - \mathbf{B}(\mathbf{U}) \right) = 0, \quad z = b,\, t > 0 \ . \end{aligned} \tag{5.1.50}$$

$\mathbf{l}_1$ and $\mathbf{l}_2$ being the eigenvectors of matrix $\mathbf{H}$. A way to apply these conditions in a finite element scheme is to rewrite the weak form (5.1.46) by letting $\psi_h \in V_h$ (beware that in this case we cannot drop the boundary terms which originate from the integration by parts). Now using as test function the finite element functions associated to the two boundary nodes we obtain two relations per boundary node. We may then form a linear combination of the equations associated to node $z = a$ (resp. $z = b$) with coefficients $\mathbf{l}_2$ (resp. $\mathbf{l}_1$), thus producing one equation for each boundary node. They effectively represent a discretisation of (5.1.50) which conforms to the adopted numerical scheme. In fact, a linearisation is usually required to this purpose, for instance by evaluating the eigenvectors $\mathbf{l}_i$, $i = 1, 2$, in (5.1.50) at the previous time step t^n. These two extra equations are then added to the ones produced by (5.1.46) and, together with the assigned boundary conditions, allow to solve the discrete problem.
This technique has been tested as well, yet in this work we preferred the method based on the extrapolation of the characteristics, for its simplicity.

5.2 Coupling the 3D model with the 1D model

We consider now two domains Ω_{3D} and Ω_{1D} as in Fig. 5.2 and we solve, in the first, the 3D fluid-structure model while in the second we consider the simplified 1D model.

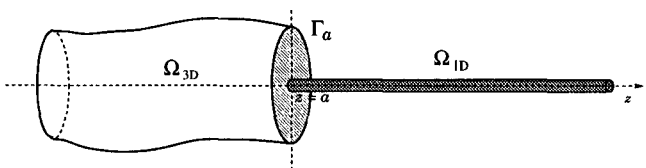

Figure 5.2: Coupling a 3D model with a 1D model

On the right side of Γ_a the 1D model supplies the quantities $A(a^+)$, $Q(a^+)$, $\overline{p}(a^+) = \psi(A)$ and $\overline{u}(a^+) = Q/A$. We define, then, the same quantities also on the left side of Γ_a as

$$A(a^-) = |\Gamma_a|; \qquad \overline{u}(a^-) = \frac{1}{|\Gamma_a|}\int_{\Gamma_a} \mathbf{u}\cdot\mathbf{n}\, d\sigma$$

$$\overline{p}(a^-) = \frac{1}{|\Gamma_a|}\int_{\Gamma_a} p\, d\sigma; \qquad Q(a^-) = |\Gamma_a|\,\overline{u}(a^-).$$

Moreover, we assume that at Γ_a the wall displacement is a function of the section area,

$$\boldsymbol{\eta}\big|_{\Gamma_a} = \mathbf{g}(A(a^-)), \tag{5.2.1}$$

being $\mathbf{g}$ a given function. For instance, we can assume that Γ_a is a circle in which case $\boldsymbol{\eta}\big|_{\Gamma_a} = \left(\sqrt{A(a^-)/\pi} - R_0\right)\mathbf{e}_r$.

It is a priori reasonable to look for the continuity of the following quantities at the interface Γ_a:

[A] area : $A(a^-) = A(a^+)$

[B] mean pressure : $\overline{p}(a^-) = \overline{p}(a^+)$

[C] flux : $Q(a^-) = Q(a^+)$

[D] entering characteristic : $\overline{u}(a^-) + 2\sqrt{\frac{2}{\rho}}\left(\sqrt{\overline{p}(a^-) - p_{ext} + p^*} - \sqrt{p^*}\right) = W_1(a^+)$

Since in the 1D model viscous terms have been (partially) neglected, the variable $\overline{p}$ can be either interpreted as a mean pressure or as a mean normal stress. The condition [B] may then be replaced with the continuity of the averaged normal stress, i.e. $\bar{\sigma} = \overline{\mathbf{T} \cdot \mathbf{n} \cdot \mathbf{n}}$. Analogously, the characteristic variable on the left hand side can be calculated using the averaged normal stress in place of the mean pressure. We have then two conditions alternative to B and D, respectively. Namely,

[B1] averaged normal stress : $\bar{\sigma}(a^-) = \overline{p}(a^+)$

[D1] char. entering variable : $\overline{u}(a^-) + 2\sqrt{\frac{2}{\rho}}\left(\sqrt{\bar{\sigma}(a^-) - p_{ext} + p^*} - \sqrt{p^*}\right) = W_1(a^+)$

In view of the splitting procedure that will be described in Section 5.2.1 to solve the coupled 3D-1D model, we are allowed to enforce, at the interface point a, only those conditions that will generate well posed individual subproblems in Ω_{3D} and Ω_{1D}.
To this aim, we advocate six different set of coupling conditions:

- **Interaction Model 1**: conditions A, B, D
  We note that B and D imply the continuity of $\overline{u}$. With the further continuity of A we obtain that of Q. Thus also C is satisfied.

- **Interaction Model 2**: conditions A, C, D
  We note that A and C imply the continuity of $\overline{u}$. If we further add D we have the continuity of $\overline{p}$. Thus also B is satisfied.

- **Interaction Model 3**: conditions A, B1, D1
  We note that B1 and D1 imply the continuity of $\overline{u}$ and , with the continuity of A we obtain that of Q. Thus also C is satisfied.

- **Interaction Model 4**: conditions A, C, D1
  We note that A and C imply the continuity of $\overline{u}$. If we further add D we have the continuity of $\bar{\sigma}$. Thus also B1 is satisfied.

- **Interaction Model 5**: conditions A, B, C
  We note that A and C imply the continuity of $\overline{u}$ and , with the continuity of B we obtain that of W. Thus also D is satisfied.

- **Interaction Model 6**: conditions A, B1, C
  We note that A and C imply the continuity of $\overline{u}$. If we further add B1 we have the continuity of W. Thus also D1 is satisfied.

5.2.1 Sub-domain iterations between 1D and 3D models

Each Interaction Model presented above can be split into two subproblems:

- A 1D problem with condition D (or D1) or B (B1), depending on which interaction model we consider, as boundary condition at the interface and an absorbing condition on the right end (i.e. zero entering characteristic variable). The first case (condition D or D1) corresponds to impose the entering characteristic variable at the interface; on the other hand, condition B (or B1) can be viewed as a condition on the area at the interface since in the 1D model, the pressure and the area are related through an algebraic relation. Both situations have been faced in Section 5.1.5.

- A 3D fluid-structure problem with condition A as boundary condition for the structure equation and condition B (B1) or C, depending on which interaction model we consider, as boundary condition for the Navier-Stokes equations. On the inflow section $\mathcal{S}_1$ we might impose ordinary Dirichlet or natural conditions; for instance we could assign the velocity profile for the fluid and the displacement of the wall.

  With these choices the structure problem turns out to be well posed, while conditions B or C as such are not sufficient to close the fluid equations since they only provide averaged and not pointwise values on Γ_a.

  The problem of how to impose this kind of *defective boundary conditions* to the Navier-Stokes equations has been deeply investigated in the paper by L. Formaggia, J.F. Gerbeau, F. Nobile and A. Quarteroni *Numerical treatment of defective boundary conditions for the Navier-Stokes equations* [28]. The ideas proposed therein are briefly summarized in Section 5.2.2.

We present, now, two possible iterative algorithms to couple the 3D and the 1D model. They correspond to the Interaction Model 3 and 6 respectively and both have been used pro the numerical simulations presented in Section 5.3 (see also the numerical results in [29] and [28]). Observe that these two interaction models are equivalent in the sense they provide the continuity of the same quantities at the interface.

Algorithm 1
Given the solution of the coupled problem at time $t = t^n$, let's say $\mathbf{u}^n$, p^n, $\boldsymbol{\eta}^n$ for the 3D model, and Q^n, A^n for the 1D one, we look for the solution $\mathbf{u}^{n+1}$, p^{n+1}, $\boldsymbol{\eta}^{n+1}$, Q^{n+1} and A^{n+1} using the following iterative algorithm :
we set $\mathbf{u}_{(0)} = \mathbf{u}^n$, $p_{(0)} = p^n$, and $\boldsymbol{\eta}_{(0)} = \boldsymbol{\eta}^n$ and for $k = 0, 1, \ldots$

1. we solve the 1D model (5.1.1) with at $z = a$

$$W_{1,(k+1)}(a^+) = \overline{u}_{(k)}(a^-) + 2\sqrt{\frac{2}{\rho}}\left(\sqrt{\bar{\sigma}_{(k)}(a^-) - p_{ext} + p^*}) - \sqrt{p^*}\right),$$

   where

$$\overline{u}_{(k)}(a^-) = \frac{1}{|\Gamma_{a,(k)}|}\int_{\Gamma_{a,(k)}} \mathbf{u}_{(k)} \cdot \mathbf{n}\, d\sigma \quad \text{and}$$

$$\bar{\sigma}_{(k)}(a^-) = \frac{1}{|\Gamma_{a,(k)}|}\int_{\Gamma_{a,(k)}} \mathbf{T}(\mathbf{u}_{(k)}, p_{(k)}) \cdot \mathbf{n} \cdot \mathbf{n}\, d\sigma,$$

and at $z = b$ the absorbing boundary condition $W_2(b) = 0$. We obtain $Q_{(k+1)}$ and $A_{(k+1)}$ in Ω_{1D};

2. we solve then the 3D fluid/structure problem by imposing for the structure at $z = a$

$$\boldsymbol{\eta}_{(k+1)}|_{\Gamma_a} = \left(\sqrt{\frac{A_{(k+1)}(a^+)}{\pi}} - R_0\right)\mathbf{e}_r$$

and for the Navier-Stokes equations, on $\Gamma_{a,(k+1)}$ the defective condition

$$\frac{1}{|\Gamma_{a,(k+1)}|}\int_{\Gamma_{a,(k+1)}} \mathbf{T}(\mathbf{u}_{(k+1)}, p_{(k+1)})\cdot\mathbf{n}\cdot\mathbf{n}\,d\sigma = p_{ext} + \beta\sqrt{A_{(k+1)}(a^+)} - p^*. \quad (5.2.2)$$

On the inflow section we prescribe suitable boundary conditions. We obtain, thus, $\mathbf{u}_{(k+1)}$, $p_{(k+1)}$, $\boldsymbol{\eta}_{(k+1)}$ in Ω_{3D}.

We iterate until the coupling conditions are satisfied within a fixed tolerance and we finally set the solution at time t^{n+1} equal to the converged value. We may eventually add a relaxation step on the variable $W_{1,(k)}(a^+)$.

Algorithm 2

Given the solution of the coupled problem at time $t = t^n$, we look for the solution $\mathbf{u}^{n+1}$, p^{n+1}, $\boldsymbol{\eta}^{n+1}$, Q^{n+1} and A^{n+1} using the following iterative algorithm :

we set $\mathbf{u}_{(0)} = \mathbf{u}^n$, $p_{(0)} = p^n$, and $\boldsymbol{\eta}_{(0)} = \boldsymbol{\eta}^n$ and for $k = 0, 1, \ldots$

1. we solve the 1D model (5.1.1) with, at $z = a$,

$$A_{(k+1)}(a^+) = \frac{1}{\beta^2}\left(\bar{\sigma}_{(k)}(a^-) - p_{ext} + p^*\right)^2$$

where

$$\bar{\sigma}_{(k)}(a^-) = \frac{1}{|\Gamma_{a,(k)}|}\int_{\Gamma_{a,(k)}} \mathbf{T}(\mathbf{u}_{(k)}, p_{(k)})\cdot\mathbf{n}\cdot\mathbf{n}\,d\sigma$$

and at $z = b$ the absorbing boundary condition $W_2(b) = 0$. We obtain $Q_{(k+1)}$ and $A_{(k+1)}$ in Ω_{1D};

2. we solve then the 3D fluid/structure problem by imposing for the structure at $z = a$

$$\boldsymbol{\eta}_{(k+1)}|_{\Gamma_a} = \left(\sqrt{\frac{A_{(k+1)}(a^+)}{\pi}} - R_0\right)\mathbf{e}_r$$

and for the Navier-Stokes equations on $\Gamma_{a,(k+1)}$ the defective condition

$$\int_{\Gamma_{a,(k+1)}} \mathbf{u}_{(k+1)}\cdot\mathbf{n}\,d\sigma = Q_{(k+1)}(a^+) \quad (5.2.3)$$

We obtain $\mathbf{u}_{(k+1)}$, $p_{(k+1)}$, $\boldsymbol{\eta}_{(k+1)}$ in Ω_{3D}.

We iterate until the coupling conditions are satisfied within a fixed tolerance and we finally set the solution at time t^{n+1} equal to the converged value. We may eventually add a relaxation step on the variable $A_{(k)}(a^+)$.

As we have already pointed out, in step 2. of both algorithms we need to solve Navier-Stokes equations with defective boundary conditions either on the flux through the interface Γ_a or on the averaged stress.

5.2.2 Defective boundary conditions for the Navier Stokes equations

Let us consider the domain $\Omega \subset \mathbb{R}^d$, $d = 2$ or 3 shown in figure 5.3. Its boundary $\partial\Omega$ is

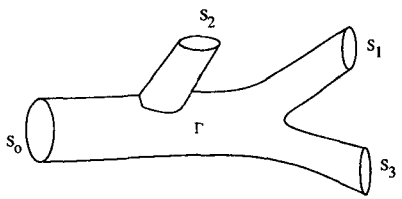

Figure 5.3: The partition of the boundary of the domain Ω.

decomposed into the union of Γ and several disjoint sections S_0, $S_1, \ldots, S_n$, $n \geq 1$.
We formalize the problem of fluid equations with defective boundary conditions in the following way : we are interested in solving the Navier-Stokes equations

$$\begin{cases} \partial_t \mathbf{u} + \mathbf{u} \cdot \nabla \mathbf{u} + \nabla p - \nu \triangle \mathbf{u} = \mathbf{f}, & t > 0 \\ \text{div } \mathbf{u} = 0, & t > 0 \\ \mathbf{u} = \mathbf{u}_0, & t = 0, \end{cases} \tag{5.2.4}$$

in the domain Ω whose boundary Γ may be deformable or not. In the former case equations (5.2.4) are supplemented by non-homogeneous boundary conditions

$$\mathbf{u}|_\Gamma = \dot{\boldsymbol{\eta}}, \tag{5.2.5}$$

where $\dot{\boldsymbol{\eta}}$ is the velocity at which the boundary moves; in the latter case, homogeneous boundary conditions will be considered

$$\mathbf{u}|_\Gamma = \mathbf{0}. \tag{5.2.5'}$$

On sections S_i, $i = 0, \ldots, n$ we consider three possible defective conditions :

prescribed mean pressure problem

$$\frac{1}{\text{meas}(S_i)} \int_{S_i} p\, ds = P_i, \quad i = 0, \ldots, n, \tag{5.2.6}$$

where each P_i is a prescribed function of the time t.

prescribed averaged normal stress

$$\frac{1}{\text{meas}(S_i)} \int_{S_i} \left(p\mathbf{n} - \nu \frac{\partial \mathbf{u}}{\partial \mathbf{n}} \right) \cdot \mathbf{n}\, ds = P_i, \quad i = 0, \ldots, n, \tag{5.2.7}$$

where each P_i is a prescribed function of the time t.

prescribed flux problem

$$\int_{S_i} \mathbf{u}\cdot\mathbf{n}\,ds = Q_i, \quad i=1,\dots,n, \qquad \text{and} \qquad \left(p\mathbf{n} - \nu\frac{\partial \mathbf{u}}{\partial \mathbf{n}}\right)\Big|_{S_0} = 0, \tag{5.2.8}$$

where the Q_i's are assigned functions of time.

We could also have imposed the flux on every section S_i, $i=0,\dots,n$. In this case, due to the incompressibility of the fluid, a compatibility relation must exist among the fluxes Q_i and the pressure is defined up to a constant.

The initial-boundary value problem (5.2.4)-(5.2.5) with either (5.2.6) or (5.2.7) or (5.2.8) is not well-posed from a physical point of view, since its solution is not unique. Indeed, on every section S_i, we are prescribing just one scalar condition rather than d conditions at every point $\mathbf{x}\in S_i$, as it should be.

To solve the *prescribed mean pressure problem* we follow the so-called *do-nothing* approach proposed in [46] : let us introduce the functional spaces

$$V = \left\{\mathbf{v}\in \left[H^1(\Omega)\right]^d, \mathbf{v}|_\Gamma = 0\right\} \qquad \text{and} \qquad M = L^2(\Omega).$$

We suppose that $\mathbf{f}\in V'$ and we introduce the functional $\phi_i\in V'$, $i=0,\dots,n$ which measures the flux of a vector function through the surface S_i. Precisely

$$< \phi_i, \mathbf{v} >= \int_{S_i} \mathbf{v}\cdot\mathbf{n}\,ds, \quad \forall \mathbf{v}\in V.$$

For this reason ϕ_i is called the *flux functional* on S_i. Then, the "do-nothing" formulation for the *prescribed mean pressure problem* reads : find $\mathbf{u}\in [H^1(\Omega)]^d$, satisfying conditions (5.2.5) (or (5.2.5')) and $p\in M$ such that, for all $\mathbf{v}\in V$ and $q\in M$,

$$\begin{cases} (\partial_t\mathbf{u} + \mathbf{u}\cdot\nabla\mathbf{u}, \mathbf{v}) + \nu(\nabla\mathbf{u}, \nabla\mathbf{v}) - (p, \text{div } \mathbf{v}) =< \mathbf{f}, \mathbf{v} > - \displaystyle\sum_{i=0}^{n} P_i < \phi_i, \mathbf{v} >, \\ (q, \text{div } \mathbf{u}) = 0, \end{cases} \tag{5.2.9}$$

for all $t>0$, with $\mathbf{u}=\mathbf{u}_0$ for $t=0$.
It follows easily, by using the Green formula, that the solution of (5.2.9) satisfies

$$\left(p - \nu\frac{\partial u_n}{\partial \mathbf{n}}\right)\Big|_{S_i} = P_i, \qquad \frac{\partial \mathbf{u}_\tau}{\partial \mathbf{n}}\Big|_{S_i} = 0, \quad \text{for } i=0,\dots,n,$$

where we have set $u_n = \mathbf{u}\cdot\mathbf{n}$ and $\mathbf{u}_\tau = \mathbf{u} - u_n\mathbf{n}$.
Thus

$$\frac{1}{\text{meas}(S_i)}\int_{S_i} p\,ds = P_i + \frac{\nu}{\text{meas}(S_i)}\int_{S_i}\frac{\partial u_n}{\partial \mathbf{n}}\,ds. \tag{5.2.10}$$

We conclude that the desired condition (5.2.6) is recovered exactly only in those cases where the last integral in (5.2.10) vanishes. This occurs, for instance, when S_i is a plane section perpendicular to a cylindrical pipe.

Otherwise, P_i will be the mean value of the normal component of the normal stresses on S_i. Thus, the same approach can be used to impose conditions (5.2.7) as well.
At the moment we are not able to propose a formulation which allows to impose only the averaged quantity (5.2.6) or (5.2.7) without resorting to a constant normal stress on each section S_i.
The formulation of the *prescribed mean pressure problem* may be easily discretised as it can be regarded as a classical Navier-Stokes problem with Neumann boundary conditions.

To solve the *prescribed flux problem*, instead, we adopt an approach based on the use of Lagrange multipliers. The formulation reads as follows : we look for $\mathbf{u} \in [H^1(\Omega)]^d$, satisfying conditions (5.2.5) (or (5.2.5')), $p \in M$ and $\lambda_1, \ldots, \lambda_n \in \mathbb{R}$ such that, for all $\mathbf{v} \in V$ and $q \in M$,

$$\begin{cases} (\partial_t \mathbf{u} + \mathbf{u} \cdot \boldsymbol{\nabla} \mathbf{u}, \mathbf{v}) + \nu(\boldsymbol{\nabla} \mathbf{u}, \boldsymbol{\nabla} \mathbf{v}) + \displaystyle\sum_{i=1}^{n} \lambda_i < \phi_i, \mathbf{v} > - (p, \operatorname{div} \mathbf{v}) = < \mathbf{f}, \mathbf{v} >, \\ (q, \operatorname{div} \mathbf{u}) = 0, \\ < \phi_i, \mathbf{u} > = Q_i, \qquad i = 1, .., n, \end{cases} \tag{5.2.11}$$

for all $t > 0$, with $\mathbf{u} = \mathbf{u}_0$ for $t = 0$.
It can be shown (see [28]) that any smooth solution of (5.2.11) satisfies the additional boundary conditions

$$\left(p - \nu \frac{\partial u_n}{\partial \mathbf{n}} \right) \Big|_{S_i} = \lambda_i, \quad \text{and} \quad \frac{\partial \mathbf{u}_\tau}{\partial \mathbf{n}} \Big|_{S_i} = 0, \quad i = 1, \cdots n. \tag{5.2.12}$$

In particular, this yields that both $\dfrac{\partial \mathbf{u}_\tau}{\partial \mathbf{n}}$ and $p - \nu \dfrac{\partial u_n}{\partial \mathbf{n}}$ are indeed constant over S_i for $i = 1, \cdots, n$. Moreover, the Lagrange multipliers represent the normal component of the normal stress on each section S_i and have then the dimension of a pressure.
In the cited paper, we have shown that, for a stationary Stokes problem, formulation (5.2.11) is well posed. In the same paper, we proposed different strategies to solve efficiently problem (5.2.11) discretised with finite elements. We recall, here, briefly the ones based on the Yosida algebraic factorisation scheme.
We introduce a Galerkin approximation based on the finite dimensional spaces $V_h \subset V$ and $M_h \subset M$, which we assume to satisfy the LBB condition

$$\forall q_h \in M_h \quad \exists \mathbf{v}_h \in V_h,\ \mathbf{v}_h \neq 0 : \quad (q_h, \operatorname{div} \mathbf{v}_h) \geq \beta_h \|q_h\|_{L^2} \|\mathbf{v}_h\|_{H^1}. \tag{5.2.13}$$

Let $(\mathbf{u}_h, p_h, \lambda_{1h}, \ldots, \lambda_{nh})$ be the solution of the discrete problem. We denote by $(u_i)_{i=1..dN}$ (resp. $(p_i)_{i=1..M}$) the components of $\mathbf{u}_h$ (resp. p_h) with respect to a basis $\{\mathbf{v}_i\}$ of V_h (resp. $\{q_i\}$ of M_h). Finally, we introduce the vectors $U = (u_1, .., u_{dN}) \in \mathbb{R}^{dN}$, $P = (p_1, .., p_M) \in \mathbb{R}^M$ and $\Lambda = (\lambda_{1h}, \ldots, \lambda_{nh}) \in \mathbb{R}^n$.
Proceeding as in Chapter 3 to discretise problem (5.2.11) in time (see section 3.5.1), we will obtain at each time step k a system of the form

$$\begin{bmatrix} A & D^T & \Phi^T \\ D & 0 & 0 \\ \Phi & 0 & 0 \end{bmatrix} \begin{bmatrix} \mathbf{U}^k \\ \mathbf{P}^k \\ \boldsymbol{\Lambda}^k \end{bmatrix} = \begin{bmatrix} \mathbf{f}_1^k \\ \mathbf{f}_2^k \\ \mathbf{Q}^k \end{bmatrix}. \tag{5.2.14}$$

The matrix $A \in \mathbb{R}^{dN \times dN}$ will have typically the form

$$A = \frac{1}{\Delta t} M + C$$

where C accounts for the convective and diffusive terms. $D \in \mathbb{R}^{M \times dN}$ is the matrix associated to the divergence operator and Φ is the $n \times dN$ matrix whose lines are given by the vectors $\phi_i = (\int_{S_i} \mathbf{v}_1 \cdot \mathbf{n}\, ds, \ldots, \int_{S_i} \mathbf{v}_{dN} \cdot \mathbf{n}\, ds)$, $i = 1, \ldots, n$. Finally $\mathbf{f}_1^k$ and $\mathbf{f}_2^k$ account for the forcing term, the non-homogeneous boundary conditions and the solution at previous time steps, while $\mathbf{Q}^k = [Q_1(t^k), \ldots, Q_n(t^k)]^T$.

We present hereafter two possible algorithms to solve system (5.2.14) :

Reordering + fractional step I

System (5.2.14) can be reordered in a Stokes-like form as

$$\begin{bmatrix} \tilde{A} & \tilde{D}^T \\ \tilde{D} & 0 \end{bmatrix} \begin{bmatrix} \tilde{\mathbf{U}}^k \\ \mathbf{P}^k \end{bmatrix} = \begin{bmatrix} \tilde{\mathbf{f}}^k \\ \mathbf{f}_2^k \end{bmatrix} \tag{5.2.15}$$

where

$$\tilde{A} = \begin{bmatrix} A & \Phi^T \\ \Phi & 0 \end{bmatrix} \in \mathbb{R}^{(dN+n)\times(dN+n)}, \qquad \tilde{D} = \begin{bmatrix} D & 0 \end{bmatrix} \in \mathbb{R}^{M\times(dN+n)},$$

$$\tilde{\mathbf{U}}^k = \begin{bmatrix} \mathbf{U}^k \\ \mathbf{\Lambda}^k \end{bmatrix} \in \mathbb{R}^{dN+n}, \qquad \tilde{\mathbf{f}}^k = \begin{bmatrix} \mathbf{f}_1^k \\ \mathbf{Q}^k \end{bmatrix} \in \mathbb{R}^{dN+n}$$

By applying the Yosida factorisation scheme to (5.2.15) we obtain the three step algorithm

(i) $\tilde{A}\tilde{\mathbf{U}}_0^k = \tilde{\mathbf{f}}^k$

(ii) $\tilde{D}\tilde{H}^{(1)}\tilde{D}^T P = \tilde{D}\tilde{\mathbf{U}}_0^k$.

(iii) $\tilde{A}\tilde{\mathbf{U}}^k = \tilde{A}\tilde{\mathbf{U}}_0^k - \tilde{D}^T\mathbf{P}^k$

where $\tilde{H}^{(1)}$ is an approximation of $\tilde{A}^{-1}$. In [28] a possible expression for $\tilde{H}^{(1)}$, preserving the accuracy of the Yosida scheme, is proposed. Yet, this expression is not straightforward to implement. On the other hand, step *(iii)* in the algorithm allows to recover exactly the constraints on the fluxes. Indeed, from step *(i)* we have $\Phi\mathbf{U}_0^k = \mathbf{Q}^k$ and in step *(iii)* we are imposing $\Phi\mathbf{U}^k = \Phi\mathbf{U}_0^k$.

Reordering + fractional step II

System (5.2.14) can also be reordered in a different manner as

$$\begin{bmatrix} A & \tilde{D}^T \\ \tilde{D} & 0 \end{bmatrix} \begin{bmatrix} \mathbf{U}^k \\ \tilde{\mathbf{P}}^k \end{bmatrix} = \begin{bmatrix} \mathbf{f}_1^k \\ \tilde{\mathbf{f}}^k \end{bmatrix} \tag{5.2.16}$$

where

$$\tilde{D} = \begin{bmatrix} D \\ \Phi \end{bmatrix} \in \mathbb{R}^{(M+n)\times dN}, \qquad \tilde{\mathbf{P}}^k = \begin{bmatrix} \mathbf{P}^k \\ \mathbf{\Lambda}^k \end{bmatrix} \in \mathbb{R}^{M+n}, \qquad \tilde{\mathbf{f}}^k = \begin{bmatrix} \mathbf{f}_2^k \\ \mathbf{Q}^k \end{bmatrix} \in \mathbb{R}^{M+n}$$

The three steps Yosida algorithm reads then

(i) $A\mathbf{U}_0^k = \mathbf{f}_1^k$

(ii) $\tilde{D}H^{(1)}\tilde{D}^T\tilde{\mathbf{P}}^k = \tilde{D}\mathbf{U}_0^k - \tilde{\mathbf{f}}^k$

(iii) $A\mathbf{U}^k = A\mathbf{U}_0^k - \tilde{D}^T\tilde{\mathbf{P}}^k$.

In this case, $H^{(1)}$ is an approximation of A^{-1} and can be taken equal to $H^{(1)} = \Delta t M^{-1}$, as in standard Yosida scheme.
This algorithm can be easily implemented starting from an existing Navier-Stokes solver which uses factorization methods. Indeed, it suffices to add to the matrix D the few lines of matrix Φ, and apply the chosen factorization method.
On the contrary, the constraints on the fluxes are not exactly satisfied. In [28] we have shown that the error introduced, i.e. $|\Phi\mathbf{U}^k - \mathbf{Q}^k|$ behaves as $O(\Delta t^2)$. This result has been confirmed numerically in the cited paper.

5.3 Numerical results

First test case. We have considered again the second test case presented in chapter 4. Precisely, we have solved the 2D fluid structure problem with the *MP/CN* coupled algorithm, on the mesh given in figure 4.9, with the input pressure profile as in figure 4.8 and a time step $\Delta t = 10^{-4}$. Yet, this time, instead of imposing homogeneous Neumann boundary conditions at the outflow section, we have coupled the 2D fluid-structure problem with a 1D model as shown in figure 5.2.
The 1D model adopted here is the one derived from a 2D geometry, i.e. system (5.1.1) with algebraic wall law given by (5.1.16). The parameters characterizing the fluid and wall dynamics both in the 2D and 1D models have been taken equal to those used in the simulations of Chapter 4. Moreover, the Coriolis coefficient α in (5.1.1) has been taken equal to 1. We have simulated the 1D model on the interval $[6\,cm,\ 12\,cm]$ discretised with a uniform mesh of 30 intervals and with a time step $\Delta t = 10^{-4}$ equal to the one adopted for the 2D simulation. The initial solution is the equilibrium state $Q = 0$ and $A = A_0$ and the CFL corresponding to this equilibrium position is about 0.22. At the right end ($z = 12\,cm$) we have imposed a zero entering characteristic variable.
About the 2D/1D coupling, we have tested both Algorithms 1 and 2 presented in Section 5.2.1, corresponding to Interaction models 3 and 6, respectively.
In the first case, to get convergence of the iterative algorithm, we have introduced a relaxation step on the entering characteristic variable $W_1(a^+)$

$$W_{1,(k+1)}^{new}(a^+) = \theta W_{1,(k+1)}(a^+) + (1-\theta)W_{1,(k)}(a^+)$$

with a relaxation parameter $\theta = 0.75$. The stopping criterion used for the 2D/1D sub-iterations is

$$\left|W_{1,(k+1)}(a^+) - W_{1,(k)}(a^+)\right| \leq 5 \cdot 10^{-5} \tag{5.3.1}$$

We remind that we are employing two sub-structuring algorithms at the same time: one for the fluid-structure problem and the other for the 2D/1D coupling. The strategy we have adopted consists in making 10 fluid-structure sub-iterations each 2D/1D sub-iteration and continuing until both stopping criteria (4.11.1) and (5.3.1) are satisfied.

Concerning Algorithm 2, we have added a relaxation step on the variable $A_{(k)}(a^+)$ with a much smaller relaxation parameter than in the previous case, i.e. $\theta = 0.02$. The stopping criterion in this case reads

$$\left| \frac{A_{(k+1)}(a^+) - A_{(k)}(a^+)}{A_0} \right| \leq 10^{-7}. \tag{5.3.2}$$

The use of Lagrange multipliers to impose flux conditions influences the convergence of the fluid-structure sub-iterations. In this case we have to take a relaxation parameter ω for the fluid-structure algorithm smaller that the one needed in Algorithm 1. We have verified that the solutions obtained by the two Algorithms are very similar. Indeed, as already remarked, these two algorithms provide the continuity of the same quantities at the 2D/1D interface. The results presented in the following of this section refer to Algorithm 1.

In figure 5.4 we present at different time instants the solution obtained. In the 2D part we visualize the pressure together with the structure deformation. On the other hand, the 1D model has been represented with a thick line and the colors correspond to the mean pressure computed. The color scale is the same as the one adopted in figures 4.10 and 4.19. Observe that almost no spurious reflections are present now. These results should be compared with those shown in figure 4.19 where homogeneous Neumann boundary conditions were imposed at the outflow section.

We have computed in the 2D region, on each vertical section, the mean pressure, the flow rate and the area, as it has been done in Chapter 4. In the 1D region, the same quantities are naturally provided by the 1D model (precisely, the 1D model provides A and Q, while the mean pressure can be recovered from the algebraic relation (5.1.16)).

Figures 5.5 and 5.6 represent these three quantities in the segment $[0, 12\,cm]$. The blue/solid line corresponds to the solution computed by the 2D model while the red/dashed line is the solution of the 1D model. Observe that the flow rate Q and the area A computed by the 2D and the 1D model, respectively, glue perfectly thanks to the coupling conditions imposed at the 2D/1D interface. On the contrary, the mean pressure $\bar{p}$ is not perfectly continuous at the interface, since in the adopted Interaction Model we are imposing the continuity of the averaged normal stress $\bar{\sigma}$ and not that of $\bar{p}$.

Second test case. To better highlight the effectiveness of this technique to "absorb" outgoing pressure and flow rate waves, we have compared the coupled 2D/1D solution of the previous test case with the solution obtained by solving only the 2D model (without any coupling with the 1D model) on a tube of length $12\,cm$ with homogeneous Neumann boundary conditions on the outflow section. At those instants at which the pressure wave is still far away from the outflow boundary, we can assume that this solution is not perturbed by the imposed boundary conditions. Then, in left half of the tube ($z \in [0, 6]$), this solution can be considered the "exact" solution of the 2D model, i.e. not perturbed by any boundary condition.

In figure 5.7 we compare the pressure and the wall deformation in the two cases at different time instants. It may be observed that the 1D model propagates the wave at a speed slightly higher than the 2D model.

In figure 5.8 we have put on the same plot the averaged pressure in $z \in [0, 6]$ obtained with the simulation of Chapter 4, i.e. with reflective boundary conditions, the one obtained with the 2D/1D coupling and the "exact" one obtained by solving the 2D model on the tube of double length. In this figure it is really evident how the 2D/1D coupling allows to dramatically reduce the spurious reflections at the outflow section with respect to the case considered in

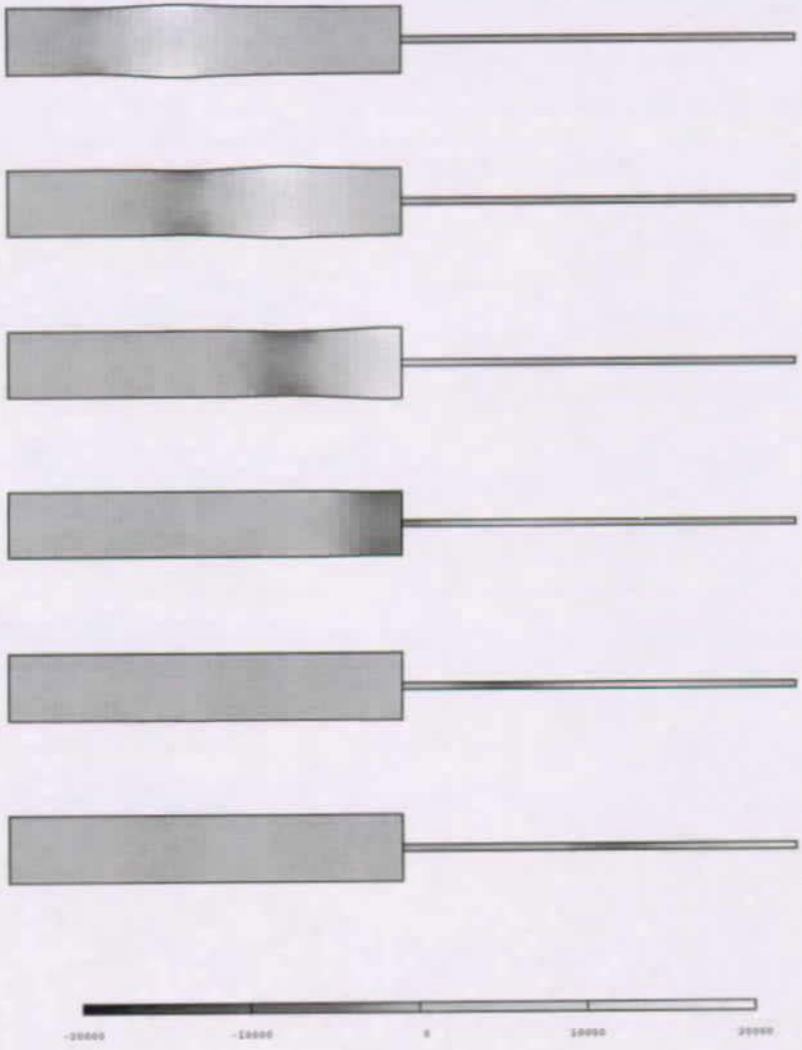

Figure 5.4: Coupling 2D simulation with the 1D reduced model; solution every $4\,ms$, starting form $t = 9\,ms$. Note how the pressure wave exits the domain with almost no spurious reflections. These results should be compared with those shown in figure 4.19.

Chapter 4. We may also observe that in the coupled 2D/1D simulation, the pressure wave is slightly accelerated with respect to the "exact" solution obtained by the only 2D model. This is due to the presence of the 1D model that, as already mentioned, features a wave speed a little higher than that of the 2D model.

Third test case. We would like, now, to quantify the reflections introduced by the coupling with the 1D model. Precisely, we aim at comparing the solution computed by the 2D/1D coupling, with the solution (taken as the "exact" one) obtained by solving only the 2D model on a tube of double length, as shown in the previous test case. To better highlight the spurious reflections, we have taken a different input pressure profile at the inflow; precisely, we have considered a pressure step of $5000\,dyne/cm^2$, i.e.

$$\mathbf{T}\cdot\mathbf{n} = \boldsymbol{\sigma}_1 = 5000\,dyne/cm^2, \quad \text{on } \mathcal{S}_1,\ \forall t > 0.$$

Let us denote with $(\mathbf{u}, p)$ the restriction of the "exact" solution to the left half of the tube $\Omega_1 = [0,6]\times[0,1]$ and with $(\mathbf{u}_1, p_1)$ the 2D solution in the same domain Ω_1 obtained with the coupled 2D/1D algorithm (see also figure 5.7). Figure 5.9 shows the relative error in the L^2 norm between the two solutions, i.e.

$$\varepsilon_p = \frac{\|p - p_1\|_{L^2(\Omega_1)}}{\|p\|_{L^2(\Omega_1)}}, \qquad \varepsilon_u = \frac{\|\mathbf{u} - \mathbf{u}_1\|_{L^2(\Omega_1)}}{\|\mathbf{u}\|_{L^2(\Omega_1)}}.$$

The simulation has been stopped at $t = 30\,ms$, i.e. before the pressure wave reaches the outflow at $z = 12\,cm$. The error on the velocity is about 2.5% with a peak over 3% when the wave crosses the 2D/1D interface. The pressure error, instead, is always less than 2%.

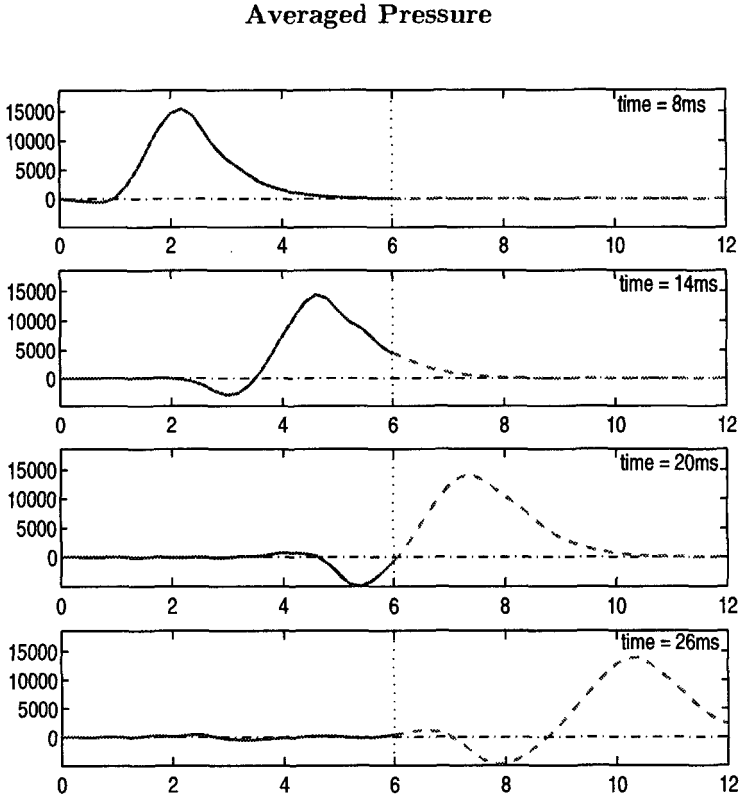

Figure 5.5: Averaged pressure at different time instants; in the left part of each plot ($z \in [0, 6\,cm]$), solution of the 2D model (blue/solid line); in the right part ($z \in [6\,cm, 12\,cm]$), solution of the 1D model (red/dashed line).

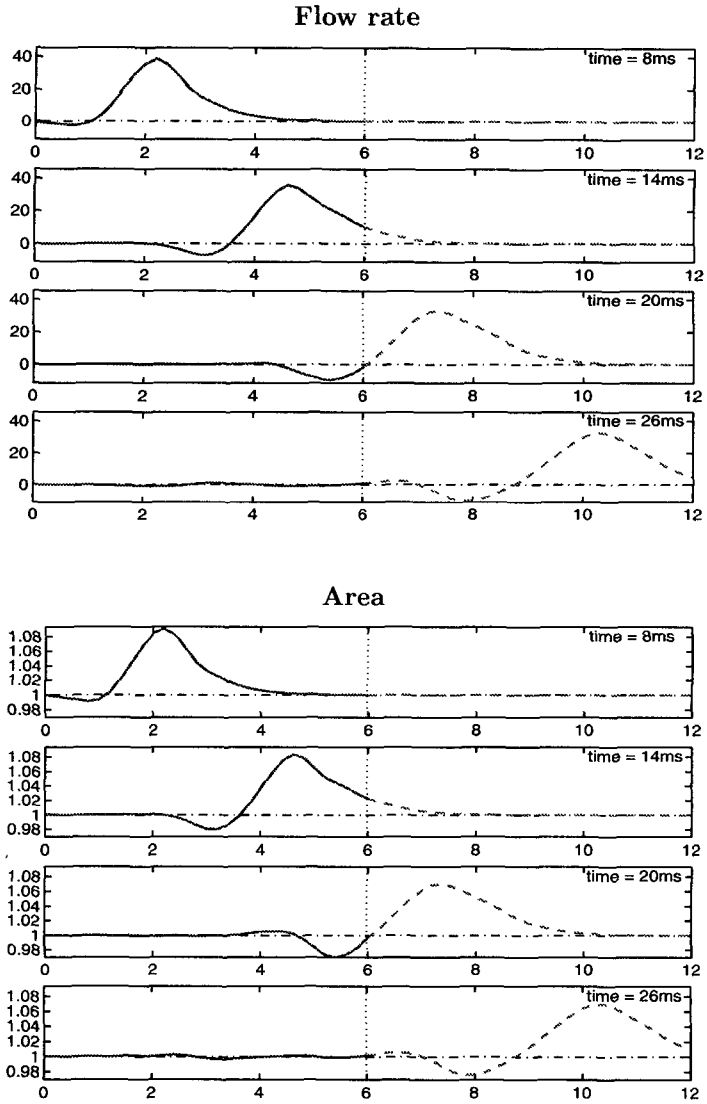

Figure 5.6: Flow rate (on the top) and Area of each section of the tube (on the bottom) at different time instants; in the left part of each plot ($z \in [0, 6\,cm]$), solution of the 2D model (blue/solid line); in the right part ($z \in [6\,cm, 12\,cm]$), solution of the 1D model (red/dashed line).

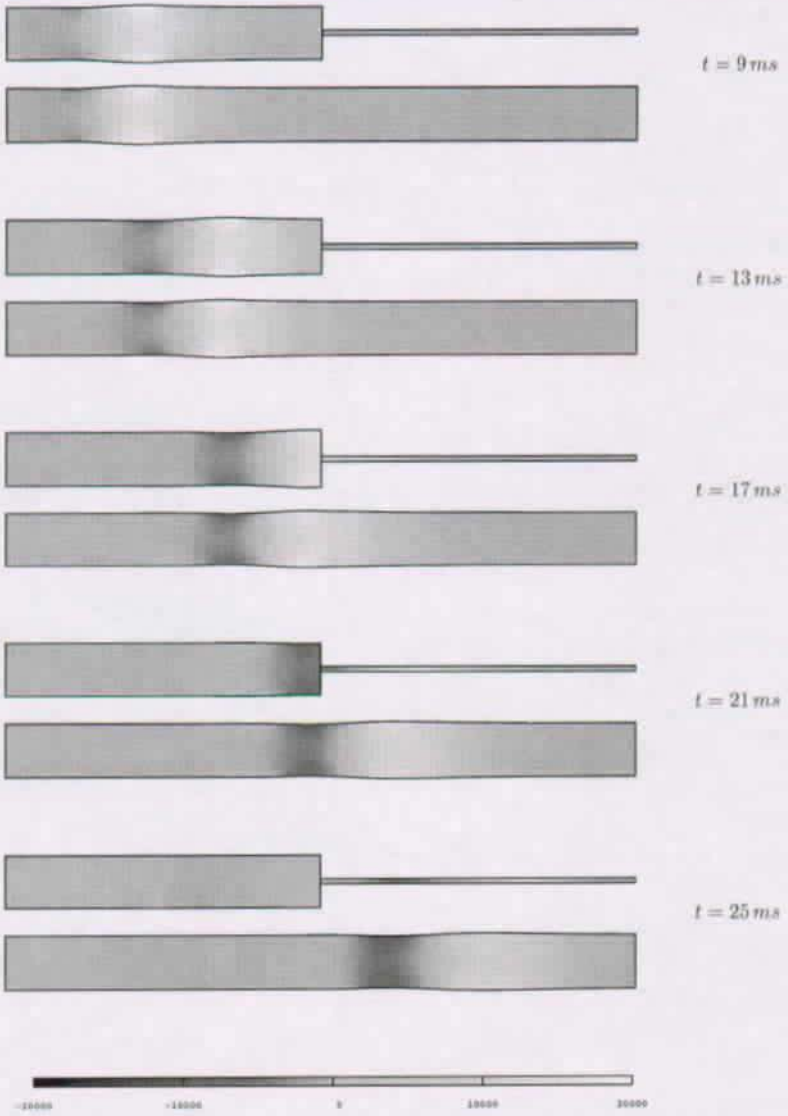

Figure 5.7: Comparison between the solution obtained with the 2D/1D coupling and the solution computed by the only 2D model on a tube of double length. In the plots we visualize the pressure inside the tube

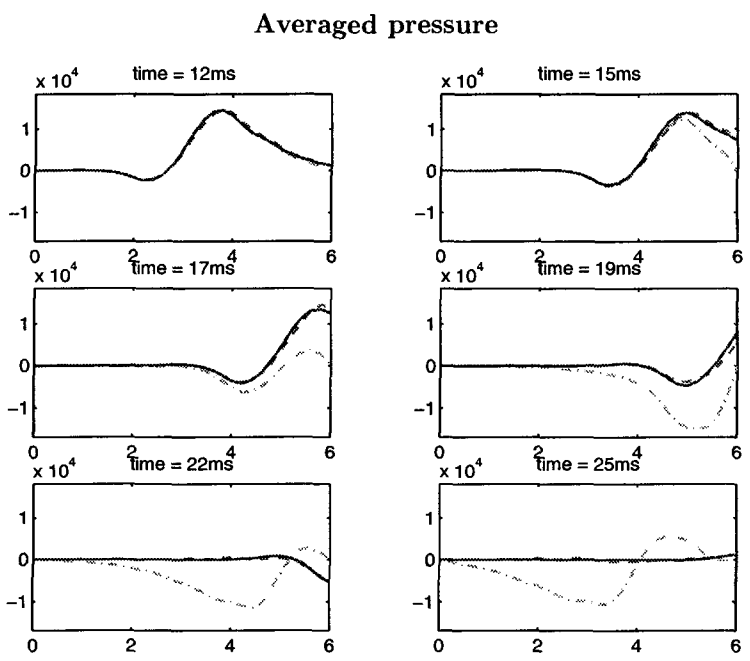

Figure 5.8: Averaged pressure along the tube $[0, 6\,cm]$ at different time instants. Blue/solid line: "exact" solution; red/dashed line: solution obtained by the 2D/1D coupling; green/dash-dotted line: solution obtained with homogeneous Neumann conditions at the outflow.

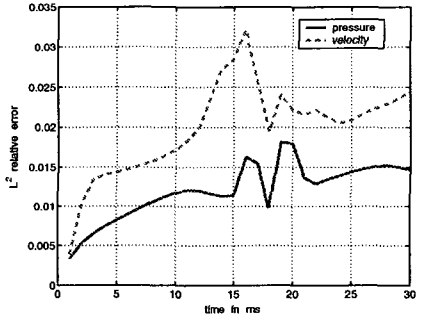

Figure 5.9: Relative error in L^2 norm both for pressure and velocity field, between the solution of the coupled 2D/1D model and the solution of the fluid-structure interaction problem on a vessel of double length.

Conclusions

In this thesis we have investigated some aspects of the numerical approximation of the fluid structure interaction problem appearing in the study of blood flow in large arteries.
In the first part, we have deeply investigated the ALE formulation for parabolic equations. in the context of a finite element approximation.
We have analysed and compared two formulations, a conservative and a non-conservative one; both have been proposed in the literature and employed for numerical simulations. They are equivalent at the differential level but lead to different numerical schemes.
We have considered a few temporal discretisations (first and second order accurate), applied to both the conservative and the non-conservative formulation and we have derived the associated Geometric Conservation Laws. We have analysed stability and convergence properties of these schemes and their relation with the GCL.
We have obtained an unconditional stability result for the Implicit Euler scheme, that satisfies the GCL, applied to the conservative formulation. On the contrary, we have shown that other time discretisation schemes, which are unconditionally stable when applied to a differential equation on a fixed domain, do not preserve the same stability properties when written in ALE form, even though GCL are satisfied.
On the other hand, the accuracy of time discretisation schemes does not degrade when solving problems on moving domains in ALE form; we have proved this theoretically for one scheme and numerically for others. In this regard, GCL seem not to play any relevant role in the accuracy of the numerical schemes.
Finally, we have generalised these results to the incompressible Navier-Stokes equations. Moreover, we have shown how inexact factorisation schemes can be extended straightforwardly to the ALE framework.

In the second part of this thesis we have studied the fluid-structure interaction model arising in hemodynamic applications and we have proved an a priori stability result for the differential model, under a condition on the positivity of the kinetic energy flux at the outflow.
We have then considered the quite general case of a non-conforming finite element approximation in space and fully implicit coupled discretisations in time. Indeed, we have experienced that staggered algorithms are unstable when applied to the problem at hand with physiological parameters. We have proposed three implicit coupled algorithms that make use of the Implicit Euler scheme (indicated *IE*), satisfying the GCL, that has been proposed in Chapter 1. What changes among them is the structure discretisation, that has been taken as the first order BDF (*BDF*), the mid-point (*MP*) and the Leap-Frog (*LF*) scheme, respectively, as well as the coupling conditions between fluid and structure. For the first two coupled algorithms we have proved an unconditional stability result. For the third one, we have proved a conditional stability result where the stability constant is governed only by the structure

discretisation. We have also proposed a fourth implicit coupled algorithm that employs a Crank-Nicolson discretisation (*CN*) for the fluid and a mid point one for the structure. For this algorithm we could not obtain an unconditional stablility result since the Crank-Nicolson scheme, applied to the fluid equations in ALE form, is not unconditionally stable, as we have shown in Chapter 3. Yet, we have proved that the energy exchange between fluid and structure at the discrete level is perfectly balanced in this coupled algorithm.
We have also shown on a numerical test case that the algorithm *MP/IE* is first order accurate and *MP/CN* is second order accurate in time.
To solve the non-linear system that arises at each time step, we have considered a simple Block Gauss-Seidel iterative algorithm that consists in sub-iterating between fluid and structure until the coupling conditions are satisfied within a fixed tolerance. We have used this iterative algorithm for all the numerical simulations presented in Chapters 4 and 5. Yet, as we have pointed out, this iterative algorithm needs a small relaxation parameter and demands for a very large number of sub-iterations. Thus, at the moment, it can not be used for realistic applications. The investigation of accelerating techniques in mandatory.
Strategies as Aitken extrapolations or non-linear GMRES iterations may be considered in the hope of dramatically reduce the number of fluid-structure sub-iterations and consequently the CPU time. This aspect will be investigated in an ongoing research.
Another attractive idea might be that of using the simplified mono-dimensional model, presented in Chapter 5, as a "preconditioner" of the coupled fluid-structure problem. This algorithm should be formalized as a non-linear multigrid/multimodel strategy. Since the 1D model is well suited to describe propagative phenomena, we feel that it could provide a good prediction of the solution of the coupled fluid-structure model. Preliminary numerical tests (see [27]) gave very encouraging results. This idea will be furtherly investigated in an ongoing research.
Finally, in the last Chapter of this work we have proposed a technique to devise absorbing boundary conditions for the fluid-structure problem, by the coupling with a reduced mono-dimensional model and we have shown its effectiveness on a numerical test case.
This approach is motivated also by the prospect of implementing multi-scale models for the human cardiovascular system (see [32]). It is clear that a realistic detailed numerical simulation of the flow in a segment of an artery (like, for instance, the carotid bifurcation or a trait of a coronary) may not be fully accomplished without accounting for the interactions with the remaining part of the cardiovascular system. One possibility to that direction is offered by the coupling of the detailed 2D/3D simulation with a simplified 1D or even lumped parameter modeling of the rest of the global system. The work carried out in this thesis represents a necessary step towards the goal of setting up an accurate and robust solver of the whole cardiovascular system.

Bibliography

[1] Y. Achdou, Y. Maday, and O.B. Widlund. Iterative substructuring preconditioners for mortar element methods in two dimensions. *Siam j. Numer. Anal.*, 36(2):551–580, 1999.

[2] R. Aris. *Vectors, Tensors, and the Basic Equations of Fluid Mechanics.* Dover Publications Inc., 1989.

[3] M. Bathe and R.D. Kamm. A fluid-structure interaction finite element analysis of pulsatile blood flow through a compliant stenotic artery. *Transaction of the ASME: J. Biomech. Engrg.*, 121:361–369, 1999.

[4] F.B. Belgacem. The mortar finite element method with lagrange multipliers. *Numer. Math.*, 84:173–197, 1999.

[5] F.B. Belgacem and Y. Maday. The mortar element method for three dimensional finite elements. *M2AN*, 31(2):289–302, 1997.

[6] C. Bernardi, Y. Maday, and A.T. Patera. A new non-conforming approach to domain decomposition: the mortar element method. In H. Brezis and J.L. Lions, editors, *Collège de France Seminar*, pages 64–84. Pitman, Boston, 1990.

[7] H. Brezis. *Analyse fonctionnelle, théorie et applications.* Masson, 1983.

[8] F. Brezzi and R.S. Falk. Stability of higher-order Hood-Taylor methods. *SIAM J. Numer. Anal.*, 28(3):581–590, 1991.

[9] F. Brezzi and M. Fortin. *Mixed and hybrid finite element methods.* Springer-Verlag, New York, 1991.

[10] R.M. Brown, W. Hu, and G.M. Lieberman. Weak solutions of parabolic equations in non-cylindrical domains. *Proc. Amer. Math. Soc.*, 125(6):1785–1792, 1997.

[11] P. Cannarsa, G. Da Prato, and J.P. Zolésio. Evolution equations in non-cylindrical domains. *Atti Acc. Lincei Rend. fis.*, 8:73–77, 1989.

[12] Y.C. Chang, T.Y. Hou, B. Merriman, and S. Osher. A level set formulation of eulerian interface capturing methods for incompressible fluid flows. *J. Comput. Phys.*, 124(2):449–464, 1996.

[13] P. G. Ciarlet. *Introduction to linear shell theory.* Gauthier-Villars, Paris, 1998.

[14] P.G. Ciarlet. *Mathematical elasticity. Volume 1: three dimensional elasticity,* volume 20 of *Studies in Mathematics and its Applications.* North Holland, 1988.

[15] P.G. Ciarlet and J.L. Lions, editors. *Handbook of numerical analysis - Finite element methods (Part I)*, volume 2. North-Holland, 1991.

[16] G.R. Cokelet. The rheology and tube flow of blood. In R. Skalak and S. Chen, editors, *Handbook of Bioengineering*. McGraw-Hill, 1987.

[17] C. Conca, J. San Martín, and M. Tucsnak. Motion of a rigid body in a viscous fluid. *C. R. Acad. Sci. Paris, série I*, 328:473–478, 1999.

[18] B. Desjardins and M. Esteban. Existence of weak solutions for the motion of rigid bodies in a viscous fluid. *Arch. Rational Mech. Anal.*, 146:59–71, 1999.

[19] B. Desjardins, M. Esteban, C. Grandmont, and P. Le Tallec. Weak solutions for a fluid-elastic structure interaction model. submitted.

[20] J. Donea. Arbitrary Lagrangian Eulerian methods. In *Computational Methods for Transient Analysis*, volume 1 of *Computational Methods in Mechanics*. North-Holland, Elsevier, 1983.

[21] G. Duvaut and J.L. Lions. *Les inéquations en mécanique et en physique*. Dunod, Paris, 1972.

[22] B. Engquist and A. Majda. Numerical radiation boundary conditions for unsteady transonic flow. *J. Comput. Phys.*, 40(1):91–103, 1981.

[23] C. Farhat, P. Geuzaine, and G. Brown. Application of a three-field nonlinear fluid-structure formulation to the prediction of the aeroelastic parameters of an F-16 fighter. proceeding of AMIF 2000 Conference, to appear on Comp. Vis. Science.

[24] C. Farhat and M. Lesoinne. Two efficient staggered algorithms for the serial and parallel solution of three-dimensional nonlinear transient aeroelastic problems. *Comput. Methods Appl. Mech. Engrg*, 182:499–515, 2000.

[25] C. Farhat, M. Lesoinne, and P. Le Tallec. Load and motion transfer algorithms for fluid/structure interaction problems with non-matching discrete interfaces: Momentum and energy conservation, optimal discretization and application to aeroelasticity. *Comput. Methods Appl. Mech. Engrg.*, 157:95–114, 1998.

[26] C. Farhat, M. Lesoinne, and N. Maman. Mixed explicit/implicit time intergration of coupled aeroelastic problems: three-field formulation, geometry conservation and distributed solution. *Int. J. Num. Meth. Fluids*, 21:807–835, 1995.

[27] E. Finzi. Résolution d'écoulements sanguins avec une technique multigird/multimodèles. Travail de fin d'études, Ecole Nationale Supérieure de Techniques Avancées, Paris, September 2001.

[28] L. Formaggia, J.F. Gerbeau, F. Nobile, and A. Quarteroni. Numerical treatment of defective boundary conditions for the Navier-Stokes equations. Report EPFL-DMA 20.2000 and INRIA-4093.

[29] L. Formaggia, J.F. Gerbeau, F. Nobile, and A. Quarteroni. On the coupling of 3D and 1D Navier-Stokes equations for flow problems in compliant vessels. Comp. Methods in Appl. Mech. Engng., in press.

[30] L. Formaggia and F. Nobile. A stability analysis for the Arbitrary Lagrangian Eulerian formulation with finite elements. *East-West Journal of Numerical Mathematics*, 7:105–132, 1999.

[31] L. Formaggia, F. Nobile, and A. Quarteroni. A one dimensional model for blood flow: Application to vascular prosthesis. to appear in MSCOM2000, Lecture Notes in Computational Science and Engineering, T. Miyoshi Ed., Springer-Verlag, Berlin, 2001.

[32] L. Formaggia, F. Nobile, A. Quarteroni, and A. Veneziani. Multiscale modelling of the circulatory system: a preliminary analysis. *Comput. Visual. Sci*, 2:75–83, 1999.

[33] H. Fujita and N. Sauer. On existence of weak solutions of the Navier-Stokes equations in regions with moving boundaries. *J. Fac. Sci. Univ. Tokyo, sect. 1A*, 17(403–420), 1970.

[34] L. Gastaldi. A priori estimates for the arbitrary lagrangian eulerian formulation with finite elements. submitted to East-West Journal of Numerical Mathematics.

[35] M.B. Giles. Non-reflecting boundary conditions for Euler equation calculations. *AIAA Journal*, 28(12):2050–2058, 1990.

[36] D. Givoli. Non-reflecting boundary conditions. *J. Comput. Phys*, 94:1–29, 1991.

[37] R. Glowinski, T.W. Pan, and J. Periaux. A fictitious domain method for dirichlet problem and applications. *Comp. Meth. Appl. Mech. Engrg.*, 111(3-4):283–303, 1994.

[38] R. Glowinski, T.W. Pan, and J. Periaux. A fictitious domain method for external incompressible viscous flow modeled by Navier-Stokes equations. *Comp. Meth. Appl. Mech. Engrg.*, 112(1-4):133–148, 1994.

[39] E. Godlewski and P.-A. Raviart. *Numerical approximation of hyperbolic systems of conservation laws*, volume 118 of *Applied Mathematical Sciences*. Springer, New York, 1996.

[40] C. Grandmont and Y. Maday. Existence for an unsteady fluid-structure interaction problem. *M2AN*, 34(3):609–636, 2000.

[41] C. Grandmont and Y. Maday. Fluid structure interaction: A theoretical point of view. submitted to Revue Européenne des éléments finis, 2001.

[42] C. Grandmont, Y. Maday, and V. Guimet. Results about some decoupling techniques for the approximation of the unsteady fluid-structure interaction. In *ENUMATH 97 (Heidelberg)*, pages 319–326. World Sci. Publishing, River Edge, NJ, 1998.

[43] Céline Grandmont. *Analyse mathématique et numérique de quelques problèmes d'interaction fluide-structure*. PhD thesis, Univ. Paris 6, 1998.

[44] H. Guillard and C. Farhat. On the significance of the geometric conservation law for flow computations on moving meshes. *Comput. Methods Appl. Mech. Engrg*, 190:1467–1482, 2000.

[45] K. Hayashi, K. Handa, S. Nagasawa, and A. Okumura. Stiffness and elastic behaviour of human intracranial and extracranial arteries. *J. of Biomech.*, 13:175–184, 1980.

[46] J.G. Heywood, R. Rannacher, and S. Turek. Artificial boundaries and flux and pressure conditions for the incompressible Navier–Stokes equations. *International Journal for Numerical Methods in Fluids*, 22:325–352, 1996.

[47] T.J. Hughes. *The finite element method, linear static and dynamic finite element analysis.* Prentice-Hall, Englewood Cliffs, 1987.

[48] T.J.R. Hughes, W.K. Liu, and T.K. Zimmermann. Lagrangian-eulerian finite element formulation for incompressible viscous flows. *Comp. Meth. Appl. Mech. Engrg.*, 29:329–349, 1981.

[49] A. Inoue and M. Wakimoto. On existence of solutions of the Navier-Stokes equations in a time dependent domain. *J. Fac. Sci. Univ. Tokyo, sect. 1A*, 24:303–319, 1977.

[50] D. Jaubert and V. Moreau. Fluid-structure interaction: applications in the context of a flow in arterial medium. CRS4 Tech. Rep., 1997.

[51] Y. Jiongmin. Weak solutions of second order parabolic equations in non-cylindrical domains. *J. Partial Differential Equations*, 2(2):76–86, 1989.

[52] B. Koobus and C. Farhat. Second-order time-accurate and geometrically conservative implicit schemes for flow computations on unstructured dynamic meshes. *Comput. Methods Appl. Mech. Engrg*, 170:103–129, 1999.

[53] G.L. Langewouters, K.H. Wesseling, and W.J.A. Goedhard. The elastic properties of 45 human thoracic and 20 abdominal aortas *in vitro* and the parameters of a new model. *J. of Biomesh.*, 17:425–435, 1984.

[54] P. Le Tallec and J. Mouro. Structures en grands déplacements couplées à des fluides en mouvement. Rapport de Recherche RR-2961, INRIA, August 1996.

[55] P. Le Tallec and J. Mouro. Fluid structure interaction with large structural displacements. *Comput. Methods Appl. Mech. Engrg*, 190:3039–3067, 2001.

[56] M. Lesoinne and C. Farhat. Geometric conservation laws for aeroelastic computations using unstructured dynamics meshes. AIAA-95-1709, Presented at the 12th AIAA Computational Fluid Dynamics Conference, San Diego, June 1995.

[57] J.L. Lions. Sur les problèmes mixtes pour certains systèmes paraboliques dans des ouverts non cylindriques. *Annales Institute Fourier*, 7:143–182, 1957.

[58] J.L. Lions. *Quelques méthodes de résolution des problèmes aux limites non linéaires.* Dunod, Paris, 1969.

[59] A. Masud and T.J.R. Hughes. A space-time galerkin/least squares finite element formulation of the Navier-Stokes equations for moving domain problems. *Comput. Methods Appl. Mech. Engrg.*, 146:91–126, 1997.

[60] D.A. McDonald. *Blood Flow in Arteries.* Edward Arnold Ltd. - London, 1990. Third edition edited by W.W. Nichols and M.F. O' Rourke.

[61] S. Mittal and T.E. Tezduyar. Parallel finite element simulation of 3D incompressible flows: fluid-structure interactions. *Int. j. numer. methods fluids*, 21:933–953, 1995.

[62] B. Nkonga and H. Guillard. Gudonov type method on non-structured meshes for three dimensional moving boundary problems. Rapport de Reserche RR-1883, INRIA, April 1993.

[63] K. Perktold and G. Rappitsch. Mathematical modeling of local arterial flow and vessel mechanics. In J.M. Crolet and R. Ohayon, editors, *Computational Methods for Fluid Structure Interaction*. Pitman Research Notes in Mathematics (306) - Longman, 1994.

[64] K. Perktold and G. Rappitsch. Computer simulation of local blood flow and vessel mechanics in a compliant carotid artery bifurcation model. *J. of Biomech.*, 28:845–856, 1995.

[65] K. Perktold, M. Resch, and H. Florian. Pulsatile non-Newtonian flow characteristics in a three-dimensional human carotid bifurcation model. *ASME J. of Biomech. Eng.*, 113:463–475, 1991.

[66] K. Perktold, E. Thurner, and T. Kenner. Flow and stress characteristics in rigid walled and compliant carotid models. *Medic. and Biolog. Eng. and Comp.*, 32:19–26, 1994.

[67] B. Perot. An analysis of the fractional step method. *J. Comp. Phys.*, 108:51–58, 1993.

[68] C.S. Peskin. Numerical Analysis of Blood Flow in the Heart. *J. of Comp. Phys.*, 25:220–252, 1977.

[69] C.S. Peskin and D.M. McQueen. A Three-Dimensional Computational Method for Blood Flow in the Heart - I Immersed Elastic Fibers in a Viscous Incompressible Fluid. *J. of Comp. Phys.*, 81(2):372–405, 1989.

[70] F. Phythoud, N. Stergiopulos, and J.-J. Meister. Forward and backward waves in the arterial system: nonlinear separation using Riemann invariants. *Technology and Health Care*, 3:201–207, 1995.

[71] S. Piperno. Explicit/Implicit fluid/structure staggered procedures with a structural predictor and fluid subcycling for 2D inviscid aeroelastic simulations. *Int. J. Num. Methods Fluids*, 25:1207–1226, 1997.

[72] S. Piperno, C. Farhat, and B. Larrouturou. Partitioned procedures for the transient solution of coupled aeroelastic problems - Part I: Model problem, theory and two-dimensional application. *Comput. Methods Appl. Mech. Engrg*, 124:79–112, 1995.

[73] S. Piperno, C. Farhat, and B. Larrouturou. Partitioned procedures for the transient solution of coupled aeroelastic problems - Part II: energy transfer analysis and three-dimensional applications. *Comput. Methods Appl. Mech. Engrg*, 190:3147–3170, 2001.

[74] G. Pontrelli and E. Rossini. Modelling the fluid-wall interaction in a blood vessel. Internal communication, 2001.

[75] A. Quarteroni. Introduction to the mathematical modeling of vascular flows, 2001. Lecture Notes of the course "Modelisation A"; Mathematical Department, EPFL, Switzerland.

[76] A. Quarteroni and A.Valli. *Domain Decomposition Methods for Partial Differential Equations.* Oxford University Press, Oxford, 1999.

[77] A. Quarteroni, F. Saleri, and A. Veneziani. The Yosida method for the numerical approximation of Navier-Stokes equations. *J. Pure Appl. Math.*, 78:473–503, 1999.

[78] A. Quarteroni, F. Saleri, and A. Veneziani. Factorization methods for the numerical approximation of Navier-Stokes equations. *Comput. Methods Appl. Mech. Engrg.*, 188(1-3):505–526, 2000.

[79] A. Quarteroni, M. Tuveri, and A. Veneziani. Computational Vascular Fluid Dynamics: Problems, Models and Methods. *Comp. Vis. Science*, 2:163–197, 2000.

[80] A. Quarteroni and A. Valli. *Numerical Approximation of Partial Differential Equations.* Springer Verlag, 1994.

[81] P.A. Raviart and J.M. Thomas. *Introduction à l'analyse numérique des équations aux dérivées partielles.* Masson, Paris, 1983.

[82] H. Reismann. *Elastic plates: theory and application.* Wiley, New York, 1988.

[83] V.C. Rideout and D.E. Dick. Difference-differential equations for fluid flow in distensible tubes. *IEEE Transactions on Bio-Medical Eng.*, BME-14(3):171–177, 1967.

[84] R. Salvi. On the existence of weak solutions of a non-linear mixed problem for the Navier-Stokes equations in a time dependent domain. *J. Fac. Sci. Univ. Tokyo, sect. 1A*, 32:213–221, 1985.

[85] R. Salvi. The exterior non-stationary problem for the Navier-Stokes equations in regions with moving boundaries. *J. Math. Soc. Japan*, 42(3):495–509, 1990.

[86] V. Selmin and L. Formaggia. Unified construction of finite element and finite volume discretizations for compressible flows. *Int. Journal. Num. Meths Engng.*, 39(1):1–32, January 1996.

[87] R. Temam. *Navier-Stokes equations.* North Holland, 1984.

[88] T.E. Tezduyar, M. Behr, and J. Liou. A new strategy for finite element computations involving moving boundaries and interfaces - the deforming-spatial-domain/space-time procedure: I. the concept and preliminary numerical tests. *Comp. Meth. Appl. Mech. Engrg*, 94:339–351, 1992.

[89] T.E. Tezduyar, M. Behr, S. Mittal, and J. Liou. A new strategy for finite element computations involving moving boundaries and interfaces - the deforming-spatial-domain/space-time procedure: Ii. computation of free-surface flows, two-liquid flows and flows with drifting cylinders. *Comp. Meth. Appl. Mech. Engrg*, 94:339–351, 1992.

[90] A. S. Tijsseling. Fluid-structure interaction in liquid filled pipe systems: a review. *Journal of Fluids and Structures*, 10:109–146, 1996.

[91] A. Tozeren. Elastic properties of arteries and their influence on the cardiovascular system. *ASME J. Biomech. Eng.*, 106:182–185, 1984.

[92] J. Y. Trépanier, M. Reggio, M. Paraschivoiu, and R. Camarero. Unsteady Euler solution for arbitrary moving bodies and boundaries. *AIAA Journal*, 31(10):1869–1876, 1993.

[93] A. Veneziani. Block factorized preconditioners for the time-dependent Navier-Stokes equations. Technical Report DST University of Veron, 2000, submitted to Num. Meth. Par. Diff. Eqs.

[94] H. Watanabe. The initial-boundary value problems for the heat operator in non-cylindrical domains. *J. Math. Soc. Japan*, 49(3):399–430, 1997.

[95] N. Westerhof, F. Bosman, C.D. Vries, and A. Noordergraaf. Analog studies of the human systemic arterial tree. *J. of Biomech.*, 2:121–143, 1969.

[96] X.Y. Xu, M.W. Collins, and C.J.H. Jones. Flow studies in canine aortas. *ASME J. of Biomech. Eng.*, 114(11):504–511, 1992.

[97] H. Zhang, M. Reggio, J.Y. Trèpanier, and R. Camarero. Geometric form of the GCL for moving meshes and its implementation in CFD schemes. *Computers in Fluids*, 22(1):9–23, 1993.

Fabio Nobile est né à Milan le 10 janvier 1974. Il a effectué son école secondaire au Lycée A. Volta à Milan où il a obtenu en 1992 son Baccalauréat Scientifique. Ensuite, il a poursuivi ses études à l'Ecole Polytechnique de Milan pour obtenir en 1998 un diplôme d'ingénieur en électronique avec mention. Depuis juillet 1998 il a été engagé comme assitant dans la chaire de modélisation et calcul scientifique du Professeur Alfio Quarteroni. Il a participé à plusieurs conférences internationales et il est co-auteur des publications suivantes :

- L. Formaggia, F. Nobile, A. Quarteroni, *A One Dimensional Model for Blood Flow: Application to Vascular Prosthesis*, à apparaître dans MSCOM2000, Lecture Notes in Computational Science and Engineering, T. Miyoshi Ed., Springer-Verlag, Berlin, 2001.

- L. Formaggia, J.F. Gerbeau, F. Nobile, A. Quarteroni, *Numerical treatment of defective boundary conditions for the Navier-Stokes equations*, Report EPFL-DMA 20.2000 and INRIA-4093, soumis à SIAM J. Num. Analysis.

- L. Formaggia, F. Nobile, A. Quarteroni, A. Veneziani, P. Zunino, *Advances on numerical modelling of blood flow problems*, Proceedings of ECCOMAS2000.

- L. Formaggia, J.F. Gerbeau, F. Nobile, A. Quarteroni, *On the Coupling of 3D and 1D Navier-Stokes equations for Flow Problems in Compliant Vessels*, Report EPFL-DMA 03.2000 and INRIA-3862, à apparaître sur Comp. Methods in Appl. Mech. Engng.

- L. Formaggia, F. Nobile, A. Quarteroni, A. Veneziani, *Multiscale Modelling of the Circulatory System: a Preliminary Analysis*, Comput. Visual. Sci 2 (1999) 2/3, 75-83.

- L. Formaggia and F. Nobile, *A Stability Analysis for the Arbitrary Lagrangian Eulerian Formulation with Finite Elements*, East-West Journal of Numerical Mathematics, vol. 7, 105-132, 1999.

- F. Nobile, A. Veneziani, *Fluid Structure Interaction in blood flow problems*, ZAMM Z. Angew. Math. Mech. 79 (1999) S1, S255-S258 (Proceedings of the GAMM meeting 1998, Bremen).